# ROLE OF OUTER MEMBRANE VESICLES IN *LEGIONELLA PNEUMOPHILA* PATHOGENESIS AND HOST IMMUNE MODULATION

**AYESHA**

**PhD**

**The Hong Kong Polytechnic University**

**2026**

The Hong Kong Polytechnic University

Department of Health Technology and Informatics

# Role of Outer Membrane Vesicles in *Legionella pneumophila* Pathogenesis and Host Immune Modulation

AYESHA

A thesis submitted in partial fulfilment of the requirements for the degree of Doctor of Philosophy

December 2025

# CERTIFICATE OF ORIGINALITY

I hereby declare that this thesis is my own work and that, to the best of my knowledge and belief, it reproduces no material previously published or written, nor material that has been accepted for the award of any other degree or diploma, except where due acknowledgment has been made in the text.

(Signature)

AYESHA (Name)

# Abstract

**Background:** *Legionella pneumophila* is a gram-negative bacterium widely distributed in natural and artificial freshwater systems. Amoebas residing in aquatic environments are essential for the survival of *L. pneumophila.* Upon ingestion by an amoeba, *L. pneumophila* continues to grow and replicate inside without dying. Hence, the amoeba host enables the propagation of *L. pneumophila* in aquatic environments. Being an opportunistic pathogen, *L. pneumophila* infects humans when they inhale aerosols containing *Legionella* from artificial water systems, leading to community-acquired pneumonia known as Legionnaires' disease (LD). *L. pneumophila* persistence in the host depends on its effective evasion of the host's conserved phagocytic mechanisms. Within the infected cells, the organism communicates with host cells through various methods. One well-known method is a specialized T4SS secretion system that modifies host cell signaling and metabolic processes by delivering approximately 330 effector proteins. Multiple factors influence the mortality rate of LD, particularly the host immune response. In clinical patients, Legionnaires' disease severity is associated with hyperinflammation and immunoparalysis, as well as a high bacterial load in the patient's lungs.

Over the last 50 years, researchers have identified bacterial outer membrane vesicles as a means of communication. It is now recognized that Gram-negative bacteria intentionally release outer membrane vesicles (OMVs) to facilitate bacterial communication with the environment and the host. Recent studies have also elucidated their function as immune modulators. However, the effects of OMV-host interaction on disease pathogenesis are poorly understood. Additionally, knowledge about the composition of components transferred by OMVs is limited.

**Aims:** Based on the literature on the immunomodulatory properties of OMVs and the clinical symptoms of Legionnaires' disease, it is hypothesized that *L. pneumophila* OMVs contribute to disease severity by modulating host immune responses and enhancing bacterial survival and replication within the host. To evaluate this hypothesis, pure OMVs were first isolated and briefly characterized to determine their molecular cargo and their biological implications in bacterial pathogenesis. Subsequently, THP-1 derived macrophages were sorted following OMV internalization, and single-cell RNA sequencing was performed to characterize high-resolution transcriptional responses to *L. pneumophila* OMVs in comparison to untreated THP-1-derived macrophages. Finally, transcriptional responses were verified through functional assays.

**Key findings:** *L. pneumophila* OMVs contain a diverse range of cell components, with proteins constituting the most considerable fraction, followed by DNA and RNA. Numerous virulence factors were identified among the OMV-associated proteins, and functional pathways were predicted. However, the direct roles of these components in bacterial pathogenesis require further investigation.

Differentially expressed gene (DEG) analysis after single-cell RNA sequencing revealed that the majority of altered genes were associated with cytokines, chemokines, and inflammatory mediators. Notably, *L. pneumophila* OMVs were found to modulate THP-1 derived macrophages toward an M2b phenotype, characterized by an immunoregulatory state that facilitates bacterial persistence while minimizing host cell damage. Additionally, M1 bactericidal phenotype and anti-legionellae responses, including caspase-1 activation, reactive oxygen species (ROS), and interferon gamma production, were not observed. In addition to transcriptional profiling, functional

production of cytokines and chemokines was validated using a cytokine array comprising 105 chemokines, cytokines, and growth factors. Among 105, 46 factors were upregulated in OMV-treated macrophages. Ingenuity Pathway Analysis (IPA) demonstrated enrichment of inflammatory pathways, such as NF-κB signaling, pathogen-induced cytokine storm signaling, and IL-17 signaling, as well as anti-inflammatory pathways including wound healing and IL-10 signaling, further confirming the M2b macrophage phenotype.

Furthermore, the immune modulation by OMVs did not induce cell death in the host cells, as no cytotoxicity was observed. MTT assays showed that OMVs were not toxic and promoted macrophage proliferation. Finally, the impact of *L. pneumophila* OMV-mediated modulation on bacterial replication and survival within the host was assessed using a CFU assay. Pre-treatment of THP-1 derived macrophages with *L. pneumophila* OMVs for 24 hours resulted in increased bacterial replication within host cells.

**Conclusion:** Together, these findings indicate that *L. pneumophila* OMVs contribute to disease severity by converting the host cell into an immunoregulatory, bacterium-permissive niche, thereby increasing bacterial survival and replication.

# Publications arising from the thesis

**Review paper:**

1. Ayesha, Chow FWN, Leung PHM (2023). Role of *Legionella pneumophila* outer membrane vesicles in host-pathogen interaction. *Frontiers in Microbiology, 14*, 1270123. https://www.frontiersin.org/journals/microbiology/articles/10.3389/fmicb.2023.1270123/full

**Conference abstracts:**

1. Ayesha, Chow FWN, Leung PHM (2024). *Legionella pneumophila* outer membrane vesicles promote macrophage survival while *Legionella pneumophila* induce inflammatory cell death pathways. *International Society for Extracellular Vesicles Annual Meeting 2024, Abstract Book.* Wiley; 2024. p. 64–65. Abstract no. OT02.O05. Available from: https://isevjournals.onlinelibrary.wiley.com/doi/10.1002/jev2.12444

2. Ayesha, Chow FWN, Leung PHM (2025). Single-cell RNA-Seq revealed that *Legionella pneumophila*-derived extracellular vesicles reprogram host macrophages to facilitate pathogen survival and spread. *International Society for Extracellular Vesicles Annual Meeting 2025, Abstract Book* 2025. p. 11. Abstract no. OT03.4. Available from: https://pmc.ncbi.nlm.nih.gov/articles/PMC12560119/#jev270157-sec-0070

**Research article**

3. Single-cell RNA-Seq revealed that *Legionella pneumophila*-derived outer membrane vesicles reprogram host macrophages to facilitate pathogen survival and spread **(Manuscript in preparation).**

# Acknowledgments

First and foremost, I am profoundly grateful to my chief supervisor, Professor. Polly Leung, for providing me with a valuable chance to receive PhD research training. Her patient guidance was of great assistance in overcoming the challenges and problems I encountered during my research. I also thank my co-supervisor, Dr. Franklin Chow, for his valuable mentorship and thoughtful feedback that greatly enhanced the quality of this work.

I am indebted to the lab personnel whose assistance has been invaluable. Special thanks to Dr. Raymond and Dr. Ryan Chow for their technical expertise and assistance with numerous experiments.

I am grateful to my assessors for their time and constructive suggestions during my PhD confirmation and seminars: Prof. SIU Gilman, Prof. ZOU Xiang, Prof. Wong Chi Ming, and Prof. HUANG Chien-ling. Their guidance and critical feedback have significantly shaped this dissertation.

To my lab mates, Dr. Abebe and Dr. Ying, thank you for your guidance in data analysis and for the collaborative spirit that made the research process enjoyable and productive. I also thank Dr. Yao, Dr. Daniel, Tadesse, Abera, Jiang, Jiaying, Zhipeng, and Tilaye for their support and suggestions during lab meetings.

Special thanks to my office friends Riham, Shama, and Thashma for making my time in the department enjoyable and memorable.

Finally, I am deeply grateful to my parents, my husband, and my friends (for their moral support throughout this journey.

This work would not have been possible without the collective assistance and encouragement of all these individuals. Thank you.

# Table of contents

**Abstract**.....ii

**Publications arising from the thesis**.....v

**Acknowledgments**.....vi

**Table of contents**.....i

**List of Figures**.....i

**List of Tables**.....i

**Abbreviations**.....ii

**Chapter 1. Introduction**.....1

**1.1 *Legionella pneumophila*: A leading cause of severe CAP (Community-Acquired Pneumonia) requiring ICU admission**.....1

**1.1.1 Legionnaires' disease history**.....2

**1.1.2 *L. pneumophila*- Accidental pathogen, but the prevalence of LD is rising**...3

**1.1.2.1 Strategies to control spread**.....7

**1.1.3 Intracellular replication of *L. pneumophila* within alveolar macrophages is a key feature of its pathogenicity**.....7

**1.1.4 Factors contributing to LD severity in clinical patients**.....12

**1.1.5 *L. pneumophila*'s ways to manipulate host cells and the need to explore beyond classical virulence mechanisms**.....14

**1.2 Extracellular vesicles/ Outer membrane vesicles: Emerging Players in Bacterial Pathogenesis**.....19

**1.2.1 All bacteria produce OMVs**.....19

**1.2.2 Composition of bacterial OMVs**.....21

**1.2.3 Mechanisms of OMVs interaction with host cells**.....23

**1.2.4 Functions of OMVs** ..... 26

**1.2.4.1 OMVs: Functions in the environment and bacterial communities** ..... 26

**1.2.4.2 Outer membrane vesicles: Functions in the human host** ..... 28

***1.2.5*** **Significance of OMVs in the disease pathogenesis of *L. pneumophila*** ..... 30

**1.3 Macrophages are model cells to study immune modulation by pathogens** ..... 34

**1.3.1 Macrophage in pathogen recognition and clearance** ..... 34

**1.3.1.1 Pathogen recognition receptors** ..... 36

**1.3.1.2 Opsonisation** ..... 40

**1.3.1.3 Phagocytosis** ..... 41

**1.3.1.4 Other microbicidal mechanisms in macrophages** ..... 43

**1.3.2 Macrophage polarization states and metabolism** ..... 45

**1.3.2.1 Macrophage activation states** ..... 45

**1.3.2.2 Macrophage metabolism** ..... 51

**1.3.2.3 Role of macrophage polarization in bacterial infections** ..... 52

**1.3.3 Cytokines and signalling pathways** ..... 54

**1.3.4 Lung macrophage responses to *L. pneumophila* and identifying a model for studying the role of *L. pneumophila* OMVs in disease pathogenesis** ..... 61

**1.3.4.1 Host immune responses to *L. pneumophila*** ..... 61_Toc221275595

**1.3.5 Importance of THP-1 derived Macrophage as a disease model for *L. pneumophila* OMV studies** ..... 67

**1.3.5.1 Introduction to THP-1 derived macrophages** ..... 68

**1.3.5.2 Applications of THP-1 cell line** ..... 70

**1.3.5.3 Use of THP-1 cells in *L. pneumophila* studies** ..... 71

**Chapter 2. Aims and Objectives ..... 76**

**2.1. Research Gaps** ..... 76

**2.2. Aims:** ..... 79

**2.3. Objectives:** ..... 80

**Chapter 3. Materials and Methods** ..... **81**

**3.1. Overview of workflow** ..... 81

**3.2 Bacterial strain and THP1 cell line** ..... 82

**3.2.1 *L. pneumophila*** ..... 82

**3.2.2 Cell line** ..... 82

**3.3 Isolation and characterization of *L. pneumophila* OMVs** ..... 82

**3.3.1 Growth curve of *L. pneumophila*** ..... 82

**3.3.2 Isolation of *L. pneumophila* OMVs** ..... 83

**3.3.3 Purification by Opti-Prep density gradient ultracentrifugation (DEG)** ..... 84

**3.3.4 Purification by Size Exclusion Chromatography (SEC)** ..... 85

**3.3.5 Qubit analysis** ..... 86

**3.3.6 TEM examination** ..... 86

***3.3.6.1*** **Preparation of staining solution (X-solution)** ..... 87

***3.3.6.2*** **Preparation of samples:** ..... 87

**3.3.7 NTA measurements** ..... 88

**3.3.8 OMV Proteomics analysis** ..... 88

***3.3.8.1*** **Sample preparation for proteomic analysis** ..... 88

***3.3.8.2*** **LC-MS Analysis** ..... 88

***3.3.8.3*** **Data analysis** ..... 89

**3.3.9 OMV DNA analysis by Illumina sequencing** ..... 90

***3.3.9.1*** **OMV preparation for total-DNA sequencing and internal-DNA sequencing** ..... 90

***3.3.9.2*** **DNA extraction by QIAamp MinElute ccfDNA Kit (Qiagen) kit** ..... 90

***3.3.9.3*** **Illumina library preparation and sequencing** ..... 91

***3.3.9.4*** **Data analysis** ..... 91

**3.3.10 OMV RNA analysis:** ..... 92

**3.4 *L. pneumophila* OMVs interaction with the Host** ..... 93

**3.4.1 THP-1 growth and differentiation** ..... 93

**3.4.2 Confocal laser scanning microscopy** ..... 93

**3.4.3 Flow cytometry analysis for OMV uptake** ..... 94

***3.4.3.1*** **Flow cytometry setup** ..... 94

**3.4.4 Single-cell RNA-seq (scRNA-seq) analysis** ..... 95

***3.4.4.1*** **Sample preparation** ..... 95

***3.4.4.2*** **10x genomics library preparation** ..... 96

**3.4.5 Cytokine array analysis** ..... 100

***3.4.5.1*** **Pathway analysis by IPA** ..... 102

***3.4.6*** **RNA isolation and two-step RT-quantitative PCR** ..... 102

***3.4.6.1*** **RNA isolation:** ..... 102

***3.4.6.2*** **cDNA synthesis:** ..... 103

***3.4.6.3*** **Quantitative real-time PCR analysis:** ..... 103

**3.4.7 Flow cytometry for macrophage cell surface markers** ..... 106

**3.4.8 Cytotoxicity assay by MTT** ..... 106

**3.4.9 Pyroptosis assay** ..... 107

**3.4.10 ROS assay** ..... 107

**3.4.11 Impact of OMVs on *L. pneumophila* survival and replication within Host Cell** 108

**3.4.12 Statistical analysis** ..... 109

**3.4.13 Data reliability** ..... 109

**Chapter 4. Results ..... 110**

**4.1. Isolation and molecular characterization of *L. pneumophila* OMVs** ..... 110

**4.1.1. Growth kinetics and viability of *L. pneumophila* in growth media** ..... 110

**4.1.2. Isolation of *L. pneumophila* OMVs** ..... 112

**4.1.2.1. SEV gives a higher yield of *L. pneumophila* OMVs compared to DEG** ..... 112

**4.1.3. Molecular Characterization of *L. pneumophila* OMVs:** ..... 117

**4.1.3.1. LPS estimation** ..... 117

**4.1.3.2. Proteomic and virulome profile of *L. pneumophila* OMVs** ..... 118

**4.1.3.3. Nucleic acids associated with *L. pneumophila* OMVs** ..... 127

**4.2. Transcriptional and functional impact of *L. pneumophila* OMVs on host cell survival and inflammatory responses** ..... 139

**4.2.1. OMVs were efficiently up-taken by THP-1 derived macrophages** ..... 139

**4.2.2. ScRNA-seq of THP-1 derived macrophages reveals heterogeneity in macrophage responses following OMV internalization.** ..... 142

**4.2.2.1. Gating and Sorting cell populations for ScRNA-seq analysis:** ..... 142

**4.2.2.2. Sample integration and clustering** ..... 145

**4.2.2.3. Differential gene expression (DEG) following OMV internalization** ..... 146

**4.2.2.4. Macrophage activation markers in clusters 3 and 4** ..... 151

**4.2.2.5. Clusters 3 and 4 reveal hallmarks of M2b macrophage activation** ..... 153

**4.2.2.6. Validation by qPCR** ..... 155

**4.2.2.7. Expression of PRRs and NLRs in clusters 3 and 4** ..... 158

**4.2.2.8. Anti-bacterial immunity (Interferon, RNS, and ROS production) in clusters 3 and 4** 159

**4.2.2.9. Enriched GO terms and KEGG pathways in cluster 3 and cluster 4** ..... 162

**4.2.2.10. Summary of ScRNA-seq results:** ..... 167

**4.2.3. Functional characterization of macrophage responses following *L. pneumophila* OMVs exposure** ..... 168

**4.2.3.1. Cytokine Array** ..... 168

**4.2.3.2. Surface marker analysis** ..... 183

**4.2.3.3. Cell viability assay** ..... 186

**4.2.3.4. ROS assay** ..... 188

**4.2.3.5. Active caspase-1 assay** ..... 190

**4.2.3.6. Effects of OMVs on bacterial survival and replication inside host cell** ..... 192

**Chapter 5. Discussion** ..... **194**

**5.1. Isolation of *L. pneumophila* OMVs** ..... 194

**5.2. Molecular Characterisation of *L. pneumophila* OMVs** ..... 197

**5.2.1. Significance of LPS in *L. pneumophila* OMVs** ..... 197

**5.2.2. Functional diversity in the protein composition of *L. pneumophila* OMVs** 198

**5.2.3. Nucleic acids associated with *L. pneumophila* OMVs: Gaps in understanding** 203

**5.3. Functional implications of *L. pneumophila* OMVs on host cell physiology** ..... 207

**5.3.1. ScRNA-seq reveals how OMVs promote *L. pneumophila* pathogenesis by reprogramming host macrophage responses** ..... 209

**5.3.2. *L. pneumophila* OMVs support host survival and increase bacterial replication inside the host** ..... 215

**5.3.3. OMVs contribute to the pathogenesis of *L. pneumophila* and present a promising therapeutic strategy** ..... 217

**Chapter 6. Conclusion and future directions** ..... **219**

**6.1. Conclusion** ..... 219

**6.2. Limitations and future directions** ..... 222

**Appendices** ..... **225**

**Appendix 1** ..... 226

**References** ..... **296**

# List of Figures

**Figure 1.1: Introduction points:** ..... 1

**Figure 1.2: *Legionella* spread route from the environment to humans.** ..... 4

**Figure 1.3: LD cases in Hong Kong from 1994 to 2023.** ..... 6

**Figure 1.4: Life cycle of *L. pneumophila* within the alveolar macrophage.** ..... 11

**Figure 1.5: Typical composition of OMVs.** ..... 22

**Figure 1.6: Uptake mechanisms of OMVs by the host cell.** ..... 25

**Figure 1.7: Functions of bacterial outer membrane vesicles in pathogenic and non-pathogenic bacteria**. (Ayesha et al., 2023). ..... 29

**Figure 1.8: Diverse roles of Macrophages during intracellular bacterial infections. (Created with BioRender.com)** ..... 36

**Figure 1.9: Spectrum of Macrophage polarization**. ..... 50

**Figure 1.10: Innate immune responses against *L. pneumophila*.** ..... 66

**Figure 1.11: Comparison of reported cell lines being used in *L. pneumophila* studies overall and in the recent 10 years by PUBMED** ..... 75

**Figure 3.1 Project workflow for investigating the role of *L. pneumophila* OMVs in disease pathogenesis and host immune modulation.** ..... 81

**Figure 3.2: Workflow for OMV isolation from *L. pneumophila.*** ..... 84

**Figure 3.3: Purification of crude OMVs by density gradient centrifugation (DEG) and size exclusion chromatography (SEC).** ..... 86

**Figure 3.4: Overview of ScRNA-seq data analysis** ..... 99

**Figure 3.5: Human XL Cytokine array kit map** ..... 101

**Figure 4.1: Growth assay and cell death assay.** ..... 111

**Figure 4.2: TEM examination of *L. pneumophila* OMVs isolated by UC and**

**purified by DEG and SEC.** ..... 113

**Figure 4.3: Qubit estimation of fractions of OMVs purified using qEV1 and OptiPrep techniques.** ..... 116

**Figure 4.4: LPS detection in *L. pneumophila* OMVs.** ..... 117

**Figure 4.5: SDS-PAGE analysis of three OMV replicates.** ..... 118

**Figure 4.6: Topology of OMV proteins based on protein types and protein abundance.** ..... 119

**Figure 4.7: Functional annotation of OMV proteins from *L. pneumophila* with EggNOG.** ..... 125

**Figure 4.8: KEGG pathway classification of *L. pneumophila* OMV proteins.** ..... 125

**Figure 4.9 Go term clustering of DAVID functional annotation data for OMV proteins from** ..... 126

***L. pneumophila*.** ..... 126

**Figure 4.10: Analysis of DNA content of *L. pneumophila* OMVs, with and without DNase treatment.** ..... 128

**Figure 4.11: Venn diagram illustrating the overlap of coding sequences identified in OMVs from *L. pneumophila*.** ..... 130

**Figure 4.12: Genome-wide distribution of DNA associated with *L. pneumophila* OMVs.** ..... 132

**Figure 4.13: Annotation of dense DNA regions in total DNA derived from the *L. pneumophila* OMVs.** ..... 133

**Figure 4.14: Top 10 KEGG pathways enriched in dense regions of total DNA from *L. pneumophila* OMVs** ..... 134

**Figure 4.15: RNA content associated with *L. pneumophila* OMVs.** ..... 137

**Figure 4.16: Confocal laser scanning microscopy of *L. pneumophila* OMVs uptake by THP-1 derived macrophage.** ..... 140

**Figure 4.17: OMV uptake of *L. pneumophila* OMVs by THP-1 derived macrophages.** ..... 141

**Figure 4.18: Workflow for the preparation of THP-1-derived macrophage samples for scRNA-seq.** ..... 143

**Figure 4.19: Flow cytometry gating approach for the selection of control and OMV treated THP-1-derived macrophages for scRNA-seq.** ..... 144

**Figure 4.20: UMAP illustration of single-cell transcriptome profiling of control and treated THP-1 derived macrophages.** ..... 145

**Figure 4.21: Overall differential expression analysis of THP-1-derived macrophages subjected to *L. pneumophila* OMVs compared to untreated controls.** ..... 147

**Figure 4.22: Cluster-specific differential gene expression in THP-1 derived macrophages after treatment with *L. pneumophila* OMVs, as determined by scRNA-seq.** ..... 149

**Figure 4.23: This heatmap illustrates the top differentially expressed genes (DEGs) between control and OMV treated conditions across all eight macrophage clusters.** ..... 150

**Figure 4.24: Cluster localization and expression plot of selected immune response genes in THP-1 derived macrophages following *L. pneumophila* OMV treatment.** ..... 152

**Figure 4.25: Dot plot analysis of M2b macrophage phenotypic marker expression in the cell clusters following *L. pneumophila* OMV treatment.** ..... 154

**Figure 4.26: qPCR evaluation of M1 and M2 markers expression in THP-1 derived macrophages following treatment with increasing doses of *L. pneumophila* OMVs.** .....156

**Figure 4.27: Dot plot analysis of DEGs related to PRR activation in THP-1 derived Macrophages following *L. pneumophila* OMV treatment in Cluster 3.**.....159

**Figure 4.28: Dot plot analysis of oxidative stress-related genes in THP-1 derived macrophages following *L. pneumophila* OMV treatment in cluster 3.**.....161

**Figure 4.29: Gene Ontology (GO) enrichment of DEG in THP-1 derived macrophages following *L. pneumophila* OMV treatment.** .....164

**Figure 4.30: KEGG pathway enrichment analysis of DEG in THP-1 derived macrophages following *L. pneumophila* OMV treatment.** .....166

**Figure 4.31: Analysis of cytokine profiles in THP-1-derived macrophages following treatment with increasing doses of *L. pneumophila* OMVs using a proteome profiler array.** .....169

**Figure 4.32: Analysis of cytokines and chemokines following treatment with *L. pneumophila* OMVs using cytokine array.**.....172

**Figure 4.33: Analysis of Growth factors following treatment with *L. pneumophila* OMVs using cytokine array.**.....173

**Figure 4.34: Analysis of Enzymes and Transporters following treatment with *L. pneumophila* OMVs using cytokine array.**.....174

**Figure 4.35: Analysis of other factors following treatment with *L. pneumophila* OMVs using cytokine array.** .....175

**Figure 4.36: STRING interaction network of 46 cytokines**. .....178

**Figure 4.37: Top enriched pathways from IPA for cytokine fold change of THP-**

**1 derived macrophages following *L. pneumophila* OMV treatment:** .....180

**Figure 4.38: IPA analysis of disease and function pathways enriched in THP-1 derived macrophages following *L. pneumophila* OMV treatment.**.....182

**Figure 4.39 Surface markers were analyzed for THP-1-derived macrophages following treatment with *L. pneumophila* OMVs utilizing flow cytometry.** .....184

**Figure 4.40 Surface markers were analyzed for THP-1 derived macrophages following treatment with *L. pneumophila* OMVs utilizing flow cytometry.** .....185

**Figure 4.41: Cell viability of THP-1 derived macrophage following treatment with *L. pneumophila* OMVs utilizing MTT assay.**.....187

**Figure 4.42: Visualisation of THP-1-derived macrophage by plan confocal microscopy with or without treatment with *L. pneumophila* OMVs.**.....188

**Figure 4.43: *L. pneumophila* OMVs stimulate antioxidant responses and reduce ROS generation in THP-1 derived macrophages.**.....189

**Figure 4.44: Analysis of caspase-1 activity (Pyroptosis) in THP-1 derived macrophages following treatment with *L. pneumophila* OMV.** .....191

**Figure 4.45: Impact of OMV pre-treatment on the intracellular replication of *L. pneumophila* in THP-1 derived macrophages.** .....193

# List of Tables

Table 1.1 Comparison of popular cell lines used to study *L. pneumophila* disease 73

Table 3.1 Primers used in this study: .....105

Table 4.1: Comparison of OMVs size and concentration among fractions obtained from DEG and SEC methods. .....115

Table 4.2: Virulence factors identified in *L. pneumophila* OMVs.....123

Table 4.3: Significantly enriched genes in OMV internal DNA between 1098 kbps and 1170 kbps. .....135

Table 4.4: qPCR verification of macrophage phenotype marker expression in 20 µg OMV treated macrophages relative to untreated macrophages (Tables A–E). .....157

Table 5.1 Comparison of particle to protein ratio of OMVs obtained by SEC and DEG .....196

# Abbreviations

| | |
|---|---|
| ATCC | American Type Culture Collection |
| BYCE | Buffered charcoal yeast extract |
| CFU | Colony-forming unit |
| cDNA | Complementary deoxyribonucleic acid |
| FACS | Fluorescence-activated cell sorting |
| GAPDH | Glyceraldehyde-3-phosphate dehydrogenase |
| KEGG | Kyoto encyclopedia of genes and genomes |
| GO | *Legionella-containing vacuole* |
| LCV | *Legionella*-containing aerosol |
| MOI | Multiplicity of infection |
| NFκB | Nuclear factor–κB |
| PCR | Polymerase chain reaction |
| PMA | Phorbol-12-myristate 13-acetate |
| RNA | Ribonucleic acid |
| RT | Reverse transcription |
| TEM | Transmission Electron Microscopy |
| LD | Legionnaires' disease |
| T4SS | Type IV secretion system |
| RTM | Respiratory tract microbiome |
| ICU | Intensive care unit |
| PRRs | Pattern-recognition receptors |
| DAMPs | Damage-associated molecular patterns |
| ROS | Reactive oxygen species |

| | |
|---|---|
| LIMPII | Lysosomal Integral Membrane Protein II |
| iNOS | Inducible nitric oxide synthase |
| CAM | Classically Activated Macrophages |
| AAM | Alternatively Activated Macrophages |
| TLR | Toll-like receptor |
| CSF2 | Colony-stimulating factor 2 |
| ISGs | Interferon-stimulated genes |
| IPA | Ingenuity Pathway Analysis |
| OMVs | Outer membrane vesicles |
| PBS | Phosphate-buffered saline |
| ScRNA-seq | Single cell RNA sequencing |

# Chapter 1. Introduction

The introduction of this thesis focuses on three main themes: the biology and pathogenicity of *Legionella pneumophila*, the emerging role of outer membrane vesicles (OMVs) in *L. pneumophila* pathogenesis, and the importance of macrophages in investigating OMV-mediated host-pathogen interactions. These concepts are illustrated in Figure 1.1.

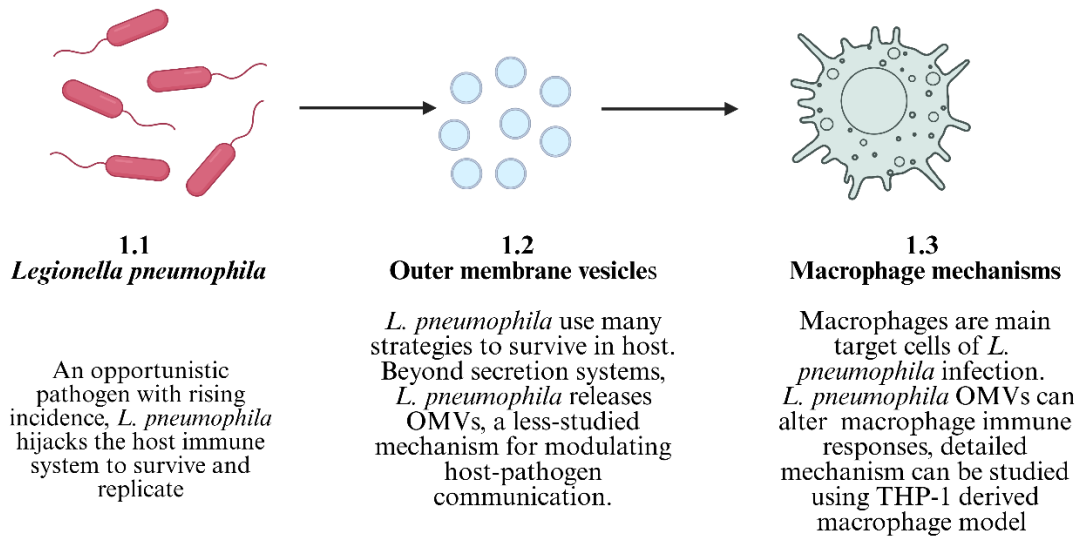


**Figure 1.1: Introduction points:** Overview of the main concepts addressed in this thesis: (1) *Legionella pneumophila*, (2) outer membrane vesicles, and (3) macrophage mechanisms.

## 1.1 *Legionella pneumophila*: A leading cause of severe CAP (Community-Acquired Pneumonia) requiring ICU admission

*Legionella* species (spp.) are among the most common microbiological causes of

community-acquired pneumonia (CAP) in the literature, responsible for severe CAP in 2% to 15% of patients who require hospitalization (Cunha, 2006; Garau & Calbo, 2008; Stout & Yu, 1997; Woodhead, 2002). Although there are approximately 65 known species of *Legionella*, 80 to 90% of infections in Europe and the US are caused by the species *Legionella pneumophila* (Beauté, 2017). According to recent meta-analysis, the proportion of *L. pneumophila* associated with CAP is 4.6% (Graham et al., 2022), and it was nearly twice as high in patients admitted to the intensive care unit. Although advances in diagnosis and appropriate medication have reduced its role as a cause of ICU admission over the past decade (Ferreira-Coimbra et al., 2020; Ruiz-Spinelli et al., 2023), historically, it still ranks as one of the top three causes of severe CAP resulting in ICU admission. (Gattarello et al., 2015; Polverino et al., 2013). CAP linked to *L. pneumophila* is named as "Legionnaires' disease (LD).

### 1.1.1 Legionnaires' disease history

The 1976 Philadelphia pneumonitis epidemic led to the discovery of the *Legionella* species. Thirty-four people died as a result of this rare respiratory illness, which affected 221 participants during the American Legion's 58th annual conference (Fraser et al., 1977). In December 1976, Joseph McDade and Charles Shepard identified this bacterium from the infected lungs of the patient. This gram-negative, rod-shaped bacterium was named *Legionella* after the American Legion incident. After the

bacterium was identified, further studies revealed that *Legionella* had actually been discovered in 1947 but had not yet been defined (Fliermans, 1996). Additionally, it was found that *Legionella* was the cause of previously unexplained flu-like illness epidemics, including the 1968 outbreak in Pontiac, Michigan, which gave rise to the clinical condition known as Pontiac fever (Glick et al., 1978). Since then, *Legionella* has been acknowledged as the prominent causative agent for community-acquired pneumonia worldwide.

### 1.1.2 *L. pneumophila*- Accidental pathogen, but the prevalence of LD is rising

*L. pneumophila* harbors everywhere, including natural environments like freshwater, moist soil, decomposed material, and man-made water systems like decorative fountains, cooling towers, etc (Newton et al., 2010). In these niches, the bacterium predominantly grows within a biofilm structure, colonizes protozoa such as amoebae of the genus *Acanthamoeba*, or resides as a free-living bacterium. From these sources, *L. pneumophila* move into man-made water systems, and once aerosolized, they can be transferred to humans and cause disease (Figure 1.2). *L. pneumophila's* potential to multiply among protozoan hosts, such as aquatic amoebae, provided insight into its ability to replicate in human lung macrophages (Escoll et al., 2014; Rowbotham, 1980). As *L. pneumophila* can also grow in multiple protozoan hosts, it has been suggested

that the ability to acquire foreign genes is the explanation for its ability to generate a replicative niche in evolutionarily diverse hosts, such as Amoeba and humans (Escoll et al., 2014; Gomez-Valero et al., 2019).

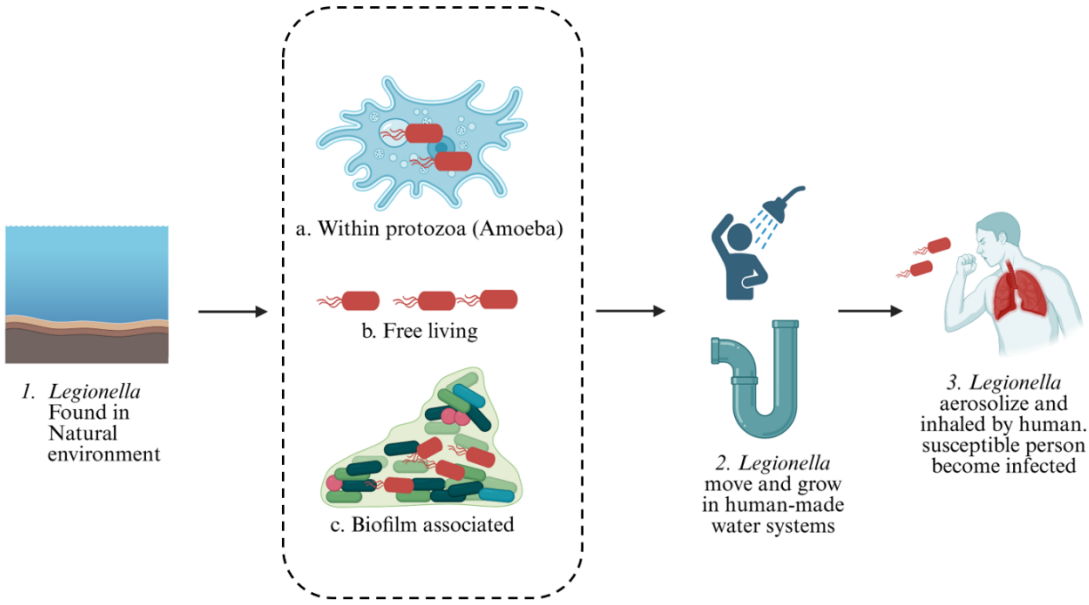


**Figure 1.2: *Legionella* spread route from the environment to humans.**

*Legionella* is found in natural habitats, such as freshwater, wet soil, and decaying matter. The bacterium primarily grows as part of a biofilm, colonizes protozoa, or can also live independently. These three forms can also be found in man-made water systems, such as showers and building pipes. From these artificial systems, once aerosolized, *Legionella* can be inhaled by humans and cause disease. **(Created with BioRender.com)**

LD can affect anybody, although it is more likely in smokers, older males, and people with medical conditions or immunosuppression (Cunha & Cunha, 2017). Similar reporting rates, geographical distribution, and epidemiology are seen in both Europe and the United States, where the prevalence of LD is increasing annually. A similar trend can also be seen in Hong Kong (Figure 1.3) (Yu et al., 2002). LD is common yet

underdiagnosed as a CAP, although recent advances in rapid detection kits have improved its diagnosis. In temperate climates, most LD cases happen from late spring to early summer fall. (Allgaier et al., 2021; Samuelsson et al., 2023). In the tropics, cases are observed throughout the year (Eshwara et al., 2020). A notable trend in LD prevalence has been observed in Europe, the US, Canada, and Australia in recent years. The specific reasons behind these increases are unclear; however, they are strongest in the older age groups (over 60 years old) and display an increased seasonal trend, despite no changes in diagnostic practices. Increased temperature, precipitation, and relative humidity are positively associated with LD events, particularly high temperatures, high humidity, low wind, and increased precipitation (Conza et al., 2013; Pampaka et al., 2022). Climate change and extreme weather events, such as sharp temperature variations and heavy rains, may intensify and create favorable conditions for *L. pneumophila* growth, which would raise the prevalence of LD (Dupke et al., 2023). According to reports, LD accounts for between 2% and 9% of all community-acquired pneumonia cases globally; however, the actual number is difficult to determine due to underdiagnosis, variations in diagnostic techniques, awareness, and reporting requirements.

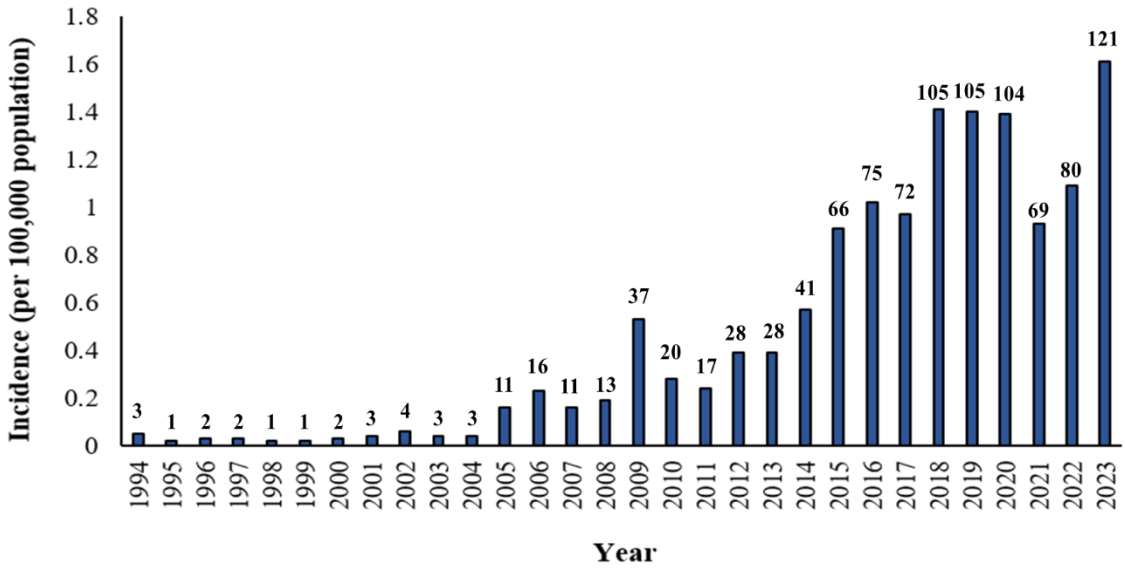


**Figure 1.3: LD cases in Hong Kong from 1994 to 2023.**

Data collected from the website (https://www.chp.gov.hk/en/static/24012.html), Centre for Health Protection, Department of Health, Hong Kong (Protection, 2024). The number value on bars shows the number of reported cases each year, while the height of the bar shows incidence per 100,000 population.

*L. pneumophila* is an opportunistic pathogen that inadvertently infects humans. Ideologically, LD represents an evolutionary dead-end for the bacterium, either clearance of the pathogen by human immune system or death of the patient. Thus, human infections are insignificant in spreading and restrict the bacterium's capacity to acquire human-specific adaptations. This explains the rare transmission of *L. pneumophila* from human to human (Currie & Beattie, 2015). This may also justify why *L. pneumophila* often demonstrates relatively low levels of antibiotic resistance compared to other human pathogens, which experience intense selection due to the use of antibiotics.

#### 1.1.2.1 Strategies to control spread

Cooling towers, spas, and water network systems are the primary sources of contamination. Temperatures above 20 °C are a significant risk factor for *L. pneumophila* colonization in dental chair equipment, according to risk factor analysis. Aerosols produced by water-bearing equipment and therapy in dental chair units that need water lines pose a danger of infection for both patients and dental personnel (Optenhövel et al., 2023). Biofilms in polluted pipes can cause infections in hospitalized patients or dialysis units. To reduce the risk of infection, it is advised to apply routine disinfection techniques and conduct routine water quality monitoring to detect the presence of substantial *L. pneumophila* loads. Additionally, to stop *L. pneumophila* from growing inside a water network, a minimum temperature for hot water > 60 °C, and a maximum temperature for cold water < 20 °C must be maintained. To determine the source of contamination, LD episodes must be reported to public health authorities (Cullom et al., 2020).

### 1.1.3 Intracellular replication of *L. pneumophila* within alveolar macrophages is a key feature of its pathogenicity

It is noteworthy that both the host's immunity and the bacterial virulence factors determine the outcome of infection. It may range from asymptomatic disease to mild respiratory illness to ICU admission requiring pneumonia.

The most frequent method of transmitting *L. pneumophila* is through inhaled aerosols from man-made water systems, including showers, hot tubs, plumbing networks, air conditioning systems, humidifiers, and whirlpool spas (Currie & Beattie, 2015). After inhalation of aerosols from these sources, human infection occurs. Similar to the strategies it employs to thrive within its protozoan hosts, *L. pneumophila* invades lung alveolar macrophages after inhalation, preventing their bactericidal action and converting them into a niche for its proliferation called the *Legionella-containing vacuole* (LCV) (Chauhan & Shames, 2021; Gonçalves et al., 2021; Mondino et al., 2020). This LCV differs from the classical endocytic compartment of phagocytic cells in both appearance and fate (Gruenberg, 2001). The formed LCV does not show any of the standard markers of the endocytic pathway, including the lysosomal transmembrane protein Rab7, which is usually found at late endosomes, Rab5, which is located at early endosomes, and LAMP-1 (Alan et al., 1984; Roy et al., 1998). Furthermore, there is no acidification of the LCV; instead, a steady pH of roughly 6.1 is maintained (Horwitz & Maxfield, 1984). Bypassing the endocytic route, the LCV thus becomes an environment that supports *L. pneumophila* replication. The LCV outer membrane is embellished with smooth vesicles and ribosomes, which are actively drawn to the LCV from the endoplasmic reticulum (ER), forming a distinct ER-like compartment, according to microscopy studies (Horwitz, 1983a; Ninio & Roy, 2007; Tilney et al., 2001). The role

of mitochondria relocalization at the LCV is also unclear, but it appears to cause a metabolic change in cells infected with *L. pneumophila* that probably promotes bacterial reproduction (Escoll et al., 2017; Finsel & Hilbi, 2015; Naujoks et al., 2016). *L. pneumophila* begins to multiply after residing in the altered phagosome for 4–10 hours, and about 24 hours of bacterial invasion by the host cell, the LCV completes full replication (Horwitz, 1983b). A crucial virulence mechanism required for *L. pneumophila* to establish infection is the type IV secretion system (T4SS), which is encoded by the dot/icm genes (Cianciotto, 2005; Galán, 2009). Shortly after a successful invasion, *L. pneumophila* activates the production of the 27-protein multiprotein complex known as the T4SS. Strains of *L. pneumophila* lacking Dot/Icm T4SS components, like ΔdotA, are incapable of replication and enter the endocytic pathway, which is defined by the fusion of the phagosome with the lysosome, acidification, and ultimately the degradation of the vacuolar trapped microorganism (Ge & Shao, 2011; Roy & Isberg, 1997). Apart from the Dot/Icm T4SS, *L. pneumophila* possesses additional secretion systems that are necessary for pathogenicity and the effective establishment of infection. A T2SS system (Lsp), a T1SS system (Lss), and an additional T4SS (Lvh) are among them (Gomez-Valero et al., 2019; Qin et al., 2017). T2SS and T4SS have received considerable attention in *L. pneumophila* research due to their crucial roles in infection (Cianciotto, 2005). It has been shown that *L.*

*pneumophila's* potential to infect diverse hosts is reduced by mutations in one of these systems; additionally, this also affects cell invasion, reproduction, survival, and biofilm formation (Newton et al., 2010; Söderberg et al., 2008). The translocation of over 300 effector molecules into the host cytosol is made possible by the functional Dot/Icm T4SS. Through various actions on the host cell, these effectors enable the LCV to create a replication-permissive environment. Following successful multiplication, *L. pneumophila* then exits the LCV into the alveolar space, lysing its previous host cell and initiating a fresh infection cycle (Figure 1.4).

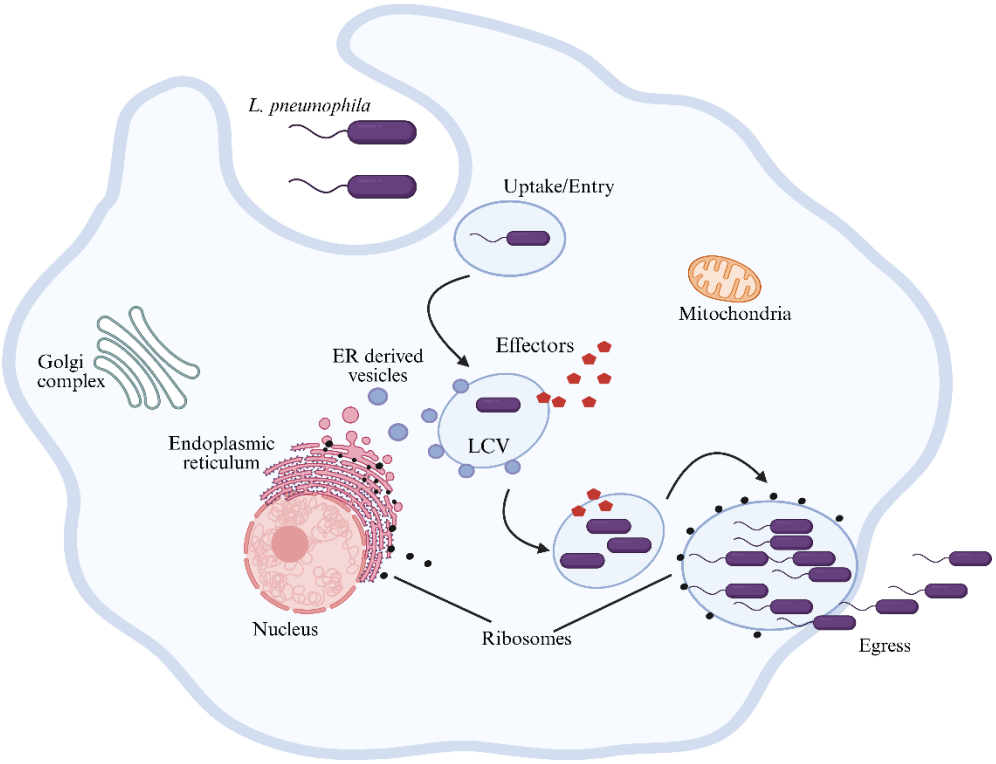


**Figure 1.4: Life cycle of *L. pneumophila* within the alveolar macrophage.**

The figure shows the infection cycle of *L. pneumophila* in a host cell. Upon entry, the bacterium shifts toward the "replicative (non-flagellated) stage" surrounded by a vacuole, and employs the Dot/Icm T4SS to deliver effector proteins (red) into the host cytoplasm. These effectors hijack host-cell processes in order to promote the biogenesis of the *Legionella*-containing vacuole (LCV). Following LCV establishment, *L. pneumophila* replicates extensively within the LCV and shifts towards the "transmissive (flagellated) stage", before eventually escaping (egressing) to infect new cells. Major organelles, such as the nucleus, endoplasmic reticulum (ER), Golgi complex, mitochondria, and ribosomes, are illustrated to demonstrate how the pathogen and host cellular machinery interact with each other. **(Created with BioRender.com)**

Typically, the life cycle of *L. pneumophila* consists of replicative and transmissive stages known as the biphasic life cycle. While the transmissive phase is considered virulent, the replicative phase is thought to be avirulent (Molofsky & Swanson, 2004). Growth occurs in both intracellular and extracellular situations, but involves metabolic

changes and is influenced by a particular gene expression pattern (Oliva et al., 2018). When conditions are favourable for reproduction and nutrient abundance, bacteria reproduce and suppress the expression of transmission traits. In contrast, when conditions are unfavourable for reproduction and nutrient deficiency, organisms express transmission traits and suppress replicative genes (Brüggemann et al., 2006). As a result, the cycle is restarted when the bacteria escape the cell and spread to other hosts. The exponential and stationary growth stages of bacterial development in liquid media indicate the replicative and transmissive phases of bacteria, respectively (Byrne & Swanson, 1998). In conclusion, the metabolic state of the cell is necessary for both the infection of the host cell and the survival of *L. pneumophila* inside the cell (Molofsky & Swanson, 2003).

### 1.1.4 Factors contributing to LD severity in clinical patients

The molecular basis of severe LD is not well understood, although many virulence factors involved in different stages of pathogenesis have been identified. (Shames et al., 2017). In a recent review of the extracellular and surface-exposed virulence factors, the functions of zinc metalloprotease (ProA), macrophage infectivity potentiator (Mip), and the flagellin (FlaA) were discussed in terms of virulence, tissue degradation, and immune system evasion (Scheithauer et al., 2023). In the human lung, ProA may specifically support bacterial growth and spread, as well as lung tissue destruction

through extracellular protease activity, which could lead to pneumonia severity. However, in the clinical picture, no *L. pneumophila* virulence factor has been linked to the severity of Legionnaires' disease (LD). The load of *L. pneumophila* DNA in respiratory specimens is associated with high pneumonia severity scores, intensive care unit (ICU) admission, or extended length of hospitalization (Maurin et al., 2010; Mentasti et al., 2012). The balance of the respiratory tract microbiome (RTM) is disrupted in severe lung disease (LD). Low microbial diversity has been identified in patients undergoing invasive mechanical ventilation (IMV), and the presence of opportunistic pathogens (fungi, archaea, and protozoa) is also believed to contribute to pneumonia progression. Since *L. pneumophila* biomass is associated with the severity of disease and can be linked to comorbidities, estimating the pathogen load is a component of patient surveillance. Secondly, IMV **(**Intermittent Mandatory Ventilation), prolonged hospitalization durations, and the combined use of antibiotics influence the lung microbiota. The relationship between respiratory microbiome homeostasis, pathogen load dynamics, and interventions related to hospitalization is a key factor in the recovery from pneumonia. In terms of immunity, the extent of NF-Kb (Nuclear Factor kappa B) pathway activation in vitro is strain dependent (Guillemot et al., 2022; Wang et al., 2018). Strains that cause more NF-κB activation in vitro cause more weight loss, greater mortality, more severe lung inflammation, and higher levels of serum

cytokines in mice. In humans, there are only a few data reports. In a small number of patients, an increased intensity of the inflammatory cytokine response is observed in the most severe cases (Fernández-Serrano et al., 2003). A recent study demonstrated that severe LD patients under mechanical ventilation experienced an early rise in systemic secretion of seven pro-inflammatory mediators, followed by leukocyte hypo-responsiveness for the cytokine secretion known as immunoparalysis (Allam et al., 2023). In conclusion, LD severity depends on *L. pneumophila* loads and hyperactivation of the immune system.

### 1.1.5 *L. pneumophila*'s ways to manipulate host cells and the need to explore beyond classical virulence mechanisms

Pathogens that reside in the host cells have evolved sophisticated tactics for modifying the host cell to generate and/or maintain the niches, in which they replicate, survive and, sometimes, even spread. Protein effectors are utilised by a wide variety of bacteria such as *Salmonella enterica, Shigella flexneri and Chlamydia trachomatis* (Galán, 2009; Kellermann et al., 2021). These effector proteins often in turn engage in remodeling the structure and function of organelles such as endosomes, ER, Golgi, and mitochondria, or in the regulation of diverse cellular activities (Kellermann et al., 2021). *L. pneumophila* effectors are selectively delivered from the LCV into the host cytoplasm

temporally and hierarchically through T4SS. Although the entire repertoire of effectors of *L. pneumophila* and their modes of action remain under studied, the effectors of *L. pneumophila* have been found to affect various host cell processes including metabolism, phagosome maturation, small GTPase signaling, ubiquitination, apoptosis, autophagy, cell cycle, cytoskeleton, and mitochondrial dynamics, mRNA transcription, and protein synthesis (Belyi et al., 2022; Galán, 2009; Ge & Shao, 2011; Kellermann et al., 2021; Mondino et al., 2020). For example, *L. pneumophila* effectors Lgt1-3, SidI, SidL, LegK4 and RavX target host protein synthesis by affecting the eukaryotic protein synthesis machinery by phosphorylation (reducing its protein refolding capacity) (Belyi, 2020). Wild-type *L. pneumophila* also inhibits eIF4E, thus blocking cap-dependent translation initiation (Ivanov & Roy, 2013). This leads to an attenuation of global protein translation and a decrease in the production of proinflammatory cytokines, such as TNFα, IL-6, and IL-12 in infected cells (Asrat et al., 2014; Copenhaver et al., 2014; Hempstead & Isberg, 2015; Liu & Shin, 2019; Treacy-Abarca & Mukherjee, 2015; Walter & Ron, 2011). *L. pneumophila* effectors also target host ubiquitin pathways that are required for efficient replication of the bacterium (Kitao et al., 2020; Qiu & Luo, 2017). SidE family effectors promote LCV biogenesis and control mTOR kinase activity that is important for nutrient uptake (De Leon et al., 2017; Kotewicz et al., 2017; Qiu et al., 2016). The MavC and MvcA effectors manipulate the ubiquitination of

Ube2N, which affects the ubiquitin-mediated degradation of the NF-κB suppressor IκBα and transcription of inflammatory genes (Gan et al., 2020; Gan et al., 2019). *L. pneumophila* is an auxotroph for host-derived amino acids for replication (Tesh & Miller, 1981). The AnkB effector brings polyubiquitinated proteins to the LCV for proteolysis and the generation of amino acids. Effectors also regulate mTORC1, which in turn controls such processes as autophagy and translation initiation (Efeyan et al., 2012). During infection, macrophages become "Warburgized" with enhanced glycolysis and repressed oxidative phosphorylation metabolism to support bacterial replication (Escoll et al., 2017). In summary, *L. pneumophila* effectors contribute to bacterial survival and modulate host responses. These trigger an "effector-triggered response", which impacts transcriptional regulators and extends expression of NF-κB-regulated transcripts. Some proinflammatory genes, such as IL-1α, are translated despite translational repression, as guided by TLR ligation and distinct mRNA motifs.

While bacterial effector proteins are one molecular weapon of *L. pneumophila,* which is well studied, *L. pneumophila* uses several other strategies to survive in the host and environmental reservoirs. Among these mechanisms are stress response systems (RpoS), drug efflux pumps, quorum sensing, and outer membrane vesicle production (Battesti et al., 2011; Green & Mecsas, 2016; Martinez et al., 2009; Toyofuku, 2019).

Chemical communication or quorum sensing, drug efflux pumps play an important role in the survival of *L. pneumophila* in bacterial communities (Rutherford & Bassler, 2012). *L. pneumophila* uses a chemical signal called *Legionella* autoinducer-1 LAI) as a quorum-sensing system that controls its life cycle and virulence by monitoring cell density in the environment (Personnic et al., 2018). In the context of host-pathogen interaction, outer membrane vesicles (OMVs) are one of the most intriguing and least characterized among these strategies. Only soluble molecules are released by secretion systems; however, OMVs can secrete both insoluble and soluble molecules together. Further, molecules on the surface of OMVs can bind to host receptors, thereby allowing the bacterial protein/enzymes to be targeted to specific cells or distal sites. OMVs are different from secretion systems in that they can transport bacterial components over long distances, i.e., to non-infected host cells without the need for direct contact. This feature may provide *L. pneumophila* with more flexible and extensive capability to regulate and control host responses.

Additionally, as previously described, the severity of *L. pneumophila* infection in clinical patients is influenced by immune system hyperactivation or dysregulation, as well as a high bacterial load in the lungs. OMVs produced by *L. pneumophila* may also

contribute to the severity of LD by modifying host cell responses, thereby catalyzing bacterial growth inside the host cell and resulting in a high bacterial load within host.

## 1.2 Extracellular vesicles/ Outer membrane vesicles: Emerging Players in Bacterial Pathogenesis

Extracellular vesicles (EVs) are lipid-bound vesicles secreted by cells into the extracellular space. EVs are produced by all life forms, but depending upon their biogenesis, release pathways, and their origin, they have different names, such as micro vesicles, exosomes, and membrane vesicles.

### 1.2.1 All bacteria produce OMVs

The secretion of extracellular vesicles (EVs) is a conserved process present across all life forms, including bacteria, archaea, fungi, and complex eukaryotes (Deatherage & Cookson, 2012). These small lipid-membrane-bound particles, measuring 20 to 400 nm in size, are released from cells but cannot self-replicate (Liu et al., 2022; Maas et al., 2017). Bacterial vesicle production was initially observed in 1960. Since then, OMVs have been widely studied across various bacteria, including *Escherichia coli, Neisseria, Vibrio, Bacteroides, Pseudomonas aeruginosa, Campylobacter jejuni, and Actinobacillus* (Chatterjee & Das, 1967; Devoe & Gilchrist, 1973; Grenier & Mayrand, 1987; Hoekstra et al., 1976; Kadurugamuwa & Beveridge, 1995; Logan & Trust, 1982; Nowotny et al., 1982; Toyofuku et al., 2019). In gram-positive bacteria, EVs bud from the cytoplasmic membrane and contain cytoplasmic contents, often called membrane vesicles (MV). In contrast, in gram-negative bacteria, EVs originate from the outer

membrane and include both periplasmic and cytoplasmic components, known as outer membrane vesicles (OMVs) (Brown et al., 2015; Toyofuku et al., 2019). Recent research suggests that gram-negative bacteria release not only OMVs but also double- and triple-membrane vesicles. These are believed to result from bacterial cell lysis, which can occur with or without the involvement of bacteriophages (Toyofuku et al., 2019).

Although different bacterial species produce OMVs, their rates of OMV production differ (de Freitas et al., 2022; Devoe & Gilchrist, 1973; Gankema et al., 1980; Wensink & Witholt, 1981). Additionally, growth and nutrient conditions impact the production and composition of OMVs within the same bacterial species. Numerous studies indicate that bacteria produce more vesicles after exposure to specific antibiotics (Orench-Rivera & Kuehn, 2016). This increased OMV production can either release more enzymes, like beta-lactamases, to break down antibiotics or serve as decoys to capture surrounding antibiotics, thereby protecting bacteria. The host's presence can also affect bacterial vesiculation. Studies have shown variations in OMV production when bacteria are exposed to host components and tissue. Using a mouse model of enterotoxigenic *E. coli* infection, electron microscopy revealed that vesicles were more abundant on ETEC cells recovered from the small intestine post-infection (Ellis & Kuehn, 2010).

### 1.2.2 Composition of bacterial OMVs

Elements of OMVs purified by ultracentrifugation, filtration, or chromatography included mainly membrane components like proteins and lipids from the periplasm, along with other cytoplasmic elements (Roier et al., 2016). Protein analysis of OMVs revealed the presence of outer membrane (OM) proteins, periplasmic proteins, and flagellin, indicating they derive from motile bacteria. Lipid analysis identified lipopolysaccharide (LPS) and lipoproteins. Notably, all OMVs from gram-negative bacteria showed a high abundance of LPS components (Toyofuku et al., 2019). Flagellin, LPS, OM proteins, and lipoproteins are also suggested to be key contributors in OMV biogenesis mechanisms (Avila-Calderón et al., 2021). Oligosaccharides, or glycans, are located in the outer membrane and are often associated with OMVs. Because OMVs play a role in interactions between bacteria and between bacteria and hosts, their ability to dock successfully with bacterial or host cell surfaces depends on the presence of adhesive oligosaccharides within the OMVs (Knoke et al., 2020). Moreover, the oligosaccharide composition in OMVs differs across various bacterial strains or species. Consequently, the oligosaccharides in OMVs can act as molecular fingerprints for identifying specific OMV types. Nonetheless, more research is needed to thoroughly understand the diversity and functional roles of oligosaccharides in OMVs from different bacteria.

Besides flagellin, oligosaccharides, outer membrane, and periplasmic proteins, OMVs carry a diverse array of cargos, including nucleic acids like plasmids, DNA, and RNA, as well as cytosolic proteins such as virulence factors (Figure 1.5). While many components have been found in the OMVs of various gram-negative bacterial species, some key elements remain consistent, suggesting a common origin. OMVs also protect the contained enzymes from extracellular degradation, enhancing their functional reach (Kulp & Kuehn, 2010).

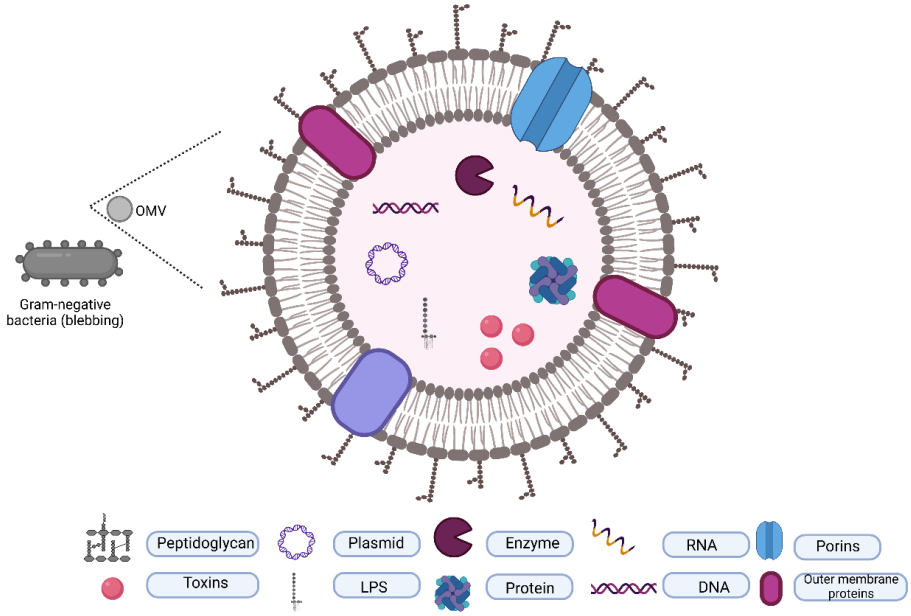


**Figure 1.5: Typical composition of OMVs.**

OMVs are originated by outer membrane blubbing and contain a lipid layer packaged with proteins, toxins, DNA, and RNA (Ayesha et al., 2023).

### 1.2.3 Mechanisms of OMVs interaction with host cells

While there is substantial evidence that OMVs can infiltrate host cells and deliver their contents to influence cellular functions, the exact processes by which OMVs engage with and are internalized by host cells remain unclear. OMVs derived from pathogenic bacteria interact with diverse cell types, including immune cells (epithelial cells, macrophages, dendritic cells, and neutrophils) and non-immune cells (endothelial cells, osteoblasts, and synovial cells) (Jäger et al., 2014; Kaparakis-Liaskos & Ferrero, 2015; Kaparakis et al., 2010; Kim et al., 2013; Lappann et al., 2013; Maldonado et al., 2011; Schultz et al., 2007). Typically, five endocytic pathways for OMVs entry into host cells: macropinocytosis, clathrin-mediated endocytosis, caveolin-mediated endocytosis, lipid-raft-mediated endocytosis, and direct membrane fusion, as illustrated in Figure 1.6. Each pathway is supported by examples found in the literature.

Evidence of macropinocytosis or actin-mediated endocytosis appeared when the uptake of *P. aeruginosa* OMVs by airway epithelial cells decreased following treatment with an actin polymerization inhibitor, which is essential for actin-dependent processes macropinocytosis (Bomberger et al., 2009). Interestingly, *P. aeruginosa* OMVs also depend on the lipid-raft-mediated endocytosis pathway to enter human lung epithelial cells (Bauman & Kuehn, 2009). OMVs from *Listeria monocytogenes* engaged with Caco-2 cells through actin-driven endocytosis or the macropinocytosis pathway

(Karthikeyan et al., 2019). Clathrin-mediated endocytosis was identified as the entry pathway for OMVs in *Brucella abortus* within human monocytes (Pollak et al., 2012), Enterohemorrhagic *E. coli* in human brain microvascular endothelial cells (HBMEC) and Caco-2 cells (Bielaszewska et al., 2013), *Aggregatibacter actinomycetemcomitans* in HeLa cells and human gingival fibroblasts (HGF) (Thay et al., 2014; Vanaja et al., 2016). Finally, OMVs can also be incorporated into host cells through direct membrane fusion, as shown in *P. aeruginosa, A. actinomycetemcomitans,* and *L. pneumophila* by labeling OMV membranes with Rhodamine R-18 fluorescent dyes (Bomberger et al., 2009; Jäger et al., 2015; Rompikuntal et al., 2012).

Studying how OMVs interact with host cells is complex because many pharmacological inhibitors of endocytic pathways influence multiple mechanisms, making it difficult to pinpoint the exact uptake process. Furthermore, a single bacterial species can utilize more than one mechanism for OMV uptake. The content and size of OMVs can also affect how they are taken up pathway.

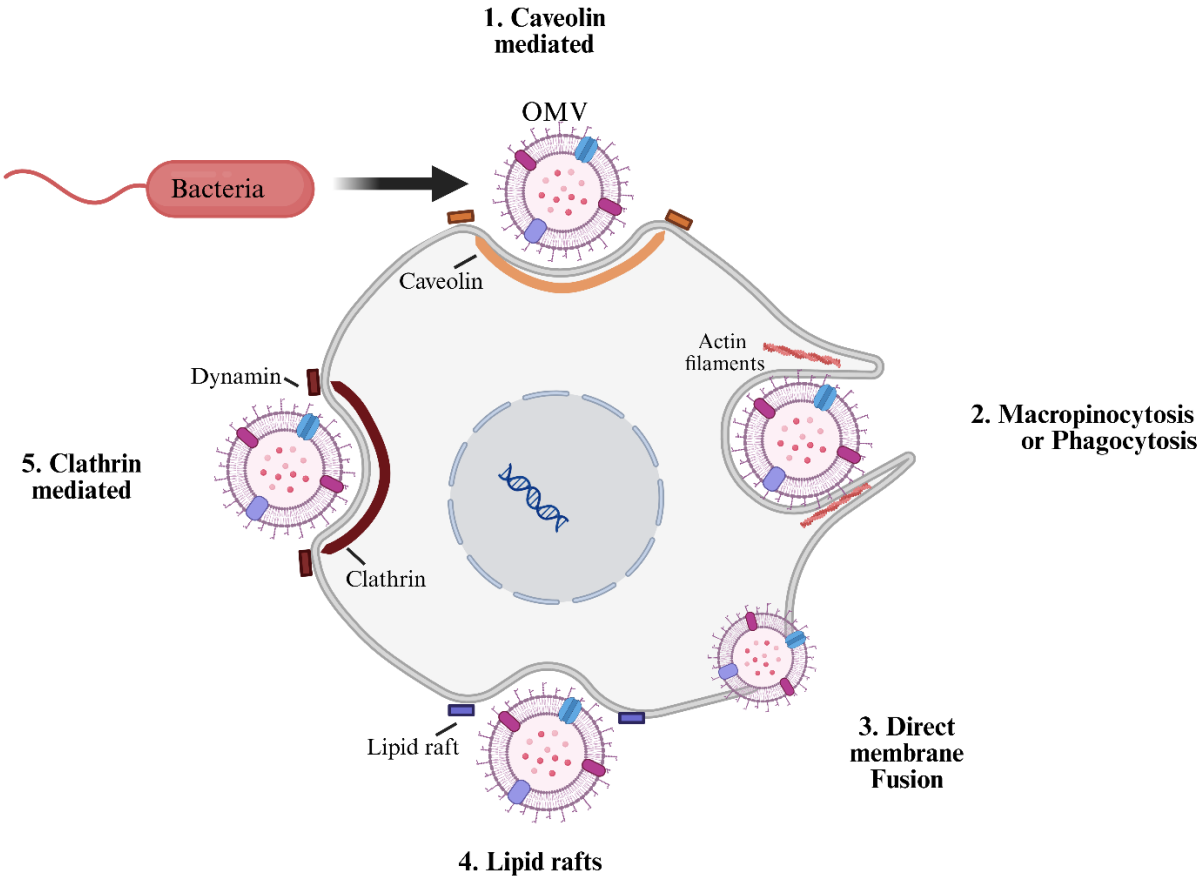


**Figure 1.6: Uptake mechanisms of OMVs by the host cell.**

The scheme illustrates the potential pathways by which bacterial outer membrane vesicles (OMVs) can enter host cells. OMVs can be taken up via lipid raft-mediated routes, clathrin-dependent and caveolin-dependent endocytosis, and direct internalization through membrane fusion. Alternatively, OMVs can be taken up by host cells via macropinocytosis or phagocytosis, which are actin-mediated events. Representative protein and lipid molecules involved in those pathways are shown to indicate means of OMV entry. **(Created with BioRender.com)**

### 1.2.4 Functions of OMVs

Previous research viewed OMV production as a by-product of cell lysis, but current studies indicate that all gram-negative bacteria actively produce OMVs. These vesicles are rich in cytoplasmic, periplasmic, virulence proteins, and specific lipids, implying a deliberate release by bacteria. This could serve two main purposes: facilitating interactions with other bacteria and the host, or aiding survival in stressful conditions (McBroom et al., 2006).

#### 1.2.4.1 OMVs: Functions in the environment and bacterial communities

OMVs play myriad biological functions. In non-pathogenic bacteria, OMVs serve as carriers for intercellular communication within bacterial communities. They transport signaling molecules, quorum-sensing factors, and small RNAs that promote coordination and cooperation among bacteria. This form of communication helps to manage microbial community behavior and can also influence the host's homeostasis. OMVs have been shown to contribute to nutrient acquisition under stressful conditions either by carrying nutrient-generating degrading enzymes like proteases or by using transporters like siderophores for nutrient scavenging. For example, OMVs of *P. aeruginosa* contain PQS, a hydrophobic molecule that enables bacteria to scavenge iron. (Dubern & Diggle, 2008). During bacterial growth, OMV-associated DNA and proteins serve as a source of carbon and nitrogen. OMVs have also shown to participate in

biofilm formation and maintenance. OMVs produced by *P. aeruginosa* biofilms contain 52 % of LPS and are responsible for the entire biofilm matrix formation(Schooling & Beveridge, 2006). Matrix-assisted biofilms showed the presence of polysaccharides, lipids, nucleic acids, and protein components like flagella, pili, and OMVs. OMVs facilitate the transport of growth factors and extracellular matrix elements in the biofilm communities. Besides, the exopolysaccharide released from OMVs leads to an increase in cell co-aggregation in biofilms. Exposure of bacteria to environmental stress have been shown to induce the production of OMVs and helps in bacterial survival (McBroom & Kuehn, 2007). Exposure to antibiotics has led to the evolution of bacterial OMVs either with multidrug efflux pumps or by accelerating the release of enzymes to degrade the antibiotic structure. To cope with bacteriophage and antimicrobial peptides present in the environment is always one of the main challenges for bacteria. OMVs have the ability to adsorb substances such as T4 bacteriophage and antimicrobial peptides. OMVs interact with AMPs in a dose-dependent manner, resulting in the loss of their efficacy by fully absorbing the antimicrobial activity. In the case of bacteriophage, once they bind to OMVs, they significantly lose their capacity to infect. (Manning & Kuehn, 2011). Horizontal gene transfer by OMVs was also reported in the literature. The transfer of both DNA cargo and related functions, such as antibiotic resistance, has been observed in the recipient bacteria (Yaron et al., 2000).

#### 1.2.4.2 Outer membrane vesicles: Functions in the human host

OMVs from human commensal bacteria can provide some beneficial effects. Recent research emphasizes the positive role of OMVs produced by gut microbiota or commensal bacteria. One study found that OMVs from *Akkermansia muciniphila*, which inhabits the intestinal mucous layer, can help restore gut microbiota balance by promoting the growth of beneficial bacteria and inhibiting opportunistic pathogens. Additionally, OMVs enhance mucosal immune functions by switching antibody production from IgM to IgA (Xinyue Wang et al., 2023).

On the contrary, OMVs from pathogenic bacteria can contribute to disease pathogenesis. Given their diverse cargo, OMVs are essential players in various biological activities that regulate host-pathogen interactions (Reimer et al., 2021; Sartorio et al., 2021). For example, OMVs can induce the death of host cells by transferring cytotoxic substances, such as cytozines, and activating cell-mediated immunity, which leads to tissue destruction (Cecil et al., 2017; Chmiela et al., 2018). The study of Yoshimura et al. showed that OMVs of *Porphyromonas gingivalis* (Murphy, 2006), *Tannerella forsythia* (Månsson et al., 2010), and *Treponema denticola* (Varghese et al., 2021) induce an intense proinflammatory response. These effects were associated with increased TNF-α, IL-8, and IL-1β secretion and the stimulation of the ASC inflammasome, ultimately resulting in induced inflammatory cell death and tissue

damage in vitro and in vivo (Cecil et al., 2017).

In addition to activating the immune system, its potential role in mediating the translocation of virulence factors has also been reported, facilitating bacterial establishment within host tissues (Sartorio et al., 2021). In a pivotal study, Bomberger et al. demonstrated that OMVs from *P. aeruginosa* induce inflammation as well as deliver alkaline phosphatase, β-lactamase, hemolytic phospholipase C, and Cif into airway epithelial cells. Remarkably, these effects were observed in the absence of viable bacteria, highlighting the central role of OMVs in modulating host physiology and in stimulating pathogenic potential, without direct contact with the originator bacteria (Bomberger et al., 2009). A summary of OMV functions is shown in Figure 1.7.

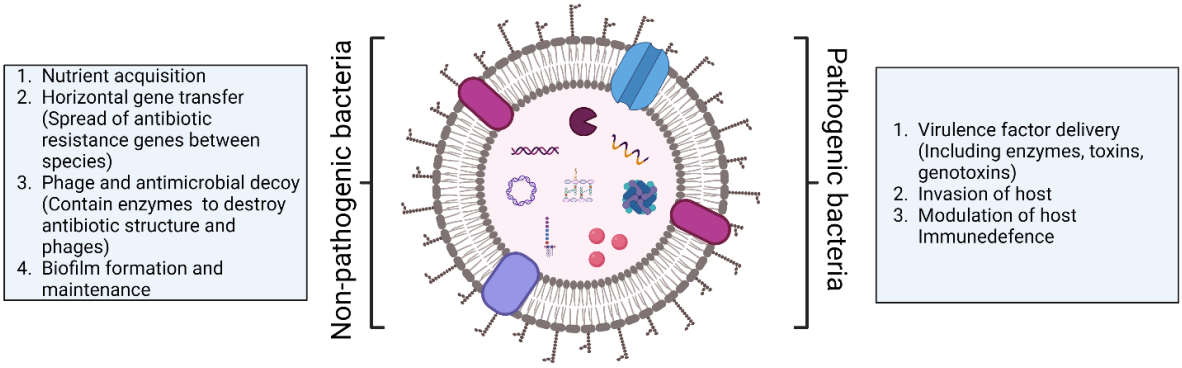


**Figure 1.7: Functions of bacterial outer membrane vesicles in pathogenic and non-pathogenic bacteria**. (Ayesha et al., 2023).

### *1.2.5* Significance of OMVs in the disease pathogenesis of *L. pneumophila*

Research over the past forty years on the biology of *L. pneumophila* and Legionnaires' disease has shed light on how this bacterium infects hosts. Recently, OMVs have emerged as a new factor in the pathogenesis of various bacterial infections. In 1979, Flesher et al. first identified OMVs in *L. pneumophila* as membrane blebs during electron microscopy of the bacterium's cell envelope (FLESHER et al., 1979). These vesicles were subsequently isolated by ultracentrifugation of bacterial culture supernatants after filtering *L. pneumophila* through a 0.22 µm filter. Their purity was assessed using negative-stain electron microscopy (EM) and atomic force microscopy (AFM) in 2008. Under the microscope, they measured between 100 and 200 nm. (Galka et al., 2008). AFM and EM are considered standard methods for visualizing and validating the purity of OMV fractions (Théry et al., 2018). Although the Dot/Icm Type IV secretion system has long been the primary focus of *L. pneumophila* virulence, the biological significance of OMVs in disease remained poorly understood until more recent history. Some studies indicate that OMVs play a role in immunomodulation and in promoting intracellular bacterial replication. Nevertheless, most of these studies remain preliminary, and the mechanisms underlying OMV-induced host manipulation in *L. pneumophila* are far from understood.

Since OMVs are packaged bacterial components lacking viable bacteria and bacterial machinery, host manipulation depends entirely on the variety of OMV-containing microbial components transported, including LPS, peptidoglycan, flagellin, proteins and nucleic acids (Bernadac et al., 1998; Cañas et al., 2018; Sartorio et al., 2021). The outer membrane of *L. pneumophila* is enriched LPS. Since OMVs are produced from the outer membrane, LPS can be incorporated into OMVs and it is crucial for understanding their immunogenicity and biological activity, as LPS mediates binding and ligation via toll-like receptor (TLR) signalling pathways. Apart from LPS, profiling the proteins, DNA, and RNA transported in OMVs by *L. pneumophila* is an essential step toward understanding the molecular processes of LD. The proteomic profile of OMVs provides functional information about the pathogenic mechanisms of *L. pneumophila*. OMVs frequently harbor a wide range of proteins, including outer membrane (OM) proteins, metabolic enzymes, adhesins, toxins, and type IV secretion system (T4SS) effectors. Such vesicle-bound proteins may support bacterial adhesion, intracellular survival, or influence host cellular pathways. In addition, a comparative analysis of OMV-associated molecules may facilitate the discovery of biomarkers or vaccine targets, thereby possessing translational potential for diagnostic and prophylactic applications. Overall, the systematic profiling of nucleic acids and proteins in *L. pneumophila* OMVs is important for the full understanding of bacterial

pathogenesis and immunomodulation. Recently, the identification of bacterial DNA and RNA in OMVs has emerged as a tool for manipulating host immune responses. For example, cytosolic pattern recognition receptors (PRRs), including RIG-I-like receptors and the cGAS-STING pathway, can detect bacterial RNA and DNA, induce inflammatory signalling, and influence infection outcomes.

From the host's perspective, the host response begins with recognition of these microbial components. Central to this response are pattern-recognition receptors (PRRs), a set of germline-encoded proteins that recognize pathogen-associated molecular patterns (PAMPs). These include Toll-like receptors (TLRs), among which TLR1, TLR2, and TLR6 are involved in recognizing bacterial lipoproteins and peptidoglycan and TLR4 in LPS detection, and others such as TLR3, TLR7, and TLR9, in microbial RNA or DNA detection (Kawasaki & Kawai, 2014). The interface between PRRs and their corresponding PAMPs or damage-associated molecular patterns (DAMPs) results in the stimulation of host immune and inflammatory effects (Newton & Dixit, 2012). Although inflammation is necessary for the elimination of pathogens, an exaggerated and/or uncontrolled inflammation can lead to a breach of collateral tissue (Kakihana et al., 2016). It is essential to understand how *L.*

*pneumophila* OMVs interact with host immune factors to elucidate their role in pathogenesis.

Macrophages are the primary cells of the innate immune system that are targeted during infection and are central in the sensing and response to pathogens. OMVs are demonstrated to adhere to, fuse with, and deliver their cargo to macrophages, potentially modulating immune signaling, cytokine production, and phagosome maturation. The elucidation of interactions of OMVs with Macrophages is crucial to understanding how OMVs play a role in immuno-evasion and disease progression.

## 1.3 Macrophages are model cells to study immune modulation by pathogens

Macrophages, as key players in the innate immune response, are the first line of defense against pathogen attacks. Due to their ability to recognize, phagocytose, and kill microorganisms, they are used as a cellular model to investigate host-pathogen interactions. Given its plasticity and ability to respond to environmental cues, the macrophage can rapidly adjust its phenotype and function, which aligns well with studies of immune modulation. For *L. pneumophila,* whose central infections occur in alveolar macrophages, these cells serve as a biologically meaningful model for analyzing the pathogen's immune escape strategies. Moreover, macrophages are a major contributor to subsequent immune response by secreting cytokines and chemokines that link innate immunity with the adaptive immune response. Macrophages play diverse roles in fighting with intracellular infections, as discussed below (Figure 1.8).

### 1.3.1 Macrophage in pathogen recognition and clearance

Macrophages were discovered as professional phagocytes by the Russian zoologist Elie Metchnikoff, who observed them in studying how certain cells can migrate toward foreign particles and then proceed to engulf and degrade them (Mechnikov, 1988). The term "macrophage" is derived from the Greek, meaning "big eater," prompted by the

ability of these cells to effectively recognize and ingest pathogens, dead cells, and foreign particles. Although often referred to as "professional phagocytes" (Rabinovitch, 1995), macrophages are also involved in tissue homeostasis and wound healing, tissue remodelling, and in crosstalk with the adaptive immune system (Geissmann et al., 2003; Wynn et al., 2013).

Macrophages modulate their phenotype in response to recognizing pathogens; thus, they customize innate immune responses to the identified pathogen (Mosser, 1994). They express a wide variety of pattern recognition receptor (PRR) families on their surface, which participate in phagocytosis upon pathogen detection. This dynamic infection is initiated by the pathogen binding to host cell receptors, followed by the remodeling of the actin cytoskeleton, which aids in invasion. The engulfed pathogens are sequestered in vesicles named phagosomes, which subsequently mature into phagolysosomes via ecto- and endocytosis fusion/fission activities (Desjardins, Celis, et al., 1994), where the engulfed pathogens are forced into a hostile microenvironment containing an acidic pH and oxidizing molecules such as ROS (reactive oxygen species) and lysozyme (acid hydrolases), which lead to the eradication of the pathogens (Flannagan et al., 2009).

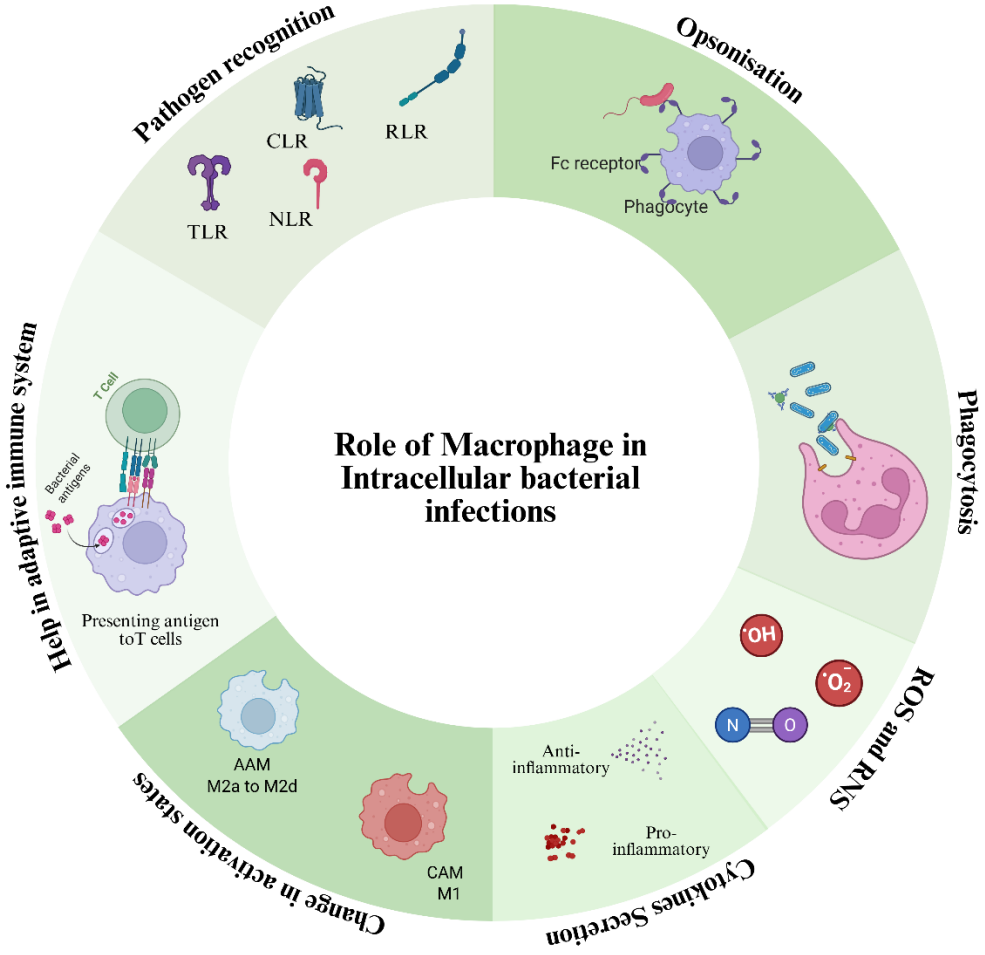


**Figure 1.8: Diverse roles of Macrophages during intracellular bacterial infections. (Created with BioRender.com)**

### 1.3.1.1 Pathogen recognition receptors

PRRs are abundantly expressed in macrophages, which are considered paradigms of intrinsic immune sensors, but they are present as well in other APCs, including dendritic and B-cells, and at lower levels in other innate immune cells such as epithelial cells. PRRs can be divided into five major families: TLRs, NLRs, RLRs, cytosolic DNA receptors and CLRs.

#### 1.3.1.1.1 Toll-like Receptors

The TLR family represents the first and best-characterized PRR family. In humans, 10 TLR molecules (TLR1-10) have been identified, and in mice, 12 (TLR1-9 and TLR11-13) (Kawai & Akira, 2010). TLRs are present on the cell surface and in endosomal membranes. TLR1, 2, 4, 5, and 6 detect bacterial products similarly to LPS or flagellin, and TLR3, 7, 8, and 9, located in endocytic compartment membranes, react in response to nucleic acids of viruses and bacteria (Kawai & Akira, 2010; Kumar et al., 2009; Takeuchi & Akira, 2010). By recognizing PAMPs, TLRs trigger signal pathways that involve adaptor proteins such as MyD88 and TRIF, which in turn promote pro-inflammatory cytokines, including TNF-α and IL-6, as well as type I interferons, through the transcription factors NF-κB and IRF3 (Kawai & Akira, 2010; Kawasaki & Kawai, 2014).

#### 1.3.1.1.2 NOD-like Receptors

NLRs sense a wide array of ligands in the cytosol. Humans have 23 of these NLRs; the mouse genome has approximately 34 (Franchi et al., 2009). NLRs include three domains: carboxy-terminal PAMPs recognition domain composed of the LRR, an intermediary activation domain known as the NOD, and an amino-terminal domain that separates NLRs into subgroups. The two most studied NLRs, NLR family apoptosis

inhibitory protein (NAIP) inflammasome NOD1 and NOD2, recognize bacterial peptidoglycans, resulting in inflammation signals and generation of cytokines such as IL-1 and IL-18 (Keestra-Gounder & Tsolis, 2017). Others, such as NLRP3, assemble inflammasomes that induce caspase-1 activity, triggering the maturation of cytokines or pyroptosis.

#### 1.3.1.1.3 RIG-I like Receptors

RLRs are a family of cytosolic sensors for RNA, each representing a minimal set of RNA-sensing. RLRs comprise a subfamily of cytosolic RNA-sensing receptors, consisting of three members RIG-I, MDA-5, and LGP2 (Loo & Gale, 2011). RIG-I and MDA-5 sense viral double-stranded RNA and initiate signaling pathways that promote the production of type I IFNs and pro-inflammatory cytokines via the adaptor MAVS, which in turn activate the transcription factors IRF3 and IRF7 (Chiu et al., 2009). LGP2 predominantly controls the regulation of other 2 RLRs as it does not contain a CARD domain and therefore doesn't involve in downstream signaling in a direct manner (Rodriguez et al., 2014).

#### 1.3.1.1.4 Cytosolic DNA Receptors

Cytosolic sensors for DNA play a crucial role in detecting foreign DNA and triggering immune responses. Frequently, these receptors also stimulate the STING pathway with consequent release of type I interferon and pro-inflammatory cytokines, including IL-6 and TNF-α (Bhat & Fitzgerald, 2014; Holm et al., 2013). cGAS is an essential sensor of DNA that, upon DNA binding, activates STING to initiate downstream signaling pathways comprised of TBK1 and NF-κB. Cytosolic DNA has also been demonstrated to initiate several pathways besides STING, leading to the production of type I interferon and proinflammatory cytokines. For example, the cytoplasmic sensor in melanoma 2 (AIM2) detects double-stranded DNA (dsDNA), then recruits the adaptor protein ASC and caspase-1 to form the AIM2 inflammasome. This inflammasome orchestrates the inflammatory response by activating the maturation of cytokines, including IL-1β and IL-18, and inducing pyroptosis.(Hornung & Latz, 2010; Sharma & Fitzgerald, 2011; B. Wang et al., 2019).

#### 1.3.1.1.5 C-type Lectin Receptors

Among secreted, transmembrane proteins and intracellular adapters, CLRs represent a large family of over 1,000 proteins (Brown et al., 2018; Fischer et al., 2022). They are receptors for carbohydrates and other ligands, associated with immune responses. CLRs,

such as Dectin-1 and Dectin-2, sense fungal parts by inducing signaling cascades that drive the production of cytokines, like IL-10 and IL-23. The inhibitory receptor CLEC12A recognizes incoming uric acid crystals and/or mycolic acids, dampening immunity by modulating cytokine production and autophagy responses in infection.

#### 1.3.1.2 Opsonisation

Besides direct recognition of pathogens through surface receptors, macrophages recognize opsonised targets, which have been labeled with complement proteins or Immunoglobulin G (IgG) antibodies. Recognition by complement is programmed by soluble factors, synthesized by hepatocytes, and activated by pro-inflammatory cytokines. These proteins induce a signaling pathway in response to binding to pathogen surfaces via three major complement pathways: classical, alternative and lectin pathway. All these pathogen recognition pathways convert complement component 3 (C3) to C3b by Protein 3 convertase, leading to a coating of the pathogen with C3b (opsonisation). C3b can additionally be cleaved into iC3b, C3c, or C3dg, unveiling different, receptor-binding regions, all of which are bound by different complement receptors, thus permitting an immune response to be customized (van Lookeren Campagne et al., 2007). Complement receptors [i.e., CR1, CR3 (CD11b/CD18), CR4 (CD11c/CD18)] are expressed on macrophages and mediate

phagocytosis of C3b, C1q, and mannose binding lectin-coated targets. Immunoglobulins can also act as opsonins by coating pathogens through epitope recognition with their Fab antigen-binding sites and their Fc region, which signals the pathogen for recognition by specific Fc receptors on phagocytes. (Daëron, 1997).

#### 1.3.1.3 Phagocytosis

The most crucial function of a macrophage is phagocytosis. Several types of receptors mediate phagocytosis, and they often need to communicate with each other to induce the appropriate internalization response. Many receptors can initiate phagocytosis (complement, scavenger, and lectin receptors); however, the best-characterized and most studied is the Fc receptor-mediated pathway. Sensors such as TLRs, which are not phagocytic themselves, also contribute to the phagocytic response through signalling (Gordon, 2016). There may be different mechanisms in each route of phagocytosis, depending on the pathogen or the conditions (Kaplan, 1977).

Opsonized pathogens attach to the Fc receptors of macrophages. This molecular interaction initiates a "zipper-like" mechanism in which the plasma membrane pistol is mobilized around the pathogen, step by step, through the orderly recruitment of the array of available Fc receptors (Griffin Jr et al., 1975). This event is ITAM phosphorylation-dependent and is initiated by Src family kinases, which facilitates

receptor clustering and subsequently increases binding efficiency (Sobota et al., 2005). Actin polymerization is also essential during membrane ruffling and phagosome sealing. The GTPase Dynamin-2 is also recruited to nascent phagosomes and participates in pseudopod extension and fission from the plasma membrane (Gold et al., 1999; Marie-Anaïs et al., 2016).

Phagocytosis is also directed by signaling molecules, such as phosphoinositide 3-kinase (PI3K), phospholipase C, and Ras-family GTPases, and their inhibition arrests the process at different stages (Swanson, 2008). A “taste” and “feel” step in phagocytosis is a new term, referring to a method by which, following chemical sensing of a target, macrophages physically probe and "taste" it, resulting in appropriate immune activation (Underhill & Goodridge, 2012). Once inside, the young phagosome is approximately identical to the plasma membrane and the environment outside of the cell. To process the pathogen, it matures through fusion and fission events with endosomal and lysosomal compartments (Flannagan et al., 2009). Rab5 GTPase and effector Rabaptin-5 regulate early phagosome formation. They synergize to stimulate Rab5 activity and recruit PI3K (Vps34) and Early Endosome Antigen-1 (EEA-1), required for early phagosome function (Christoforidis et al., 1999). Once matured, Rab5 is replaced by Rab7, allowing for the fusion with lysosomes. Lysosome tethering is mediated by

SNARE proteins, VAMP7 and VAMP8. Mature phagosomes also contain LAMP1 and LAMP2, and Lysosomal Integral Membrane Protein II (LIMPII), in addition to cathepsins and an acidic pH, which help in parasite killing (Desjardins, Huber, et al., 1994).

Macrophage activation states influence phagosome maturation. For instance, classically activated macrophages (CAM) mature slowly, which is conducive to APC (antigen-presenting cell) and ROS-mediated killing. At the same time, alternatively activated macrophages (AAM) rapidly go through the endosomal pathway to facilitate the rapid clearance of apoptotic cells (Canton, 2014; Podinovskaia et al., 2013). The majority of this degradation occurs in the phagolysosomal compartment through the microbicidal mechanisms outlined below.

#### 1.3.1.4 Other microbicidal mechanisms in macrophages

##### 1.3.1.4.1 Acidification

As phagosomes acidify, their inside pH falls to 4.5–5.5 by V-type $H^+$-ATPases that pump $H^+$ into lysosomes (Futai et al., 2000). This is a hostile environment to pathogens and induces the action of hydrolases, the ROS gene, and apoptosis-mediated bacteria killing (Vatansever et al., 2013). Pathogens have developed strategies to survive, for

example, *Mycobacterium avium* avoids self-killing by inhibiting v-ATPase recruitment (Sturgill-Koszycki et al., 1994).

#### 1.3.1.4.2 ROS and RNS species production

ROS are essential for killing microbes and are produced by the NADPH oxidase system (NOX2), which consists of two membrane subunits and three cytoplasmic subunits. Transfer of electrons from NADPH via FAD (Flavin Adenine Dinucleotide) , to heme and then $O_2$ forms superoxide ($O_2^-$), which can be a source of $H_2O_2$, hydroxyl radical, and singlet $O_2$ (Bedard & Krause, 2007). ROS induce damage to bacterial DNA, protein, and membranes (Imlay & Linn, 1988; Kohanski et al., 2007)

Reactive nitrogen species (RNS) are produced by inducible nitric oxide synthase (iNOS), after being induced by inflammatory mediators. The iNOS enzyme catalyzes electron transfer between NADPH and FAD and FMN to generate nitric oxide (NO) from L-arginine. NO combines with superoxide to produce species such as peroxynitrite ($ONOO^-$), nitrogen dioxide ($NO_2$), and dinitrogen trioxide ($N_2O_3$) that interfere with bacterial respiration, enzymes, and DNA, particularly in the presence of $H_2O_2$ (Darrah et al., 2000; Pacelli et al., 1995).

#### 1.3.1.4.3 Antimicrobial molecules

Examples of non-oxidative mechanisms include antimicrobial peptides and proteins that alter bacterial membranes, sequester nutrients, and cause cell lysis. NRAMP1 effluxes metals, such as iron, manganese, and cobalt, out of the phagosome, starving bacteria of critical nutrients provided by these metals (Cellier, 2017). Defensins burst membranes and inhibit the release of intracellular organisms such as *L. monocytogenes* (Arnett et al., 2011). Another antimicrobial peptide, LL-37, a product of cathelicidin induced by TLRs upon stimulation with *Mycobacterium tuberculosis,* also facilitates phagocytosis and pathogen elimination (Rivas-Santiago et al., 2008). Bacterial destruction is aided by proteases (cathepsins and asparagine endopeptidase), which either directly degrade bacteria or indirectly modulate the host response (Bewley et al., 2011; Descamps et al., 2012).

### 1.3.2 Macrophage polarization states and metabolism

Apart from their direct function in bacterial clearance, studies have also demonstrated the implication of activation states of macrophages in the pathogenesis of various bacterial diseases.

#### 1.3.2.1 Macrophage activation states

Despite many advancements in recent decades, we are still exploring the plasticity of

macrophages. Preliminary observations demonstrated that macrophages or phagocytes could be 'activated' to increase their phagocytosis and killing of microorganisms using ROS and NO (Mackaness, 1962; Nathan et al., 1983). Subsequently, the identification of AAM throughout the late 1980s and early 1990s was characterized. It was shown that they express a distinct pattern of gene expression compared to CAM, counteracting the pro-inflammatory effector functions of these cells (Stein et al., 1992). Mills suggested calling these CAM and AAM as M1 and M2 macrophages, similar to Th1 and Th2 T-helper terminology (Mills et al., 2000). It is noteworthy that most studies on macrophage activation have been conducted on murine models, which exhibit significant differences compared to human models in terms of activation markers and heterogeneity.

Macrophages exhibit various states of activation in response to chemical and physiological stimuli, a phenomenon known as macrophage activation. Classically CAM and AAM are two extremes of the activation spectrum, with pro-inflammatory versus anti-inflammatory cytokine profiles, and the spectrum also includes many intermediate states (Figure 1.9) (Mills et al., 2000). Although specific stimulation signatures have been identified, macrophages are plastic cells that can rapidly change activation state in response to extrinsic stimulation, a process referred to as functional adaptivity (Davis et al., 2013).

#### 1.3.2.1.1 Classically activated macrophage or M1 macrophage

M1 macrophages are classically activated macrophages stimulated in response to bacterial LPS and IFN-γ and are recognized by their ability to generate high levels of proinflammatory molecules (Bach et al., 1997). CAMs are pro-inflammatory cells which are up-regulated by IL-6 and produce pro-inflammatory factors when activated by IFN-γ (which activates Janus kinase activity and STAT1 phosphorylation and hence expression of pro-inflammatory mediators) (Bach et al., 1997). Full activation requires a second signal, e.g., TNFα or products of microorganisms. (Mosser, 2003). TNFα is generated by activation of different TLRs, including TLR2 and TLR4. TLR4 detects LPS (Hoshino et al., 1999), a component released by certain Gram-negative bacteria. TLR activation induces TNFα production inside the cell, a response that is not present in TLR4 -/- knock-out mice. The signaling pathway activated by TLR4 activation results in the release of the TF NFκB, which relocates to the nucleus and induces the expression of pro-inflammatory genes (Cairo et al., 2011). Other PRRs implicated in activation of the macrophage are NLRs, which sense intracellular PAMPs and contribute to inflammasome assembly. IFN-γ priming of macrophages increases Nod2 expression and the expression of inflammasome-related genes, including members of the IL-1 cytokine family and CASP1 (CASP1 is the gene that encodes caspase-1) (Awad et al., 2017).

CAM exert bactericidal activity. Following the ingestion of microorganisms, the production of reactive oxygen intermediates, such as superoxide ($O2^-$) and hydrogen peroxide ($H_2O_2$), increases significantly, producing an "oxidative burst" necessary for microbial destruction (Murray et al., 1979). Higher enzymatic production of NO from L-Arginine is also a helpful factor to kill pathogens (Pacelli et al., 1995).

#### 1.3.2.1.2 Alternatively activated macrophage or M2 macrophage

Within the lungs during infection, the influx of activated macrophages in response to specific chemokines, with the help of TNFα, is initiated, which has been proposed to be involved in controlling and eliminating the infection (Roach et al., 2002). However, when inflammation is not resolved, the constant generation of proinflammatory factors may cause irreversible tissue damage, which intensifies chronic inflammatory symptoms (Martinez et al., 2008). Alternatively activated macrophages (AAM) were initially found to mediate the anti-inflammatory reaction. Upregulation of the AAM phenotype appears to be induced to balance the over-inflammatory stimulation and to heal the inflammatory state.

The idea of alternative macrophage activation was formulated when it became clear that IL-4 increases the expression of CD206, overriding the effect of IFN-γ. IL-13 also induces the alternatively activated phenotype. AAMs present unique surface markers

and cytokine expression signatures, controlled by STAT6 and epigenetics. They are involved in wound-healing and immune-modulation (Alan et al., 1984).

#### 1.3.2.1.3 Other activation states

David Mosser and co-workers described an AAM independent macrophage population which they named 'type II activated macrophages' or "M2b macrophages" (Anderson & Mosser, 2002). The M2b phenotype is induced by Fc receptor signaling and stimulation of TLR receptors and has some similarities with CAM. Both CAM and M2b are activated by immune-stimulating agents; this M2b phenotype is preferentially distinguished as an alternative rather than an activated phenotype, as the cells overproduce the anti-inflammatory cytokine IL-10 and underproduce the pro-inflammatory cytokine IL-12 (Gerber & Mosser, 2001). Also, M2b polarized macrophages induce IL-4 production, which contributes to the Th2 immune response. However, M2a macrophages are elicited with IL-4/IL-13, and Arginase-1 expression is up-regulated; M2b macrophages do not enhance Arginase-1 expression. It indicates that M2b macrophages are not related to the process of wound healing and regeneration, but they may be implicated in immunoregulation. Thus, M2b is functionally and transcriptionally different from M2a.

M2c macrophages are anti-inflammatory and derived from IL-10 and TGFβ. Other defined or emerging subsets that share features with CAM and AAM include those

specific to tumor-associated macrophage (TAM) and M2d, which play roles in angiogenesis and immune suppression.

These newly emerging activation states highlight a shift from a linear to a multidimensional perspective of macrophage activation, with unique profiles in response to different physiological stimuli.

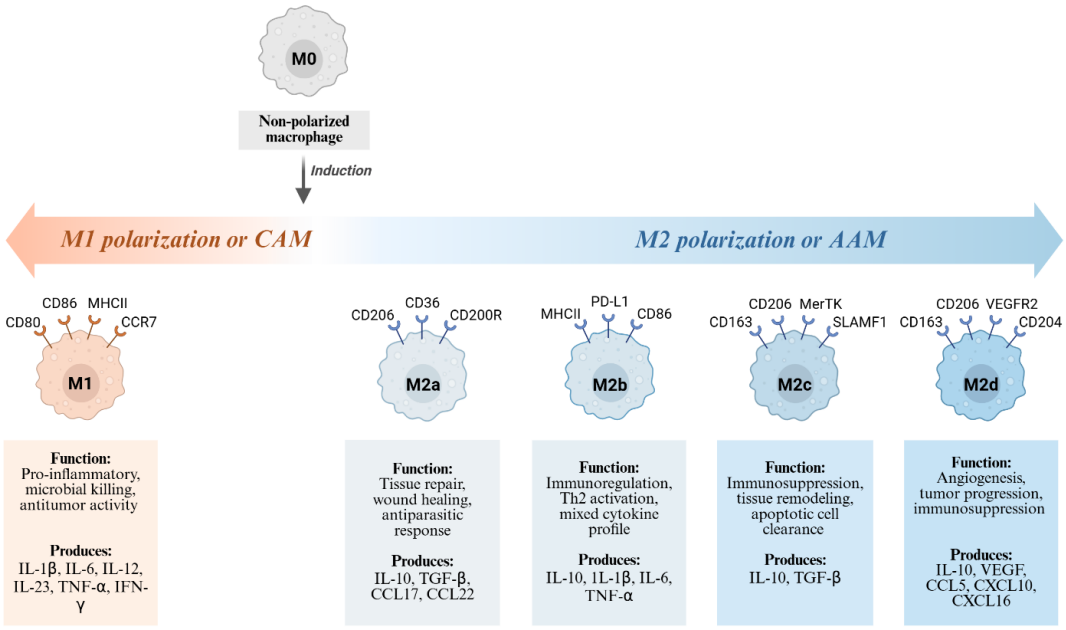


**Figure 1.9: Spectrum of Macrophage polarization**.

The continuum of macrophage activation states is depicted in the diagram, which progresses from M1 to M2. M1 macrophages typically contribute to antimicrobial and tumoricidal activities, secreting pro-inflammatory cytokines. In contrast, M2-like macrophages are activated by a variety of signals and involved in tissue repair, immune regulation, and tumor progression. The M2 subtypes are defined by their respective triggers and functions: M2a (tissue repair), M2b (immune regulation), and M2c (related to immune suppression and tissue remodeling), and M2d (tumor progression and angiogenesis). This figure illustrates the dynamic and plastic state of macrophage polarization upon other microenvironmental stimuli. (Diagram adapted from template "Spectrum of Macrophage Polarization from M0 to M1 and M2 Subtypes" from Biorender).

### 1.3.2.2 Macrophage metabolism

#### 1.3.2.2.1 Arginine metabolism

One of the most well-characterised markers of macrophage activation is the differential metabolism of L-Arginine. Hibbs and co-workers described that CAM produces NO from L-Arginine using the iNOS enzyme (Hibbs et al., 1988). In contrast, Corraliza demonstrated that AAM express Arginase-1 for L-Arginine metabolism, and iNOS enzyme is suppressed due to the presence of IL-4, IL-10, and prostaglandin E2 (PGE2) (Corraliza et al., 1994). Differential arginine metabolism is thought to be associated with macrophage function, with NO production supporting pathogen killing and Arginase-1 producing polyamine for wound healing and cell proliferation.

New evidence indicates that the mechanisms through which macrophages express Arginase-1 are more complicated than initially proposed. *Mycobacterium bovis* and *Bacillus calmette-guérin* can also induce Arginase-1 (BCG) infection, where TLR-MyD88 signals induce STAT3, which activates IL-10, thereby suppressing microbicidal activity and promoting pathogen survival (El Kasmi et al., 2008; Qualls et al., 2010). Macrophages producing Arginase-1 can suppress both Th2 cell proliferation and cytokine production, while the reduction in its production contributes to fibrotic disease.

#### 1.3.2.2.2 Mitochondrial metabolism

Metabolic pathways of glucose vary in polarized macrophages. CAMs utilize anaerobic glycolysis to provide rapid energy during infection, thereby boosting ROS production for microbicidal action (Rodríguez-Prados et al., 2010). In contrast, AAMs rely on oxidative glucose metabolism and mitochondrial biogenesis, which are well-suited for combating chronic infections and facilitating tissue repair (Odegaard & Chawla, 2011; Vats et al., 2006).

### 1.3.2.3 Role of macrophage polarization in bacterial infections

Naturally, macrophages are supposed to be bactericidal upon exposure to microbial stimuli. Given these key roles, it is reasonable to assume that pathogens have evolved strategies to modulate macrophage activation to their advantage. Transcriptome studies have revealed that innate immune cells like macrophages exhibit a standard response in gene expression upon encountering multiple pathogens (Jenner & Young, 2005; Nau et al., 2002). Upon infection with a variety of pathogens, the genes associated with macrophage polarization show the overexpression of M1-associated genes, e.g., cytokines (TNF, IL-6, IL-12, IL-1β), cytokine receptors (IL-7R, IL-15RA), chemokines (CCL2, CCL5, CXCL8), and the chemokine receptor CCR7 (Benoit et al., 2008). M1 activation state is generally associated with protection, and M1 polarization has been

shown to participate in the control of infections caused by different bacteria such as *L. monocytogenes, Salmonella typhimurium, M. tuberculosis, Mycobacterium ulcerans, and a Chlamydia* species (Benoit et al., 2008; Chacon-Salinas et al., 2005; Jouanguy et al., 1999; Kiszewski et al., 2006; Rottenberg et al., 2002).

As a consequence, most pathogenic bacteria, especially those that survive within the host cell as intracellular bacteria, have evolved ways to modulate the polarization of these immune cells to ensure their survival. Some bacteria do this by inhibiting M1 polarization, thereby attenuating inflammation and diminishing macrophage microbicidal capacity. Intracellular *Shigella flexneri*, for instance, produces a modified, hypoacetylated LPS that is not recognized by TLR4, leading to reduced production of proinflammatory cytokines by mouse bone marrow-derived macrophages (Paciello et al., 2013). *Staphylococcus aureus* activates Akt1 signaling in murine lung infection, leading to the elevation of SOCS1 (suppressor of cytokine signaling 1) and the downregulation of NF-κB, which results in the reprogramming of M1-like antimicrobial macrophages to less activated states (Xu et al., 2013). It has been reported that *M. tuberculosis* secretes virulence factors, including lipoarabinomannan and ESAT6, which inhibit M1 activation by impairing phagosome maturation and blocking activation of NF-κB, respectively (Lugo-Villarino et al., 2011). During chronic

infection, *M. tuberculosis* can also induce an M2-like macrophage phenotype by activating Wnt6 (wingless-type MMTV integration site family, member 6) signaling in infected cells and in lung granulomas (Schaale et al., 2013). *S. aureus* biofilms are often resistant to macrophage internalization, and macrophages that do infiltrate catheter-associated biofilm in vitro have diminished expression of IL-1β, TNFα, and iNOS, but upregulated Arg1 expression, consistent with an M2 phenotype (Thurlow et al., 2011). *S. typhimurium* is found to interact selectively with M2 macrophages, and the infection induces an upregulation of PPARδ in these cells. Absence of PPARδ significantly compromises the bacterium's ability to replicate and persist (Eisele et al., 2013). Remarkably, *S. typhimurium's requirement* for PPARδ stems from its metabolic needs, leading to suppression of antimicrobial responses through M2 polarization. However, it remains unknown if bacteria directly promote PPARδ expression to persist in the host.

### 1.3.3 Cytokines and signalling pathways

Cytokines are crucial coordinators of both innate and adaptive immune responses, playing an essential role in responding to infections and controlling chronic diseases. These short proteins have a significant influence on various biological activities, including inflammation, tissue repair, haematopoiesis, and communication between immune cells, which involves binding to specific cellular receptors. They act via

autocrine, paracrine, or endocrine pathways that facilitate local and systemic immunity (Dinarello, 2007).

Cytokines are functionally redundant, and one of their primary characteristics is pleiotropy, which allows them to act on various cell types and directly enhance, complement, or inhibit the action of other cytokines. It is almost impossible to specify the function of a particular cytokine. As discussed earlier, macrophages are categorized as classically activated or alternatively activated based on their activation status. Consequently, these distinct macrophage types exhibit significant variation in the cytokines they release, thereby influencing their activities (Biswas & Mantovani, 2010). Cytokine secretion is meticulously regulated through inter-organellar exchanges dependent on vesicular trafficking and cytoskeletal remodelling (Stow & Murray, 2013).

They are particularly produced by lymphocyte and macrophage cells. Even though immune cells are the primary source of cytokines, pathogens or tissue damage can cause other cell types to release them as well. Cytokines influence fundamental cell biological responses, including growth, differentiation, apoptosis, and survival, and they interact with common signaling pathways. Additionally, they create an environment that supports immune activation. To summarize, cytokines are vital mediators in immune regulation, significantly contributing to host defense against microbes. The

specific profile of cytokines released depends on both the type of antigenic stimulus and the type of stimulated immune cell. Cytokines enable macrophages to respond to challenges posed by pathogens. They are divided into six distinct families based on their structural and functional similarities, including IL-1 Superfamily, TNF Superfamily, IL17 Superfamily, IL6 family, Type I cytokine family, and Type II cytokine family (Muñoz Carrillo et al., 2017).

#### 1.3.3.1.1 Role of cytokines in bacterial infections

In response to bacterial infections, the host initially activates a rapid and nonspecific immune response to eradicate the pathogen. This natural response involves the migration of neutrophils, macrophages, and dendritic cells, the activation of the complement system, and the secretion of cytokines (Tosi, 2005). Although this response serves to control or otherwise restrict the proliferation of microbes, it can also cause damage to the host tissue. Consequently, maintaining the immune system response is of paramount importance, and cytokine secretion is a central modulatory mechanism for this maintenance. These molecules mediate intercellular communication and play a crucial role in regulating both the innate and adaptive immune systems (Baskic et al., 2017).

Upon accessing microorganisms, PRRs detect PAMPs, and this molecular recognition initiates downstream signaling pathways, particularly NF-κB and MAPK. These pathways then induce the synthesis of proinflammatory cytokines, including IL-1α, IL-1β, TNF-α, IFN-γ, IL-12, and IL-18 (Kawai & Akira, 2009). Among these, TNF-α and IL-1β play a central role in the inflammation process and in the recruitment of immune cells.

The immune response elicited during infection includes several protective measures that facilitate the elimination of microbes, stimulate lymphocytes for the adaptive immune system, and control tissue damage. IL-1β, for example, is mainly mediated by PRRs specifically, TLRs, in response to microbial and damage-associated molecular patterns (Borthwick, 2016). Ligand binding to PRRs triggers signaling pathways that include NF-κB, activator protein-1 (AP-1), MAPK, and type I interferon, leading to the induction of inflammatory mediators and chemokines (Broggi & Granucci, 2015). Pro-IL-1β is first produced as an inactive, immature form of protein (pro-IL-1β) and requires cleavage by caspase-1 to generate the biologically active molecule. This cleavage is mediated by the inflammasome, a multimeric protein complex formed by NLR family pyrin domain-containing 3 (NLRP3), the adaptor protein ASC, and caspase-1. Mature IL-1β, in turn, acts by binding to its receptor IL-1R1, whose

signalling promotes the expression of endothelial adhesion molecules and results in the influx of neutrophils and monocytes at the site of infection. IL-1β also increases phagocytosis, attracts leukocytes, activates them chemotactically, and induces the production of lipid mediators as well as other cytokines (Biondo et al., 2014).

IL-1β is crucial in vivo for host defense against some pathogens. For example, during *S. aureus* infection, IL-1β signalling through IL-1R1 is necessary for neutrophil recruitment, demonstrating its role in combating such diseases as well as possibly other infections triggered by diverse pathogens (Miller et al., 2007).

TNF-α is another cytokine that cooperates with IL-1β during bacterial infections. It is rapidly synthesized during endotoxemia and triggered by microbial products. TNF-α is also responsible for the production of acute-phase reactants by the liver (Arango Duque & Descoteaux, 2014). In vivo studies demonstrate TNF-α's role in the clearance of intraperitoneal bacterial infections by recruiting neutrophils and macrophages to the infection site. This response is also accompanied by increased expression of COX-2 and iNOS, leading to the generation of PGE2 (prostaglandin E2) and NO, respectively, which contribute to microbial clearance and the restoration of tissue homeostasis (Dinarello, 2000; Malaviya & Abraham, 2000).

Another vital cytokine in host defense against extracellular bacteria is IL-17, in particular IL-17A. It is mainly secreted by the CD4T lymphocyte subset (Th17), which differentiates and matures in response to cytokine sets such as TGF-β and IL-6, IL-21 and TGF-β, or IL-1, IL-6, and IL-23 (Chizzolini et al., 2018; Harrington et al., 2005). IL-17A has protective effects in so many ways. It induces the production of proinflammatory cytokines (e.g., IL-1β, IL-6, GM-CSF, TNF-α), chemokines (e.g., CCL2, CCL7, CXCL1, CXCL2, CXCL5, and CXCL8), and adhesion molecules, determining the recruitment of neutrophils, monocytes, and dendritic cells to the inflamed site (Kolls et al., 2008).

It has been demonstrated that TLR4 signaling is required for IL-17 induction in *Klebsiella pneumoniae* infection. IL-17 induces granulocytopoietic cytokines, which cascade into neutrophil infiltration. IL-17 receptor-deficient mice demonstrate defective neutrophil recruitment, increased bacterial burden, and decreased survival. By contrast, adenoviral overexpression of IL-17 increases the expression of MIP-2, G-CSF, TNF-α, and IL-1β and enhances neutrophil recruitment, which is associated with increased bacterial clearance and protection from *K. pneumoniae* infection (Happel et al., 2003; Ye et al., 2001). PGE2 also drives the expansion of Th17 cells by an IL-1β-dependent mechanism at infected sites. In vitro data suggest that PGE2 upregulates

CCL20 secretion by Th17 cells, thereby controlling Th17-mediated infection (Chizzolini et al., 2008).

IL-18 also mediates immune response by inducing the release of pro-inflammatory cytokines, including TNF-α, IL-1β, IL-8, and GM-CSF, that increase neutrophil chemotaxis and activation. IL-18, on the other hand, enhances the proliferation and cytotoxic activity of CD8+ T cells and NK cells (Sahoo et al., 2011). One of the most essential functions of IL-18 during bacterial infections is its capacity to stimulate IFN-γ secretion from NK cells (Novick, 2013), in turn eliciting macrophage stimulation and the induction of antimicrobial genes against intra- and extracellular pathogens (Murray, 1994). Some bacterial species, such as non-pathogenic *Lactobacillus* and *Streptococcus pyogenes*, also appear capable of inducing IL-1β, IL-6, TNF-α, IL-12, IL-18, and IFN-γ, suggesting a pronounced Th1-type cytokine response to these bacteria (Miettinen et al., 1998).

### 1.3.4 Lung macrophage responses to *L. pneumophila* and identifying a model for studying the role of *L. pneumophila* OMVs in disease pathogenesis

#### 1.3.4.1 Host immune responses to *L. pneumophila*

Lung Macrophages infected by *L. pneumophila* not only serve as niches for the bacteria that facilitate disease, but also participate in the immune response to the pathogen. After inhaling *L. pneumophila*-containing aerosols, the bacterium is recognized and taken up by alveolar macrophages (AMs). Nonetheless, these cells also support bacterial replication and can escape the endocytic maturation and evade phagolysosomal degradation of *L. pneumophila*. However, in immunocompetent hosts, an intricate network of macrophage immunity facilitates the successful clearance of bacteria and the resolution of infection (Liu & Shin, 2019; Susa et al., 1998). Various studies and literature sources demonstrate the host responses to *L. pneumophila*, summarized in Figure 1.10.

##### 1.3.4.1.1 TLRs and their roles

The detection of *L. pneumophila* by macrophages depends on multiple PRRs present at the cell surface as well as in the cytosol. Two surface PRRs, TLR2 and TLR5, are

critical. TLR2 specifically senses lipoproteins within the bacterial cell wall, whereas TLR5 responds to flagellin from *L. pneumophila* (Hawn et al., 2007; Shim et al., 2009). Mice with a deficiency in TLR2 ($TLR2^{-/-}$) have been shown to have higher bacterial burdens and reduced production of proinflammatory cytokines compared with wild-type controls (Archer & Roy, 2006; Hawn et al., 2006). In contrast, $TLR5^{-/-}$ mice do not exhibit an increase in bacterial colony-forming units (CFUs), but are found to be defective in neutrophil recruitment and cytokine production, indicating that TLR5 may play a role in controlling the resolution of inflammation (Archer et al., 2009; TR, 2003). Another TLR receptor for *L. pneumophila* is TLR9, although it detects *L. pneumophila's* DNA in endosomes, and may play a redundant function in limiting infection. Activation of these signalling cascades by TLR ligation is initiated by MyD88 and MAPKs, leading to NF-κB-dependent transcription of proinflammatory cytokines, including IL-1β and TNF-α (Newton et al., 2007).

#### 1.3.4.1.2 The NLRs and inflammasomes

Cytosolic NLRs, including NOD1 and NOD2, prefer to recognize N-linked peptidoglycan fragments, which are secreted by the Type IV secretion system (T4SS) of *L. pneumophila*. These sensors and adopter RIP2 are essential for bacterial clearance and neutrophil recruitment in vivo (Frutuoso et al., 2010; Shin et al., 2008). The

cytosolic flagellin delivered to the cytosol by T4SS is indeed recognized by the NAIP5/NLRC4 inflammasome, resulting in fusion of LCV with the lysosomes, production of cytokines, and pyroptosis by caspase-1 activation (Molofsky et al., 2006). Flagellin-deficient strains (ΔflaA) and naturally non-flagellated species such as *Legionella longbeachae* do not trigger pyroptosis and IL-1β and IL-18 maturation through this inflammasome (Cazalet et al., 2010). The NLRP3 inflammasome, along with ASC and caspase-1, functions in a compensatory manner and produces IL-1β and IL-18 when NAIP5/NLRC4 is inactive, although its role in infection is redundant (Case et al., 2009; Casson et al., 2013). Lastly, non-canonical inflammasome activation through caspase-11 is also involved, resulting in pyroptosis, LCV degradation, and NLRP3 activation (Aachoui et al., 2013; Akhter et al., 2012).

#### 1.3.4.1.3 Nucleic acid sensing in the cytosol

It is critical to detect bacterial nucleic acids in the cytosol to elicit effective antibacterial responses. The DNA sensor cGAS recognizes *L. pneumophila* DNA and triggers STING-dependent type I IFN (IFN-I) pathway through IRF3 activation (Lippmann et al., 2011; Lippmann et al., 2008). A hypomorphic variant (HAQ) of the TMEM173 gene, which encodes STING, leads to a deficiency in IFN-I responses and is associated with susceptibility to LD in humans (Ruiz-Moreno et al., 2018). Moreover, the RNA-sensors

RIG-I and MDA5, as well as the adaptor MAVS, were reported to be involved in the IFN-I induction in response to *L. pneumophila* infection (Monroe et al., 2009).

#### 1.3.4.1.4 Role of IL-1 family cytokines

Infection is controlled predominantly by inflammasome-dependent release of IL-1α and IL-1β. These cytokines can signal to bystander macrophages, recruiting and activating PMNs (polymorphonuclear leukocytes), monocytes, DCs (dendritic cells), and epithelial cells through binding to the IL-1 receptor (IL-1R). IL1R signaling activates production of proinflammatory cytokines (TNFα, IL-12) and chemokines (CXCL1, CXCL2) to facilitate neutrophil migration (Casson et al., 2013; LeibundGut-Landmann et al., 2011; Mascarenhas et al., 2015). Among two cytokines, IL-1α is likely to be more important in vivo (Casson et al., 2013). Additionally, the production of IL-18 by inflammasome activation is necessary for NK (natural killer) cell stimulation, IFN-γ production and the effective elimination of bacteria in both lung and systemic infections (Brieland et al., 2000).

#### 1.3.4.1.5 Type I and Type II Interferons

Both IFN-I (IFN-α/β) and IFN-II (IFN-γ) modulate antimicrobial gene expression and control host defenses in macrophages during an *L. pneumophila* infection. A deficiency

in the signaling of these IFNs causes a defect in bacterial elimination (Shinozawa et al., 2002). AMs secrete type I IFNs, which act through receptor IFNAR and transmit signals to transcription factors ISGF3 and GAF for the expression of a large number of interferon-stimulated genes with antibacterial functions (Kessler et al., 1988). One target interferon-stimulated gene (ISG) is the immune-responsive gene 1 (IRG1), which localizes near the LCV, where it generates itaconic acid, a TCA cycle intermediate that limits bacterial replication (Naujoks et al., 2018; Naujoks et al., 2016).

#### 1.3.4.1.6 Role of TNFα

TNFα is an important cytokine in the response to *L. pneumophila*. Clinical data have demonstrated that patients on anti-TNFα therapy/agents are more likely to develop LD (Fabroni et al., 2010; Lanternier et al., 2013). Synthesized primarily by PMNs and monocytes, TNFα activates two receptors on AMs: TNFR1 and TNFR2. TNFR1 signaling is essential for clearance of bacteria as well as PMN recruitment and IL-12 production, while TNFR2 could regulate the inflammatory response (Fujita et al., 2008). While the specific mechanisms are not yet entirely understood, TNFα was seen to aid NAIP5-mediated defense (Coers et al., 2007). Notably, TNFR1-mediated suppression of *L. pneumophila* is independent to NLRC4, caspase-1/11, and ROS, but requires activation of NF-κB, lysosomal acidification, and other caspases (Kawamoto et al.,

2017; Park et al., 2017).

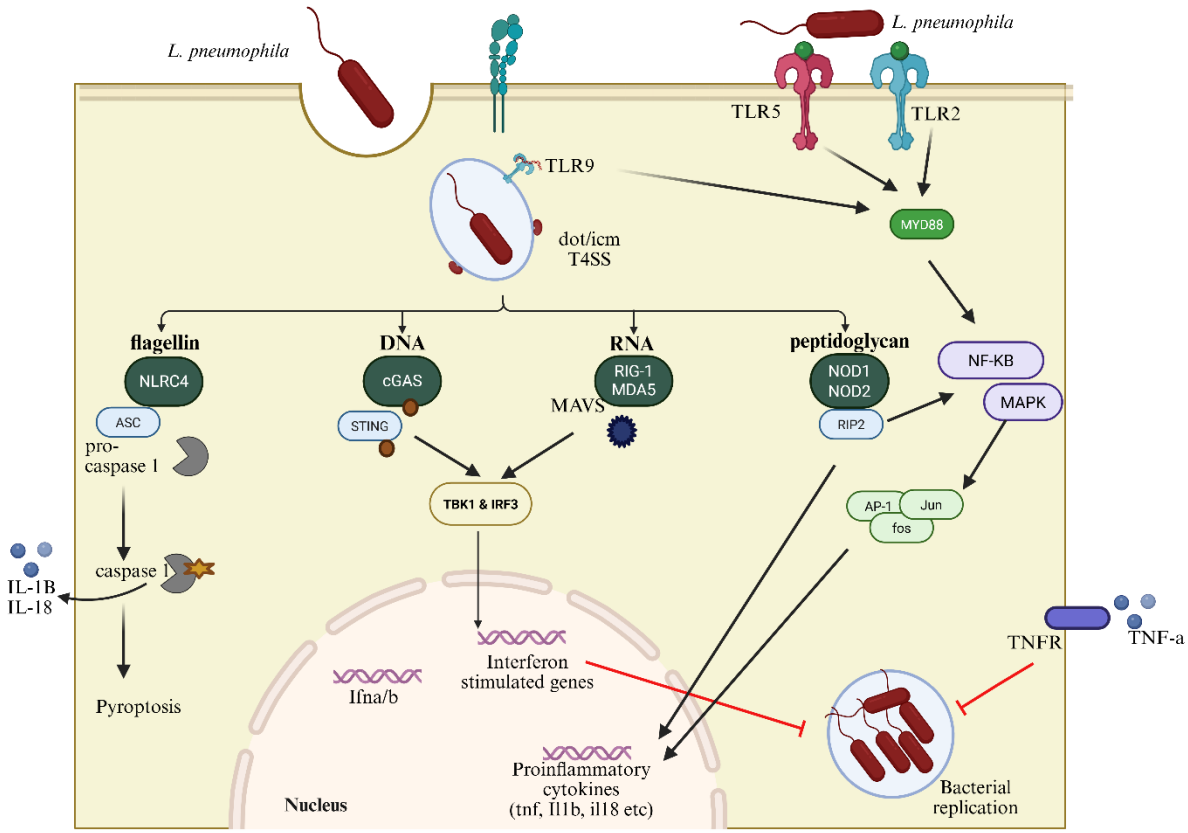


**Figure 1.10: Innate immune responses against *L. pneumophila*.**

Schematic view of the macrophage immune responses to *L. pneumophila* infection. Several pattern recognition receptors (PRRs) are involved in sensing *L. pneumophila* either at the cell membrane (e.g., TLR2, TLR5), or in the cell cytosol (NOD1/NOD2 and cGAS). Activation of these receptors leads to activation of unique intracellular signalling pathways that mediate the antibacterial immune response. Read the above main text for more information. **(Created with BioRender.com)**

### 1.3.5 Importance of THP-1 derived Macrophage as a disease model for *L. pneumophila* OMV studies

The majority of the data on the anti-*Legionella* immunity comes from cellular (primary lung cells or immortalized lines) and animal (most often murine) models. Nevertheless, wild-type mouse strains depict a fundamental resistance to *Legionella* because it is unable to replicate *L. pneumophila* intracellularly. Infection in intracellular environments only occurs in the macrophages from A/J mice, which are deficient in the NAIP5 (or Birc1e) inflammasome pathway (Wright et al., 2003). Pathogen recognition by NAIP5 occurs through the detection of flagellin. Thus, an alternative approach to investigating infection in mouse models is to employ a *L. pneumophila* strain that has non-functional flagellin (Schell et al., 2016). Therefore, Animal model studies offer an imperfect reflection of the pathogenesis and immune response in human infections, in part because of the intrinsic inability of *L. pneumophila* to replicate within mouse models. Additionally, there are ethical and laboratory facility constraints to consider when working with in vivo models for bacterial infection. Nonetheless, primary human cells and human immortalized cell lines, such as the THP-1 monocytic cell line and A549 cells, provide essential models for studying human immune responses, as they are of human origin and closely resemble human cellular responses. More importantly, *L. pneumophila* can grow in these cell lines, making them suitable for studying infection

and immune responses.

As discussed earlier, macrophages play crucial roles in the innate immune system, including: (1) recognizing invading pathogens, such as bacteria, viruses, and fungi, based on PAMPs interacting with PRRs; (2) replicating to increase the number of immune cells capable of responding to infection; (3) secreting pro- and anti-inflammatory cytokines and chemokines that help direct immune effector cells to sites of infection and inflammatory resolution once the threat has subsided; and (4) executing phagocytosis to internalize and degrade pathogens (Si-Tahar et al., 2009). Research has shown that THP-1 derived macrophage cells can perform all these functions and closely resemble alveolar macrophages in morphology and function, including the expression of differentiation markers.

#### 1.3.5.1 Introduction to THP-1 derived macrophages

The THP-1 cell line was derived from a male with acute monocytic leukaemia (Tsuchiya et al., 1980). These monocytes can be polarized to macrophages by different treatments, including PMA (phorbol-12-myristate-13-acetate), Vitamin D3 (dihydroxyvitamin D3), and M-CSF (macrophage colony-stimulating factor). While M-CSF has biological relevance in vivo, particularly for the differentiation of early hematopoietic progenitors into monocytes, it does not work well in vitro unless

combined with interferon-gamma (Phillips et al., 2005; Takahashi, 2001). Comparison of THP-1 differentiation by PMA and VitD3 showed that differentiation with 100 nM vD3 over 3 days generates macrophages with impaired phagocytic function and decreased IL-1β and TNF-α production compared to macrophages differentiated for 3 days with 200 nM PMA (Auwerx, 1991; Daigneault et al., 2010).

Further, there are different protocols for PMA differentiation. Upon treatment with PMA (e.g., for 1–3 days), THP-1 cells begin to express macrophage-like phenotypic features, including the ability to adhere to culture plates and show morphological differentiation with cell spreading and an amoeboid form. They have prominent Golgi complexes, rough endoplasmic reticulum, and increased ribosomes in their cytoplasm (Tsuchiya et al., 1982). As Daigneault and colleagues have pointed out, the induction of the macrophage-specific markers is enhanced using a protocol of 200nM PMA for 3 days, followed by 5 days of PMA-free rest (Daigneault et al., 2010). This effect leads to alterations in the cytoplasm-to-nucleus ratio, an increase in the mitochondrial-to-lysosomal compartment, and the induction of surface. Consistent with all findings (Bastiaan-Net et al., 2013; Chanput et al., 2013; Chanput et al., 2012), PMA remains the most effective and widely used agent for generating macrophage-like cells that most closely resemble human resident cells macrophages. Complete differentiation

reportedly takes 48 hours at a minimum PMA dose of 100 ng/ml (162 nM). Nonetheless, caution is required with increased PMA concentrations, as they can cause unwanted effects, especially NF-κB-dependent gene expression involved in inflammatory conditions. To increase macrophage marker expression and reduce short-term PMA-mediated NF-κB activation, a 24 h resting period in PMA-free medium following differentiation is suggested. The time required for THP-1 cells to adhere to the culture, and the level of phagocytosis, cell surface CD14, CD36, TLR2, or complement receptor 3 (CR3; CD11b/CD18) expression on the cell surface, depend on the cell line, the concentration of activator agent, and other factors.

#### 1.3.5.2 Applications of THP-1 cell line

THP-1 cells are commonly used as an in vitro model system for multiple purposes, including inflammation studies, understanding viral and bacterial infections, drug testing, cancer research, vaccine development, immunotherapy, and regenerative medicine (Tsuchiya et al., 1980). Once differentiated into macrophages, they exhibit all the functions of human macrophages.

THP-1-derived macrophages are extremely useful in infectious disease studies as the expression of a wide array of PRRs, such as TLRs and NLRs, permits these cells to sense bacterial PAMPs and trigger a series of signaling events resulting in the release

of pro-inflammatory cytokines (e.g., TNF-α, IL-1β, IL-6, and IL-8) just like alveolar macrophages (Chanput et al., 2014; Daigneault et al., 2010). It has been widely used to investigate the immunomodulatory impact of bacterial infections (*M. tuberculosis, L. pneumophila, Salmonella enterica, E. coli*, and others) (Shin et al., 2010; Verma et al., 2020). These models enable researchers to understand the molecular processes involved in bacterial evasion, inflammasome activation, cytokine secretion, and macrophage phenotype in a controlled setting. Additionally, due to their reproducibility and ease of genetic manipulation, they represent a model of choice for high-throughput assays in host–pathogen biology.

#### 1.3.5.3 Use of THP-1 cells in *L. pneumophila* studies

For the past 40 years, a wide range of human cell lines has been used as models to study the pathogenesis of *L. pneumophila* infection. The typical cell lines used for these models include U937, A549, HeLa, and THP-1 cells. Analysis of PubMed data suggests that over the last 10 years, THP-1 cells have become the most commonly used system for *L. pneumophila* studies. Many studies have demonstrated that *L. pneumophila* can infect and replicate in differentiated THP-1 cells. PMA-differentiated THP-1 cells display a very similar morphology to human primary monocyte-derived macrophages and possess a macrophage phenotype and function. This distinction is essential because,

in humans, *L. pneumophila* preferentially infects alveolar macrophages during infection. Horwitz in 1983 was the first to show that *L. pneumophila* can evade host defenses within human monocytes by interfering with phagosome-lysosome fusion to remain viable and multiply within the host (Horwitz, 1983b). Other studies have demonstrated that differentiated THP-1 cells reproduce this phenomenon by favouring *L. pneumophila* intracellular replication and eliciting cellular responses to infection that are similar to those of primary macrophages (Escoll et al., 2016).

Studies on THP-1 cells have also made important contributions to our understanding of the molecular mechanisms of *L. pneumophila* cell invasion. For instance, Abu Khweek and Amer summarized how *L. pneumophila* controls host physiological processes, like autophagy, apoptosis, and cytokine production, in THP-1-derived macrophages (Abu Khweek & Amer, 2018). In these studies, they also demonstrated that the LCVs established in THP-1 cells are comparable to those induced in primary macrophages, indicating that this model is also relevant for investigations on the intracellular trafficking and replication of *L. pneumophila* (Escoll et al., 2016)

Furthermore, the use of THP-1 cells has allowed high-throughput screening of host and bacterial factors necessary for infection. For example, THP-1 cells have been used to identify host signaling pathways regulating *L. pneumophila*, including NF-κB and

MAPK, which are activated during *Legionella* infection, and to examine the effectiveness of candidate antimicrobial agents (Shin et al., 2008). Table 1.1 compares the properties of popular cell lines used in previous studies to examine *L. pneumophila* mechanisms, and Figure 1.11 shows the number of studies that used these cell lines.

**Table 1.1 Comparison of popular cell lines used to study *L. pneumophila* disease**

| Cell Line | Origin | Occurrence of infection | Host Response | Advantages | Limitations | References |
|---|---|---|---|---|---|---|
| **U937** | Isolated from Human histiocytic lymphoma cells Pro-monocytic | Supports replication of *L. pneumophila* intracellularly; can differentiate virulent from non-virulent strains | It exhibits cytopathic effects upon infection; triggers immune responses | Reference model for studying macrophage-pathogen interactions; cytokine induction | Requires differentiation, might not fully reflect all of the functions of primary macrophages, more mature state | (Koriyama et al., 2019; Xiong et al., 2017; Zhang et al., 2024) |
| **A549** | Human alveolar epithelia cells orginated from Adenocarcinomic human alveolar basal epithelial cells | Supports replication of *L. pneumophila* intracellularly; apoptosis and cytokine induction | NF-κB pathway activation; IL-8 expression; HMGB1 release | Model for lung epithelial response in bacterial invasion studies | Non-phagocytic; not entirely representative of macrophage contacts. | (Khweek & Amer, 2010; Kunishima et al., 2000; Vinzing et al., 2008) |

| | | | | | | |
|---|---|---|---|---|---|---|
| **THP-1** | Human monocytic cell line isolated from acute monocytic leukemia patient | Efficiently internalizes and allows replication of L. pneumophila;<br><br>Undergoes necrotic cell death after infection | Associated with release of pro-inflammatory stimuli such as HMGB1; and cathepsin B-dependent necrosis | Mimic human lung alveolar macrophage response, compatible with innate immunity studies | Requires differentiation and need a standardized protocol | (Buse et al., 2011; Hoppe et al., 2017; Jung, Herkt, et al., 2017; Xiong et al., 2017) |
| **NCI-H292** | Isolated from lymph node of a pulmonary mucoepidermoid carcinoma, Lung epithelial cells | | Can induced pro-inflammatory cytokines (eg IL-8);<br><br>Implicated in pathogen translocation across epithelial barriers | Models airway epithelial responses; useful in studies of pathogen-epithelial interactions and transmigration mechanisms | Non-phagocytic and doesn't may not accurately reflect as immune cell | (Kawamoto et al., 2017; Teruya et al., 2007; Wagner et al., 2007) |

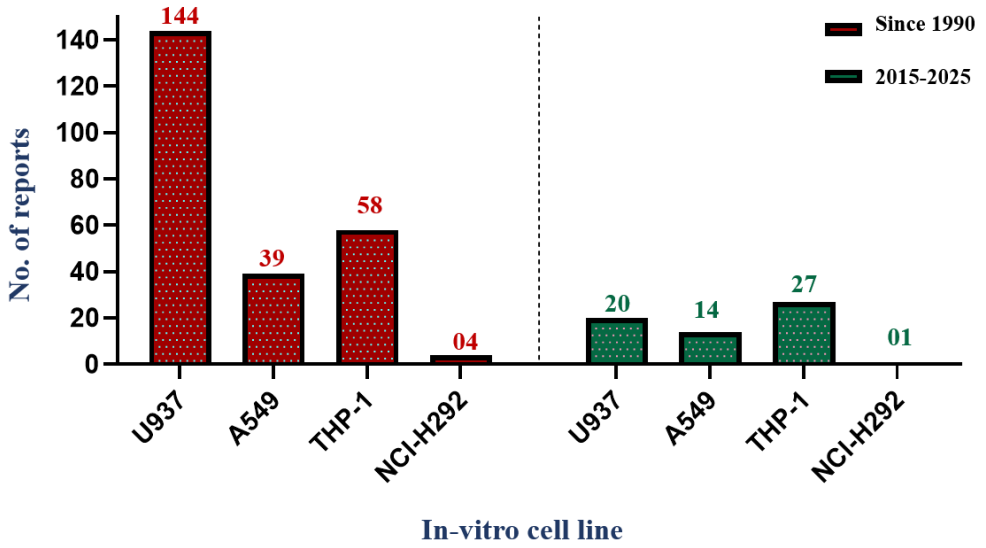


**Figure 1.11: Comparison of reported cell lines being used in *L. pneumophila* studies overall and in the recent 10 years by PUBMED**.

Comparison shows that in the recent decade, THP-1 cells have been used more frequently as an in vitro cell line model for studying the pathogenesis of L. pneumophila, due to their functional relevance and ease of handling.

Based on this literature, using THP-1 derived macrophages is a reasonable approach to assess how these *L. pneumophila* OMVs affect cellular functions, such as immunomodulation, apoptosis, and inflammation. Understanding these mechanisms helps clarify how OMVs aid *L. pneumophila* in evading the immune system.

# Chapter 2. Aims and Objectives

## 2.1. Research Gaps

1. Many studies have focused on the characterization of proteins and RNAs in OMVs of pathogenic bacteria; however, the existence of DNA in these vesicles and whether it is actively packaged and functional has been widely neglected. In *L. pneumophila,* the OMV-associated proteome was studied more than a decade ago (2008) using conservative gel-digestion approaches, whereas knowledge of DNA is not available in the literature. One study reported that *L. pneumophila* translocates regulatory RNAs via OMVs, which mimic host microRNAs and modulate host defence signalling pathways. Current approaches in OMV studies focus on individual biomolecules rather than on the entire cargo and on employing bioinformatic analyses to predict how these components can influence host-pathogen interactions together. This comprehensive approach can increase our understanding of the coordinated functions of EV-associated biomolecules in modulating host cellular processes in Legionnaires' disease.

**2.** Pathogenesis of *L. pneumophila* depends on multiple factors. The most described key factor of virulence is the type IV Dot/Icm secretion system, which participates in the modulation of key host cellular processes such as ubiquitination, pyroptosis (caspase-1), phagosome maturation, lipid remodelling, autophagy, endocytic pathway, and modulation of pathways like NF-κB and MAPK pathways via phosphorylation, which are critical for bacterial clearance. Despite the significant advances in our understanding of Dot/Icm-mediated pathogenesis, the role of OMVs in *L. pneumophila* infection remains comparatively underexplored. In particular, there is a lack of knowledge regarding how OMVs influence the same host cell pathways targeted by the Dot/Icm system. A comprehensive analysis of global transcriptomic responses in host cells following exposure to *L. pneumophila* OMVs can address these questions. Such studies have the potential to reveal previously unrecognised roles of OMVs, offering deeper insights into their wider effects on host cellular pathways and functions.

3. Many studies have elucidated the role of OMVs as potent modulators of immune responses. However, in *L. pneumophila*, it is unclear whether the host immune responses triggered by *L. pneumophila* OMVs are beneficial or protective to the host or serve the pathogen's advantage. Multiple factors influence the mortality rate of Legionnaires' disease, particularly the host immune response. In clinical patients, the severity of LD is linked to hyperinflammation or immunoparalysis and a high bacterial load in the patient's lungs. Examining the host immune profile and measuring bacterial load after exposure to OMVs can reveal whether OMVs contribute to disease severity, as shown in clinical patients.

## 2.2. Aims:

This project aimed to comprehensively characterize the molecular cargo of *L. pneumophila* OMVs, investigate the global transcriptomic changes in host cells following OMV exposure to elucidate changes in cellular processes and pathways, and to validate the findings related to immune activation, oxidative stress responses, cell death, and finally estimate the bacterial burden in host cells after OMV treatment. Through integrating molecular characterization, transcriptomics, and functional assays, the project aims to improve our understanding of how OMVs contribute to *L. pneumophila* pathogenesis.

## 2.3. Objectives:

1. To isolate and purify OMVs from *L. pneumophila* using size exclusion chromatography (SEC using qEV1) and density gradient centrifugation (DEG using Optiprep) methods, and to compare their efficiency regarding OMV quality and yield.

2. To comprehensively characterise the molecular cargo of the purified *L. pneumophila* OMVs by detecting LPS, profiling associated proteins using label-free proteomics, and analysing DNA and RNA contents.

3. To investigate the modulation of THP-1-derived macrophage processes and pathways through single-cell RNA sequencing (scRNA-seq) following OMV internalization, enabling a high-resolution assessment of transcriptomic changes across individual cell populations.

4. To examine host cell viability and bacterial replication within the host after OMV treatment, in order to determine whether OMVs confer an advantage to the pathogen or the host.

# Chapter 3. Materials and Methods

## 3.1. Overview of workflow

The workflow of this project is outlined in Figure 3.1. Initially, OMVs were isolated from *L. pneumophila* and analyzed for their molecular components, such as LPS, DNA, RNA, and proteins. These OMVs were then used to treat THP-1 derived macrophages to study their interactions, including OMV uptake, single-cell RNA sequencing, cytokine responses, macrophage polarization, host cell cytotoxicity, ROS production, and bacterial survival within OMV treated macrophages. This comprehensive approach provided a detailed assessment of how *L. pneumophila* OMVs influence host immune responses and bacterial pathogenicity.

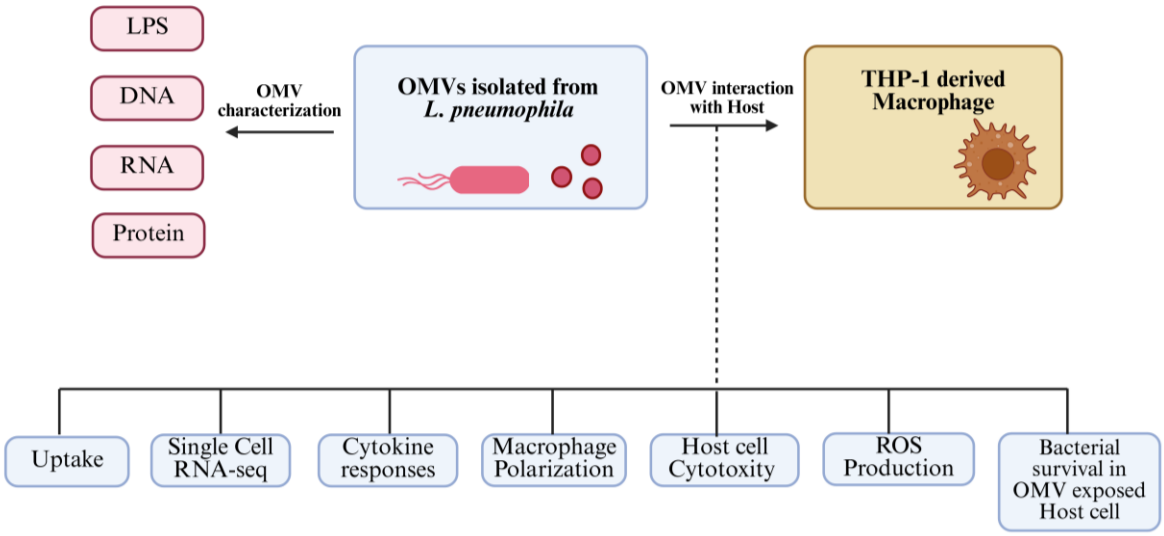


**Figure 3.1 Project workflow for investigating the role of *L. pneumophila* OMVs in disease pathogenesis and host immune modulation.**

### 3.2 Bacterial strain and THP1 cell line

#### 3.2.1 *L. pneumophila*

The Philadelphia strain of *L. pneumophila* (ATCC 33152) was employed in this study. The organism was cultivated on Buffered Charcoal Yeast Extract (αBCYE) agar plates supplemented with αBCYE growth supplement (HKM Huankai Microbial) and GVPC selective reagents (supplied by HKM Huankai Microbial). Cultures were maintained at 37°C in 5% $CO^2$ for 3 to 5 days. For liquid culture, *L. pneumophila* was cultivated in Buffered Yeast Extract (BYE) broth supplemented with additives (HKM Huankai Microbial).

#### 3.2.2 Cell line

This study utilized human monocyte THP-1 cells (ATCC TIB-202). Cells were grown in RPMI 1640 medium (Gibco, Waltham, MA, USA) supplemented with 10% fetal bovine serum (Thermo Fisher) and 1% penicillin-streptomycin (1000 U/ml) (Gibco) at 37°C in a 5% $CO_2$ atmosphere for 3 to 5 days before any experiment.

### 3.3 Isolation and characterization of *L. pneumophila* OMVs

#### 3.3.1 Growth curve of *L. pneumophila*

*L. pneumophila* growth phases were determined by creating a growth curve for the bacteria using optical density at 600 nm (OD600) at each 12-hour interval. *L. pneumophila* was initially streaked onto BCYE agar and incubated at 37°C for 2–3 days for the isolation of colonies. A colony was inoculated into 5 ml of BYE broth and incubated at 37°C with agitation at 180 rpm overnight to prepare a pre-culture. The OD600 of the preculture was measured the next day, and the culture was diluted with fresh BYE broth to an initial OD600 of 0.05 to 0.1 in a 10-ml culture. This culture was grown by shaking at 37°C, and 1 ml aliquots were taken at 12-hour

intervals; the OD600 was determined using a spectrophotometer blanked with fresh BYE broth. Samples with an OD600 greater than 1.0 were diluted as needed for measurements. The OD600 values of each time point were plotted against time, and the bacterial growth curve was plotted to show the lag, exponential, and stationary growth phases of *L. pneumophila.* All the analyses were done in triplicate.

### 3.3.2 Isolation of *L. pneumophila* OMVs

Based on the above growth curve analysis, the exponential and early stationary phase time point was selected for the isolation of OMVs. *L. pneumophila* was cultivated on BCYE agar at 37°C in a CO2 atmosphere. From this pre-culture, we inoculated 20-30 complete BYCE plates of *L. pneumophila* and incubated them at 37 °C for 3 days. The subsequent bacterial culture is collected utilizing a 10 µl inoculation loop or cotton swab, then resuspended in 20 ml of sterile phosphate-buffered saline (PBS) and vortexed for 30 seconds. Following centrifugation at 4,000 × *g* for 20 minutes at 4°C, the supernatant is collected and filtered twice through a 0.22-µm PES membrane syringe filter. The filtrates are subsequently collected for OMV separation.

Differential ultracentrifugation is the gold standard for EV separation, although SEC and other rapid commercial techniques are also becoming common these days. Crude OMVs were collected by ultra-centrifugation (UC) of supernatants at 100,000 *g* for 90 minutes, using the Ti 70.1 rotor from Beckman Coulter (Beckman Coulter, Brea, CA, USA). After the first ultracentrifugation, the EV pellet was washed once by adding 5 ml PBS (Figure 3.2).

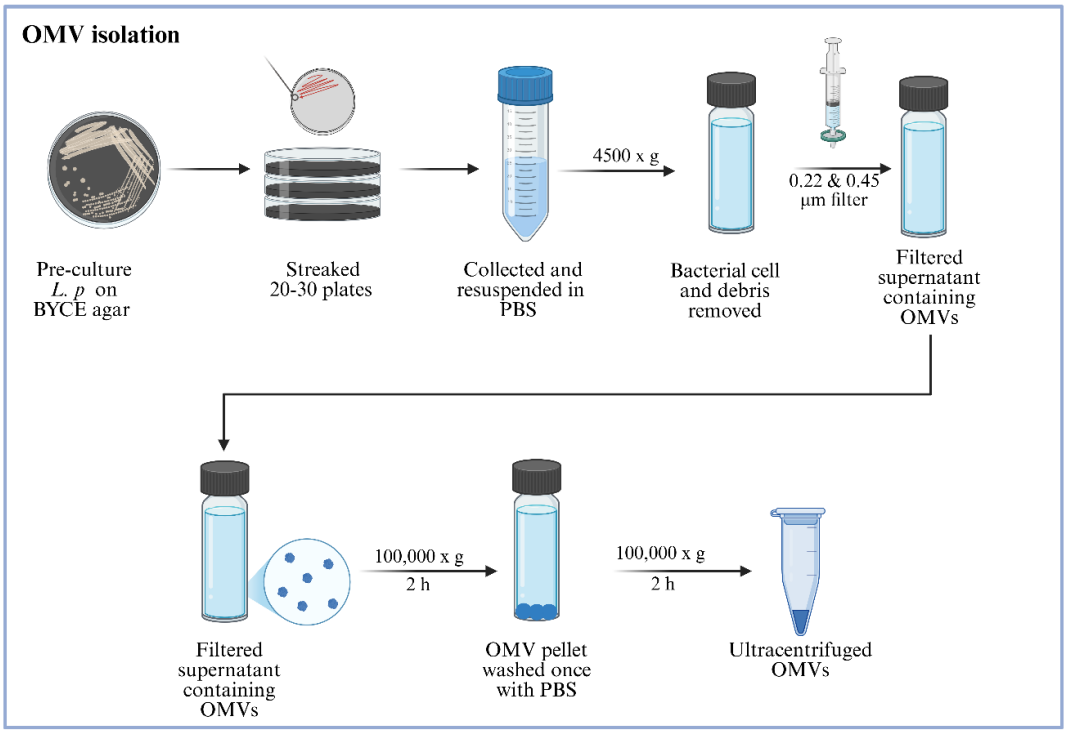


**Figure 3.2: Workflow for OMV isolation from *L. pneumophila*.**
*L. pneumophila* were streaked onto agar plates and incubated for growth. The bacterial biomass was collected and suspended in buffer, then filtered to remove bacterial debris. The resulting filtered supernatant was subjected to ultracentrifugation to pellet OMVs. The OMV pellet was washed once to obtain the final crude OMV preparation. **(Created with BioRender.com)**

### 3.3.3 Purification by Opti-Prep density gradient ultracentrifugation (DEG)

To get purified OMVs, the crude OMV pellet was resuspended in 100 – 200ul PBS and then subjected to particle separation via layered iodixanol (OptiPrep, Stemcell Technologies, Canada). The following concentrations of iodixanol were prepared in PBS: 0%, 6%, 10%, 14%, 16%, 20%, 24%, 30%, 34%, and 40%. These layers were added to the resuspended crude OMVs in a top-down approach. Following layering, density gradient ultracentrifugation was performed at 100,000 × *g* for 16 hours at 4°C. The distinct layers of varying densities were thereafter collected in sequence, and each fraction was washed with PBS by ultracentrifugation at 100,000 × *g* for 1.5 hours at 4°C, performed twice. When the EV layers became visible, only the visible layers were collected and washed. However, for the first batch, all ten layers were analysed by qubit protein assay, Transmission electron microscopy (TEM), and Nanoparticle

tracking analysis (NTA) to narrow down the layers required in the latter experiments. Next, for the downstream experiments, such as host interaction studies, pure OMV-containing fractions were pooled and concentrated by an additional ultracentrifugation step to obtain a homogenized mixture of OMVs. Additionally, the purity of OMVs was validated by confirming the absence of viable bacteria after plating out 100 µl of vesicle suspension on LB agar and incubating for 24 h at 37°C. Resulting OMVs were stored at −20 °C for one month and at −80 °C for longer time.

### 3.3.4 Purification by Size Exclusion Chromatography (SEC)

OMV-containing pellet was resuspended in 1 ml PBS and loaded onto a (qEV1/70 nm) size exclusion column (Izon Science, Christchurch, New Zealand) that was pre-washed with PBS. Fractions were collected as per the manufacturer's instructions. Using the AFC Automatic Fraction Collector, 10 fractions of 0.7 ml each were collected. Each fraction was initially screened by the qubit protein assay, TEM and NTA. For downstream experiments, such as host interaction studies, pure OMV fractions were pooled and concentrated by an additional ultracentrifugation step to obtain a homogenized mixture of OMVs. Additionally, the purity of OMVs was validated by confirming the absence of viable bacteria after plating out 100 µl of vesicle suspension on LB agar and incubating for 24 h at 37°C. Resulting OMVs were stored at −80 °C for long-term storage and −20 °C for one-month storage.

The workflow of both methods is described in Figure 3.3.

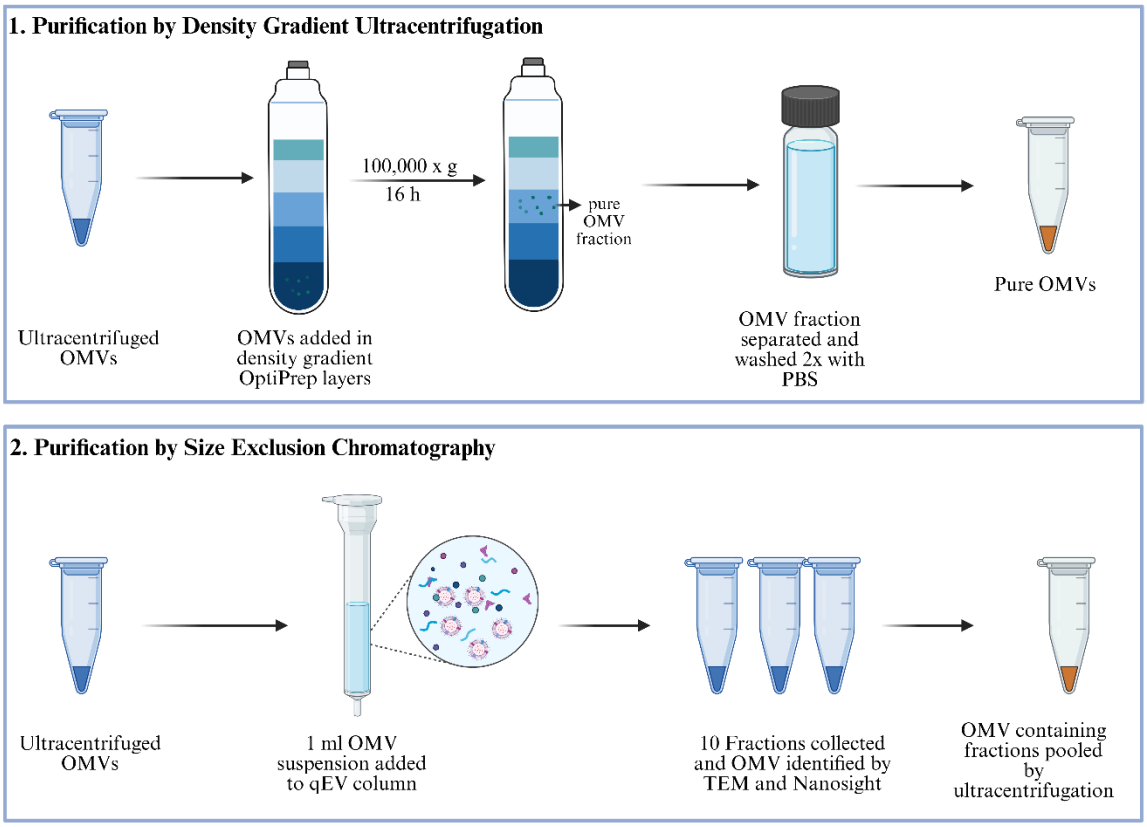


**Figure 3.3: Purification of crude OMVs by density gradient centrifugation (DEG) and size exclusion chromatography (SEC).**
(1) Crude OMVs were first subjected to density gradient centrifugation (DEG) to separate OMVs from remaining contaminants based on their buoyant density. (2) The OMV-containing fractions were purified using size exclusion chromatography (SEC), allowing separation based on particle size. **(Created with BioRender.com)**

### 3.3.5 Qubit analysis

For Protein, DNA, and RNA estimation of OMVs, we used Qubit fluorometric quantification Assay kits, catalog no. Q33212, Q32850, and Q32852 respectively. All 10 fraction layers were measured for protein, DNA, and RNA content according to the manufacturer's instructions.

### 3.3.6 TEM examination

Historically, the best staining images under TEM were achieved with uranyl acetate (UA); however, due to radiogenic concerns, some reports have mentioned alternatives to UA staining.

For this study, we used one alternative, “Uranium-free X solution” reported by Moscardini et al **(**Moscardini et al., 2020**).**

#### *3.3.6.1* Preparation of staining solution (X-solution)

The X solution was prepared by dissolving 92 mg of phospho-tungstic acid in 3.5 ml of water and partially neutralizing it with 1 M NaOH to achieve a pH of 4-5. Subsequently, 186 mg of $YbCl_3$ dissolved in 4 ml of water was incorporated into the existing mixture, and the total volume of the solution was adjusted to 8 ml with more water. Then, 2 ml of 100% ethanol was added, and the mixture was agitated at room temperature for 24 hours. The precipitate was subsequently eliminated by centrifugation, and the supernatant was mixed with 39 mg MES. The pH was then set to 4.6–4.8, and the mixture was subsequently agitated for additional 24 hours. The solution was ultimately filtered through a 0.22-µm membrane filter and kept in the dark at 4°C.

#### *3.3.6.2* Preparation of samples:

First, Formvar/Carbon-supported copper grids (Sigma-Aldrich) were plasma-treated on a gatan plasma cleaner. Samples were prepared by adding 5-7 µl of OMV suspension to the grid and incubating for 10 minutes. After which, the excess solution was blotted off with filter paper, and the grids were washed twice with filtered PBS or ultrapure water. Then, one drop of X solution (prepared as described above) was added, and the mixture was incubated for 30 seconds. Excess stain was removed by blotting, and the grids were air dried. Samples were imaged on a ThermoFisher Talos L120C 120 kV TEM and Transmission Electron Microscope (JEOL Model JEM-2010).

### 3.3.7 NTA measurements

OMV size distribution and particle concentration were measured by Nanosight NS300HSB equipped with a 405 nm laser. OMV samples were diluted 1000-fold in PBS. Standard 5-minute measurements were taken using NTA software version 3.0 with camera level 12 and a detection threshold of 5.

### 3.3.8 OMV Proteomics analysis

#### *3.3.8.1* Sample preparation for proteomic analysis

Samples for MS analysis were prepared using the EasyPep MS Sample Prep Kit (Thermo Fisher) following the manual instructions. In brief, the protein estimation of purified OMV fractions was done using Pierce BCA protein assay kit (Thermo Scientific, Waltham, MA, USA) and concentrated using a refrigerated CentriVap vacuum concentrator (Labconco Corporation). Samples were then dissolved in the lysis buffer. 100 µg of protein was obtained, and the volume was set to 100 µl Reduction and alkylation solutions were added to reduce and alkylate the sample at 95 °C for 10 minutes. Then, the protein was digested by incubating it with a trypsin/Lys-C mixture at 37 °C overnight, followed by the addition of the digestion stop solution. After that, the samples were desalted and cleaned by C18 peptide clean-up columns with a series of washes. The peptides were then eluted with the elution solution and subsequently dried by a CentriVap vacuum concentrator.

#### *3.3.8.2* LC-MS Analysis

LC-MS/MS acquisition was conducted with the Orbitrap Fusion Lumos Mass Spectrometer (Thermo Scientific, Waltham, MA, USA) coupled with a Dionex Ultimate 3000 RSLCnano System (Thermo Scientific, Waltham, MA, USA) equipped with Acclaim PepMap C18 analytical columns (Thermo Scientific, Waltham, MA, USA) and Trap Column Cartridges Holders with nanoViper Fittings (Thermo Scientific, Waltham, MA, USA). 1 µl of Samples was injected and trapped for 3 minutes before separation in the analytical columns. The

gradient settings are as follows: solvent A, 0.1% formic acid in water; solvent B, 0.1% formic acid in acetonitrile; gradient started at 2% B for 5 min, 6% B at 5–7 min, 30% B at 7–92 min, 90% B at 92–100 min that hold until 105 min and re-equilibrate with 2% B for 10 min. The flow rate was maintained at 300 ml/min. The eluted peptides were analyzed by an Orbitrap Fusion Lumos Mass Spectrometer using a data-independent acquisition (DIA) strategy in positive ion mode with a resolution of 60,000, standard automatic gain control (AGC) target, and a scan range of 400-1500 m/z. Precursors were then fragmented using high-energy collision dissociation (HCD) with a normalized collision energy set as 32%. MS/MS was acquired using an Orbitrap as mass analyzer with a mass resolution of 15,000 and standard AGC target.

#### *3.3.8.3* Data analysis

The mass spectrometry proteomics data have been deposited to the ProteomeXchange Consortium via the PRIDE (Perez-Riverol et al., 2022) partner repository with the dataset identifier PXD048599. The DIA raw files from MS and MS/MS were analyzed by Spectronuat (Version 18, Biognosys) software. Default directDIA+ (Deep) workflow was used with *L. pneumophila*'s reviewed proteome on Uniport as the searching database (Release date: 28 October 2023). Peptide searches were performed using Trypsin/P as the cleavage enzyme, allowing for up to two missed cleavages. Carbamidomethylation of cysteine residues was set as a fixed modification, while oxidation of methionine residues was included as a variable modification. 0.01 False Discovery Rate (FDR) was applied for peptides identification. The final protein groups only contain protein with at least two peptides.

### 3.3.9 OMV DNA analysis by Illumina sequencing

#### *3.3.9.1* OMV preparation for total-DNA sequencing and internal-DNA sequencing

For the analysis of total DNA associated with OMVs, the purified OMV pellets were resuspended in 1 ml of PBS.

For the OMVs internal DNA analysis, the purified pellets were first resuspended in 50 µL of PBS, and external DNA was removed using the TURBO DNA-free kit (Thermofisher) according to the manufacturer's instructions. 1 µl of DNase was added along with 5 µl of TURBO DNase buffer and incubated for 20 minutes at 37°C. Next, DNase was inactivated by adding 5 µl of DNase inactivation reagent and incubating for 5 minutes at RT. The sample was centrifuged, and the supernatant was transferred to a new tube. PBS was added to this new tube to make up the total volume of 1 ml. Extraction was done in triplicate from 3 different batches of OMVs.

#### *3.3.9.2* DNA extraction by QIAamp MinElute ccfDNA Kit (Qiagen) kit

DNA extraction was performed by using the QIAamp MinElute ccfDNA Kit according to the manufacturer's protocol. For complete lysis and release of OMV DNA, 1 ml OMV suspension was treated with magnetic bead suspension, bead binding buffer, and proteinase K in a 15 ml conical tube and incubated for 10 minutes at RT. By placing it on a magnet, the supernatant was discarded, and DNA bound to beads was eluted with Bead elution buffer. Next, buffer ACB was added to the eluted supernatant and passed through a QIAmp MinElute column. The column was washed with ACW2 buffer and dried. DNA was eluted in 20–50 µL of ultra-clean water, and the purified OMV DNA was then frozen at −20°C for subsequent analysis. DNA attached to the column was eluted by adding 30 µl of ultra-clean water into the centre of the column. DNA concentration, Quality, and size distribution were analyzed by Qubit 1x

dsDNAHS kit (Thermofisher), Nanodrop, and Bioanalyzer HS DNA kit (Bioanalyzer), respectively.

#### *3.3.9.3* Illumina library preparation and sequencing

OMV DNA libraries were prepared with the Illumina DNA Prep according to the manufacturer's protocol.

During the first step of library preparation, the OMV DNA was tagmented, which is a combined process of DNA fragmentation and tagging with adapter sequences. This was done with the Bead-Linked Transposomes (BLT) and Tagment Buffer (TB1). Following tagmentation, the tagmented DNA products were cleaned up by Tagment Stop Buffer (TSB) and Tagment Wash Buffer (TWB) buffers. Next, the tagmented DNA was PCR amplified using Enhanced PCR Mix (EPM) and index adapters i7 and i5. After that, the libraries were purified by beads, buffers and ethanol to eliminate residual primers, nucleotides, and enzymes. Lastly, libraries were quantified, normalized, and pooled as necessary for sequencing. The resultant libraries were kept at −20°C before sequencing on a Novaseq X Plus (Illumina) with 4GB output per sample.

#### *3.3.9.4* Data analysis

Sequencing data quality was analyzed by FastQC, and low-quality reads and adapters were removed by Trimmomatic. Sequence alignment and mapping were performed using BWA-MEM and SAMtools, with the reference genome of *L. pneumophila* ATCC 33152 obtained from NCBI (NC_002942.5). Genes were predicted by Prokka, and functional pathways were determined by KEGG and GO.

### 3.3.10 OMV RNA analysis:

OMV-RNA extraction was performed by the PureLink RNA Mini Kit (Thermo Scientific, Waltham, MA, USA). Purified OMV pellet was resuspended in 100 to 200 µl of PBS. Briefly, 2-Mercaptoethanol was added to the kit-provided lysis buffer. 0.3 ml of this prepared lysis buffer was added to the OMV suspension to lyse the vesicles. Next, the 0.3 ml lysate containing cells was passed through a 21-gauge syringe (Terumo, Tokyo, Japan) 5 to 10 times to homogenize. Homogenate was centrifuged for 5 minutes, and supernatants were transferred to new tubes. According to the kit instructions, 70 % ethanol was added to the homogenate, and the whole mixture was passed through a spin cartridge column. After centrifugation at 12,000 ×*g* for 15 s, the flow-through was discarded, followed by washing with Wash Buffer I and Wash Buffer II. Finally, the RNA in the spin cartridge was eluted in 50 µl of RNase-free water. RNA concentration, Quality, and size distribution were analyzed by Qubit 1x dsDNA HS kit (Thermo Scientific, Waltham, MA, USA), Nanodrop, and Bioanalyzer HS DNA kit (Agilent Technologies, Santa Clara, CA, USA), respectively. RNA was stored at -80°C before use. Genomic DNA contamination was removed by the TURBO DNA-free kit (Invitrogen, Waltham, MA, USA). RNA concentration was found to be too low for library preparation. For three trials using low-input Illumina library preparation (SMART-Seq Total RNA Mid Input), the library preparation was unsuccessful with too low concentration of library to be sequenced.

## 3.4 *L. pneumophila* OMVs interaction with the Host

### 3.4.1 THP-1 growth and differentiation

THP-1 human monocytic cell line (ATCC TIB-202) was grown at 37°C in a humidified incubator (5% $CO_2$) in RPMI 1640 media supplemented with 10% FBS and antibiotics (penicillin and streptomycin) until confluent. Cells were centrifuged and reconstituted in new medium before differentiation to achieve a concentration of $3 \times 10^5$ cells/ml for a 24-well plate, $1\times 10^6$ cells/ml for a 6-well plate, and 40,000 cells/ml for a 96-well plate.

To differentiate THP-1 cells, we followed the protocol as described previously with some modifications (Daigneault et al., 2010). For differentiation, THP-1 cells were treated with 100 ng/ml PMA (adjusted with the type of plate and its volume) for three days. After that, the medium was replaced, and the cells were allowed to rest for an additional 5 days.

For all OMV-host interaction studies, during experimental incubation with OMVs, Serum-free media Macrophage-SFM (Gibco, Waltham, MA, USA)) was used to avoid the interference of serum EVs from regular FBS.

### 3.4.2 Confocal laser scanning microscopy

THP-1 cells were seeded in a confocal dish (coated with poly-l-lysine) with a concentration of $1 \times 10^6$ cells/ml and differentiated into macrophages by PMA as described earlier. Once cells were ready, OMVs were stained with Vybrant CM dil (catalog no. V22888; Thermo Scientific, Waltham, MA, USA). OMVs were gently mixed with dye to ensure even distribution and then incubated for 20 minutes at 37°C. The unbound dye was removed by centrifugal filter MW 100K (Pall Corporation, Port Washington, NY, USA) according to the manufacturer's instructions. Then, to evaluate the OMVs' attachment to and internalization by macrophages, 10 µg of OMVs were added to a confocal dish for 4 hours at 37°C. Subsequently, the cells were

washed 3 times with PBS to remove unbound OMVs and fixed with 4% (v/v) paraformaldehyde (PFA) for 15 min. The cells were then incubated with Hoechst for 30 min at 4°C. Samples were viewed with a TCS SPE confocal microscope using 63x oil immersion lenses. Images were processed using Leica Suite Software.

### 3.4.3 Flow cytometry analysis for OMV uptake

THP-1 cells were seeded in a 12-well plate and differentiated into macrophages by PMA as described earlier. Once cells were ready, OMVs were stained with Vybrant CM dil (catalog no. V22888; Thermo Scientific, Waltham, MA, USA). OMVs were gently mixed with dye to ensure even distribution and then incubated for 20 minutes at 37°C. The unbound dye was removed by centrifugal filter MW 100K (Pall Corporation, Port Washington, NY, USA) according to the manufacturer's instructions. Following the incubation, cells were washed with PBS twice. Now, for flow cytometry analysis, differentiated THP-1 macrophages were collected by detaching with Accutase (1 ml of Accutase was added in wells for 10 minutes at 37 °C). After washing the cell samples with PBS, flow cytometry was performed.

#### *3.4.3.1* Flow cytometry setup

FACSAria III was utilized in all Flow cytometry experiments. A 10-µm nozzle was used according to the size of THP-1 cells (9-18 µm in diameter). Before starting flow cytometry analysis, the flow cytometer (FC) was calibrated with Standard beads. Flow cytometry start-up procedures were performed as indicated in the software, and the stream was allowed to become stable before turning on the sweet spot. For the analysis of OMV (as labelled with Vybrant CM-Dil red stain) uptake by THP-1-derived macrophages, a 633 nm laser was used. Gating was used to select the live population; the acquisition board was used to analyze fluorescence signals in the samples. Data were analyzed by the FlowJo software later.

### 3.4.4 Single-cell RNA-seq (scRNA-seq) analysis

#### *3.4.4.1* Sample preparation

THP-1 cells were differentiated into macrophages by PMA treatment in a 6-well plate, as described earlier. OMVs were stained with Vybrant CM dil and unbound dye was removed by centrifugal filter MW 100K according to the manufacturer's instructions. Then, macrophages were incubated with Vybrant-labelled OMVs at a concentration of 30 µg/ml (concentration optimized for high uptake) for 12 h at 37 °C or left untreated. Following incubation, cells were washed twice with PBS.

For flow cytometry, macrophages were detached using StemPro Accutase (Gibco, Waltham, MA, USA) solution. Cells were collected by centrifugation at 200 x *g* for 4 minutes. Accutase supernatant was removed, and cells were washed once with PBS. Then, the cell pellet was resuspended in PBS + 10 % FBS. 1 microliter 7-AAD was added to both OMV treated and untreated macrophages, and cells were incubated on ice for 10 to 15 minutes (to eliminate dead cells). Flow cytometry analysis was performed using Cy5.5 and PE red channel filters. Compensation was done due to excitation wavelength overlap between 7-AAD and Vybrant stain after recording the events for both stain control samples separately. Finally, the samples were analyzed, and gating was chosen. 7 AAD-negative & Vybrant-negative population was selected for untreated control, while 7 AAD-negative & Vybrant-positive population was selected for the OMV containing macrophages. Populations were sorted into tubes containing 2 ml of PBS + 10% FBS as a cushion. After sorting, cells were centrifuged and resuspended in 100 to 500 µl of PBS + 10 % FBS. Cell viability and cell count were determined by Countess Automated Cell Counter (Thermo Fisher Scientific, Waltham, MA, USA). Eighty percent cell viability and more than 50,000 cells were processed for scRNA-seqRNA-seq library preparation. Experiment was performed in three biological replicates.

### *3.4.4.2* 10x genomics library preparation

After verifying the quality of the single-cell suspension, Chromium Next GEM Single-cell 3' v3.1 Gene Expression kits were used to prepare the single-cell RNA-seq libraries by following the manufacturer's instructions. Cell concentrations were adjusted for a target recovery of 10,000 cells, and samples were sequenced with a depth of 50,000 reads per cell.

#### 3.4.4.2.1 Gel Bead-in-Emulsion (GEM) preparation

First, we prepared a master mix for the RT using the manual instructions, which is then mixed with the cell suspension. The final mixture is added into Next GEM Chip together with barcoded gel beads along with partitioning oil. while running the chip on the Chromium machine, this produces an emulsion in which every gel bead carrying a cell and the RT master mix. The GEMs are transferred to strip tubes in which the reverse transcription is carried out using a thermal cycler.

#### 3.4.4.2.2 Post-GEM-RT clean-up and amplification of cDNA

In the previous, first-strand cDNA was generated from the captured mRNA, with each cDNA molecule labelled by a unique cell-specific barcode. The emulsion was then broken and the remainder of the assay was continued as a typical Illumina library prep. Barcoded cDNA was extracted from the broken emulsion and purified on Dynabeads. Next this cleaned first strand cDNA was amplified using the primer sites of Template Switch Oligo and Read 1 adapter. The number of PCR cycles of amplification was adjusted based on the targeted cell recovery (11 cycles for >6000 cells recovery). Upon PCR completion, SPRI-select magnetic beads were used to purify the product. Finally, the prepared cDNA QC was performed by Qubit.

#### 3.4.4.2.3 **Library preparation and sequencing**

Library preparation included enzymatic fragmentation to decrease fragment sizes, then end repair and A-tailing. Subsequently, a Read 2 adapter is ligated to the A-tailed fragments, permitting the i5 and i7 sample indices and the P5 and P7 adapter sequences to be added during the final PCR step of the Single-cell Gene Expression library construction. Prior to sequencing library QC was performed by Agilent bioanalyzer.

#### *3.4.4.2.4* **Data Analysis**

An open-access Linux-based analysis pipeline named Cell Ranger was used for the QC of sequenced data. Cell Ranger was downloaded and installed from 10x Genomics support web-page and is meant for data from the Chromium Single-cell Gene Expression assay. Details on how this pipeline work is provided at the website of 10x genomics (https://support.10xgenomics.com/). After obtaining FASTQ files, Cell Ranger was also used for genome mapping and gene counting. Sequenced reads were aligned to the hg38 (Homo sapiens) reference genome.

Filtered barcode matrices obtained by Cell Ranger were used for the downstream analysis in R. For data quality purposes, cells that expressed less than 500 genes, had a low UMI per gene ratio (below 0.8), or contained more than 10% mitochondrial gene content were filtered out. Normalization and were performed through the sctransform R package (version 0.2.1). Following this transformation, samples were integrated using a rescaled integration workflow in Seurat in which Pearson residuals are harmonized across datasets. PCA was then applied to the expression matrices to reduce the dimensionality. For downstream analysis, 30 principal components were chosen, and UMAP was performed for additional dimension reduction and visualization.

Cell clusters were identified using Seurat's graph-based clustering algorithm (FindCluster function) at a specific resolution scale (0.2, 0.4, 0.6, 0.8, and 1.0) to separate transcriptionally distinct populations of resident peritoneal cells. Clusters with high cell cycle scores were excluded from further analysis. Cell types were objectively assigned using the SingleR package (version 1.0.5). Differential gene expression analysis was performed using the MASTtest and FindMarkers present in the Seurat package. For cluster-specific gene expression, each macrophage was compared with all other macrophage clusters together. Further DE analyses were performed among clusters, and between treated and untreated groups.

The gProfiler app was used to describe the enriched molecular pathways between differentially expressed genes. Gene Ontology (GO) and the Kyoto Encyclopedia of Genes and Genomes (KEGG) were used to define gene sets in the analysis. GO enrichment analyses were visualized by GO plot (1.0.2). Data analysis work flow is provided in Figure 3.4.

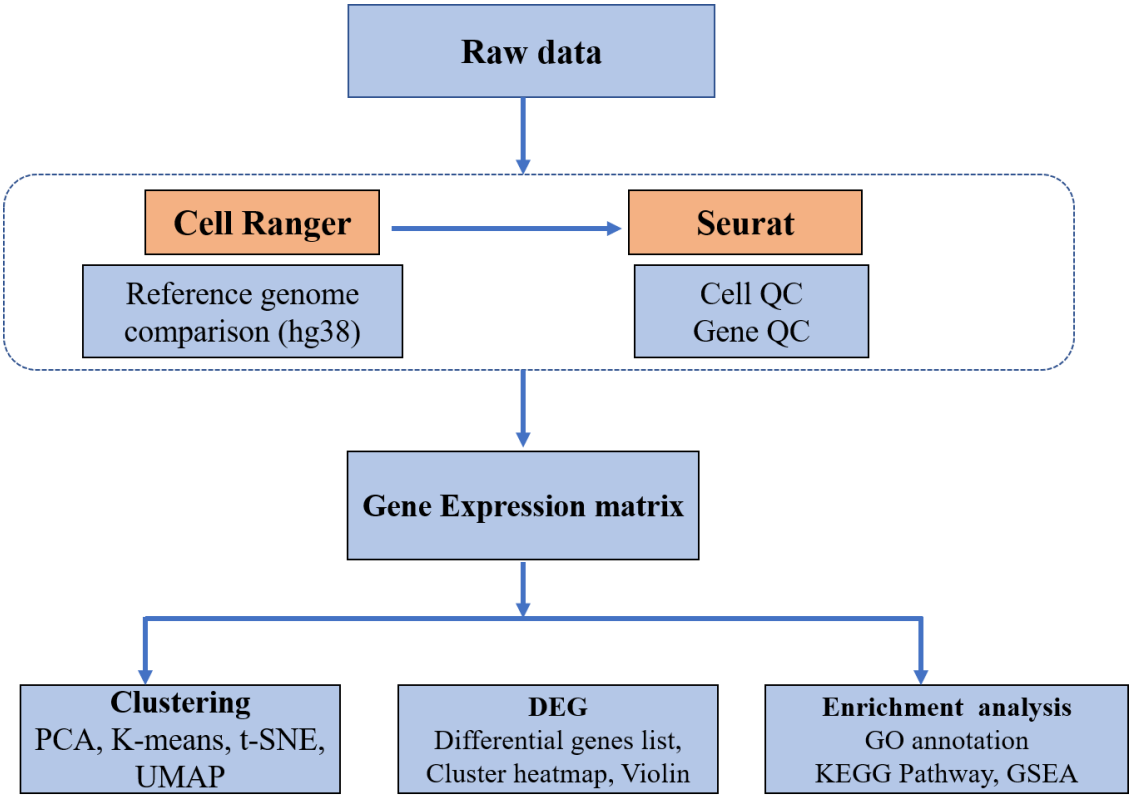


**Figure 3.4: Overview of ScRNA-seq data analysis**

Raw sequencing data were processed using Cell Ranger for reference genome comparison (hg38) and Seurat for cell and gene quality control (QC). The resulting gene expression matrix was subjected to downstream analyses including clustering (PCA, K-means, t-SNE, UMAP), differential gene expression (DEG) analysis (differential gene lists, cluster heatmaps, violin plots), and enrichment analysis (GO annotation, KEGG pathway, GSEA)

### 3.4.5 Cytokine array analysis

Differentiated macrophages were stimulated with *L. pneumophila* derived OMVs. For OMV stimulation, OMVs were added with increasing concentrations (1, 10, and 20 μg/ml) or left untreated, in triplicate and incubated at 37°C in a humidified incubator (5% $CO_2$) for 24 and 48 hours. At 24 and 48 time points, supernatants were collected and centrifuged from three biological replicates.

The Proteome Profiler Array (Human XL cytokine array kit ARY022B) was performed according to the manufacturer's instructions to assess the cytokines/chemokines in collected supernatants. Dot blots were visualized by the ChemiDoc imaging system. Signal intensities were measured by Quick Spots Image Analysis Software. Normalization was done by subtracting the intensity of the negative control reference spot from the intensities of the growth factors. The average intensity of the triplicated is calculated. $Log_2$ fold expression was determined for graphical representation in R. Cytokines with signal intensities 1.5-fold higher or lower than those of the untreated group were considered significantly expressed. Proteome Profiler Array Map Shown in Figure 3.5.

| | 1 | 2 | 3 | 4 | 5 | 6 | 7 | 8 | 9 | 10 | 11 | 12 | 13 | 14 | 15 | 16 | 17 | 18 | 19 | 20 | 21 | 22 | 23 | 24 |
|---|---|---|---|---|---|---|---|---|---|---|---|---|---|---|---|---|---|---|---|---|---|---|---|---|
| A | Reference spots | | Adiponectin | | Apolipoprotein A-I | | Angiogenin | | Angiopoietin-1 | | Angiopoietin-2 | | BAFF | | BDNF | | Complement Component C5/C5a | | CD14 | | CD30 | | Reference SpotS | |
| B | - | | CD40 ligand | | Chitinase 3-like 1 | | Complement Factor D | | C-Reactive Protein | | Cripto-1 | | Cystatin C | | Dkk-1 | | DPPIV | | EGF | | EMMPRIN | | - | |
| C | - | | ENA-78 | | Endoglin | | Fas Ligand | | FGF basic | | FGF-7 | | FGF-19 | | Flt-3 Ligand | | G-CSF | | GDF-15 | | GM-CSF | | - | |
| D | GROα | | Growth Hormone | | HGF | | ICAM-1 | | IFN-γ | | IGFBP-2 | | IGFBP-3 | | IL-1α | | IL-1β | | IL-1ra | | IL-2 | | IL-3 | |
| E | IL-4 | | IL-5 | | IL-6 | | IL-8 | | IL-10 | | IL-11 | | IL-12 p70 | | IL-13 | | IL-15 | | IL-16 | | IL-17A | | IL-18 Bpa | |
| F | IL-19 | | IL-22 | | IL-23 | | IL-24 | | IL-27 | | IL-31 | | IL-32 | | IL-33 | | IL-34 | | IP-10 | | I-TAC | | Kallikrein 3 | |
| G | Leptin | | LIF | | Lipocalin-2 | | MCP-1 | | MCP-3 | | M-CSF | | MIF | | MIG | | MIP-1/MIP-1β | | MIP-3α | | MIP-3β | | MMP-9 | |
| H | Myeloperoxidase | | Osteopontin | | PDGF-AA | | PDGF-AB/BB | | Pentraxin 3 | | PF4 | | RAGE | | RANTES | | RBP-4 | | Relaxin-2 | | Resistin | | SDF-1α | |
| I | Serpin E1 | | SHBG | | ST2 | | TARC | | TFF3 | | TfR | | TGF-α | | Thrombospondin-1 | | TNF-α | | uPAR | | VEGF | | Reference Spots | |
| J | Reference spots | | - | | Vitamin D BP | | CD31 | | TIM-3 | | VCAM-1 | | - | | - | | - | | - | | - | | Negative Controls | |

**Figure 3.5: Human XL Cytokine array kit map**

Full map of 105 cytokines is shown with three reference spots and one negative control spot labelled on the kit membrane.

#### *3.4.5.1* Pathway analysis by IPA

For the pathway analysis, the IPA system (IPA, QIAGEN Inc., Redwood City, CA, USA; www.qiagen.com/ingenuity) was used, which describes the enriched pathways and their functions in the query data.

Using cytokine array data, canonical pathways, diseases, and functions were analyzed. Based on 7 million published data points in the Ingenuity Knowledge Base, IPA uses network algorithms, built-in QC, and calculates a score for each network (Calvano et al., 2005; Irizarry et al., 2003). Fisher's exact test at the right tail is employed to determine the negative logarithm of the significance threshold. Z-score >2 is considered the threshold of activation, Z-score <−2 as the threshold of significant inhibition, and log (P-value) >2 as the threshold for the association with canonical pathway analysis, disease, and function.

### *3.4.6* RNA isolation and two-step RT-quantitative PCR

#### *3.4.6.1* RNA isolation:

THP-1 cells were seeded in a 6-well plate (Corning, NY, USA) at 1 × $10^6$ cells/ml and differentiated into macrophages with PMA as described earlier. Cells were incubated with increasing concentrations of OMVs (1, 10, and 20 µg/ml) or left untreated, in triplicate, in a humidified incubator at 37°C for 24 hours. RNA extraction was performed by the PureLink RNA Mini Kit (Thermo Scientific, Waltham, MA, USA). Briefly, 2-Mercaptoethanol was added to the kit-provided lysis buffer. 0.3 ml of this prepared lysis buffer was added to each well containing cells. Next, the 0.3 ml lysate containing cells was passed through a 21-gauge syringe (Terumo) 5 to 10 times to homogenize the cells. The homogenate was centrifuged for 5 minutes, and the supernatant was transferred to new tubes. According to the kit instructions, 70% ethanol was added to the homogenate, and the mixture was then passed through a spin cartridge column. After centrifugation at 12,000 ×*g* for 15 s, the flow-through was discarded,

followed by washing with Wash Buffer I and Wash Buffer II. Finally, the RNA in the Spin Cartridge was eluted in 50 µl of RNase-free water. RNA concentrations were measured by both Nanodrop and Qubit. Nanodrop was used to check RNA purity (A260/280). RNA was stored at -80°C before use

#### *3.4.6.2* cDNA synthesis:

For the preparation of cDNA from RNA, HiScript IV RT supermix kit (Vazyme: R423) was used. A constant amount of RNA (800 ng) was used to convert into cDNA for all samples.

1. Genomic DNA was removed by the gDNA wiper mix provided by the kit. In the reaction tube RNase-free dd$H_2O$ was added to a final volume of 15 µl with 3 µl of 5× gDNA wiper mix, and finally 800 ng of template RNA was added (volume adjusted accordingly). Mixtures were gently pipetted and incubated at 42°C for two minutes.
2. DNA-digested RNA samples were then reverse transcribed. 5 µl of 4 x HiScript IV Supermix was added to the mixture obtained from step 1 and incubated at 37°C for 15 min followed by incubation at 85°C for 5 sec. The same mixture was also prepared and incubated with a No-RT Control Mix.

#### *3.4.6.3* Quantitative real-time PCR analysis:

Real-time PCR was performed in a 20-µl reaction volume consisting of 1 µl of cDNA, 2 × Taq Pro Universal SYBR Green qPCR Master mix (Vazyme, Cat# Q712-02; Vazyme Biotech Co., Ltd., Nanjing, China), and 10 µM of each forward and reverse primer synthesized by Tech Dragon Limited (Hong Kong, China). Primers details are given in Table 3.1. The PCR was carried out on Roche LC96 thermocycler.

The thermal cycler program used for PCR consisted of 10 minutes of initial denaturation at 95°C, followed by 40 cycles of denaturation at 95°C for 30 seconds and annealing at 60°C for

1 minute. For reactions, melting curve analysis was performed to verify the specificity of the PCR products. CT values for the target genes were normalized with the reference (housekeeping) gene. Gene expression levels of targets were normalized relative to their expression of untreated samples.

For each sample, the ΔCt value was calculated as follows:

$\Delta Ct = Ct\ (target\ gene) - Ct\ (reference\ gene)$

To compare gene expression between treated and untreated groups, the ΔΔCt value was calculated:

$\Delta\Delta Ct = \Delta Ct\ (experimental) - \Delta Ct\ (control)$

The relative expression level (fold change) of the target gene was then determined using the formula:

$Fold\ change = 2^{-\Delta\Delta Ct}$

Primers were designed according to the marker genes of each macrophage subset.

**Table 3.1 Primers used in this study:**

Primers were designed by the online Primer-BLAST tool provided by NCBI

| Genes | Primers | Primer sequence (5'-3') | Amplicon size (bp) |
|---|---|---|---|
| TNF | TNF F | GAGGCCAAGCCCTGGTATG | 19 |
| | TNF R | CGGGCCGATTGATCTCAGC | 19 |
| IL12 | IL12 F | CCTTGCACTTCTGAAGAGATTGA | 23 |
| | IL12 R | ACAGGGCCATCATAAAAGAGGT | 22 |
| CCL2 | CCL2 F | CAGCCAGATGCAATCAATGCC | 21 |
| | CCL2 R | TGGAATCCTGAACCCACTTCT | 21 |
| IL4 | IL4 F | CCAACTGCTTCCCCCTCTG | 19 |
| | IL4 R | TCTGTTACGGTCAACTCGGTG | 21 |
| IL10 | IL10 F | TCAAGGCGCATGTGAACTCC | 20 |
| | IL10 R | GATGTCAAACTCACTCATGGCT | 22 |
| TGFβ | TGFβ F | GGCCAGATCCTGTCCAAGC | 19 |
| | TGFβ R | GTGGGTTTCCACCATTAGCAC | 21 |
| NOS2 | NOS2 F | AGGGACAAGCCTACCCCTC | 19 |
| | NOS2 R | CTCATCTCCCGTCAGTTGGT | 20 |
| ARG1 | ARG1 F | GGCAAGGTGATGGAAGAAAC | 20 |
| | ARG1 R | AGTCCGAAACAAGCCAAGGT | 20 |
| IL1β | IL1β F | ATGATGGCTTATTACAGTGGCAA | 23 |
| | IL1β R | GTCGGAGATTCGTAGCTGGA | 20 |
| SOD2 | SOD2 F | CACTGCAAGGAACAACAGGC | 20 |
| | SOD2 R | ACCAGGCTTGATGCACATCTT | 21 |
| IL6 | IL6 F | TGCAATAACCACCCCTGACC | 20 |
| | IL6 R | GTGCCCATGCTACATTTGCC | 20 |
| CCL4 | CCL4 F | AAGCTCTGCGTGACTGTCCTGT | 22 |
| | CCL4 R | AAGCTTCCTCGCGGTGTAAGA | 21 |
| VEGF | VEGFA F | AGGGCAGAATCATCACGAAGT | 21 |
| | VEGFA R | AGGGTCTCGATTGGATGGCA | 20 |
| GAPDH | GAPDH F | GTGAAGGTCGGTGTCAACGGATTT | 24 |
| | GAPDH R | CACAGTCTTCTGAGTGGCAGTGAT | 24 |

### 3.4.7 Flow cytometry for macrophage cell surface markers

THP-1 cells were differentiated into macrophages by PMA treatment as described earlier. Cells were incubated with increasing concentrations of OMVs (1, 10, and 20 µg/ml) or left untreated (control). The procedures were performed in triplicate. the cells were incubated in a humidified incubator at 37°C for 24 hours. Macrophage cell surface markers were analyzed by flow cytometry using PE anti-human CD163, APC anti-human CD11b, FITC anti-human CD86, and Brilliant Violet 421 anti-human CD68 (all from BioLegend, San Diego, CA, USA). The Staining process was carried out according to the cell-surface staining protocol provided by the manufacturer. Before staining, macrophages were detached and rinsed twice with cell staining buffer (BioLegend, San Diego, CA, USA). To reduce non-specific reagent binding, Fc receptors were blocked by Human TruStain FcX™ (Fc Receptor Blocking Solution, BioLegend, San Diego, CA, USA). Resuspended cells were split into four separate tubes and respective fluorescent-labelled antibodies were added and incubated for 15 to 20 minutes in the dark on ice. Next, cells were washed with cell staining buffer, 1 µl of 7-AAD cell viability stain was added for 3 to 5 minutes, and FC analysis was performed using FACSAria III using all five in-built lasers.

### 3.4.8 Cytotoxicity assay by MTT

THP-1 cells were differentiated to macrophages by PMA treatment as described earlier. Cells were incubated with increasing concentrations of OMVs (1, 10, and 20 µg/ml) or left untreated in triplicate in a humidified incubator at 37°C for 24 hours. Then, 10 µl of MTT reagent (thiazolyl blue tetrazolium bromide, 5 mg/ml) was added to the cells. After two hours of incubation, MTT-containing medium was replaced with Dimethyl Sulfoxide (DMSO), and absorbance was measured after gentle shaking at 570 nm.

### 3.4.9 Pyroptosis assay

For the analysis of pyroptosis, the Caspase-1 staining kit (Abcam, Cambridge, UK) was used according to the manufacturer's instructions. THP-1 cells were differentiated into macrophages through PMA treatment as described earlier, but in 96-well, clear, flat-bottom, black colored Tissue culture-treated plates. Cells were incubated with increasing concentrations of OMVs (1, 10, and 20 μg/ml) or left untreated, in triplicate, and maintained in a humidified incubator at 37°C for 24 hours. Cells were then washed twice with the washing buffer provided by the kit. Next, 150 μl of washing buffer was added to the cells, along with 1 μl of stain solution, and incubated for 1 hour at 37°C with 5% $CO_2$, protected from light. Cells were washed to remove unbound stain. Fluorescence intensity was measured by a Thermo Scientific Varioskan LUX Multimode Microplate Reader at Ex/Em 490/525 in fluorescence mode. For the data analysis, blank readings were subtracted from all control and treated readings, and fold change was determined between the control and OMV treated group using fluorescence intensity value.

### 3.4.10 ROS assay

The Abcam Cellular Reactive Oxygen Species (Abcam, Cambridge, UK) kit was used to estimate the intracellular reactive oxygen species using the manufacturer's instructions. THP-1 cells were differentiated into macrophages through PMA treatment as described earlier, but in 96-well, clear, flat-bottom, black tissue culture-treated plates. Cells were incubated with increasing concentrations of OMVs (1, 10, and 20 μg/ml) or left untreated, in triplicate and maintained in a humidified incubator at 37°C for 24 hours. Then, the ROS working solution was added at 100 μl/well, and the plate was incubated for 1 hour at 37°C with 5% CO2, in the dark. Positive control was treated with 1 mM H2O2 for additional 30 minutes. Fluorescence intensity was measured by Thermo Scientific Varioskan LUX Multimode Microplate Reader at Ex/Em 520/605 in fluorescence mode. For the data analysis, blank readings were subtracted from all control and treated readings, and fold change was determined between the control and

OMV treated group using the fluorescence intensity values.

### 3.4.11 Impact of OMVs on *L. pneumophila* survival and replication within Host Cell

To determine the effect of OMVs on the invasion efficiency of *L. pneumophila* in host cells, a standardized infection assay was conducted. THP-1 cells were differentiated into macrophages by PMA treatment as described earlier in a 6-well plate. Macrophages were pre-treated with increasing concentrations of OMVs (1, 10, and 20 μg/ml) or left untreated, in triplicate, and incubated at 37°C in a humidified incubator (5% $CO_2$) for 24 hours. After this pre-incubation period, cells were washed twice with PBS and cultured in an antibiotic-free medium (RPMI 1640 only). *L. pneumophila* subcultures were grown to post-exponential phase, harvested by centrifugation, and resuspended in PBS.

Now, *L. pneumophila* was added to the host cell monolayers at a multiplicity of infection (MOI) of 10 after incubation for 1 h at 37°C in a humidified $CO_2$ incubator. For the negative control, the bacteria were added to cells not pre-treated with OMVs under the same conditions. After 1hour, extracellular bacteria were removed by washing the monolayer of cells three times with PBS, and the medium was replaced with fresh medium supplemented with 100 μg/ml gentamicin for an additional 1 hour. Cells were then washed once more with PBS and incubated for 24 hours. After 24 hours, cells were detached and lysed by passing the cells through a 21-gauge syringe needle (Terumo, Tokyo, Japan) 10 times to release intracellular bacteria. The lysates were 10-fold serially diluted and spread on BCYE agar plates in colony-forming units (CFUs). Replication of *L. pneumophila* within host cells was determined based on comparison of the number of intracellular bacteria in OMV treated versus untreated groups. Each experiment was repeated in triplicate and the results were presented as the mean ± SEM.

### 3.4.12 Statistical analysis

All the data are presented as means ± SEM and analyzed by GraphPad Prism version 7.02. Graphs and bars were also plotted by using Prism. For comparing two independent groups, the unpaired t-test was used for parametric data and the Mann-Whitney test for non-parametric data. For statistical analyses involving multiple groups (i.e., fold changes, absorbance values, and flow cytometry percentages), a paired t-test or the Wilcoxon signed-rank test was performed. P values less than 0.05 were considered significant. For bivariable or multivariable grouped data, two-way ANOVA with Sidak's post-hoc tests was employed. Data collected from cytometry were analyzed using FlowJo Software version 7.

### 3.4.13 Data reliability

All experiments were performed in 3 biological replicates. For both the *L. pneumophila* ATCC strain and THP-1 cells, experiments were performed in triplicate using three different stock Additionally, a control was included for each experiment.

# Chapter 4. Results

## 4.1. Isolation and molecular characterization of *L. pneumophila* OMVs

### 4.1.1. Growth kinetics and viability of *L. pneumophila* in growth media

Before OMV isolation, the growth curve and viability of *L. pneumophila* were determined. For growth curves, both the optical density and CFU count methods were used, with measurements taken every 12 hours for four days. The bacterial density continued to increase linearly from 0 to 60 h, then entered a stationary phase between 60 and 72 h, corresponding to the onset of the post-exponential phase. The OD decreased at 96 h, indicating the onset of the decline phase (Figure 4.1A). For the CFU count, a similar growth pattern was found, as shown in Figure 4.1B. Bacterial growth increased until 60 h, then stayed in a stationary phase until 72 h, followed by a decline phase around 96 h.

The LDH assay was used to estimate cell death in broth media every 24 hours, in conjunction with the growth curve. LDH leakage is directly proportional to the estimation of bacterial cell death. Results were consistent with the growth curves. At 96 h, LDH leakage was observed, increasing from 0.5% to 7%, indicating the onset of the decline phase (Figure 4.1C). LDH release was measured for up to 114 hours to evaluate cell damage during the bacterial decline phase, which occurs after the stationary phase and might not be fully captured within the first 96 hours.

Based on the growth curve and colony morphology on BYCE agar plates, *L. pneumophila* was allowed to grow for three days before OMV isolation.

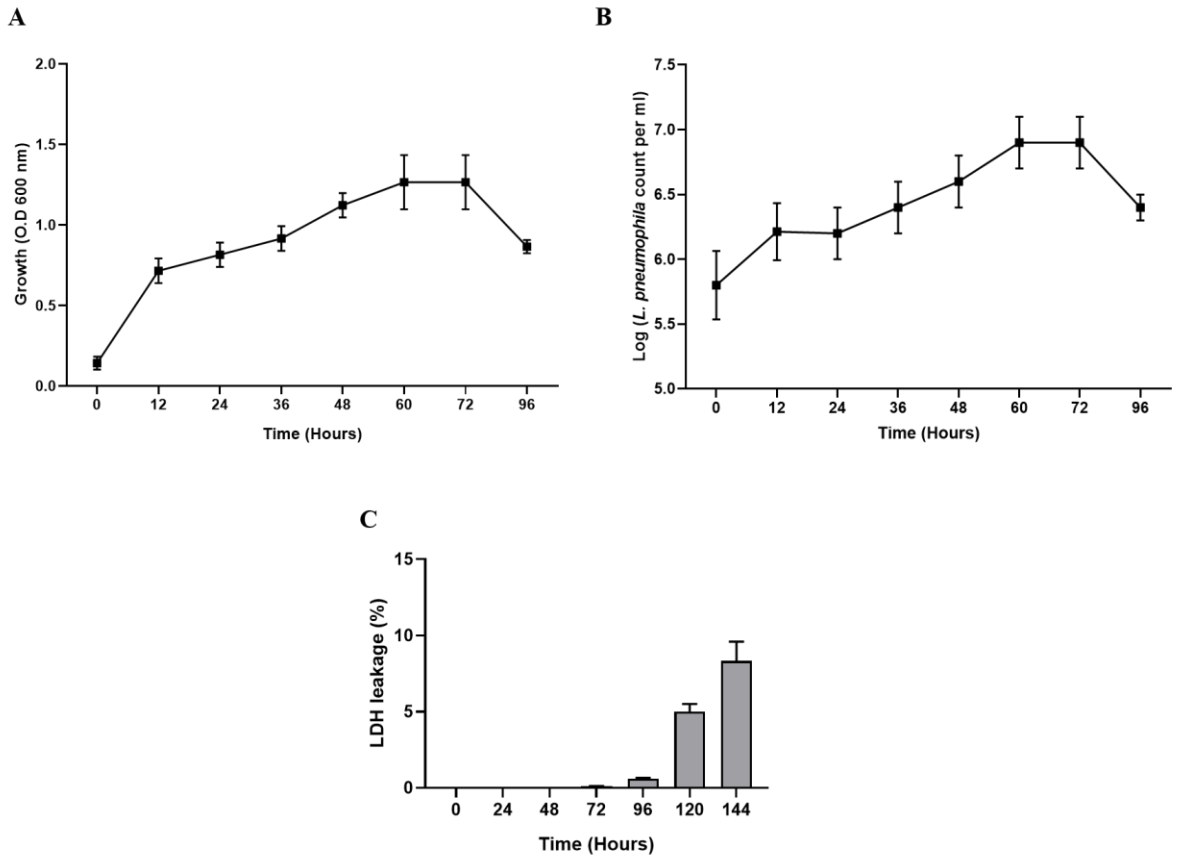


**Figure 4.1: Growth assay and cell death assay.**

**(**A) Growth curve of *L. pneumophila* assessed by optical density at 600 nm (O.D. 600 nm) during 96 hours. Cellular growth exhibits a steady increase, reaching maximum growth between 60 and 72 hours, followed by a decline phase at 96 hours. Data are shown as mean ± SEM (n=3). (B) Growth of *L. pneumophila* was quantified as log CFU per ml, at 0, 12, 24, 36, 48, 60, 72, and 96 hours. Data are shown as mean ± SEM (n=3). (C) Percentage of lactate dehydrogenase (LDH) leakage, assessed from 0 to 144 hours. Minimal cytotoxicity is seen up to 96 hours, with a significant increase at 120 and 144 hours, indicating death or the decline stage. Data are shown as mean with SD (n=3).

### 4.1.2. Isolation of *L. pneumophila* OMVs

The protocol for isolating membrane vesicles from bacteria was established long ago by Meta Kuehn in 2000 (Horstman & Kuehn, 2000), and previous studies have widely employed liquid cultures for this purpose. In this project, we adapted a more efficient vesicle isolation protocol using agar media instead of broth cultures, as this method avoids the challenges of handling large volumes (500-1000 ml) of broth for centrifugation. With the agar plate method, we can scrape growth from 20 to 40 plates, resuspend it in only 20 ml of media, and process it faster (Reis et al., 2019). Notably, the goal for both protocols is to collect the cell-free fraction from cultures for ultracentrifugation and final vesicle sedimentation, which is more effectively achieved with solid agar plates. Additionally, solid media reduces contamination from media components, as only bacterial growth is collected for subsequent EV purification. Detailed protocol can be found in the Materials and Methods section 3.3.2.

#### 4.1.2.1. SEV gives a higher yield of *L. pneumophila* OMVs compared to DEG

Both DEG (OptiPrep iodixanol) and SEC (qEV1 columns) methods were compared for OMVs purity and quantity. Using TEM, the extracted crude OMV sample contained a spherical vesicle population, but also showed obvious impurities, including membrane fragments, proteins, and flagella-like structures (Figure 4.2A). However, after purification using both methods, TEM revealed significantly cleaner images with fewer impurities, and vesicles appeared as double-membranous, well-separated spheres, exhibiting a heterogeneous OMV population. Although TEM was performed for all the fractions obtained by DEG and SEC, representative images from enriched OMV fractions are shown here (Figure 4.2B and 4.2C). Other fractions were devoid of OMVs or show contaminants (Figure 4.2D). Both purification methods yielded higher purity in the OMV fractions than simple ultracentrifugation of crude OMVs. TEM investigation also revealed the absence of bacterial debris, flagella, and proteins, indicating that both protocols were equally efficient in terms of purity.

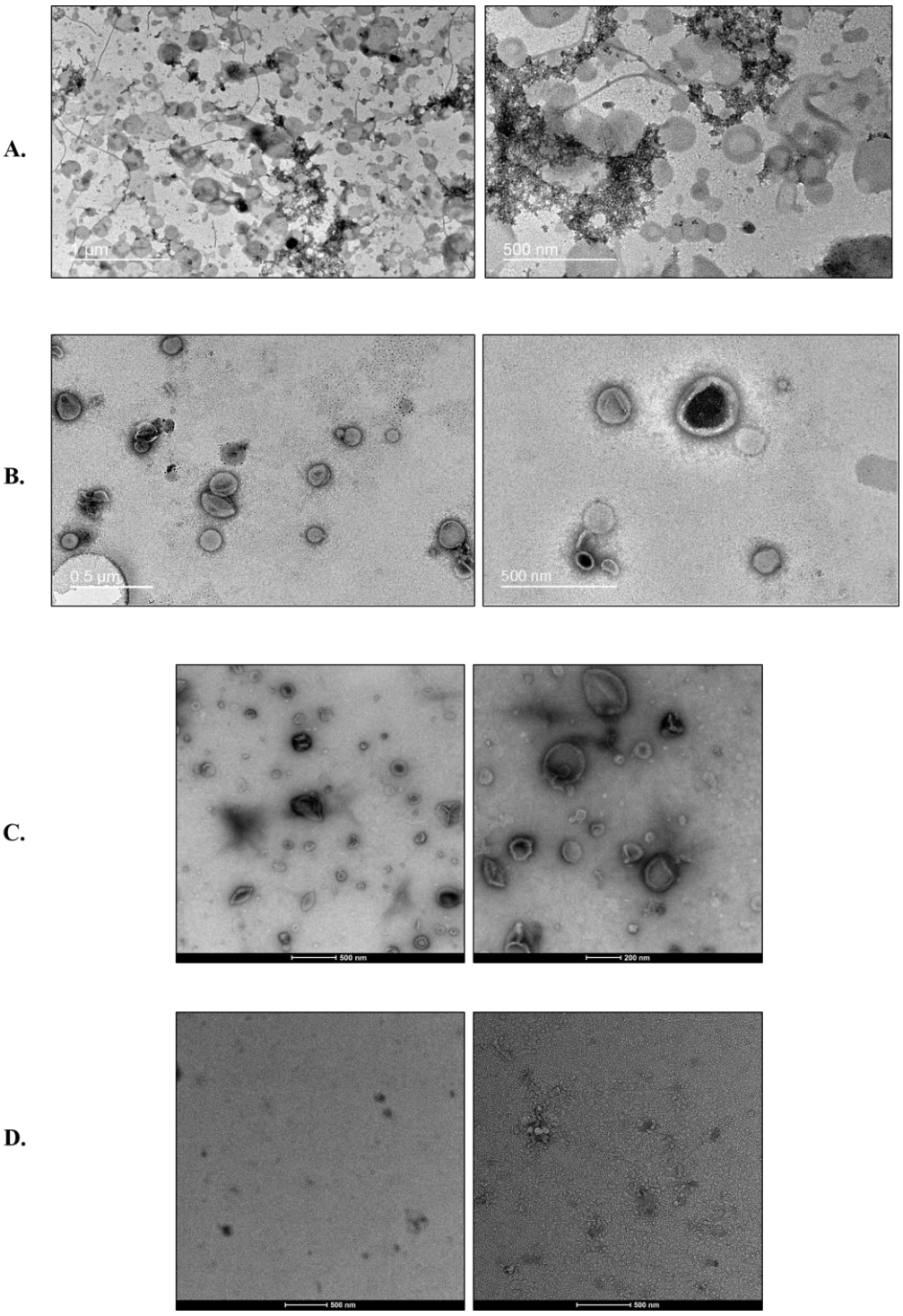


**Figure 4.2: TEM examination of *L. pneumophila* OMVs isolated by UC and purified by DEG and SEC.**

(A) Representative TEM images of crude OMVs after UC showing some debris, flagella, and contaminant proteins. (B) and (C) Representative TEM images of the purified OMVs by the DEG and SEC method, respectively. Spherical, double-membranous structures of varying sizes are OMVs. (D) OMVs were found in only a few fractions per batch; the remaining fractions were devoid of vesicles and contained a small (dots) protein-like structure, indicating the presence of contaminants. Bar size: 500 nm.

Next, the two purification methods were also compared for OMVs size distribution and yield using NTA (Malvern Panalytical Ltd., Malvern, UK). The NTA measurement of bacterial vesicles isolated using DEG and the SEC method is presented in Table 4.1. The data demonstrated substantial variation in mean particle sizes and concentrations among the fractions recovered by each method.

The particle size range for the SEC method is 127.1-232.9 nm. This high variation indicates that the DEG procedure generates a size-heterogeneous population of vesicles. In comparison, the SEC approach provides a narrower size range (131.2 nm to 175.4 nm), with the average particle size around 131.2 nm for the corresponding fractions. This suggests that the SEC may be better suited to a more homogeneous sample for downstream applications based on the objective. Furthermore, for DEG, fractions 4-6 contain enriched OMVs, while for SEC, fractions 1-3 contain enriched OMVs.

The differences between the two methods are also highly evident in particle concentration data. For the DEG fractions, particle concentration varies considerably, with a maximum of $6.31 \times 10^{12}$ particles/ml in fraction 5. In contrast, the SEC method shows the highest particle concentration, $3.59 \times 10^{13}$ particles/ml in fraction 2, which is 5.69 times higher than the most enriched fraction of DEG ($6.31 \times 10^{12}$ particles/ml). These results revealed that although vesicle distribution across fractions differs substantially between the two methods, the OMV yield and homogeneity are higher with the SEC method.

These findings also reveal the need to choose the appropriate isolation method based on the specific needs of downstream applications, as the extraction protocol may significantly affect the properties of the isolated vesicle populations.

**Table 4.1: Comparison of OMVs size and concentration among fractions obtained from DEG and SEC methods.**

| Fractions | DEG | | SEC | |
|---|---|---|---|---|
| | **Mean particle size** | **Particle concentration** | **Mean particle size** | **Particle concentration** |
| 1 | 189.1 | $6.34 \times 10^{8}$ | 175.0 | $1.70 \times 10^{12}$ |
| 2 | 189.8 | $3.32 \times 10^{10}$ | 133.1 | $3.59 \times 10^{13}$ |
| 3 | 232.9 | $3.37 \times 10^{9}$ | 154.9 | $5.20 \times 10^{12}$ |
| 4 | 136.8 | $2.06 \times 10^{12}$ | 166.6 | $2.55 \times 10^{12}$ |
| 5 | 127.1 | $6.31 \times 10^{12}$ | 175.4 | $1.63 \times 10^{10}$ |
| 6 | 148.7 | $1.94 \times 10^{12}$ | 143.7 | $6.88 \times 10^{11}$ |
| 7 | 153.4 | $6.90 \times 10^{11}$ | - | - |
| 8 | - | - | 167.3 | $6.52 \times 10^{10}$ |
| 9 | - | - | - | - |
| 10 | 95.0 | $3.32 \times 10^{12}$ | 131.2 | $1.92 \times 10^{10}$ |

Furthermore, Qubit fluorometric assay for detecting total vesicle-associated protein, DNA, and RNA showed that SEC purified OMVs contained higher concentrations of protein, DNA, and RNA than DEG purified OMVs at equivalent initial volumes (Figure 4.3).

Collectively, the results show that the vesicle quality obtained with either purification procedure was superior to that of crude OMVs; however, purification by SEC yielded the purest vesicle preparation with the highest yield. As a result, the SEC purified OMVs enriched fractions from 1-4 were pooled and used for downstream molecular characterization and functional studies of OMVs.

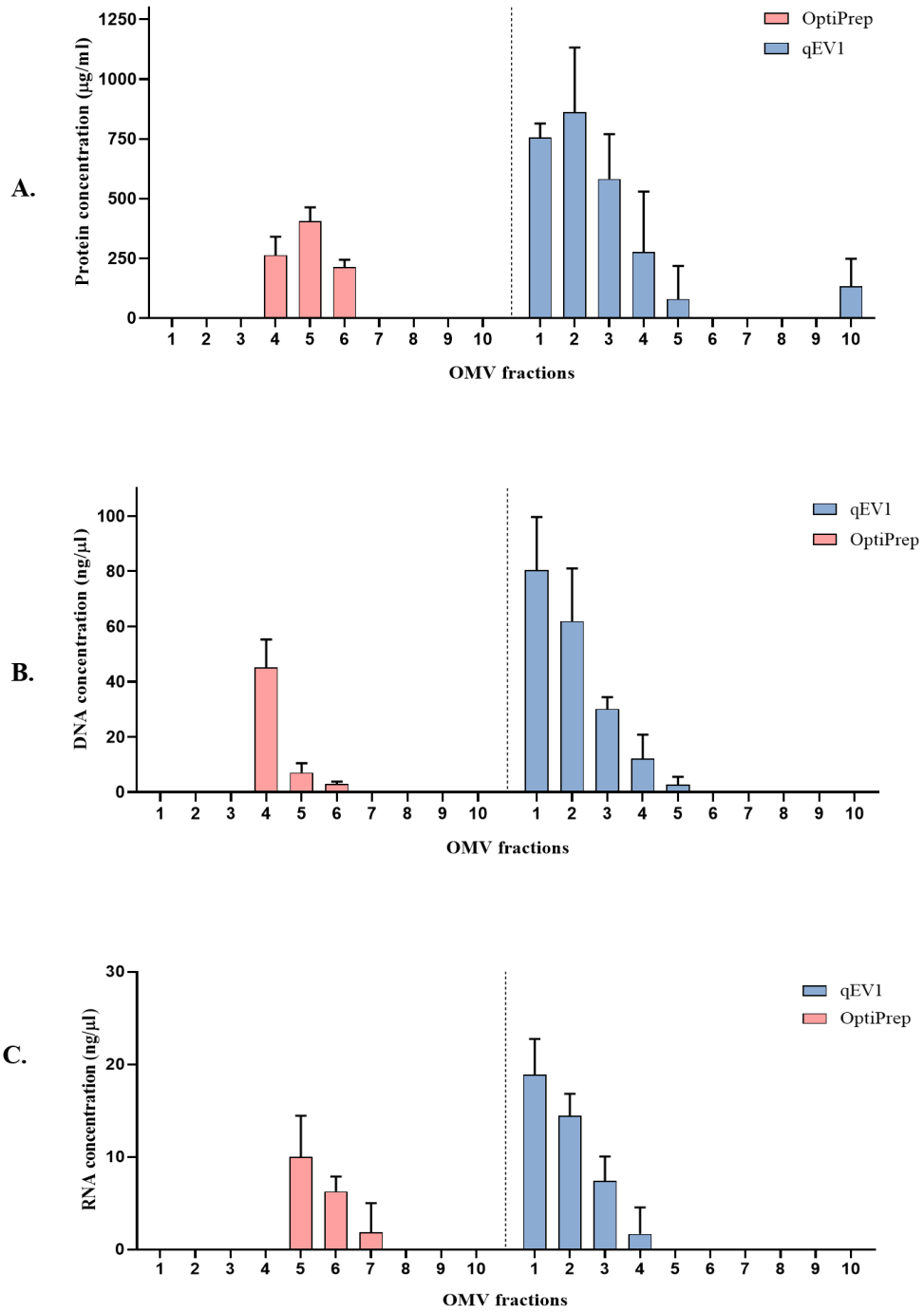


**Figure 4.3: Qubit estimation of fractions of OMVs purified using qEV1 and OptiPrep techniques.** (A) Protein concentration (B), DNA concentration, and (C) RNA concentration quantified by Qubit assay in each of the 10 fractions derived from qEV1 (blue bars) and OptiPrep (red bars) isolation techniques.

### 4.1.3. Molecular Characterization of *L. pneumophila* OMVs:

#### 4.1.3.1. LPS estimation

Quantifying the LPS content in OMVs is crucial for understanding their immunogenicity and biological activity, as LPS mediates binding and ligation via TLR signalling pathways. Relative amounts of LPS in *L. pneumophila* OMVs were determined by comparing to a PBS negative control. The results provide evidence for the presence of LPS in the OMVs, at approximately 1.3 endotoxin units (EU) per milliliter (Figure 4.4).

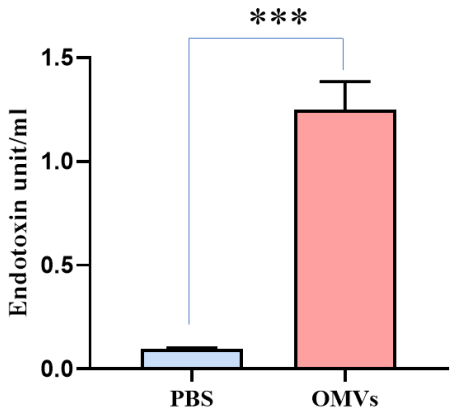


**Figure 4.4: LPS detection in *L. pneumophila* OMVs.**
The quantification of endotoxin units (EU) indicated that OMVs contain roughly 1.3 EU, while the PBS control exhibits minimal endotoxin levels, effectively zero. Data are provided as mean values from triplicate measurements. Bars indicate mean ± standard deviation (SD) of n=3, and statistical significance was evaluated using a unpaired t-test (***p-value < 0.001).

### 4.1.3.2. Proteomic and virulome profile of *L. pneumophila* OMVs

To examine the global proteome profile of OMVs, the protein constituents of OMVs from three biological replicates of *L. pneumophila* were visualized using SDS-PAGE (Figure 4.5). SDS-PAGE, stained with silver, identified many distinct bands with a similar pattern across all OMV replicates. The versatility in band location and thickness indicated distinct vesicle protein compositions in OMVs from each replicate. The predominant proteins in all OMV samples were identified at around 20 and 50 kDa.

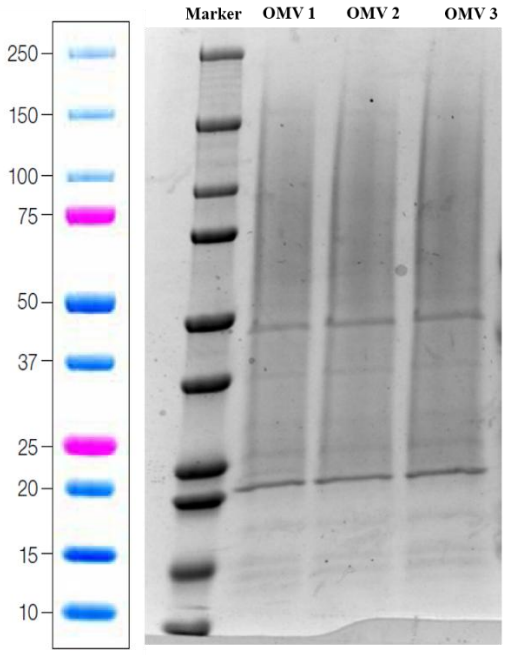


**Figure 4.5: SDS-PAGE analysis of three OMV replicates.**
Representative gel picture showing protein profiles of three distinct OMV replicates. Several protein bands are consistently detected across all samples. Prominent dense bands are seen at the 20-kDa and 50-kDa positions.

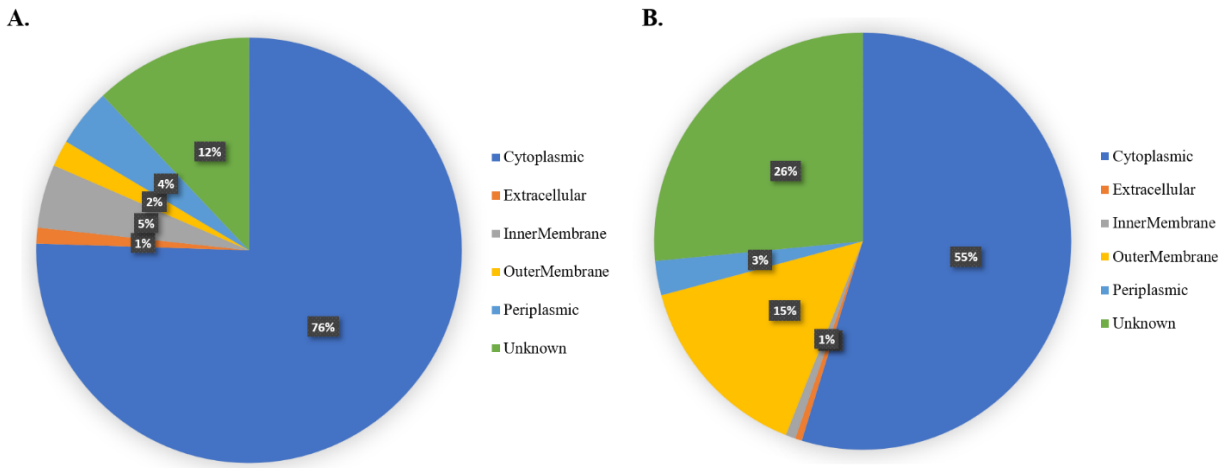


**Figure 4.6: Topology of OMV proteins based on protein types and protein abundance.**
(A) A Pie chart displaying the distribution of OMV proteins classified by various protein types, with percentages representing the proportion of proteins in each distinct group. (B) Pie chart with the distribution of OMV proteins based on their average abundance, percentages indicating the relative abundance in each distint group.

After LC-MS/MS analysis, we combined the proteomes from three biological replicates and selected proteins containing more than two peptides. A total of 250 proteins were identified in *L. pneumophila* OMVs. Topology analysis based on protein type identified 188 cytoplasmic, 12 inner membrane, 11 periplasmic, 5 outer membrane, 3 extracellular, and 30 unknown proteins. In contrast, topology analysis based on average protein abundance reveals that outer membrane proteins constitute a significant fraction of the proteome, second only to cytoplasmic proteins (Figure 4.6). Both protein-type and abundance analyses showed that most vesicular proteins are derived from cytoplasmic and internal proteins of *L. pneumophila,* indicating that *L. pneumophila* packages a repertoire of bacterial cytoplasmic proteins into OMVs, which may play a role in bacterial pathogenesis.

The 250 proteins identified covered the biochemically diverse components of bacterial physiology, stress response, and virulence. This OMV composition suggests that they are not

merely waste products but instead play a role in host-pathogen interactions and environmental survival. The complete list of OMV proteins is provided in **Appendix 1**.

The proteins can be categorized into the following categories:

1. **Translation apparatus**: A large majority of proteins found in this OMVs were annotated to ribosomes and involved in translation. This comprised 30S and 50S ribosomal subunits (RplQ, RplE, RplS, RplN, RpsG, RpsB, RpsD, RpsC, RpsF, RplY, RplB), translation initiation and elongation factors (InfA, InfB, InfC, FusA, Tsf), interestingly, many aminoacyl-tRNA synthetases (AlaS, IleS, SerS, AsnS, ProS, TyrS, LeuS, ValS, LysS, ThrS, AspS), and DNA-directed RNA polymerase (RpoA). The localization of translational components in OMVs may be linked with the delivery of functional or regulatory RNAs to host cells, or it may also suggest mechanisms for manipulating host translation.
2. **Metabolism and ABC transporters**: OMVs also harboured enzymes involved in different metabolic paths, such as: metabolism of amino acids and derivatives: HutH, HutG, DapA, DapD, AroB, AroK, AroQ, HisH1, HisF, ProA, GlyA, GcvH, GcvT, GcvPB, Nucleotide-biosynthesis: PurA, PurB, PyrF, PyrD, PyrE, PyrG and central carbon metabolism: SucC, TpiA, Mdh, Acn, Pgk, Eno, Ppa. While some components of ABC transporters, MetN and SecB, and the potassium (Kup2) transporter and the Ferric uptake regulation protein were also found. The proteome profile indicated that OMVs may contribute to nutrient scavenging and/or environmental adaptation and support bacterial persistence by exporting excess or regulatory enzymes.
3. **Cell wall and membrane biosynthesis**: Peptidoglycan biosynthesis: MurA2 MurD, MurG, lipid A biosynthesis: LpxB2, LpxD1, LpxD2, and phospholipid biosynthesis:

PlsX PlsY. These enzymes, which maintain the bacterial envelope, may control OMV curvature, release, or cargo sorting.

4. **Heat shock proteins and chaperons:** Several heat shock proteins and chaperones, GroEL, GroES, DnaK, DnaJ, GrpE, HtpG, HtpX, Tig were also observed. Their presence might indicate stress during OMV formation, or they may protect cargo proteins or support bacterial survival under stressful conditions. Hfq, an RNA chaperone protein, was also found, which is believed to play an important role in bacterial pathogenesis by influencing gene expression through interaction with small regulatory RNAs.
5. **Outer Membrane and Lipoprotein:** A set of OM and lipoprotein-related proteins was also identified: Pal, TolB, LolA, LolD, LptD, BamB, MsbA, and Mip. They are involved in maintaining the integrity of the outer membrane, LPS export, and OMV generation, supporting the idea that OMVs are formed from distinct regions of the outer membrane. Also, some lipoprotein biosynthesis-related proteins were detected, such as Lgt and lipid transport enzymes, e.g., PlsX, PlsY.
6. **Virulence-Associated Proteins and Effectors:** One of the central themes in OMV biology is virulence. Several known and predicted Dot/Icm T4SS effectors were identified in the OMV proteome by VFDB (Virulence Factor Database), as shown in Table 4.2.

   Most of the characterized effectors were identified, including HtpB, SidD, SidE, SdeA, Fur, DrrA, and Mip. It has been demonstrated that these proteins may manipulate host cell functions, including vesicle trafficking, ubiquitination, and autophagy. Their incorporation into OMVs suggests that OMVs could serve as an alternative effector-transfer vehicle, particularly during the early stages of infection or during extracellular maintenance. Some components of the Dot/Icm type IVB secretion system were also

identified, including DotL, DotM, DotN, lvgA, IcmS, and IcmW, demonstrating that OMVs can carry components of the secretion system and/or play a role in host signalling upon internalization.

Other virulence-related factors, including proteases (HtpX, ClpX, ClpP, and HslV), DNA and RNA nucleases (FabZ, XseA, Orn, Rph, RppH), and redox proteins (KatG2 and SodB), were also detected in OMVs, indicating that OMVs can be involved in manipulating host cell niches.

**Table 4.2: Virulence factors identified in *L. pneumophila* OMVs**

| VF class | Virulence factors | Related genes | Uniport Description |
|---|---|---|---|
| **Adherence** | **Hsp60** | **htpB** | Serve a protective function against the defensive mechanisms produced by infected macrophages. |
| **Intracellular survival** | **Mip** | **Mip** | Important virulence determinant associated with macrophage infectivity. Shows PPIase action. |
| | | **dnaJ** | Dnaj actively responds to hyperosmotic and heat shock by preventing stress-denatured protein aggregation and disaggregation. |
| **Iron uptake** | **Cytochrome c maturation (ccm) locus** | **ccmA** | Part of the ABC transporter complex CcmAB is involved in the biogenesis of c-type cytochromes; once thought to export heme, this seems not to be the case, but its exact role is uncertain. Responsible for energy coupling to the transport system. |
| | | **ccmE** | Heme chaperone required for the biogenesis of c-type cytochromes. Transiently binds heme delivered by CcmC and transfers the heme to apo-cytochromes in a process facilitated by CcmF and CcmH. |
| | | **Fur** | Acts as a global negative controlling element, employing $Fe^{2+}$ as a cofactor to bind the operator of the repressed genes. |
| **Secretion system** | **Dot/Icm type IVB secretion system** | **icmJ/dotN** | Component of the Dot/Icm type IVB secretion system (T4BSS), which is used to inject bacterial effector proteins into eukaryotic host cells. |
| | | **icmO/dotL** | |
| | | **icmP/dotM** | |
| | | **icmS** | |
| | | **icmW** | |
| | | **lvgA** | |
| | **Type IVB secretion effectors** | **drrA/sidM** | Virulence effector that plays a key role in hijacking the host vesicular trafficking by recruiting the small guanosine triphosphatase (GTPase) Rab1 to the cytosolic face of the Legionella-containing vacuole (LCVs). |
| | | **sdeA/laiA** | Secreted effector that interferes with the host cell ubiquitin pathway and is required for intracellular bacterial replication. |
| | | **sidD** | Virulence effector that plays a role in hijacking the host vesicular trafficking by recruiting the small guanosine triphosphatase (GTPase) Rab1 to the cytosolic face of the Legionella-containing vacuole (LCVs). |
| | | **sidE/laiD** | Effector that interferes with the host cell ubiquitin pathway and is required for intracellular bacterial replication. |

The functional pathways associated with these proteins were identified by EGGNOG, KEGG and DAVID. The eggnog mapper identified 17 functional pathways related to OMV proteins of *L. pneumophila*. Most of the proteins (around 76 of 250) were linked with translation, ribosomal structure, and biogenesis. The next enriched pathway was nucleotide transport and metabolism. Other enriched pathways included transcription, post-translational modification, protein turnover, chaperones, energy production and conversion, and defense mechanisms, indicating the diverse roles of OMV-associated proteins. The appearance of proteins involved in such a wide range of biological functions emphasizes the functional diversity within the OMV proteome. In particular, the enrichment of proteins involved in cell wall/membrane/envelope biogenesis suggests an important role for OMVs in maintaining the integrity of the cellular envelope and in the bacterium's response to external stress (Figure 4.7). Furthermore, the KEGG database identified that most proteins participate in metabolic pathways and genetic information processing, as represented in Figure 4.8. DAVID database analysis *of L. pneumophila* OMV proteome revealed similar functional enrichments (like EggNOG) for ribosomal functional annotation terms, specifically "structural constituent of ribosome" and "translation". The enrichment of RNA-binding and cytoplasmic proteins also suggests that these vesicles contain components involved in protein synthesis and RNA processing (Figure 4.9).

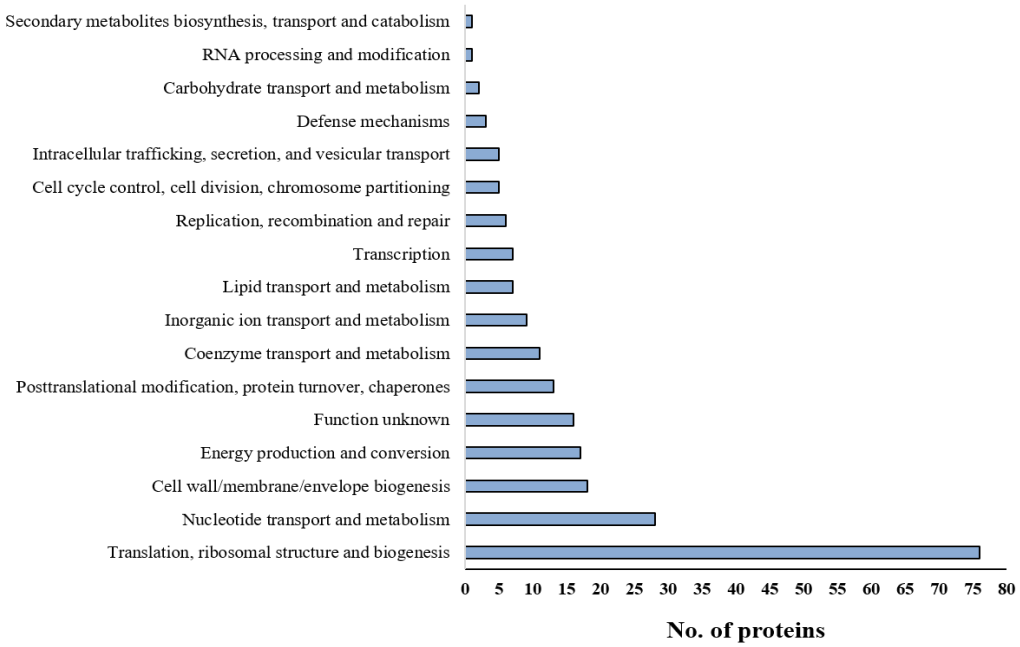


**Figure 4.7: Functional annotation of OMV proteins from *L. pneumophila* with EggNOG.**
The bar chart illustrates the distribution of observed proteins among functional categories according to EggNOG annotation. Categories include translation, ribosomal structure and biogenesis, nucleotide transport and metabolism, cell wall/membrane/envelope biogenesis, energy generation and conversion, among others. The most significant number of annotated proteins is classified under the categories of translation, ribosomal structure, and biogenesis. X-axis indicates the number of proteins found within each functional category.

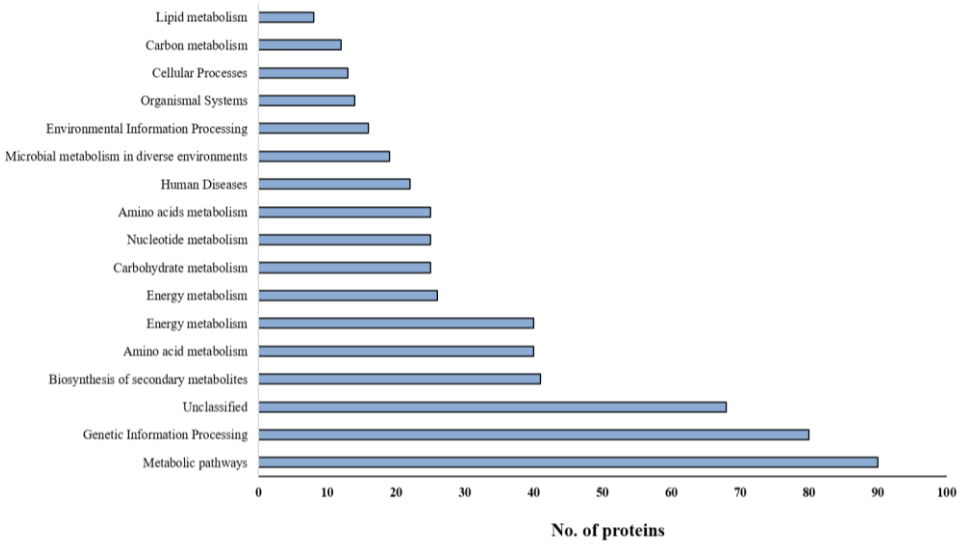


**Figure 4.8: KEGG pathway classification of *L. pneumophila* OMV proteins.**
The X-axis indicates the number of proteins classified into each pathway, and the Y-axis shows the categories of KEGG pathways. Metabolic pathways, genetic information processing, unclassified, biosynthesis of secondary metabolites, and energy metabolism are major categories.

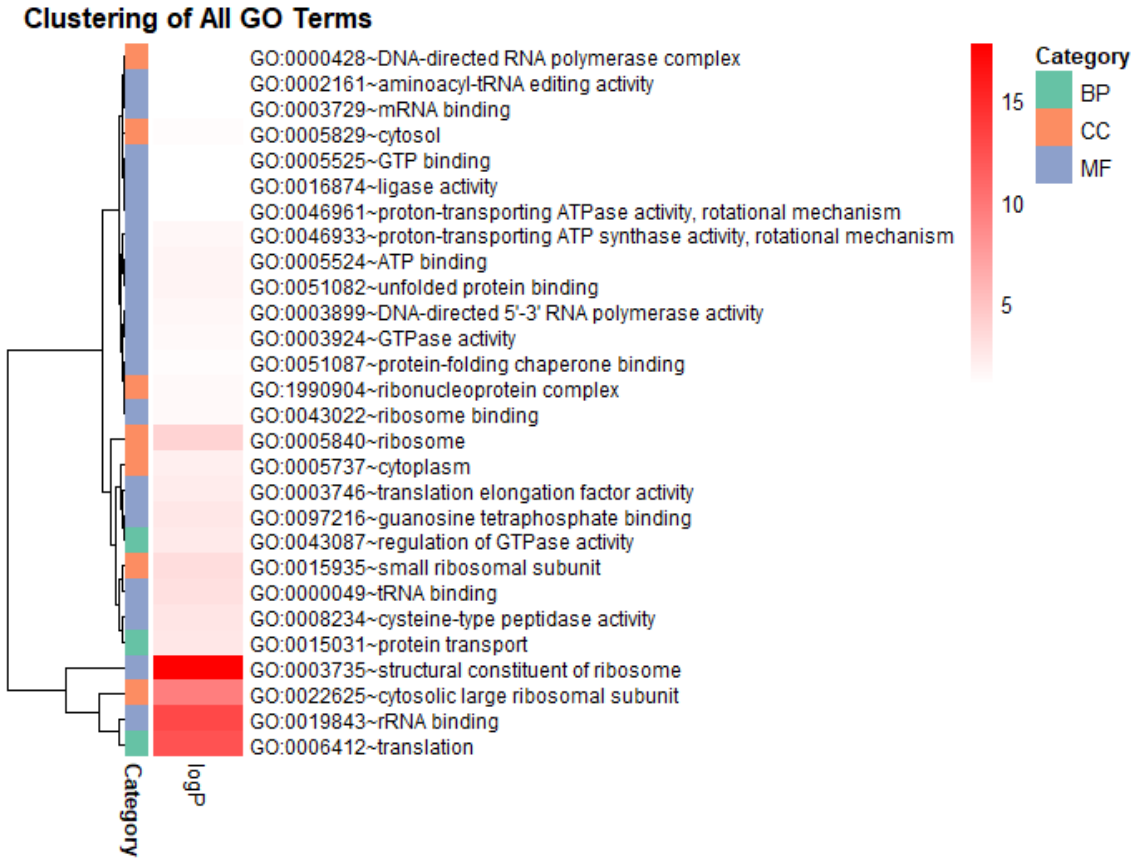


**Figure 4.9 Go term clustering of DAVID functional annotation data for OMV proteins from *L. pneumophila*.**

Heat map analysis of top 20 GO terms represented by significantly enriched pathways of (A) biological process, (B) cellular component, and(C) molecular function. The intensity of red in each cell reflects the greater biological significance of the cluster known as enrichment exposure (–logP value). Hierarchical clustering categorizes similar GO terms, emphasizing predominant functional themes among OMV proteins, including translation, RNA binding, ribosome biogenesis, and ATP binding. The annotation describes the molecular functions, cellular components and biological processes most significantly over-represented among OMV proteins *in L. pneumophila.*

Taken together, the proteomic profile indicates that *L. pneumophila* OMVs contain a diverse array of proteins, including components of the translation machinery, cell wall biosynthesis, and metabolism, as well as known virulence factors. *L. pneumophila* OMVs proteome may modulate the host immune system via lipoproteins and membrane surface proteins. At the same time, virulence factors may enhance *L. pneumophila* pathogenicity during infection if transferred to the host cell, although these findings remain to be evaluated. In contrast, the roles of other components, such as the translation machinery and metabolic proteins, in host-pathogen interactions remain unclear and require further consideration.

#### 4.1.3.3. Nucleic acids associated with *L. pneumophila* OMVs

##### 4.1.3.3.1. DNA associated with *L. pneumophila* OMVs

To date, the DNA associated with *L. pneumophila* OMVs remains uncharacterized. The schematic representation (Fig. 4.10A) summarizes the procedure applied to distinguish between total OMV-associated DNA (labelled as total DNA) and protected DNA residing inside vesicles (labelled as internal DNA). Three biological replicates were used for both total DNA and internal DNA analyses. Quantification by spectrophotometry showed that most detectable DNA was surface-associated (Fig. 4.10B). Overall, the amount of total OMV-associated DNA (average 45 ng/µl) was much higher than that recovered in an intact form within DNase-treated preparations (5 ng/µl), confirming that most OMV-bound DNA is located on their surface and minor fraction is protected within the vesicles due to the OMV bilayer.

Using the Bioanalyzer, untreated OMVs (Fig. 10C) showed a significant peak characteristic of high-molecular-weight DNA (>10 kb), in contrast, DNase-treated OMVs (Fig. 10D) demonstrated a significantly smaller fragment size.

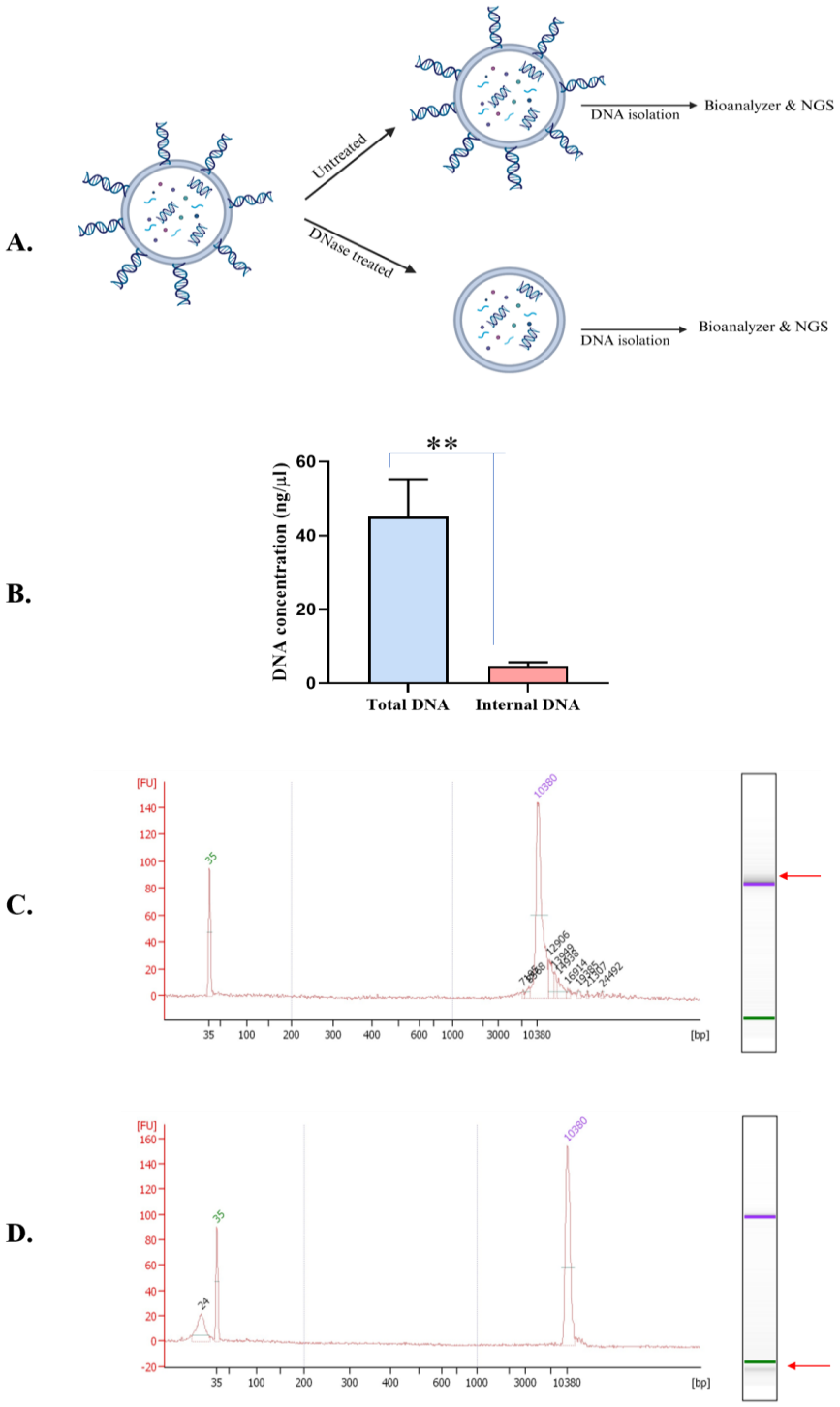


**Figure 4.10: Analysis of DNA content of *L. pneumophila* OMVs, with and without DNase treatment.** **(A)** Schematic presentation of experimental design: OMVs were either untreated (OMVs containing both extracellular and intravesicular DNA) or treated with DNase to remove extracellular DNA, exposing only intravesicular DNA. DNA from the two groups was isolated, then Bioanalyzer and next-generation sequencing (NGS) analysis were performed. (B) Measurement of total and internal (DNase-treated) DNA levels in internal OMVs was significantly lower than those in total DNA (**p < 0.01). Data are presented as mean ± standard deviation (n=3). (C, D) Representative Bioanalyzer electropherograms for untreated OMVs (C, total DNA) and from DNase-treated OMVs (D, Internal DNA). DNA maker indicating the size and the position of the band corresponding to DNA using red arrows within all gels.

Next, the Illumina platform was used to sequence the total DNA and internal DNA of OMVs released by *L. pneumophila*. DNA sequencing data revealed that, although internal DNA was significantly lower in concentration, the sequences from the total and internal DNA were fully mapped to the *L. pneumophila* ATCC reference genome (*L. pneumophila* strain Philadelphia 1, GenBank accession: AE017354.1, ATCC: 33152). The genome size/length for both samples was approximately 3,400,000 bp, matching the size of the *L. pneumophila* genome (3.4 Mb).

Comparison of the protein-coding genes (CDS) found in the total DNA, internal DNA, and *L. pneumophila* ATCC reference strain (GenBank accession: AE017354.1) was visualized as a Venn diagram shown in Figure 4.11. The findings suggested a striking overlap between the three datasets. First of all, 3,170 protein-coding genes were reported as OMV-encoded, out of which 3163 (99.8%) were present within both total DNA and internal DNA datasets. Only 7 (0.2%) genes were specific to the internal DNA and encoded hypothetical proteins. Secondly, all OMV-CDS were common to the *L. pneumophila* strain, except for 1.5%, indicating the presence of the full spectrum of *L. pneumophila* genes in both the total and internal DNA of OMVs, rather than selective packaging of some genes.

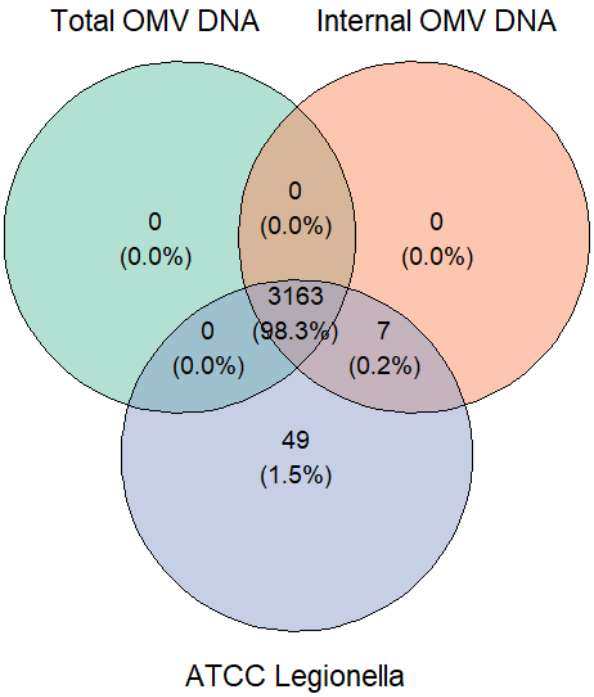


**Figure 4.11: Venn diagram illustrating the overlap of coding sequences identified in OMVs from *L. pneumophila*.**

Venn diagram illustrating the overlap of coding sequences identified in outer membrane vesicles from *L. pneumophila*. The study compares coding sequences found in total DNA (green), internal DNA (orange), and the *L. pneumophila* ATCC reference genome (blue). Three groups share a total of 3,163 coding sequences, constituting 98.3% of the total. The diagram indicates unique and common coding sequences in each subgroup, shown by numbers and percentages within each area. A limited quantity of sequences is exclusive to *L. pneumophila* (49, 1.5%) and to *L. pneumophila* with internal OMV DNA (7, 0.2%), but no unique sequences are present in total OMV DNA or internal OMV DNA alone, signifying substantial overlap and specificity of OMV-associated DNA with the *L. pneumophila* ATCC reference genome.

Next, the DNA density and read coverage for both samples were assessed. The DNA read coverage was calculated using three biological replicates for both total and internal DNA samples and mapped to the 3.4 Mb *L. pneumophila* ATCC reference genome (GenBank accession: AE017354.1). The coverage or genome-wide distribution of both total DNA (Figure 4.12A) and internal DNA (Figure 4.12B) shows some regions with read density higher than the average and others with read density lower than the average, and the pattern of this read coverage distribution varies between total and internal DNA. For example, in the total DNA sample, there is a high-density region (red color) between 1,200,000 bp and 1,800,000 bp. In contrast, the high-density regions (red color) in the internal DNA sample are distributed randomly throughout the genome.

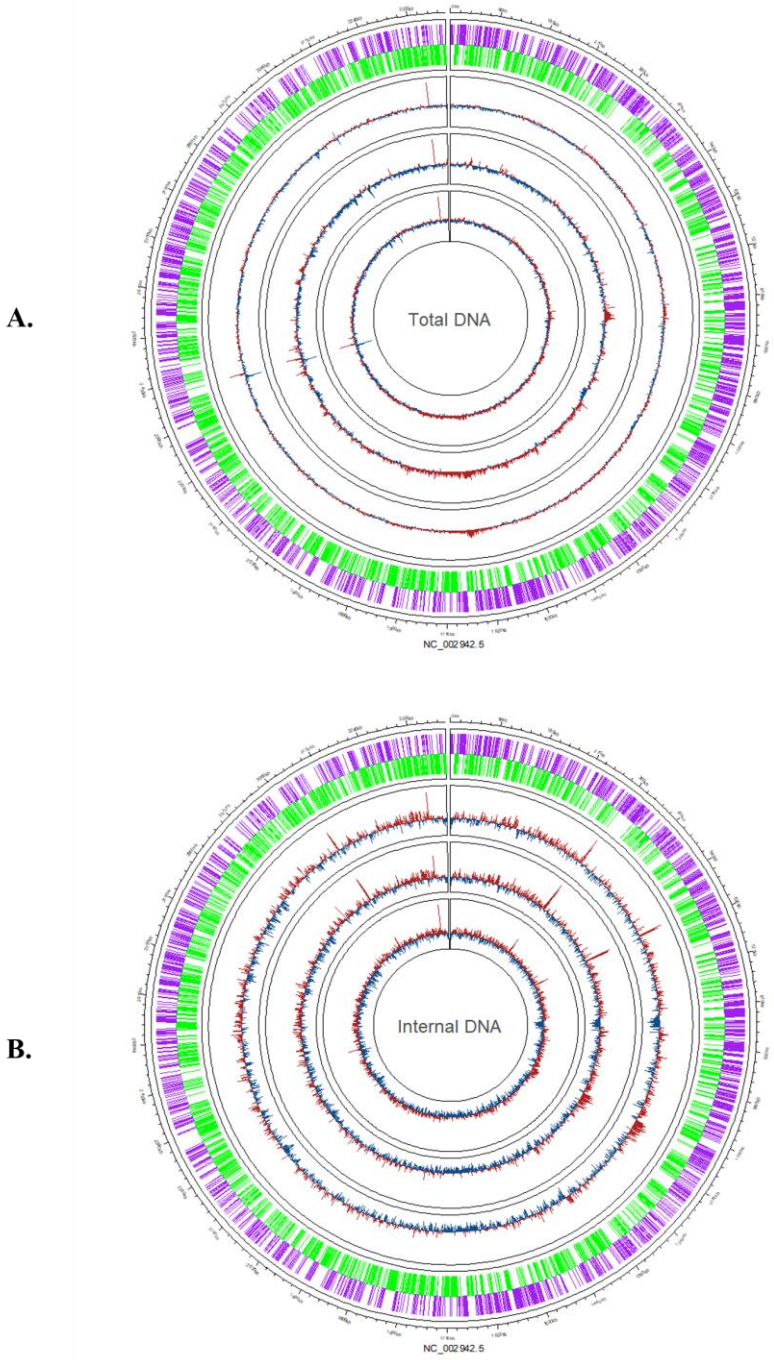


**Figure 4.12: Genome-wide distribution of DNA associated with *L. pneumophila* OMVs.**
(A) DNA density plot for total OMV DNA and (B) DNA density plot for internal OMV DNA, each presented with three biological replicates, aligned to the *L. pneumophila* ATCC reference genome. Each panel features circular plots that illustrate read coverage (red and blue lines) representing the density of DNA fragments and the peak length indicates the enrichment of regions. Positions with above-average read density are shown in red, whilst those with below-average density are marked in blue, showing a denser area in total DNA from 1200 to 1900 kbps while many dense regions are found in internal DNA distributed across the DNA. The outer rings indicate the locations of annotated protein-coding genes on the positive (purple) and negative (green) DNA strands of the *L. pneumophila* ATCC reference genome. The graphs describe the genome-wide distribution and enrichment of total and internal OMV DNA content concerning identified genes.

The biological implications of the total DNA region from 1,200 kbps to 1,800 kbps were assessed for functional involvement using GO (Figure 4.13) and KEGG (Figure 4.14). KEGG analysis revealed that most of these CDS were associated with metabolic functions, whereas GO analysis showed diverse mechanisms ranging from metabolism to cell motility to defense mechanisms.

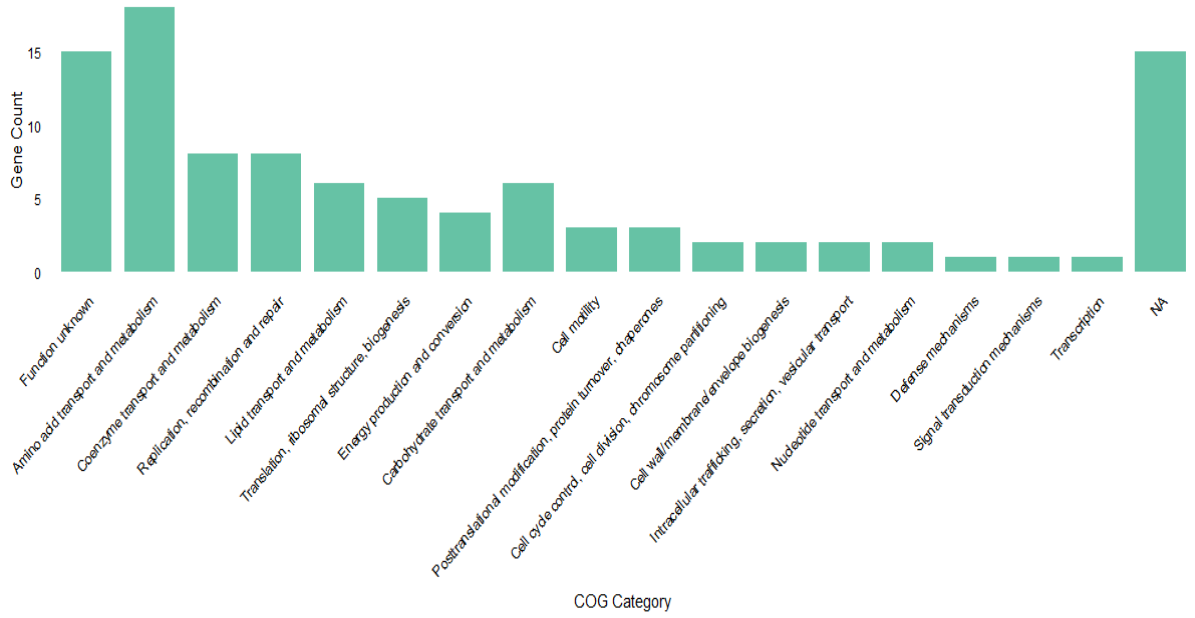


**Figure 4.13: Annotation of dense DNA regions in total DNA derived from the *L. pneumophila* OMVs.**

The bar graph shows the gene counts assigned to each functional COG (Clusters of Orthologous Groups) category counted from the annotation results of (1200 bp to 1900 kbp) total DNA. The x-axis shows COG functional categories such as Function unknown, Amino acid transport and metabolism, Replication, recombination and repair, etc. The y-axis indicates the number of genes assigned to each category. Based on gene count, the "Function unknown," "NA" (unassigned), and transport/metabolism categories contain the most genes in the dense region of total DNA.

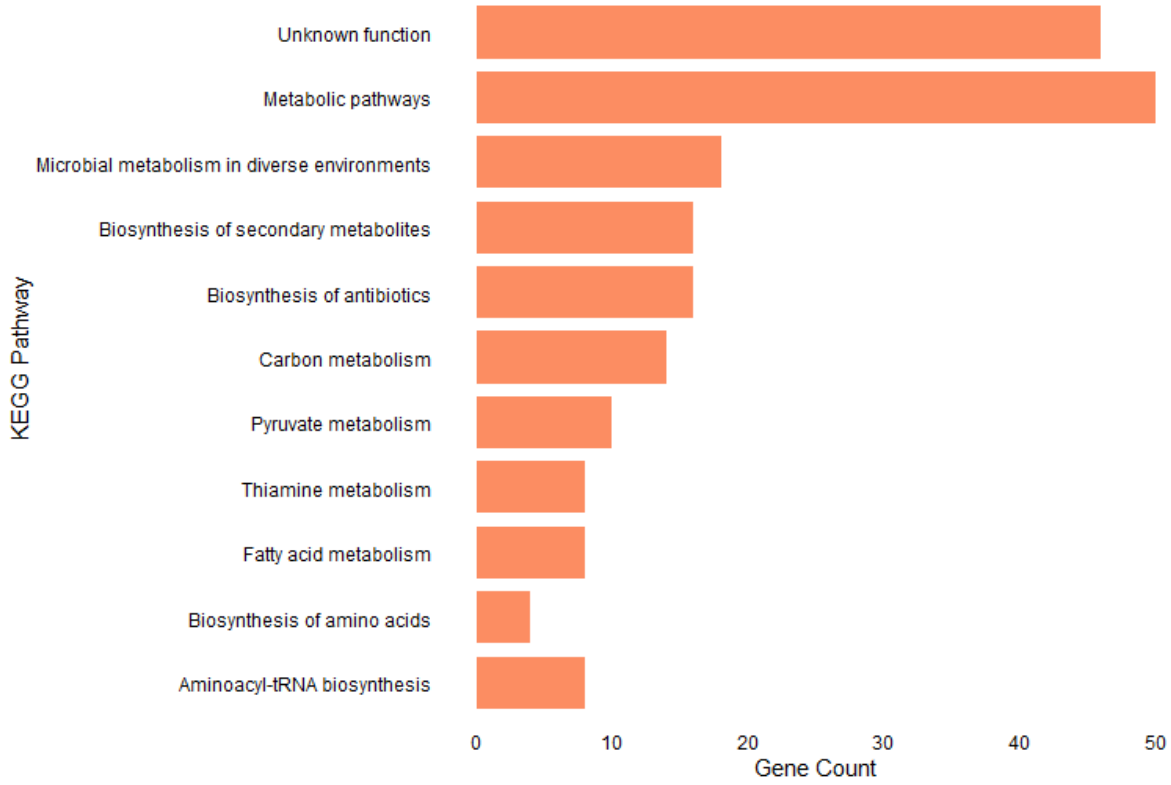


**Figure 4.14: Top 10 KEGG pathways enriched in dense regions of total DNA from *L. pneumophila* OMVs.**

The horizontal bar graph displays the gene counts for the most highly represented KEGG pathways identified within genomic loci of high DNA density (enriched red regions) in total OMV DNA. The y-axis lists the KEGG pathway names, while the x-axis shows the number of genes assigned to each pathway. Pathways with the most representation include "Metabolic pathways," "Unknown function," "Microbial metabolism in diverse environments," "Biosynthesis of secondary metabolites," and others. This analysis highlights the functional complexity and metabolic potential of genomic regions preferentially encapsulated in OMVs.

Besides DNA density, enrichment of regions by the length of red peaks was also compared. In contrast to total DNA, internal DNA exhibits a broader distribution and significant enrichment of some regions throughout the DNA, as indicated by the length of the red peaks. By filtering out regions that are significantly over-represented (coverage ratio> 1.25), we identified 15 genes in the region around the highest peak, between 1098 kbps and 1170 kbps. These include secretory immunoglobulin A-binding protein, which interferes with host immune response, while all other genes were related to metabolism and stress responses (Table 4.3).

**Table 4.3: Significantly enriched genes in OMV internal DNA between 1098 kbps and 1170 kbps.**

| Gene name | Product | Location (start) | Location (end) |
|---|---|---|---|
| czcA_2 | Cobalt-zinc-cadmium resistance protein CzcA | 1128000 | 1129000 |
| copA_1 | Copper-exporting P-type ATPase | 1122000 | 1123000 |
| cusA_1 | Cation efflux system protein CusA | 1115000 | 1116000 |
| cusB_1 | Cation efflux system protein CusB | 1114000 | 1115000 |
| phaC_2 | Poly(3-hydroxyalkanoate) polymerase subunit PhaC | 1157000 | 1158000 |
| mdtA_2 | Multidrug resistance protein MdtA | 1127000 | 1128000 |
| atpD_1 | ATP synthase subunit beta | 1150000 | 1151000 |
| ftsP | Cell division protein FtsP | 1136000 | 1137000 |
| esiB_1 | Secretory immunoglobulin A-binding protein EsiB | 1160000 | 1161000 |
| prs_2 | Ribose-phosphate pyrophosphokinase | 1121000 | 1122000 |
| - | Putative thymidine phosphorylase | 1119000 | 1120000 |
| - | Ribonuclease | 1119000 | 1120000 |
| - | Calcium-transporting ATPase 1 | 1111000 | 1112000 |
| - | putative signaling protein | 1156000 | 1157000 |
| hmp | Flavohemoprotein | 1142000 | 1143000 |

Although the genomic distribution patterns of both total and internal DNA varied, the biological significance of both total and internal DNA did not suggest any role in host-pathogen interaction. Additionally, the presence of all *L. pneumophila* genomic content within OMVs indicates that OMVs take up DNA in a random or non-specific manner. Vesicular budding from the outer membrane can trap cytoplasmic components, including chromosomal DNA fragments, and cell lysis during the stationary phase might release genomic DNA, which can then bind to the OMV surface and be internalized during vesicular formation.

The precise mechanisms underlying DNA packaging within OMVs remain unclear. These findings raise further questions about the presence of DNA in OMVs of pathogenic bacteria and highlight the need for further investigation. Nevertheless, it is important to note that this DNA may indirectly influence host-pathogen interactions, as it has the potential to activate host TLR9.

#### 4.1.3.3.2. RNA associated with *L. pneumophila* OMVs:

RNAs found in OMV fractions ranged from 10 to 20 ng/µl by qubit measurement. However, RNA was reduced to approximately 5 ng/µl after extraction and clean-up using the PureLink RNA Mini and mirVana miRNA (Thermo Fisher) commercial kits. Total RNA (mRNA, rRNA, tRNA) and small RNA-enriched RNA were separately extracted, and their concentrations and qualities were analyzed using Qubit and Bioanalyzer, respectively. Figure 4.15A shows that the proportion of small RNA was higher in OMVs compared to other RNAs. This low concentration dropped to nearly zero after RNase treatment, thereby hindering the separation of total RNA from internal RNA in OMVs.

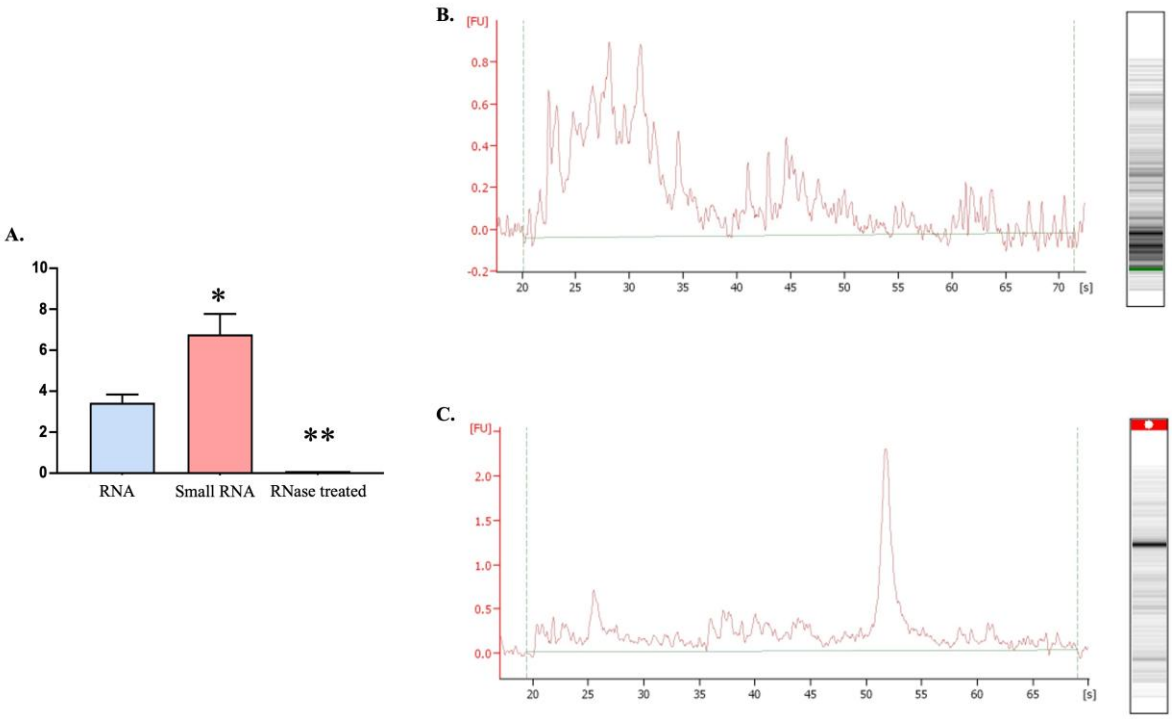


**Figure 4.15: RNA content associated with *L. pneumophila* OMVs.**
A) Measurement of RNA concentrations after OMV RNA extraction. Measurements of RNA (mRNA, rRNA, tRNA), small RNA and RNase-treated (control) OMV samples indicated a significant small RNA concentration relative to other RNA and the degradation of all RNA following RNase treatment. Data are presented as mean ± standard deviation (n=3). Paired t-test performed for significance (*$p < 0.023$, **$p < 0.049$) compared to Total RNA (B). Bioanalyzer electropherogram of small OMV RNA, illustrating the presence of many small RNAs in the lower region of the gel. (C) The Bioanalyzer electropherogram of other OMV RNA (mRNA, rRNA, tRNA) samples demonstrates a wide distribution of RNA species.

Bioanalyzer analysis showed that both small RNA and RNA (mRNA, rRNA, tRNA) had degraded profiles (Figure 4.15B and 4.15C). Agilent analysis of the RNA (mRNA, rRNA, tRNA) samples revealed a distinct, high-molecular-weight band near 7000 bp. This peak likely indicates the presence of large ribosomal RNA complexes or genomic DNA contamination, rather than the expected mRNA, rRNA, or tRNA target profiles. Despite using the Takara library preparation kit for low-input small RNA and RNA (mRNA, rRNA, tRNA), the yields did not meet the requirements for sequencing. As a result, sequencing these RNA samples was infeasible.

These trial experiments suggest that sequencing OMV-associated RNA is more difficult than sequencing OMV-associated DNA, and that OMV-associated RNA characterization requires optimization from RNA isolation to library preparation to the development of data analysis tools.

## 4.2. Transcriptional and functional impact of *L. pneumophila* OMVs on host cell survival and inflammatory responses

### 4.2.1. OMVs were efficiently up-taken by THP-1 derived macrophages

Before studying the role of OMVs in *L. pneumophila* disease pathogenesis, it is essential to explore their physical interactions with host cells.

To determine the internalization of *L. pneumophila* OMVs by host cells, THP-1 derived macrophages were treated with Vybrant labelled OMVs for 2 hours at 37°C; nuclei were counterstained with Hoechst, and the uptake was examined by confocal laser scanning microscopy after 2 hours. On confocal microscopy, distinct cytoplasmic accumulation of red fluorescent signals, indicating internalization of OMVs, was observed in THP-1 derived macrophages. In the merged images, co-localization between OMVs and nuclei was observed within cells after a 4-hour incubation, suggesting that OMVs bind to host cells and are taken up (Figure 4.16).

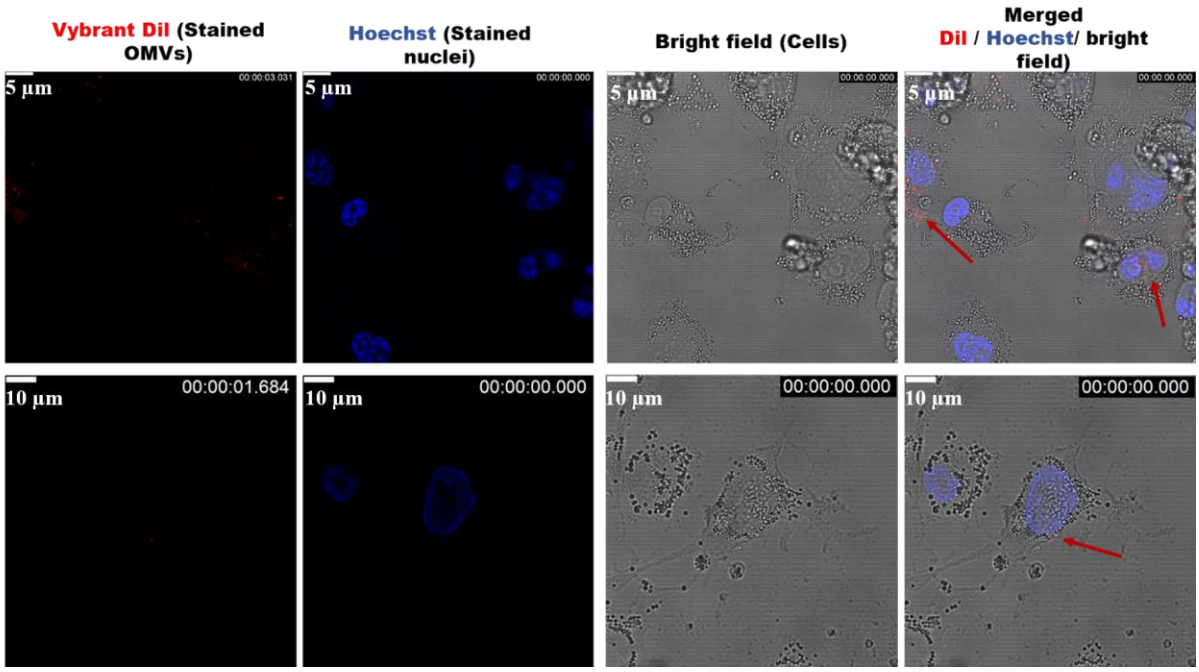


**Figure 4.16: Confocal laser scanning microscopy of *L. pneumophila* OMVs uptake by THP-1 derived macrophage.**

THP-1 cells were differentiated into macrophages by PMA treatment. OMVs were stained with Vybrant Dil dye and incubated with macrophages for 2 hours. Cells were fixed and stained with Hoechst stain and visualised under a Leica SPE confocal microscope. Representative images from two resolutions are shown. The white bars on the left side indicate the scale.

To quantify the uptake of *L. pneumophila* OMVs into THP-1 derived macrophages, OMVs were stained with the lipophilic dye Vybrant CM-Dil (red), and the level of uptake was quantified using a BD FACSAria III cell flow cytometer.

To assess the time and dose-dependent behaviour, THP-1 derived macrophages were incubated for 24 and 48 hours with 1 µg, 10 µg, and 20 µg of Vybrant labelled OMVs. Subsequently, cells were collected and washed several times to remove free vesicles before analyzing the samples for red fluorescence. Flow cytometry showed a dose-dependent increase in Vybrant fluorescence intensity in OMV treated macrophages compared to untreated control macrophages. At 24 hours, there was a non-significant increase in fluorescence within 1 µg treatment group, while significant increases were observed in the 10 and 20 µg groups. At 48 hours, fluorescence intensity significantly increased across all doses (Figure 4.18).

Interestingly, OMV uptake increased with OMV dose but not with incubation time from 24 to 48 hours, except at 1 µg of OMVs, where the Vybrant signal increased significantly from 5.68% to 15.06% between 24 and 48 hours.

These data support efficient uptake of *L. pneumophila* OMVs by THP–1–derived macrophages in a concentration-dependent manner, indicative of active internalization. In contrast, no significant increase was observed between 24 and 48 hours (Figure 4.17), which may imply that all OMVs are internalized during the first 24 hours or that they are internalized concurrently with OMV degradation, resulting in a constant overall uptake. However, no report is available for this mechanism. This uptake plateau can also be explained by receptor saturation for endocytosis and OMV internalization. Receptor saturation is critical, as this phenomenon has already been reported in the literature for OMVs (Ellis & Kuehn, 2010).

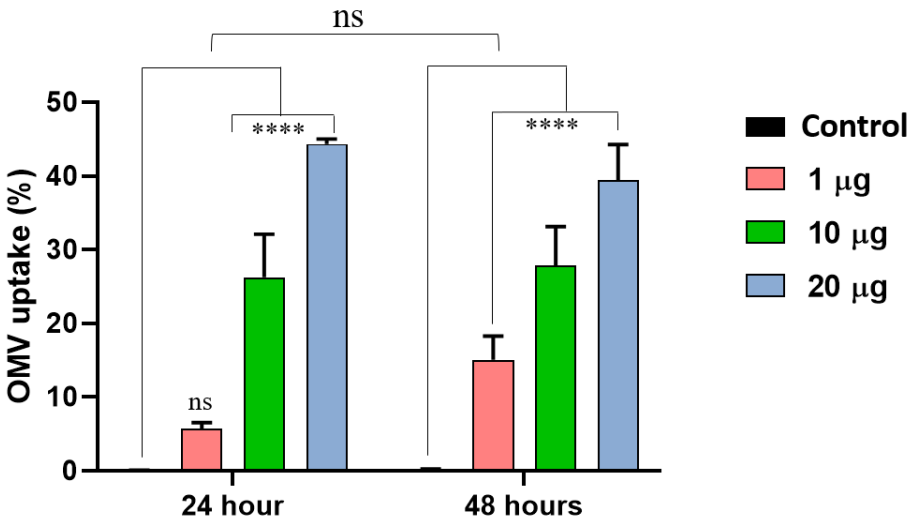


**Figure 4.17: OMV uptake of *L. pneumophila* OMVs by THP-1 derived macrophages.**
The bar graph illustrates the percentage of OMV uptake at 24 and 48 hours of incubation with increasing OMV doses (1µg, 10µg, and 20µg), in comparison to untreated control cells. The uptake of OMV was assessed using flow cytometry. Data are expressed as mean ± standard deviation from triplicate experiments. Uptake increased markedly in a dose-dependent fashion, peaking at 20µg for both the 24- and 48-hour intervals (****$p<0.0001$). No significant change (ns) was detected for 1µg OMV at 24 hours in comparison to the control. And no significant change (ns) was observed between the 24-hour and 48-hour groups. Sidak's multiple comparisons test and the 2-way ANOVA test are performed.

### 4.2.2. ScRNA-seq of THP-1 derived macrophages reveals heterogeneity in macrophage responses following OMV internalization.

To reveal the impact of *L. pneumophila* OMVs internalization on host cell processes and immune modulation, scRNA-seq was performed on THP-1-derived macrophages after OMVs internalization (three biological replicates). The resolution of single-cells enables the identification of changes in expression at the single-cell level, revealing cellular diversity and unique activation states that can be masked in bulk analyses. By profiling the transcriptional landscape at single-cell resolution, we aimed to uncover the diverse molecular responses of macrophage function and pathways in response to OMV.

#### 4.2.2.1. Gating and Sorting cell populations for ScRNA-seq analysis:

THP-1-derived macrophages were incubated for 12 h at 37°C with 5% $CO_2$ in two conditions: untreated (control) or after treatment with Vybrant labeled OMVs. Cells were analyzed by flow cytometry for OMV-uptake and populations were sorted for the subsequent scRNA-seq. Figure 4.18 describes the workflow.

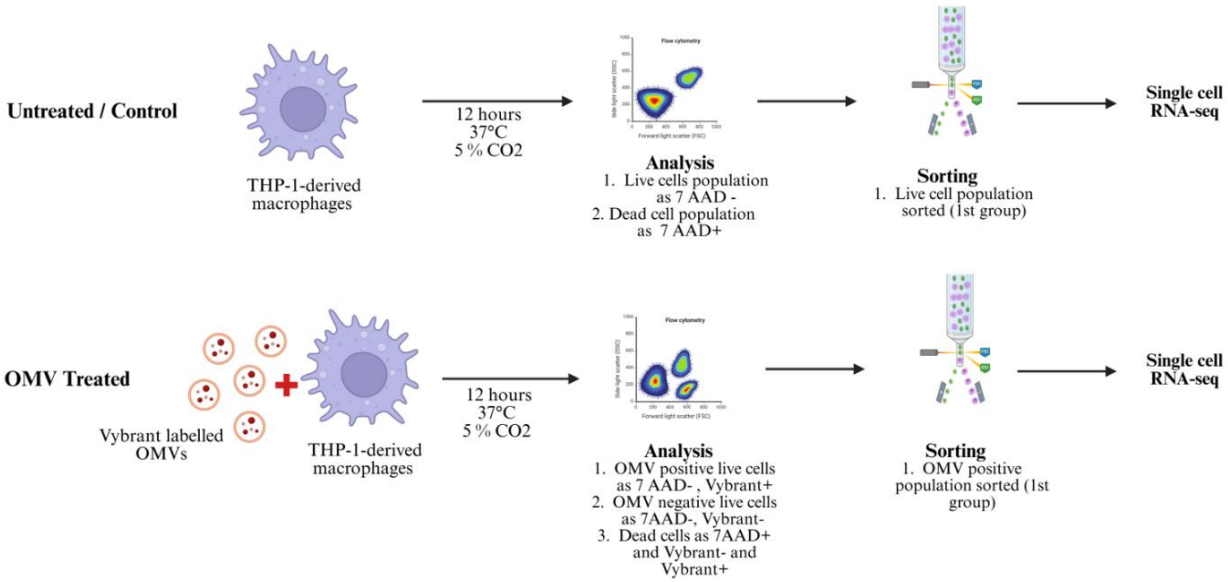


**Figure 4.18: Workflow for the preparation of THP-1-derived macrophage samples for scRNA-seq.** Schematic representation of untreated (control) and OMV treated condition. THP-1-derived macrophages were incubated for 12 hours at 37°C with 5% $CO_2$, either untreated (control) or in the presence of Vybrant-labelled OMVs (OMV treatment). Following incubation, cells were analyzed by flow cytometry to differentiate between living and dead populations (control), and to further classify OMV-positive and OMV-negative live cells in the treatment group. Live cells (control) or OMV-positive live cells (treatment) were separated and collected for further scRNA-seq. This approach ensures the separation of specific cellular subpopulations for transcriptome analysis after OMV uptake.

7-AAD staining divided macrophages into two populations: “live cells” (7-AAD negative) and “dead cells” (7-AAD positive) in the control group. Cells were then filtered based on viability, and live cells were sorted for the control group (Figure 4.19A).

In OMV treated macrophages, flow cytometry plots gated three main populations (Figure 4.19B):

1. Live cells (7-AAD negative) that were Vybrant positive due to internalized OMVs (OMV positive)
2. Live cells with no internalized OMVs (OMV-negative)
3. Dead cell population with or without OMVs (7-AAD positive).

Among these 3, the first population (live macrophages that are OMV-positive, around 10 %) was sorted and used for scRNA-seq analysis (Figure 4.20). Using this sorting strategy, macrophages containing OMVs were effectively separated from live and dead bystander cells for high-resolution transcriptomic analysis. Flow cytometry gating also ensured the separation of only live viable cell populations, which is the most essential prerequisite for good scRNA-seq. Approximately 30,000 control and 30,000 treated macrophages were sequenced across three biological replicates using the 10x Genomics platform, as each replicate can accommodate up to 10,000 cells.

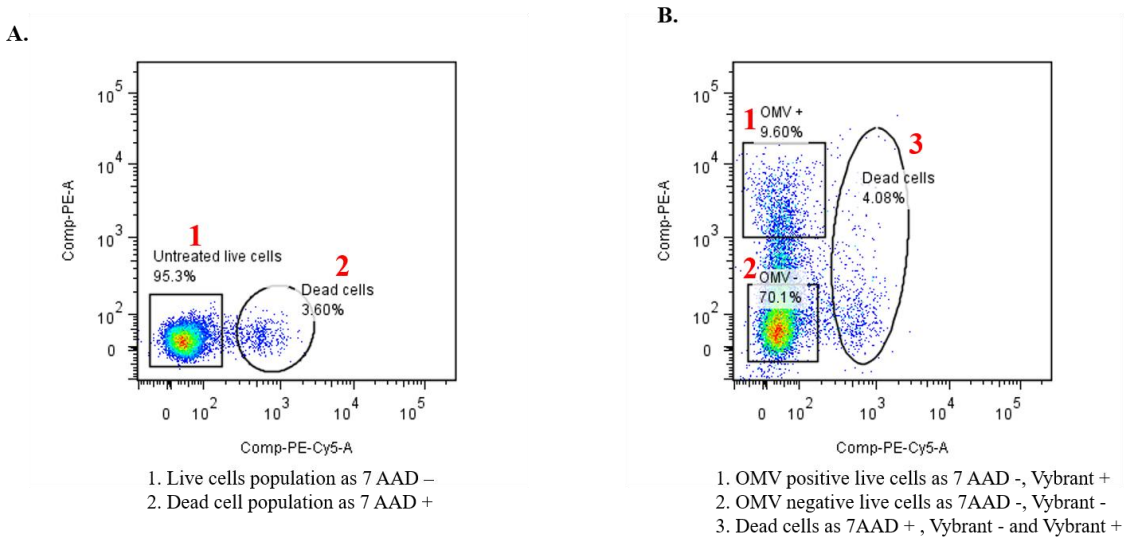


**Figure 4.19: Flow cytometry gating approach for the selection of control and OMV treated THP-1-derived macrophages for scRNA-seq.**

(A) Representative pseudocolor graph of control (untreated) macrophages, illustrating the gating of live cells (95.3%) and dead cells (3.6%) based on PE (Vybrant Dil for OMVs) and PE-Cy5 (7-AAD, dead cell staining) fluorescence. (B) Gating of OMV treated macrophages, differentiating OMV-negative (OMV−, 70.1%) and OMV-positive (OMV+, 9.6%) viable cell populations, together with dead cells (4.08%). An elevated PE signal shows OMV uptake. The specified gated populations were sorted for further scRNA-seq, facilitating transcriptome comparison between OMV-internalized and control macrophage populations.

### 4.2.2.2. Sample integration and clustering

ScRNA-seq was performed on THP-1-derived macrophages from three control and three OMV treated replicates, and the different datasets were integrated to remove batch effects. Integration of data from all six samples, visualized using UMAP, showed strong alignment with the defined cellular distributions. Samples clustered by identity and condition showed that OMV treated macrophages occupied distinct regions within the transcriptional landscape, reflecting treatment-dependent variations (Figures 4.20A & 4.20B).

The "Find marker" function built inside the Seurat Package identified or assigned eight distinct clusters, ranging from cluster 0 to cluster 7, in integrated samples of both control and treated groups, indicating the cellular heterogeneity of macrophages (Figure 4.20C). DEGs involved in each cluster are described in the following section.

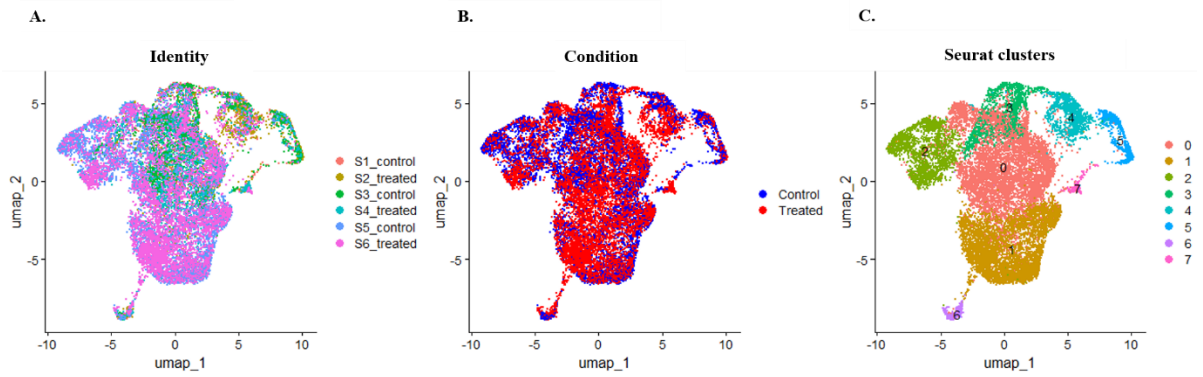


**Figure 4.20: UMAP illustration of single-cell transcriptome profiling of control and treated THP-1 derived macrophages.**
(A) Cells are color-coded according to sample identification, including control and OMV-treated biological replicates (S1_control, S2_treated, etc.), illustrating the intermingling of cells across conditions. (B) Cells categorized by experimental condition: control (blue) and OMV treated (red), exhibiting overlap in some transcriptional space while displaying some region-specific enrichments. (C) Unsupervised clustering by Seurat identified eight distinct cell clusters, each represented by a color corresponding to cluster (0–7), indicating distinctive transcriptional states among macrophage populations. These UMAP plots illustrate the diversity and relationships among transcriptional responses in macrophages under different conditions. Each dot represents a single cell, with its position reflecting the overall gene expression profile, while colors indicate the normalized expression level of a specific gene in each cell.

#### 4.2.2.3. Differential gene expression (DEG) following OMV internalization

Comparative analysis of differentially expressed genes across all three macrophage replicates treated with OMV versus control macrophages identified 720 genes that were significantly regulated by OMV exposure. The volcano plot shows 456 genes significantly upregulated and 264 significantly downregulated after treatment with OMVs (Figure 4.21). Among the most upregulated genes were CCL1, a chemokine that attracts leukocytes and is involved in inflammation; CSF2 (colony-stimulating factor 2), which enhances macrophage activation and proliferation; IL23A, an essential member of the cytokine family subunit necessary for the immune response; and TNFAIP2 (tumour necrosis factor alpha-induced protein 2), a regulator associated with TNF-alpha gene activation. CD80 is an essential stimulatory molecule for T cell activation development. Additionally, the expression of the unique long non-coding RNA (lncRNA) (ENSG00000286533) was significantly upregulated, strongly suggesting its regulatory roles in the macrophage response to OMVs. In contrast, genes that were significantly downregulated included PYROXD2 (related to redox regulation), QPRT (involved in NAD metabolism), and DLX3 (a transcription factor with potential roles in cellular differentiation), indicating the inhibition of specific metabolic or differentiation pathways following OMV treatment. These DEGs highlights the activation bias of macrophages in response to *L. pneumophila* OMVs towards pro-inflammatory and primed conditions, with several metabolic activities and some regulatory programs being simultaneously suppressed.

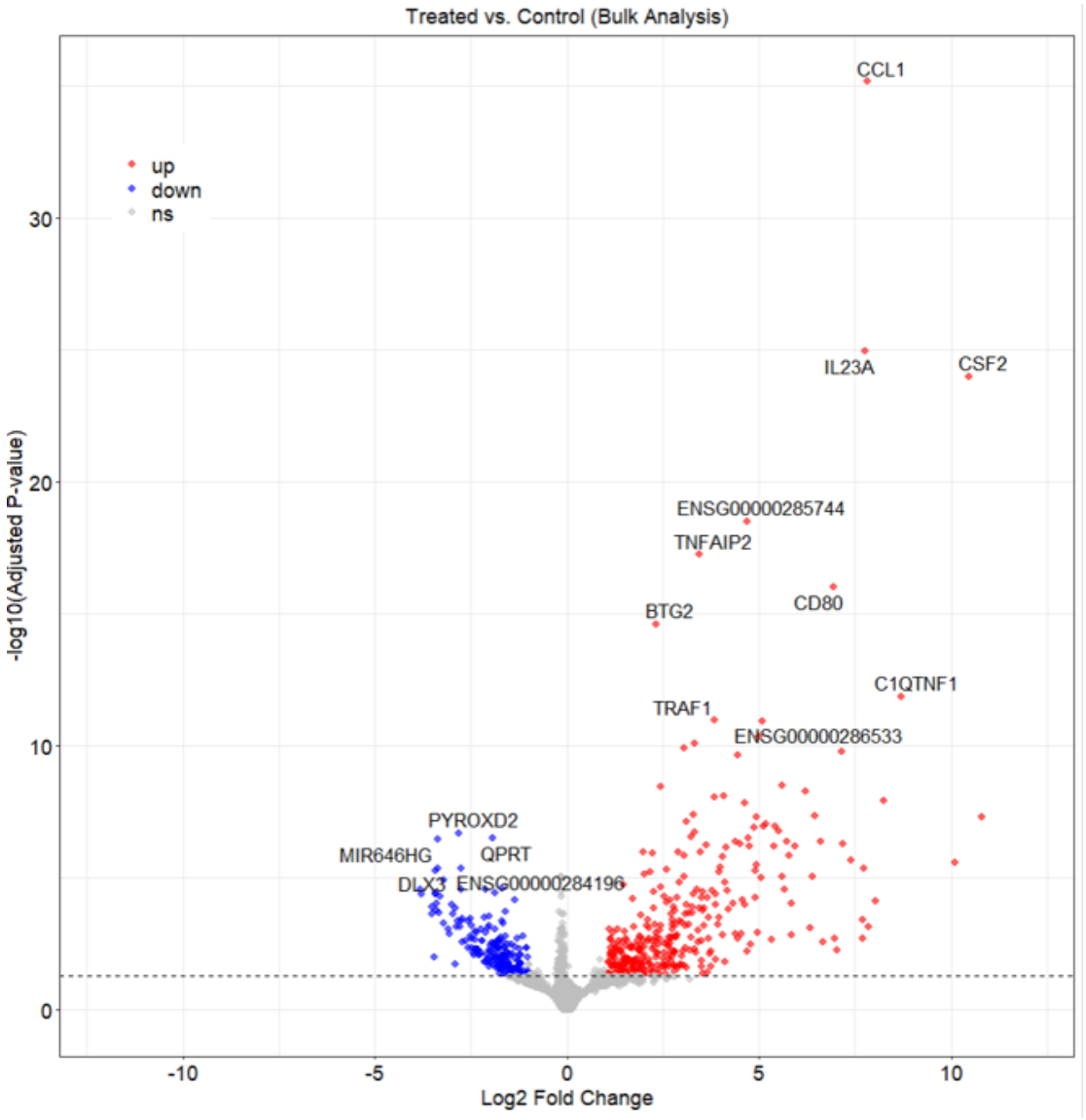


**Figure 4.21: Overall differential expression analysis of THP-1-derived macrophages subjected to *L. pneumophila* OMVs compared to untreated controls.**

The volcano figure illustrates the log2 fold-change in gene expression (x-axis) vs statistical significance (–log10 adjusted P-value, y-axis) for all identified genes. Red dots represent highly elevated genes, blue dots signify significantly downregulated genes, and grey dots suggest non-significant alterations. The highlighted genes that are upregulated considerably are CCL1, IL23A, CSF2, and TNFAIP2, whereas the downregulated genes consist of PYROXD2, QPRT, and DLX3. The plot emphasizes unique transcriptional profiles in host macrophages following OMV exposure, with several immune response genes exhibiting significant upregulation.

Differential expression analysis (DEGs) of individual clusters revealed significant heterogeneity in gene regulation between macrophage subtypes after OMV internalization (Figure 4.22), where clusters 0 and 3 showed the highest transcriptional differences, with 753 up-regulated and 598 down-regulated genes in cluster 3, and 466 up-regulated and 329 down-regulated genes in cluster 0. Cluster 0 and cluster 3 of macrophage subtypes responded more to OMV stimulus and showed broad transcriptional changes, followed by cluster 4 with 365 up-regulated and 302 down-regulated genes.

In contrast, smaller clusters, such as 7 and 1, had fewer DEGs overall, which may reflect more subtle transcriptional shifts or less involvement in the OMV response. Cluster 7 had the least DEGs, with just 70 up-regulated and only 12 down-regulated genes.

In general, the number of activated genes was greater than that of inhibited genes in most clusters, suggesting overall activation or increased functional activity of macrophages after OMV entry. The varying numbers of DEGs across clusters highlight the presence of diverse macrophage subpopulations with unique transcriptional signatures. Such complexity mirrors the physiological reality in humans, where macrophages exhibit multiple activation states beyond the classical M1 and M2 states, including M2a, M2b, M2c, and M2d phenotypes, that are often masked in bulk RNA analyses (Martinez & Gordon, 2014; Sica & Mantovani, 2012). Heatmap for the top DEGs between both control and OMV treated macrophages among clusters is also shown in Figure 4.23. The pattern of gene expression across clusters (from cluster 0 to cluster 7) was not distinct; however, clear activation of these markers is evident in OMV treated macrophages compared to controls within individual clusters. KEGG analysis of these DEGs in all clusters revealed similar pathways related to the immune system; however, clusters 3 and 4 are described below due to their significant involvement in the regulation of

macrophage activation. GO and KEGG pathways of other clusters can be found in **Appendix 2.**

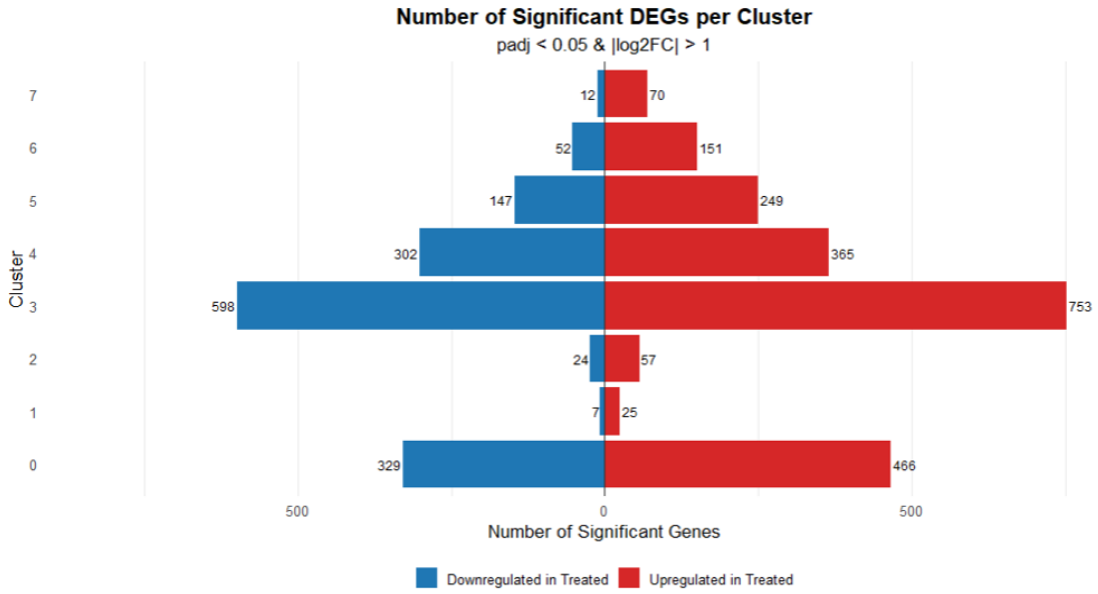


**Figure 4.22: Cluster-specific differential gene expression in THP-1 derived macrophages after treatment with *L. pneumophila* OMVs, as determined by scRNA-seq.**
The bar plot illustrates the number of substantially differentially expressed genes (DEGs) in each cluster (0–7), identified by an adjusted P-value of less than 0.05 and a $\log_2$ fold change above 1. Blue bars denote genes that are downregulated in OMV treated cells, whereas red bars highlight genes that are increased in OMV treated macrophages relative to controls. The y-axis represents the identity of cell clusters, whereas the x-axis denotes the number of DEGs per cluster. Cluster 3 had the highest number of DEGs. The results describe the transcriptional variability and cluster-specific responses of macrophages to OMV exposure. Vertical bars represent the number of upregulated (red) and downregulated (blue) genes in each cluster with an adjusted p-value of 1.

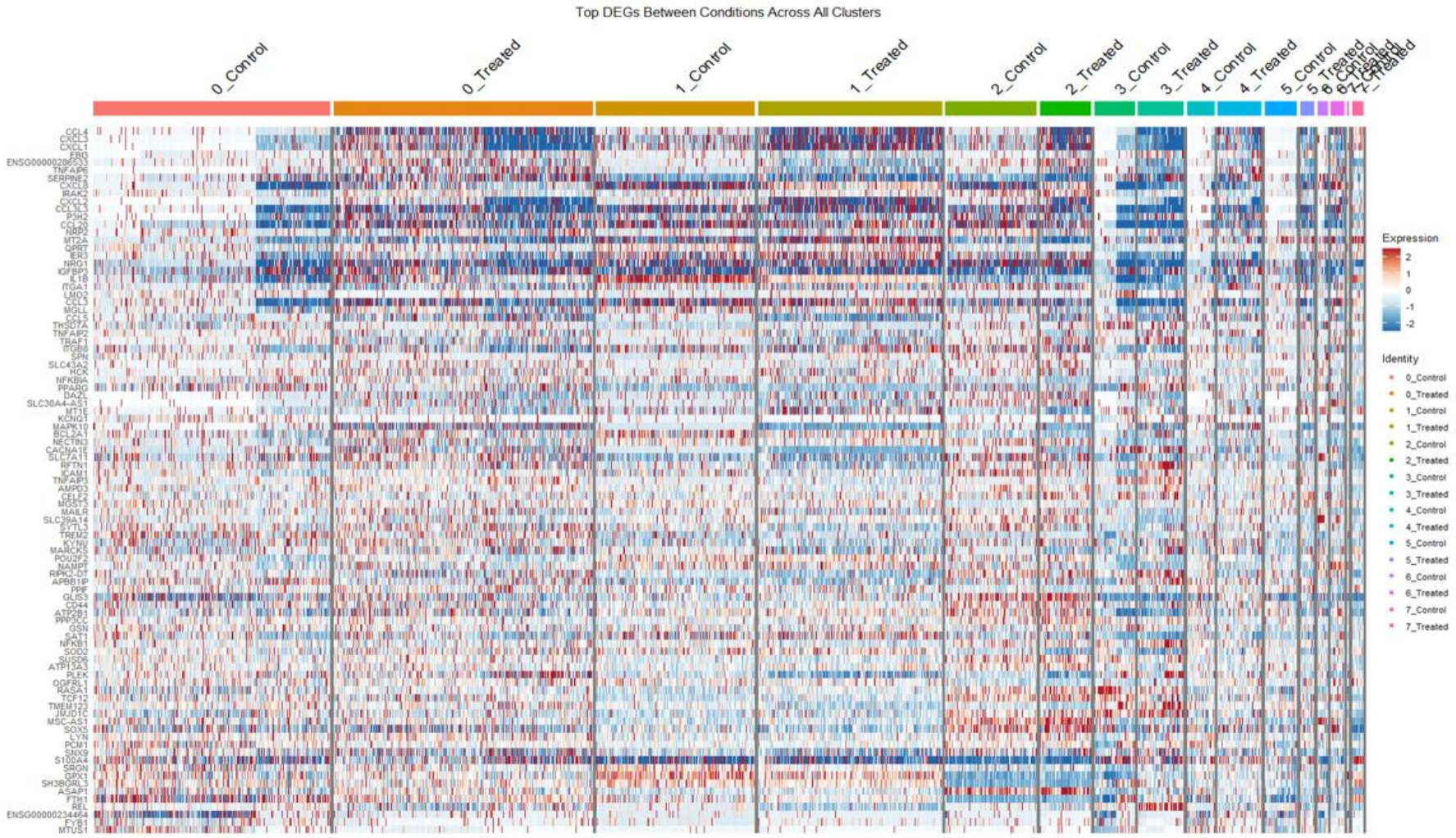


**Figure 4.23: This heatmap illustrates the top differentially expressed genes (DEGs) between control and OMV treated conditions across all eight macrophage clusters.** Each vertical section represents a cluster with separate columns for control and treated macrophages, showing gene expression patterns. Red indicates higher expression, while blue indicates lower expression. The figure highlights distinct transcriptional changes induced by OMV treatment that vary between clusters, reflecting heterogeneity in macrophage responses at the single-cell level.

#### 4.2.2.4. Macrophage activation markers in clusters 3 and 4

Clustering of single-cell RNA data revealed that clusters 3 and 4 exhibited significantly higher levels of immune-related gene activation after OMV exposure. DEG analysis revealed the highest upregulation of immune markers, including TNFAIP2, CD80, CD83, IL1B, CCL1, and CCL20. Some representative markers are shown in Figure 4.24 of violin plots. These markers belong to classical macrophage activation and immune response: TNFAIP2, an inflammatory signal, immediately inducible by TNF-α; CD80 and CD83, co-stimulatory molecules crucial for antigen presentation and T cell stimulation; IL1B encodes interleukin-1β which is synthesized to perform protective role for human body being a central mediator of innate immunity; CCL1 and CCL20 are immunocyte chemokines responsible for the recruitment of immune cells to site of inflammation. Moreover, clusters 3 and 4 elicited similar immune responses, with corresponding upregulation of the expression profiles of most key immune markers following OMV exposure.

These exceptionally high levels of pro-inflammatory cytokines and co-stimulatory molecules suggest that the regulatory activities in cluster 3 are crucial in controlling the host's immune response during OMV exposure. Consequently, our further analyses focused on these two clusters to determine the cellular and molecular mechanisms by which OMV-driven immune activation is mediated.

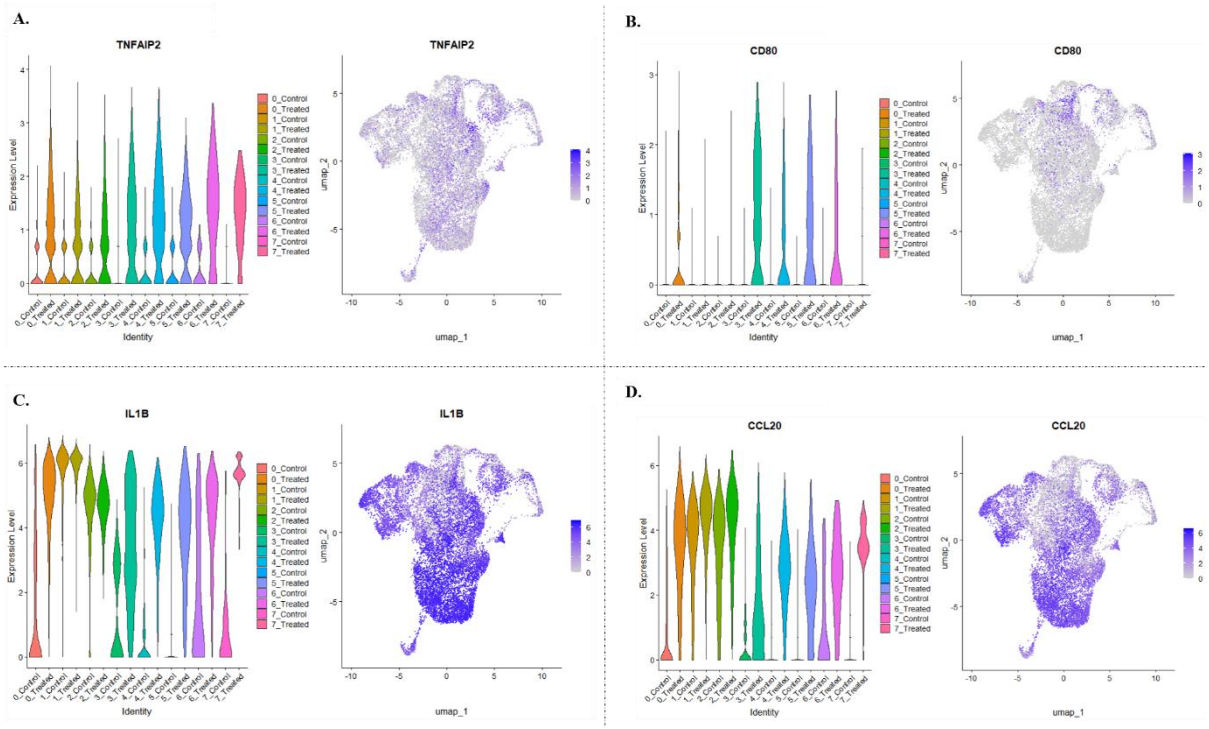


**Figure 4.24: Cluster localization and expression plot of selected immune response genes in THP-1 derived macrophages following *L. pneumophila* OMV treatment.**

Violin plots (left panels) illustrate single-cell gene expression levels for (A) TNFAIP2, (B) CD80, (C) IL1B, and (D) CCL20 throughout eight cellular clusters (0–7), categorized by control and OMV treated conditions. Each violin illustrates the distribution of expression within a specific cluster and condition. UMAP plots (right panels) depict the expression of each gene on the single-cell manifold, illustrating the spatial distribution and intensity of gene expression within individual cells. Expression levels are represented by a color gradient, with increased expression shown by a deeper shade of blue.

#### 4.2.2.5. Clusters 3 and 4 reveal hallmarks of M2b macrophage activation

Next, to understand the functional role of these clusters during disease pathogenesis, macrophage subtype activation markers were analyzed in clusters 3 and 4. Notably, these clusters exhibited significant upregulation of canonical M2b macrophage activation markers, including *CSF2*, *IL1B*, *CCL1*, *CCL20*, *IL6*, and *TNF*.

The dot plot in Figure 4.25 illustrates the average expression levels (dot size) and percentages of cells expressing each marker gene across clusters. All M2b phenotype markers showed significantly higher expression levels in clusters 3 and 4 compared to other clusters and controls (P-value < 0.05), indicating a strong, statistically significant activation.

Taken together, these findings indicate that cell populations in clusters 3 and 4 are preferentially activated by OMV exposure and polarize toward the M2b macrophage phenotype. M2b macrophage phenotype is characterized by both pro-inflammatory and anti-inflammatory immune responses. This skewing toward an M2b subpopulation suggests that OMVs contribute to the establishment of an immunoregulatory niche, potentially facilitating bacterial persistence and survival within the host environment.

**A.**

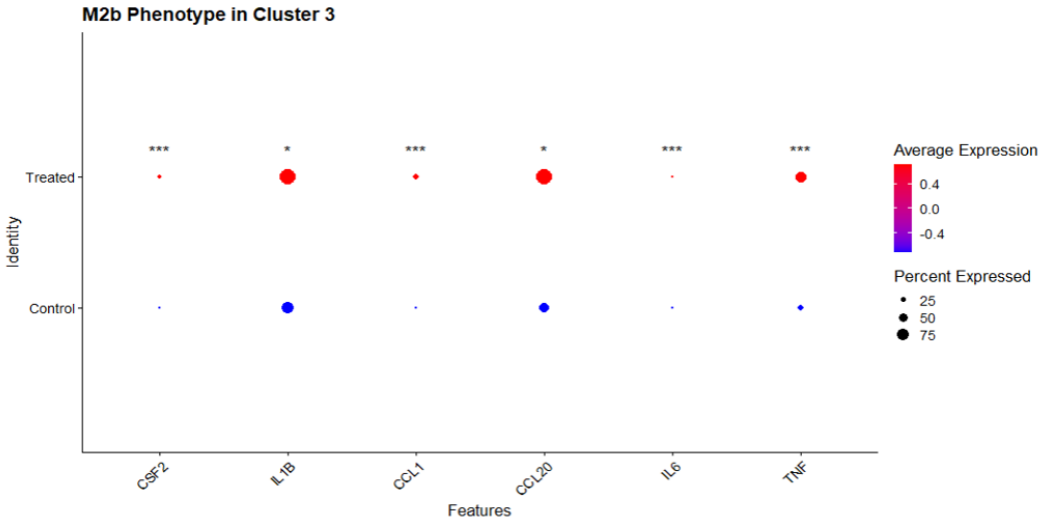


**B.**

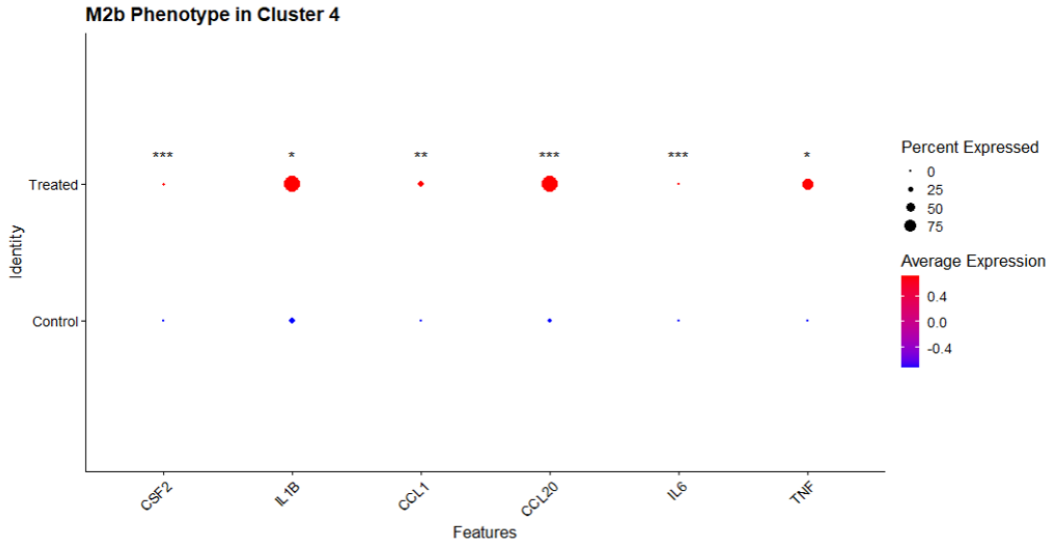


**Figure 4.25: Dot plot analysis of M2b macrophage phenotypic marker expression in the cell clusters following *L. pneumophila* OMV treatment.**

(A) Cluster 3 and (B) Cluster 4 dot plot illustrates the expression of certain M2b marker genes (CSF2, IL1B, CCL1, CCL20, IL6, TNF) in control and OMV treated THP-1 derived macrophage populations. Rows represent cell identity (Control versus Treated), whereas columns display marker genes. The color of each dot signifies the average gene expression (red = up-regulated, blue = down-regulated), while the size of the dot represents the proportion of cells in each group that exhibit the marker. Asterisks indicate statistical significance (*$p < 0.05$, **$p < 0.01$, ***$p < 0.001$) for differential expression between treatment and control groups. Both clusters exhibit significant activation of M2b signature genes in OMV treated macrophages, signifying the development of the immunoregulatory M2b phenotype following OMV exposure.

#### 4.2.2.6. Validation by qPCR

To validate our identification of the M2b macrophage subtype activation phenotype in scRNA-seq data, we conducted quantitative PCR to assess representative markers of M1, M2, and M2b macrophage subsets.

For single-cell experiments, THP-1-derived macrophages were treated with 20 μg/ml of OMVs. For validation, we incubated macrophages with increasing doses of OMVs (1 μg, 10 μg, and 20 μg) for 12 hours. We measured the expression of classical M1 markers, typical M2 markers, and M2 subtype-associated markers compared to untreated controls (Figure 4.26). The results indicated a strong, dose-dependent upregulation of all significant M2b markers tested: IL-6, TNF-α, IL-1β, and IL-10, with IL-6 and IL-10 increasing 79- to 85-fold compared with untreated controls respectively. TNF-α and IL-1β were upregulated almost 40-fold. In contrast, for the M1 marker sets, as well as the typical M2a, M2c, and M2d marker sets, there is a non-significant expression of some key markers. These observations support the scRNA-seq data and indicate that OMV exposure seems to induce a macrophage activation state towards the M2b side, with hallmark pro-inflammatory IL-1β, and anti-inflammatory IL-10 being expressed at the same time and at a high level. Table 4.4 summarizes the fold changes of marker sets for macrophage subtypes for classical M1 (bactericidal), M2a (tissue repair), M2b (immunoregulatory), M2c (anti-inflammatory), and M2d (tumor-associated) following highest dose treatment of *L. pneumophila* OMV.

To sum up, the qPCR results validated single-cell sequencing results and underline the importance of M2b polarization in macrophage response to OMV exposure, which can be critical for bacterial survival and immune evasion. qPCR analysis of these markers was also performed following 24- and 48-hour incubations; however, no significant changes were observed. Therefore, the results are tabulated in **Appendix 3.**

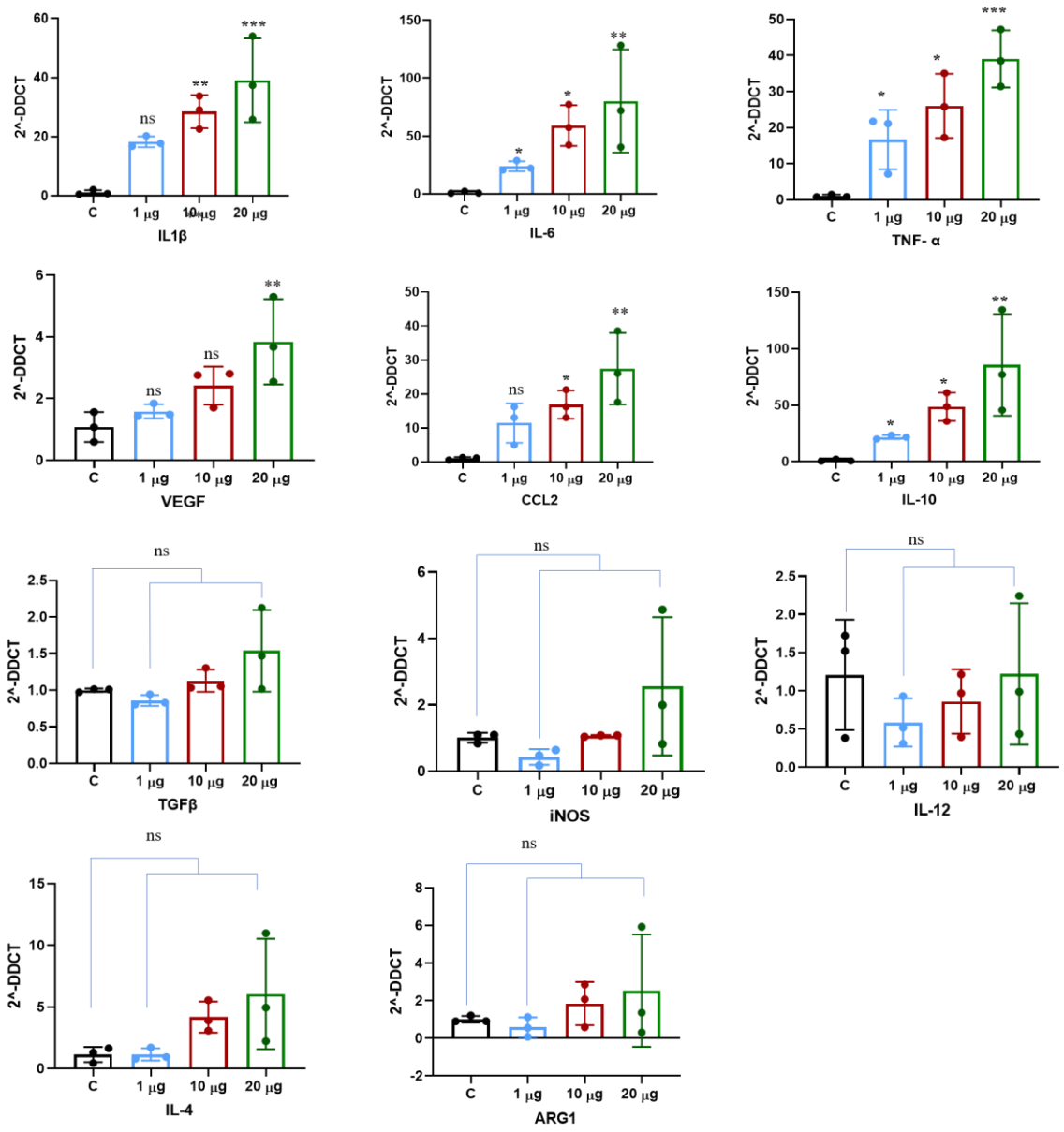


**Figure 4.26: qPCR evaluation of M1 and M2 markers expression in THP-1 derived macrophages following treatment with increasing doses of *L. pneumophila* OMVs.**

Bar graphs illustrate relative expression levels (2^-ΔΔCT) for specific genes: proinflammatory cytokines (IL1β, IL6, TNF-α), chemokines (CCL2), growth factors (VEGF), anti-inflammatory markers (IL-10), and polarization markers (TGFβ, iNOS, IL-12, IL-4, ARG1), after exposure to OMVs at concentrations of 1 µg (blue), 10 µg (red), or 20 µg (green), in comparison to untreated controls (black). The data indicate the mean ± standard deviation of three biological replicates for each condition. Marked elevations in gene expression are noted for proinflammatory markers (IL1β, IL6, TNF-α, CCL2, IL-10) in a dose-dependent fashion (*p < 0.05; **p < 0.01; ***p < 0.001), whereas polarization markers (TGFβ, iNOS, IL-12, IL-4, ARG1) exhibit no significant alterations (ns) among treatment groups.

**Table 4.4: qPCR verification of macrophage phenotype marker expression in 20 µg OMV treated macrophages relative to untreated macrophages (Tables A–E).**

**A**

| M1 type makers | Fold change | P-value | Significance |
|---|---|---|---|
| iNOS | 2.5 | 0.2685 | ns |
| IL6 | 79 | 0.036 | ** |
| TNF-α | 39 | 0.0011 | *** |
| IL1β | 39 | 0.0098 | *** |
| IL12 | 1.2 | 0.9862 | ns |

**B**

| M2a type markers | Fold change | P-value | Significance |
|---|---|---|---|
| IL4 | 6.05 | 0.1330 | ns |
| ARG | 1.5 | 0.4275 | ns |
| IL10 | 85 | 0.0295 | ** |
| CCL2 | 25 | 0.0062 | ** |

**C**

| M2b type markers | Fold change | P-value | Significance |
|---|---|---|---|
| IL1β | 39.08 | 0.0098 | *** |
| IL10 | 85 | 0.0295 | ** |
| IL6 | 79 | 0.036 | ** |
| TNF-α | 39 | 0.0011 | *** |

**D**

| M2c type markers | Fold change | P-value | Significance |
|---|---|---|---|
| IL10 | 85 | 0.0295 | ** |
| TGFβ | 1.5 | 0.1704 | ns |
| ARG | 1.5 | 0.4275 | ns |

**E**

| M2d type markers | Fold change | P-value | Significance |
|---|---|---|---|
| IL10 | 85 | 0.0295 | ** |
| VEGF | 3.8 | 0.0309 | ** |
| IL12(LOW) | 1.2 | 0.9862 | ns |
| TNF-α (LOW) | 39 | 0.0011 | *** |

#### 4.2.2.7. Expression of PRRs and NLRs in clusters 3 and 4

Immune responses are activated after recognition of a foreign antigen by PRRs (cell surface receptors) and NLRs (intracellular/ cytosol receptors). To understand how host macrophages can sense OMVs and activate specific pathways, we analyzed PRR and NLR expression in cluster 3 and cluster 4. Among all PRRs examined, TLR2 and CLEC4E (Mincle) were activated in cluster 3, indicating their active engagement in sensing OMV components. Among NLRs, NLRP3 was activated while STING1 was downregulated (Figure 4.27).

The involvement of TLR2 in *L. pneumophila* recognition is consistent with the literature, with TLR2 reportedly mediating macrophage responses to *L. pneumophila's* components that include lipoproteins and LPS (Shim et al., 2009). Whereas Mincle (CLEC4E) is known for its interaction with glycolipids on bacterial outer membrane vesicles. The above expression pattern of PRRs not only confirmed our hypothesis that LPS and glycolipids derived from OMV were the main stimuli for immune responses and M2b polarization in cluster 3, but also demonstrated that bacterial pathogens like *L. pneumophila* can hijack macrophage functions by the Mincle signalling pathway (Stegmann et al., 2024).

NLRP3 is a cytosolic receptor that identifies bacterial components such as bacterial RNA, extracellular ATP, and ion flow induced by bacterial toxins or cell wall fragments. STING1 detects cyclic dinucleotides—distinct bacterial second messengers, including c-di-GMP and c-di-AMP—typically present in bacterial DNA or released into the host cytosol. Activation of STING1 leads to the production of interferon gamma, which limits bacterial infection within the cell. Interestingly, *L. pneumophila* OMVs downregulate this receptor as an escape mechanism to prevent the host cell from interferon gamma immunity.

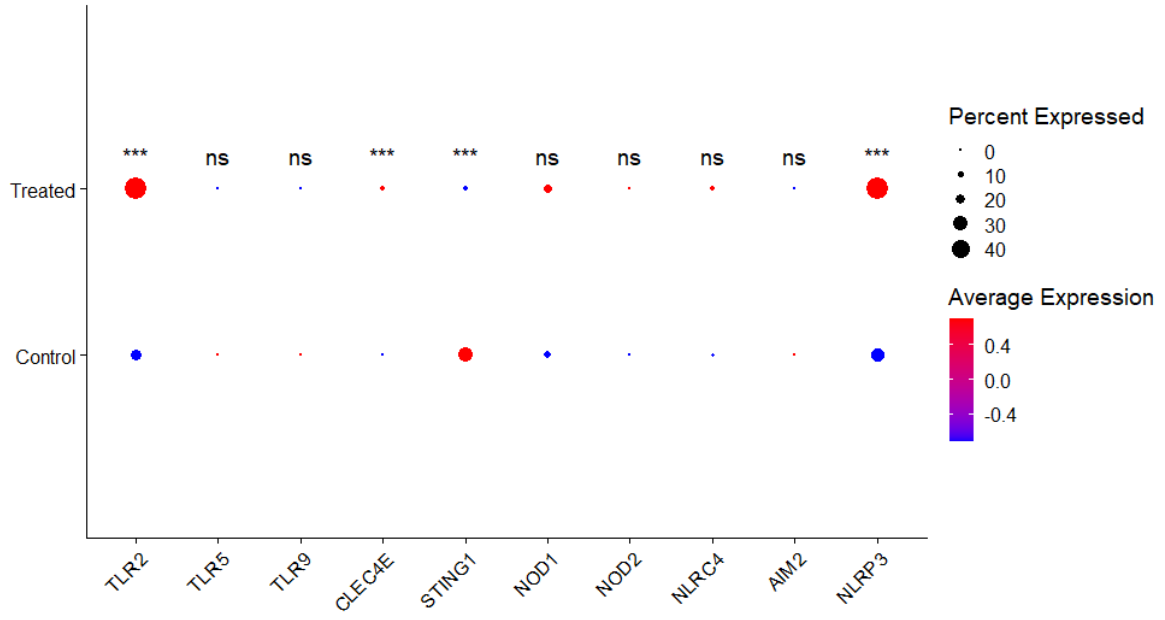


**Figure 4.27: Dot plot analysis of DEGs related to PRR activation in THP-1 derived Macrophages following *L. pneumophila* OMV treatment in Cluster 3.**

Dot plots illustrate the average expression (color scale: red = increased, blue = decreased) and the percentage of cells expressing each PRR genes (circle size) between untreated (Control) and OMV treated (Treated) macrophage populations for cluster 3. The investigated genes comprise TLR2, TLR5, TLR9, CLEC4E, STING1, NOD1, NOD2, NLRC4, AIM2, and NLRP3. Asterisks above each gene denote the statistical significance of differential expression between treatment and control conditions (***$p < 0.001$; ns = not significant). The OMV treatment significantly upregulated and elevated the expression frequency of numerous critical PRR genes, namely TLR2, CLEC4E, STING1, and NLRP3, in cluster 3 macrophages, demonstrating robust activation of innate immune sensing pathways in response to OMV exposure.

### 4.2.2.8. Anti-bacterial immunity (Interferon, RNS, and ROS production) in clusters 3 and 4

Interferons and the induction of ROS / RNS play key roles in the innate immune response elicited against intracellular pathogens. Previous work has shown that interferon signalling is critical to control *L. pneumophila* replication in macrophages, as it enhances the bactericidal capacity of host cells and thereby limits the bacterial burden (Stetson & Medzhitov, 2006) . In the same way, it is well recognized that the production of ROS and RNS is an established inactivation mechanism by which macrophages kill engulfed bacteria and prevent their intracellular proliferation.

Therefore, we evaluated the expression of interferon genes (type I and II), interferon-stimulated genes (ISGs), and genes linked to the generation of ROS and RNS to better describe the immune response triggered by *L. pneumophila* OMVs. These genes are essential components of classical antibacterial immunity. After OMV exposure, scRNA-seq revealed no upregulation of interferon genes or ISGs across any clusters. In fact, these interferon-related genes were undetectable in cleaned data. Similarly, OMV treatment did not lead to an increased expression of genes like NOS2 and CYBB, which are involved in the production of ROS and RNS (Figure 4.28). However, antioxidant genes SOD2, GLSM were found to be up-regulated that works in contrast to ROS and RNS generation.

The absence of these traditional antimicrobial responses further confirms that *L. pneumophila* OMVs do not trigger typical activation pathway of M1 macrophages, which is characterized by strong interferon signalling and the production of bactericidal ROS and RNS. Instead, the upregulation of immunoregulatory markers suggests a selective induction of the M2b macrophage polarization state, without the corresponding activation of potentially harmful antimicrobial effector mechanisms.

This pattern of selective immune modulation by *L. pneumophila* OMVs is likely advantageous for both the host and the pathogen. *L. pneumophila* may be able to escape host bactericidal mechanisms and increase its intracellular survival by promoting an immunoregulatory niche through M2b polarization using OMVs. Interestingly, the integrity of the host cells is also maintained for more bacterial replication, as there are no inflammatory or cytotoxic responses.

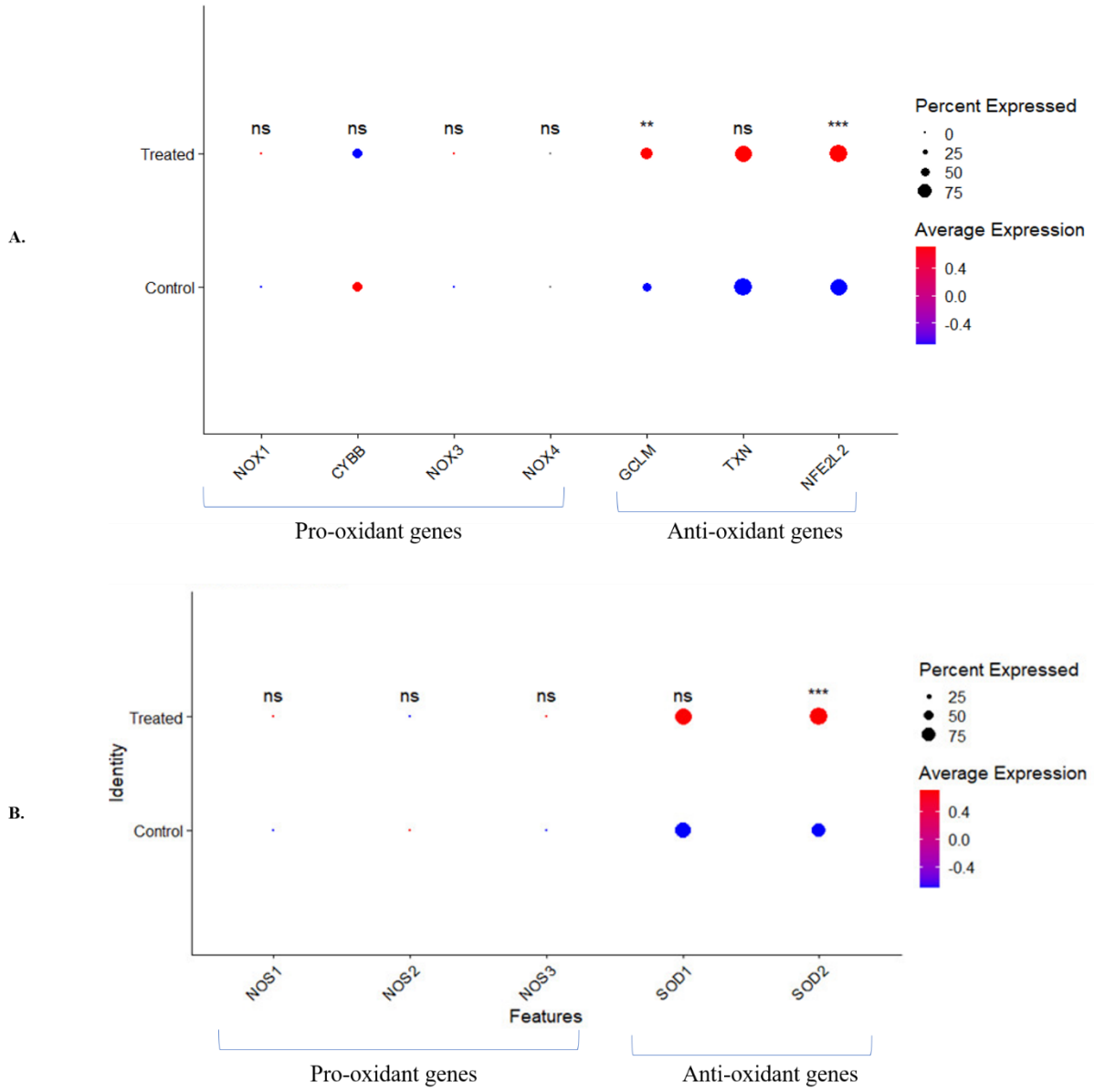


**Figure 4.28: Dot plot analysis of oxidative stress-related genes in THP-1 derived macrophages following *L. pneumophila* OMV treatment in cluster 3.**

Expression levels of pro-oxidant genes (NOX1, CYBB, NOX3, NOX4) and anti-oxidant genes (GCLM, TXN, NFE2L2) in macrophages treated with OMV compared to untreated (control) macrophages. (A) Expression of supplementary pro-oxidant genes (NOX1, CYBB, NOX3) and antioxidant genes (GCLM, NFE2L2) for reactive nitrogen species. (B) Expression of supplementary pro-oxidant genes (NOS1, NOS2, NOS3) and antioxidant genes (SOD1, SOD2) for reactive nitrogen species. For each gene, the color of the dot signifies average expression (red = elevated, blue = diminished), while the size of the dot represents the proportion of cells expressing the gene. Comparisons are shown for the control and experimental groups. Statistical significance is denoted above each dot: ns (not significant), **$p < 0.01$, ***$p < 0.001$. After exposure to OMVs, macrophages exhibited a notable elevation of critical antioxidant genes (particularly NFE2L2, GCLM, SOD2) with no impact on pro-oxidant genes, suggesting a transcriptional shift towards antioxidant state in response to *L. pneumophila* OMV OMVs.

#### 4.2.2.9. Enriched GO terms and KEGG pathways in cluster 3 and cluster 4

Further, gene ontology (GO) enrichment analysis was performed to gain insight into the biological functions of macrophage clusters 3 and 4 following OMV internalization. GO enriched terms were classified into three categories, including Biological Process (BP), Cellular Component (CC), and Molecular Function (MF).

GO enrichment for cluster 3 shows that down-regulated genes were associated with synapse assembly, the control of cell component size, and actin filament polymerization (Figure 4.29). These terms relate to cytoskeletal remodelling and membrane organization, factors necessary for alterations in macrophage morphology and phagocytic capacity. Similarly, molecular functions, including actin and phosphatidylinositol binding, also related to cytoskeletal and membrane lipid interactions, were downregulated. In comparison, upregulated genes were associated with migration, chemotaxis, and cellular responses to IL-1.

However, GO enrichment analysis of cluster 4 revealed that down-regulated genes were associated with mononuclear cell migration and phagocytosis. In comparison, up-regulated genes were enriched for leukocyte and myeloid leukocyte migration, cell chemotaxis, response to interleukin-1, and chemokines. These observations are parallel to increased inflammation and cell migration responses in macrophages triggered by bacterial infection. Enriched terms for down-regulated genes at the cellular component level included synaptic membrane and neuron synapse, indicating the decreased potential interactions with neural membrane elements. Cytokine activity is one of the molecular function enrichments observed in up-regulated genes, highlighting cytokine-mediated immune regulation after OMV exposure.

GO enrichment profiles of clusters 3 and 4 (Figure 4.29) together suggest slightly different functions of both macrophage populations: cluster 4 is enriched for immune activation, inflammatory response, and cell migration pathways, indicative of immune modulatory role; while cluster 3 is enriched in cytoskeletal and membrane structural processes likely

contributing to adaptation of these cells for bacterial uptake as well as cell-to-cell interactions and tissue maintenance.

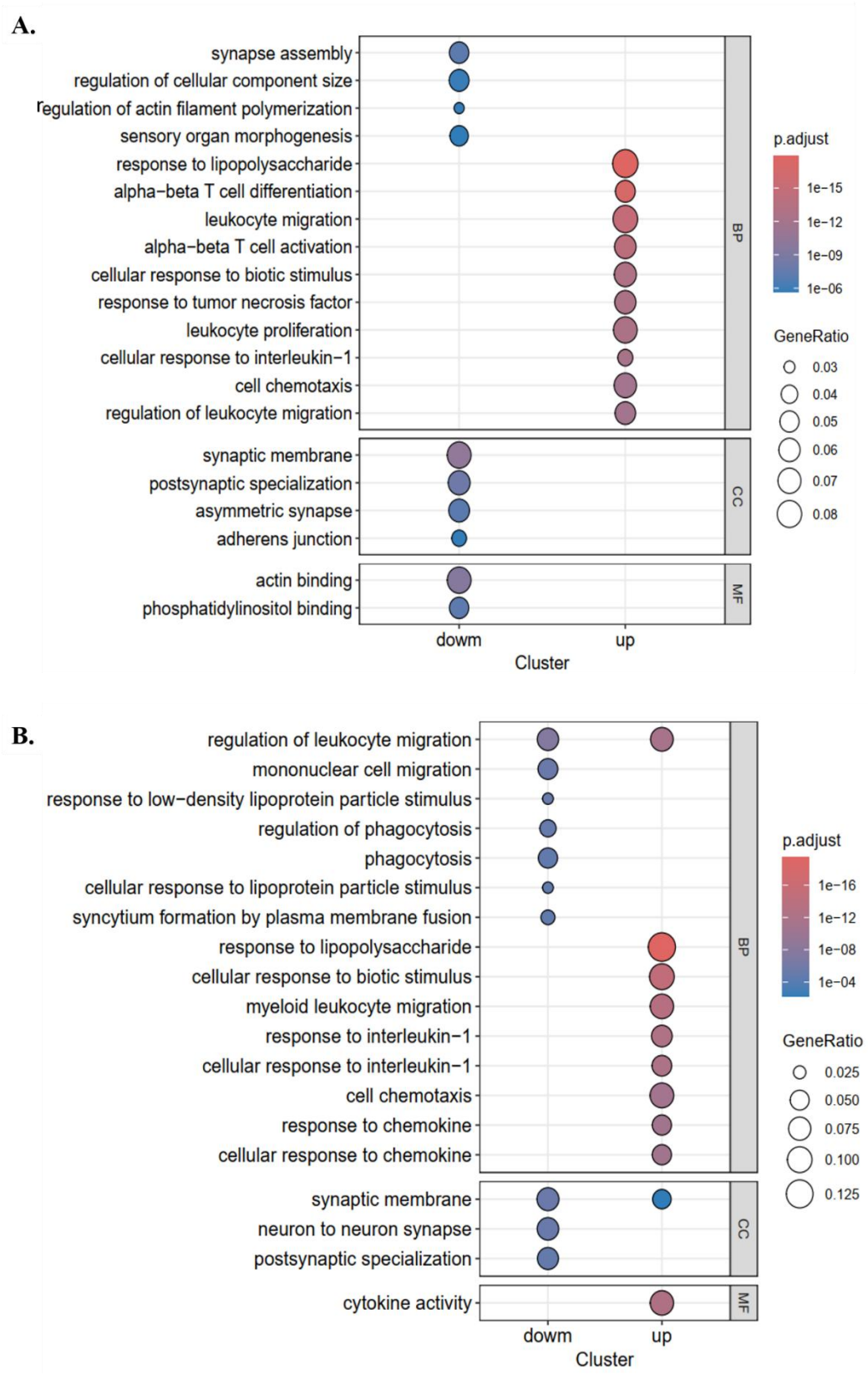


**Figure 4.29: Gene Ontology (GO) enrichment of DEG in THP-1 derived macrophages following *L. pneumophila* OMV treatment.**

(A) A dot plot illustrating substantially enriched Gene Ontology (GO) for genes of cluster 3 that are upregulated (right) and downregulated (left) after OMV treatment, classified by Biological Process (BP), Cellular Component (CC), and Molecular Function (MF). Dots symbolize distinct GO words, differentiated by adjusted p-value

(p.adjust; red indicates higher significance, blue indicates lower significance) and scaled according to gene ratio (the proportion of genes associated with that term). Upregulated genes are related to immunological activation and leukocyte migration (biological process), whereas downregulated terms pertain to synapse and cytoskeletal architecture. (B) A dot plot illustrating Gene Ontology enrichment for genes unique to clusters 4 within single-cell data, contrasting downregulated words (left) with upregulated terms (right). The enriched Gene Ontology words in the upregulated group encompass leukocyte movement, chemotaxis, and responsiveness to inflammatory stimuli, whereas the downregulated terms pertain to neural and synaptic activities.

KEGG analysis also verified that down-regulated pathways in cluster 3 were related to the cytoskeleton, adherens junctions, and Wnt signalling pathways, which are cell communication networks that regulate cell processes and central tissue regeneration. In comparison, immune activation pathways were up-regulated, like the TNF-signalling pathway, NOD-like receptor signalling pathway, NF-KB pathway, and JAK-stat pathway. Similarly, cluster 4 had upregulated pathways related to the TNF-signalling pathway, the NOD-like receptor signalling pathway, the NF-KB pathway, and IL-17 signalling pathways. In contrast, some processes related to metabolism and cell signalling were down-regulated (Figure 4.30).

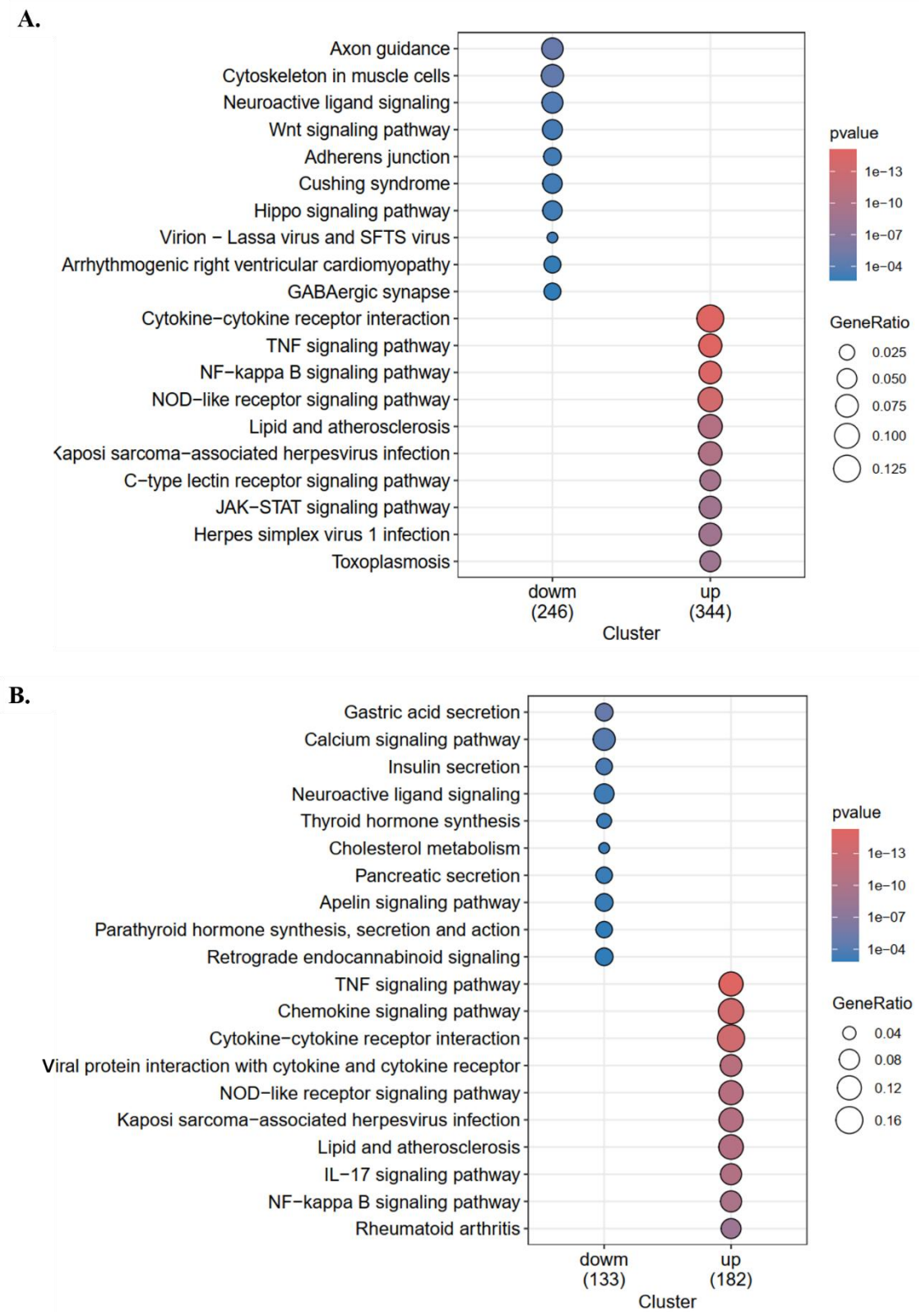


**Figure 4.30: KEGG pathway enrichment analysis of DEG in THP-1 derived macrophages following *L. pneumophila* OMV treatment.**

Dot plots illustrate the predominant KEGG pathways enriched in genes that are upregulated (right) and downregulated. The y-axis displays the names of the pathways. Dots signify distinct pathways, with color denoting the corrected p-value (red = higher significance; blue = lower significance) and size reflecting the gene ratio (the fraction of differentially expressed genes associated with each route). (A) Genes elevated in Cluster 3 are enriched

in immunological and inflammatory pathways, including cytokine-cytokine receptor interaction, TNF signaling, NF-κB signaling, and associated infection and immune response pathways. Downregulated genes include metabolic and signaling processes, such as axon guidance, calcium signaling, and stomach acid production. (B) Cluster 4 exhibits a similar increase in immunological signaling and infection-associated pathways. In contrast, downregulated words pertain to metabolic and secretory processes. This investigation emphasizes the functional specialization and immune activation pathways in macrophage subpopulations following OMV exposure.

#### 4.2.2.10. Summary of ScRNA-seq results:

Key findings are summarized as follows:

1. Macrophages are highly plastic and heterogeneous by nature. Our scRNA-seq revealed heterogeneity by detecting multiple macrophage subpopulations within a single macrophage cell type. Additionally, these heterogeneous populations also exhibit varying responses to OMV stimuli; some sub-populations of macrophages (clusters 0, 3 and 4) are more responsive compared to others (clusters 1, 2, 5,6, and 7).

2. Among the various activation states of macrophages, it was identified that *L. pneumophila* OMVs modulate macrophages toward the M2b polarization state, which is characterized by the presence of both pro-inflammatory and anti-inflammatory factors. This immunoregulatory niche is known to benefit pathogens by providing an environment in which they can survive and replicate more effectively.

3. Anti-bacterial defence mechanisms like interferon, reactive oxygen species, and reactive nitrogen species were not activated, confirming the immunoregulatory profile of these macrophage clusters 3 and 4.

4. PRR analysis revealed that these immune responses could be generated by TLR2 and CLEC4E (Mincle) cell surface receptors, after recognizing LPS and glycolipids from the *L. pneumophila* OMVs membrane, respectively.

5. Finally, we assumed that M2b polarization is primarily driven by activation of the NF-κB signalling pathway from KEGG analysis, as literature shows that NF-κB signalling drives mixed cytokine production (pro-inflammatory and anti-inflammatory), necessary for M2b activation state.

### 4.2.3. Functional characterization of macrophage responses following *L. pneumophila* OMVs exposure

To validate the significance of the transcriptional changes identified at single-cell resolution, a series of functional assays was conducted on macrophages treated with OMVs. Additionally, the effects of OMV dosages and exposure duration were evaluated in these functional assays to assess their impact.

These tests include a cytokine array to profile 105 secreted inflammatory mediators, an MTT assay, which measures cellular viability and metabolic state, the ROS assay, which quantifies levels of oxidative stress, caspase activity assessments for apoptosis detection, and bacterial survival assays to determine the implications of OMVs on *L. pneumophila* replication within macrophages. Collectively, these studies offer complementary views on the functional implications of transcriptional responses to OMVs.

#### 4.2.3.1. Cytokine Array

To validate the immune-modulatory potential of *L. pneumophila* OMVs at protein levels, THP-1 cell-derived macrophages were treated with increasing doses of OMVs. For the time point study, we used 24 and 48 hours, which are essential for measuring the early and late cytokine responses, respectively. After incubation at different dose and time conditions, cytokine profiles were examined in both control and OMV-treated macrophages.

Blot intensities were measured from control, 1 µg, 10 µg, and 20 µg OMVs groups in triplicate. Representative images of one blot group for the 24-hour time point are shown in Figure 4.31 here. The remaining blot images are shown in **Appendix 4.**

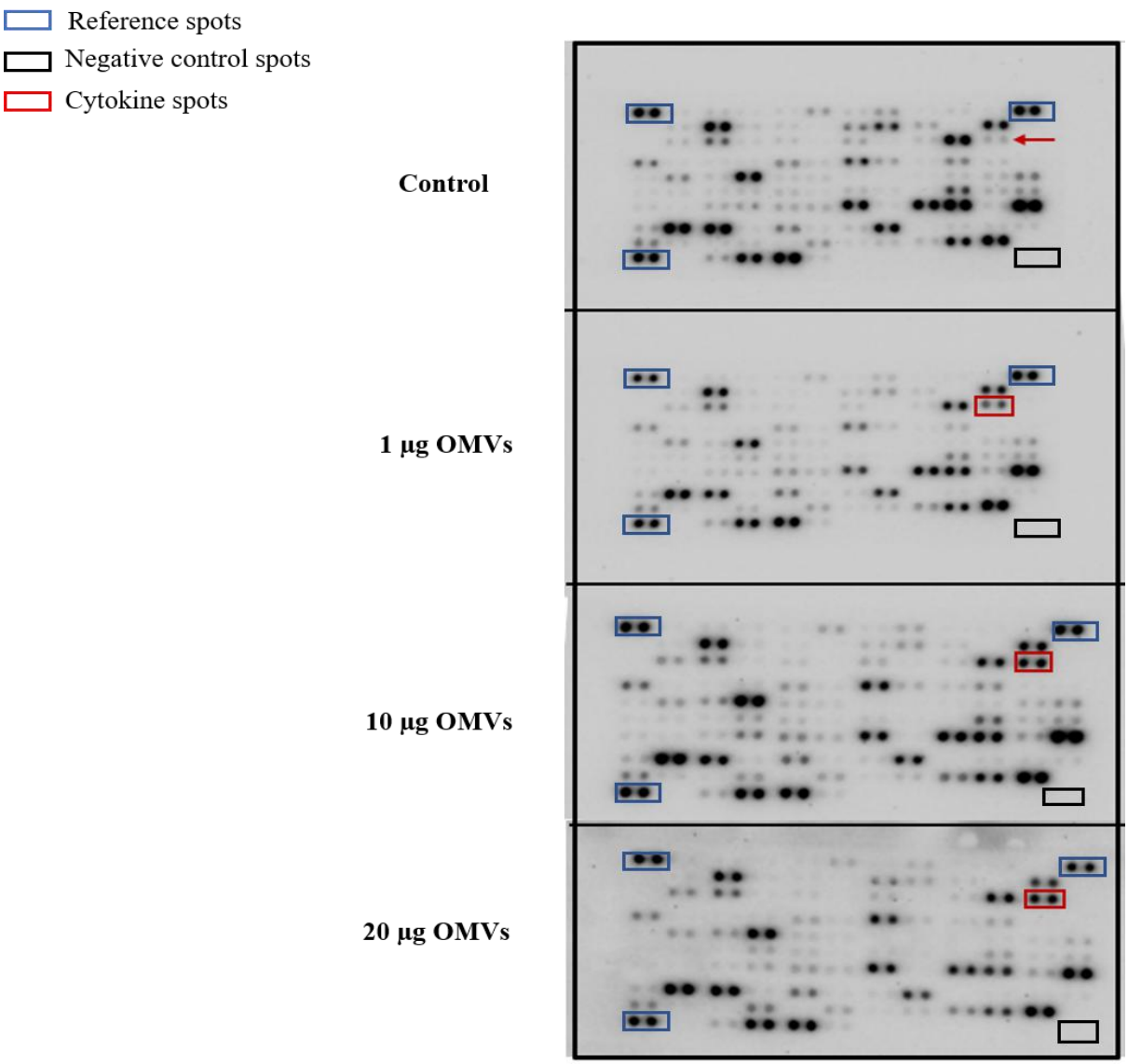


**Figure 4.31: Analysis of cytokine profiles in THP-1-derived macrophages following treatment with increasing doses of *L. pneumophila* OMVs using a proteome profiler array.** Representative cytokine profiles from control (untreated) macrophages and those treated with increasing doses of OMV (1µg, 10µg, 20µg). Each panel exhibits replicated locations for various cytokines, positive reference locations (blue boxes), and negative control locations (black boxes). One cytokine of interest is shown here inside red boxes, demonstrating an increase in the expression of several proinflammatory cytokines after OMV exposure. Arrays exhibit a total of 105 cytokines. The Experiment was performed in triplicate. One representative blot experiment is shown.

The cytokine profiles of THP-1-derived macrophages after *L. pneumophila* OMVs treatment at 24 h and 48 h revealed that among 105 cytokines, 46 cytokines were found to be differentially expressed. However, the expression profile showed a varied pattern for both dose and time series. Regarding the time point, expression of all cytokines was reduced at 48 hours compared to those at 24 hours, highlighting the greater modulation of the host cell immune responses at 24 hours.

Regarding the dosage effect, the expression of some cytokines showed a definite dose-related increase. For example, at 24 hours, GM-CSF and IL-19 levels correlated with increasing OMV concentrations, consistent with a dose-dependent stimulatory effect of OMVs on their release. The same pattern was observed for CD30 and Cripto-1 (Figure 4.32 and 4.33).

In contrast, some cytokines showed a non-linear response to OMV stimulation. Interestingly, the highest expression was observed at 1 µg and was variable at 10 µg and 20 µg. The most differentially expressed cytokines showed non-linear response. Important cytokines of this category are IL-1β, IL-2, IL-3, IL-4, IL-5, IL-32, IL-27, IL-22, IL-10, Flt-3 ligand, Fas ligand etc. Some of these cytokines exhibit a reverse pattern, with high expression at low doses and the lowest expression at the highest dose. For example, at 24 hours, the fold change for IL-27 was approximately 2.86 at the

lowest dose and 2.21 at the highest dose, suggesting an inhibitory effect at the highest dose. Furthermore, most of these cytokines exhibited disparate patterns in terms of dose. For instance, anti-inflammatory cytokines IL-4 and IL-10 exhibited the highest expression at 1 μg and 20 μg, respectively, while the lowest expression was at 10 μg at 24 h. Likewise, the expression of certain growth factors, such as growth hormone, leptin, and HGF, was also not well-defined by dose, indicating a complex mode of regulation for these various cytokines in response to OMV contact. Cytokines were categorized into different subgroups based on their functions, as described by the IPA. The bar charts of the 46 differential cytokines are shown in Figures 4.32-4.35.

Additionally, these 46 cytokines were also differentially expressed in scRNA-seq data with same pattern. Dot plot of these can be found in **Appendix 5.**

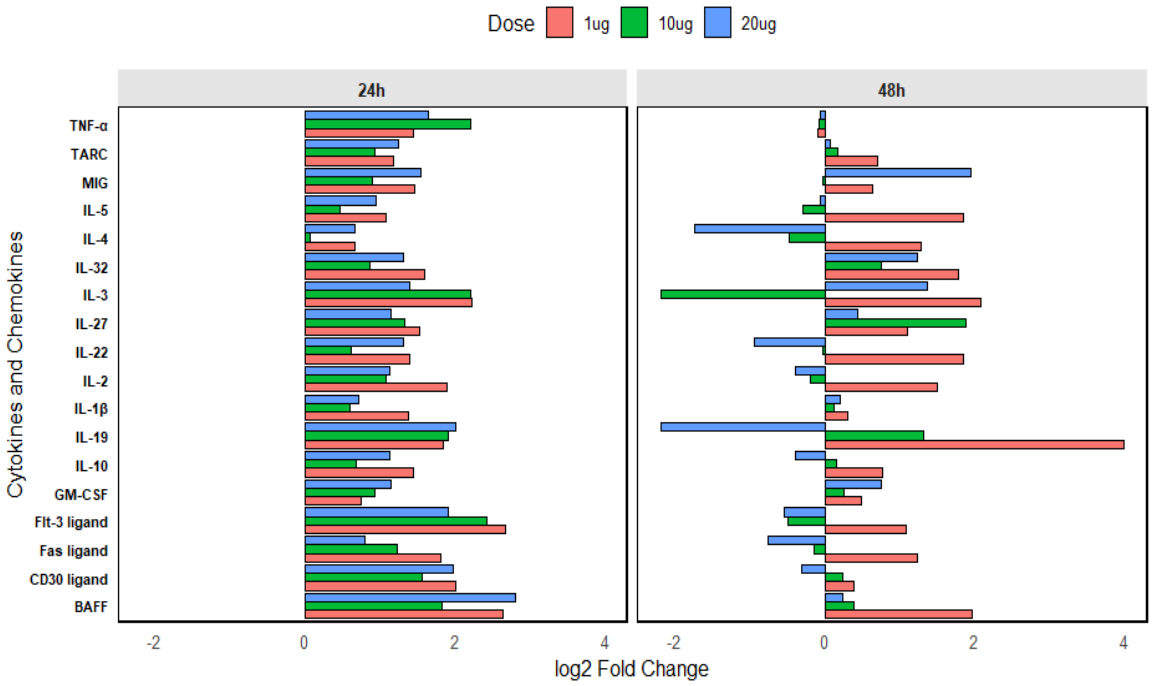


**Figure 4.32: Analysis of cytokines and chemokines following treatment with *L. pneumophila* OMVs using cytokine array.**

Bar graphs illustrate the log2 fold change in the expression of specific cytokines and chemokines at 24 hours (left panel) and 48 hours (right panel) after exposure to increasing OMV doses (1 µg, red; 10 µg, green; 20 µg, blue). The y-axis shows identified cytokines and chemokines, whilst the x-axis represents log2 fold-change to untreated controls.

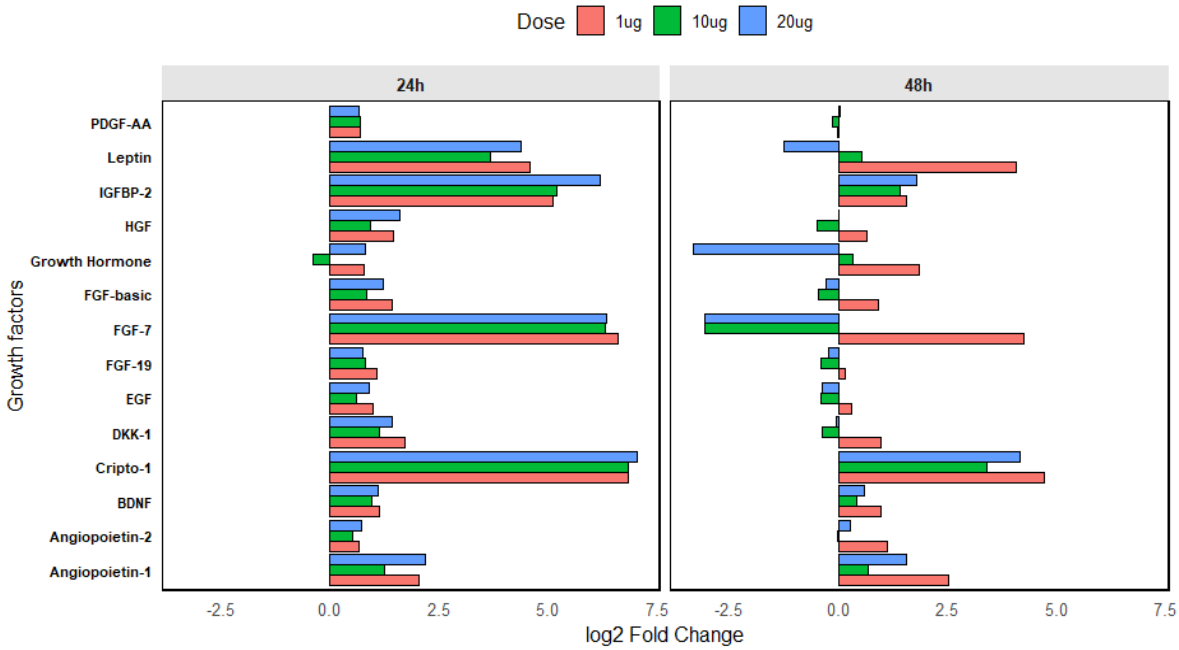


**Figure 4.33: Analysis of Growth factors following treatment with *L. pneumophila* OMVs using cytokine array.**

Bar graphs illustrate the log2 fold change in the expression of specific cytokines and chemokines at 24 hours (left panel) and 48 hours (right panel) after exposure to increasing OMV doses (1 µg, red; 10 µg, green; 20 µg, blue). The y-axis shows identified growth factors, whilst the x-axis represents log2 fold-change to untreated controls.

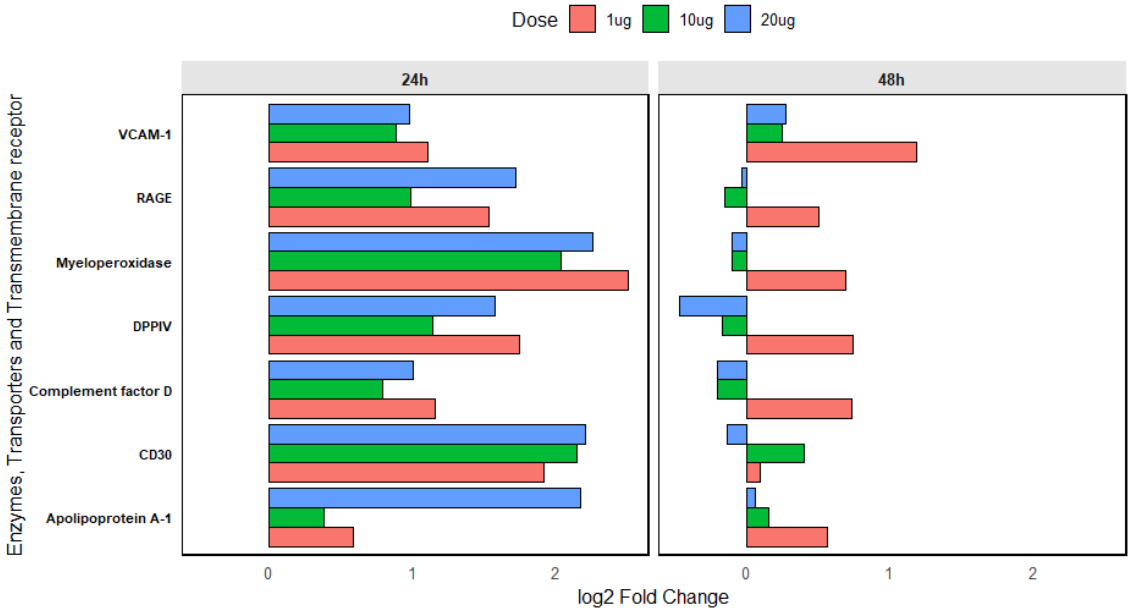


**Figure 4.34: Analysis of Enzymes and Transporters following treatment with *L. pneumophila* OMVs using cytokine array.**

Bar graphs illustrate the log2 fold change in the expression of specific cytokines and chemokines at 24 hours (left panel) and 48 hours (right panel) after exposure to increasing OMV doses (1 µg, red; 10 µg, green; 20 µg, blue). The y-axis shows identified factors, whilst the x-axis represents log2 fold-change to untreated controls.

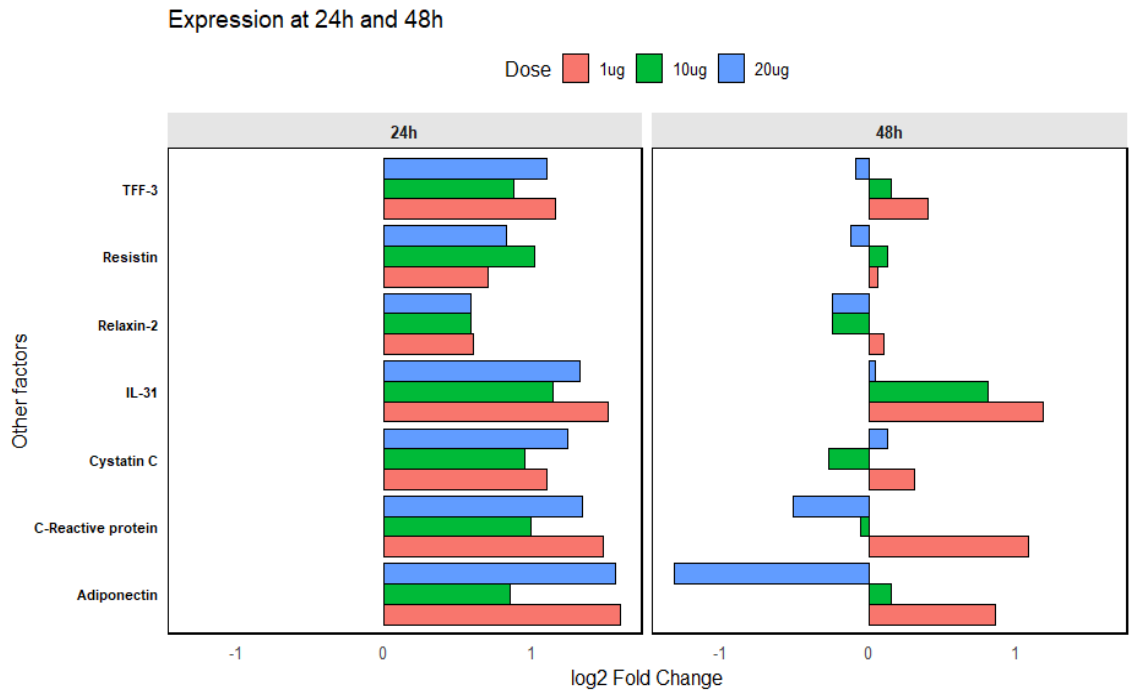


**Figure 4.35: Analysis of other factors following treatment with *L. pneumophila* OMVs using cytokine array.**

Bar graphs illustrate the log2 fold change in the expression of specific cytokines and chemokines at 24 hours (left panel) and 48 hours (right panel) after exposure to increasing OMV doses (1 µg, red; 10 µg, green; 20 µg, blue). The y-axis shows identified factors, whilst the x-axis represents log2 fold-change to untreated controls.

In summary, the following are key findings from the cytokine array.

1. This functional study confirmed the potent capacity of OMVs to regulate the host's immune response. OMVs can stimulate the production of a vast array of immune mediators in the host, including pro-inflammatory and anti-inflammatory cytokines and growth factors. Co-induction of pro-inflammatory cytokines (including TNF-α and IL-1β) and anti-inflammatory mediators (including IL-10) is consistent with scRNA-seq data that highlight an immune-regulatory M2b macrophage phenotype. High production of growth factors suggests a role for OMVs in tissue remodelling, repair, or immune cell survival, creating an environment that may support bacterial persistence/survival.
2. Heterogeneous cytokine responses were observed across varying doses of OMV. This can be attributed to the pleiotropic regulation of cytokines and the high degree of interdependence between these immune effectors. STRING interaction analysis supports this idea, as the 46 identified molecules are significantly interconnected proteins, indicating that OMVs do not act separately on individual pathways; instead, they coordinate a sophisticated, global immune response (Figure 4.36). The large size of this network of

cytokines enables them to work together to achieve an integrative immune response.

3. Lastly, the induction of more cytokines at 24 hours also highlights the activation of the innate immune system, while a decrease in cytokine responses at 48 hours can be related to the host cell transition from acute infection to resolution. Therefore, for downstream studies, a 24-hour time window was used to understand the mechanisms of *L. pneumophila* OMVs.

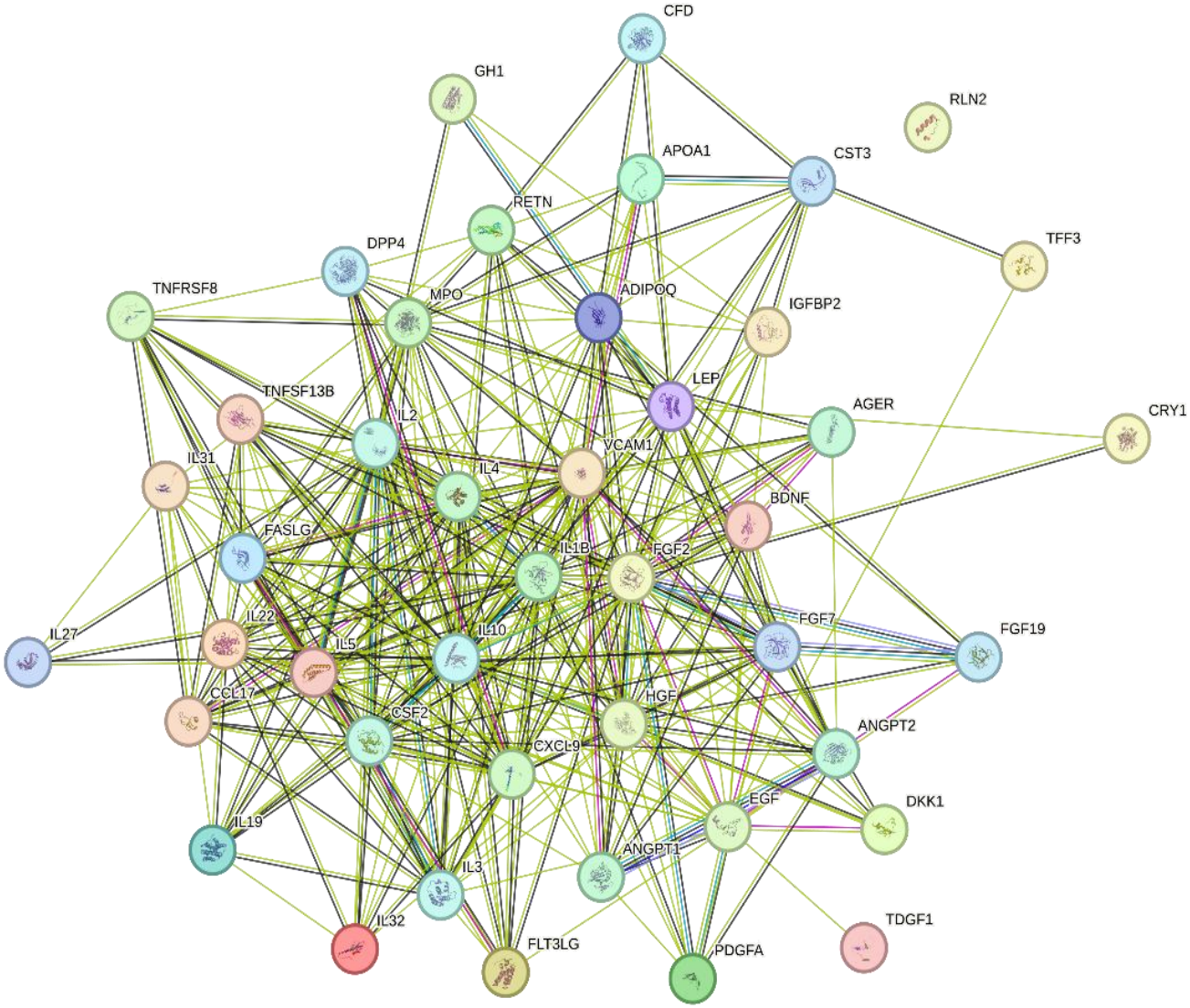


**Figure 4.36: STRING interaction network of 46 cytokines**.

The STRING interaction network for the cytokines appears to be closely linked and densely packed. Nodes represen each cytokine, and lines represent interactions. This extensive interconnectedness illustrates the significance o cytokine crosstalk, redundancy, and feedback in the regulation of immune system homeostasis and reactivity.

#### 4.2.3.1.1. Canonical pathway enrichment

To gain insight into the potential biological significance of these 46 cytokines, the fold change data for the 24-hour time point were analysed using the IPA tool to identify canonical pathways, diseases, or functions associated with the observed cytokine changes, which enabled the detection of the major signalling pathways and immune-related processes disrupted by OMV treatment. The canonical pathway enrichment plot (Figure 4.37) displays the most significantly altered pathways, sorted by -log(p-value) and coloured by predicted activation z-score. Orange colour bars show activation of the pathway, while blue/purple shows inhibition (Figure 4.37). Among canonical pathways, Pathogen-induced cytokine storm was the most enriched and activated pathway, followed by IL-17 signalling, macrophage classical activation, NF-κB Signalling, Chemokine Signalling, and IL-10 signalling. These observations are also in conjunction with scRNA-seq data. A subset of pathways has negative z-scores, including CLEAR Signalling and Autophagy, indicating that OMV treatment suppressed these essential host defense pathways, which may enhance the survival and replication of *L. pneumophila* within host cells.

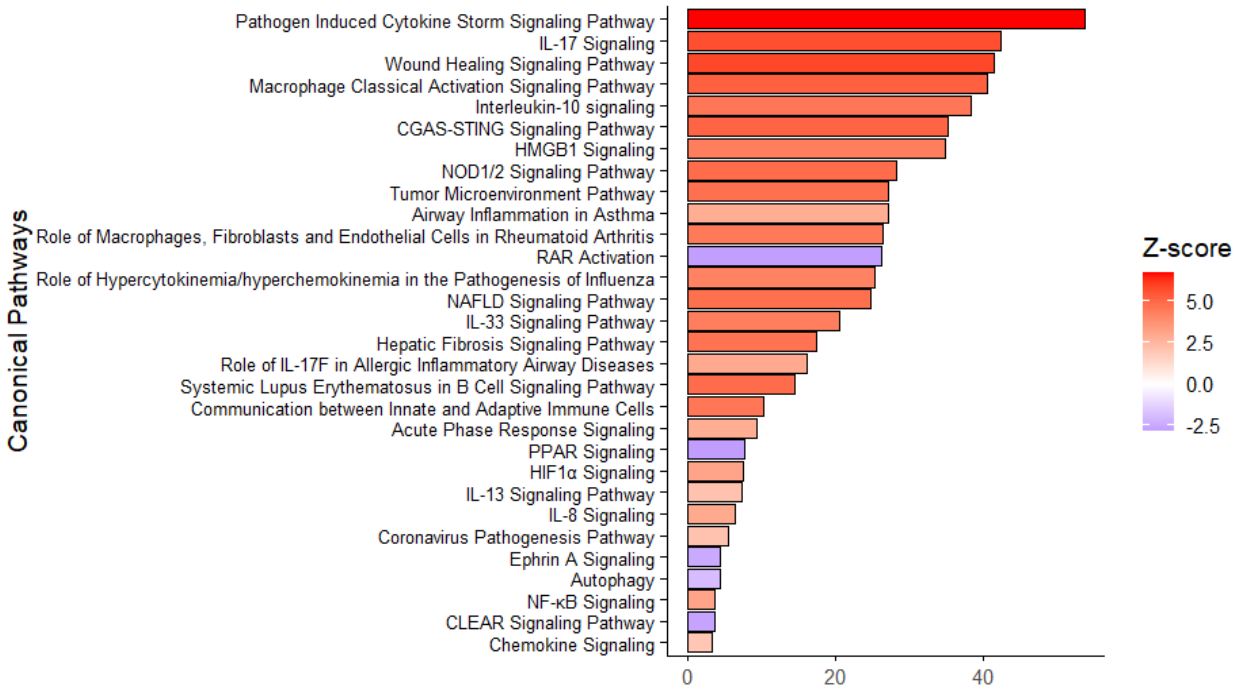


**Figure 4.37: Top enriched pathways from IPA for cytokine fold change of THP-1 derived macrophages following *L. pneumophila* OMV treatment:**

Length of bars shows the association of the path to the data based on the – log p value. While the colours of bars show the activation or inhibition of pathways, orange shows pathway activation, while purple shows pathway inhibition.

Furthermore, disease or function annotation indicated that these modified cytokines were associated with leukocyte migration, leukocyte cell movement, and chemotaxis (in conjunction with scRNA-seq GO results Figure 4.29). In addition, cell invasion, cell survival, and cell viability were increased (Figure 4.38).

Although the recruitment of immune cells to the infection site is generally considered to be advantageous to the host, some pathogens can exploit this process by attracting and infecting macrophages, thereby creating a niche for their replication. Similarly, activation of cell survival and cell viability helps bacteria replicate and survive, especially in chronic diseases.

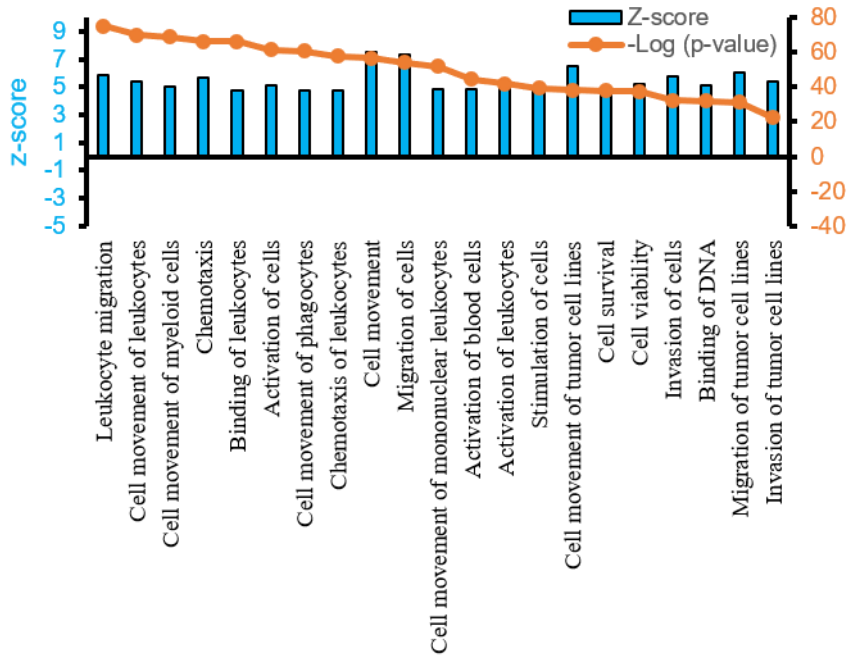


**Figure 4.38: IPA analysis of disease and function pathways enriched in THP-1 derived macrophages following *L. pneumophila* OMV treatment.**

The bar and line graph illustrates the most enriched diseases and biological activities found from the IPA analysis of cytokine fold change data following treatment with *L. pneumophila* OMV. The x-axis describes disease or biological processes (e.g., leukocyte migration, cellular mobility, chemotaxis, immune cell activation, cell survival, invasion). The left y-axis (blue) displays the IPA Z-score, signifying the anticipated activation or inhibition of each route. The right y-axis (orange) shows the statistical significance (–log p-value) for the enrichment of each function. The functions exhibiting the highest activation include leukocyte migration, chemotaxis, and the movement of myeloid and phagocytic cells.

#### 4.2.3.2. Surface marker analysis

To validate the expression of inflammatory and anti-inflammatory markers in OMV-treated macrophages, THP-1-derived macrophages were subjected to increasing doses of OMVs or left untreated as a control for 24 hours. Subsequently, flow cytometry was conducted to evaluate the surface expression of CD86 and CD163. CD11b was utilised as a universal antigen-presenting cell (APC) marker to confirm the macrophage features acquired from THP-1 cells after differentiation. About 80% of the cell population was positive for CD11b in both control and OMV treated groups, therefore affirming a uniform macrophage population for the specific marker's detection (Figure 4.39A).

In the control macrophages, approximately 1.5% of cells were positive for CD86. Nevertheless, OMV treatment resulted in a substantial increase in CD86-positive cells, reaching approximately 30%. CD86 is expressed in both M1 and M2b macrophage subsets, but is missing in M2a and M2c phenotypes. In contrast, the expression of CD163, a marker specific to M2d macrophages, was markedly reduced following OMV treatment at all OMV doses. No dose-dependent variations in the expression of CD86 or CD163 were seen in the flow cytometry study (Figure 4.39B).

This data indicates that OMV treatment alters macrophage polarization towards a phenotype characterised by elevated CD86 and reduced CD163 expression, one of the features of the M2b macrophage state. Histograms shown in Figure 4.40.

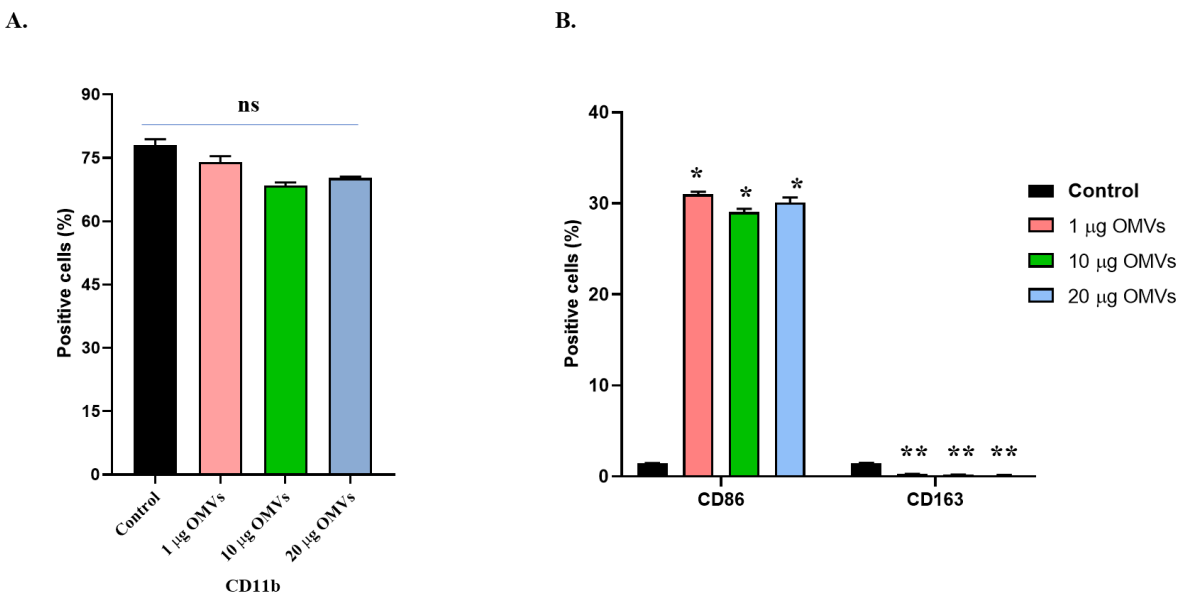


**Figure 4.39 Surface markers were analyzed for THP-1-derived macrophages following treatment with *L. pneumophila* OMVs utilizing flow cytometry.**

(A) Flow cytometry measured CD11b expression in macrophages subjected to increasing doses of OMVs (1 µg, 10 µg, 20 µg) relative to untreated controls. The bar graph illustrates the proportion of CD11b-positive cells (mean ± SD). No statistically significant variations in CD11b expression were seen across the treatment groups. (B) Assessment of macrophage polarization markers CD86 and CD163 using flow cytometry after OMV treatment. The bar graph illustrates the proportion of CD86- and CD163-positive cells for the control group and each OMV dosage. The OMV treated groups had a statistically significant elevation in CD86-positive cells (*$p < 0.05$) relative to the control, whereas CD163 signals were significantly decreased in the OMV treated groups (***$p < 0.001$ vs. control).

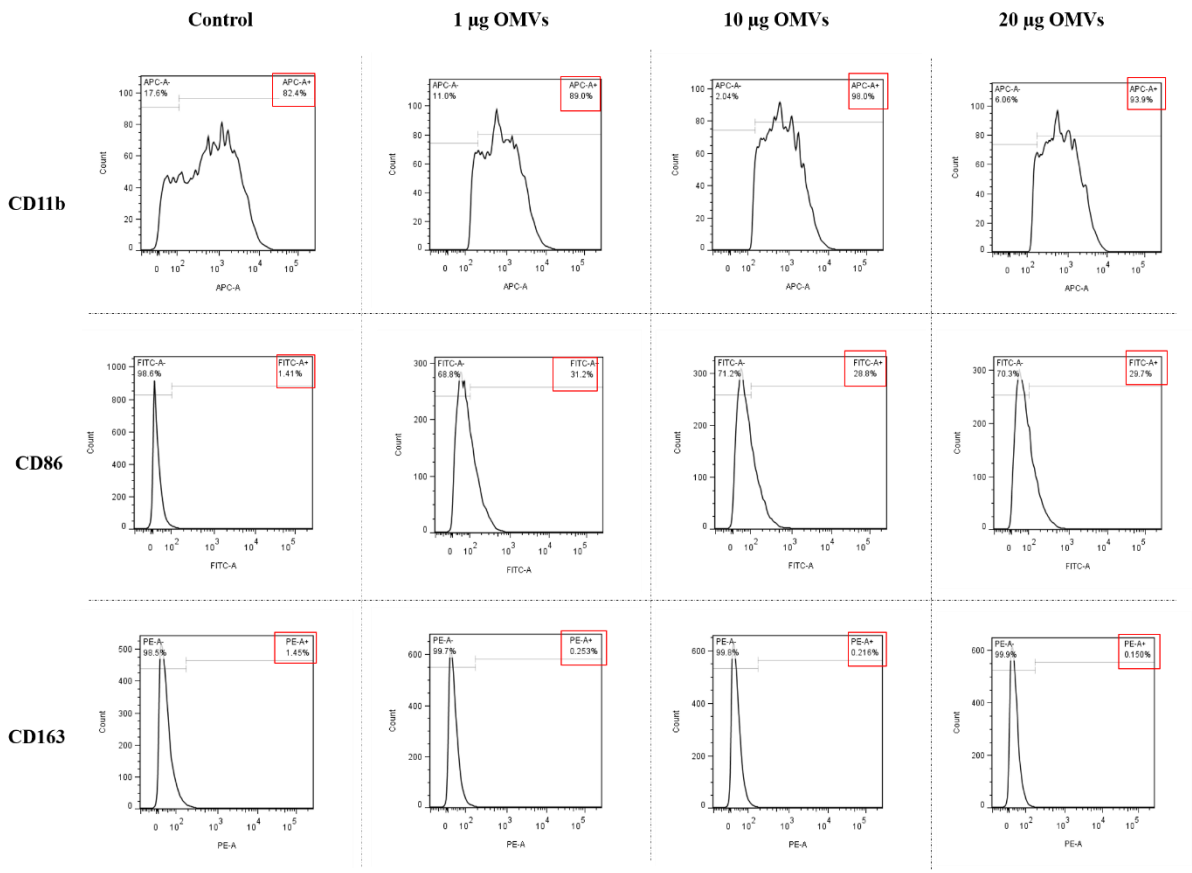


**Figure 4.40 Surface markers were analyzed for THP-1 derived macrophages following treatment with *L. pneumophila* OMVs utilizing flow cytometry.**

Representative histograms illustrate the expression patterns of three principal macrophage markers, including CD11b (top row), CD86 (middle row), and CD163 (bottom row), in control and OMV treated macrophages (1 µg, 10 µg, 20 µg OMVs). The percentage of marker-positive cells is displayed in the upper right corner of each figure in a red box. The rate of CD11b+ cells remained consistent (~82–93%) across all groups, demonstrating a persistent identity of THP-1 differentiated macrophages. CD86 (FITC): OMV treatment significantly increased CD86 expression, with CD68+ cells increasing from 4% in the control group to around 29–31% in the OMV treated groups, indicating macrophage activation (M1/M2b). CD163 (PE): The expression of CD163, a marker for regulatory M2c/M2a macrophages, is low (<1.5%) and diminishes further with exposure to OMV, indicating a suppression of the M2c/M2a phenotype.

#### 4.2.3.3. Cell viability assay

scRNA-seq data revealed the immunoregulatory profile of macrophages, with no cell-damage genes or pathways observed. Cytokine array with IPA analysis also showed that *L. pneumophila* OMVs promote host cell survival.

To confirm this, cell viability was assessed using the MTT assay. THP-1-derived macrophages were treated with increasing concentrations of OMVs for 24 hours or left untreated. Results were normalized with untreated control cells.

After 24 hours of incubation with *L. pneumophila* OMVs, no decrease in cell viability was observed; instead, all OMV treated groups showed increased cell viability compared to the untreated control. This increment was observed across all concentration levels, but was significantly higher at 1 μg/ml OMVs. The data indicate that OMV treatment is not cytotoxic to macrophages and may favour cell survival or proliferation under the conditions tested. The highest viability at 1 μg OMVs is also consistent with the above cytokine array results, which showed the highest secretome levels for most cytokines at 1 μg OMVs (Figure 4.41). Moreover, the increase in cell viability was also observable at the morphological level under the microscope (Figure 4.42).

The enhancement in cell viability by OMV treatment can be attributed to OMV-stimulated chemokines and growth factors, which drive large numbers of inflammatory

monocytes to the site of stimulation in response to chemokine gradients and adhesion molecules. During human pathophysiology, the recruited macrophages will reach and outnumber the resident macrophages. As macrophages are highly plastic, consequently, growth factors and cytokines in the local tissue environment mediate proliferation and substantial phenotypic and functional differentiation of both recruited and resident macrophages (Jenkins et al., 2013), resulting in extended cell viability.

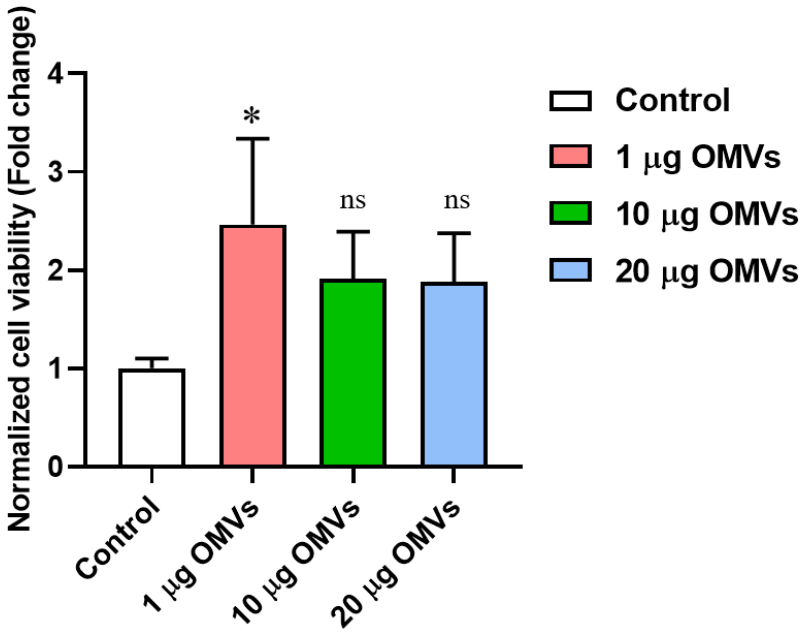


**Figure 4.41: Cell viability of THP-1 derived macrophage following treatment with *L. pneumophila* OMVs utilizing MTT assay.**

The bar graph illustrates the normalized cell viability (fold change) of THP-1 derived macrophages following a 24-hour incubation with OMVs at doses of 1 μg, 10 μg, and 20 μg, in comparison to untreated control cells. Data are expressed as mean ± standard deviation from biological replicates. A one-way ANOVA was conducted, followed by Tukey's post hoc test for multiple comparisons. OMV treatment did not pose any cytotoxic effect. Instead, treatment with 1 μg OMVs markedly enhanced cell viability relative to the control (*$p < 0.05$).

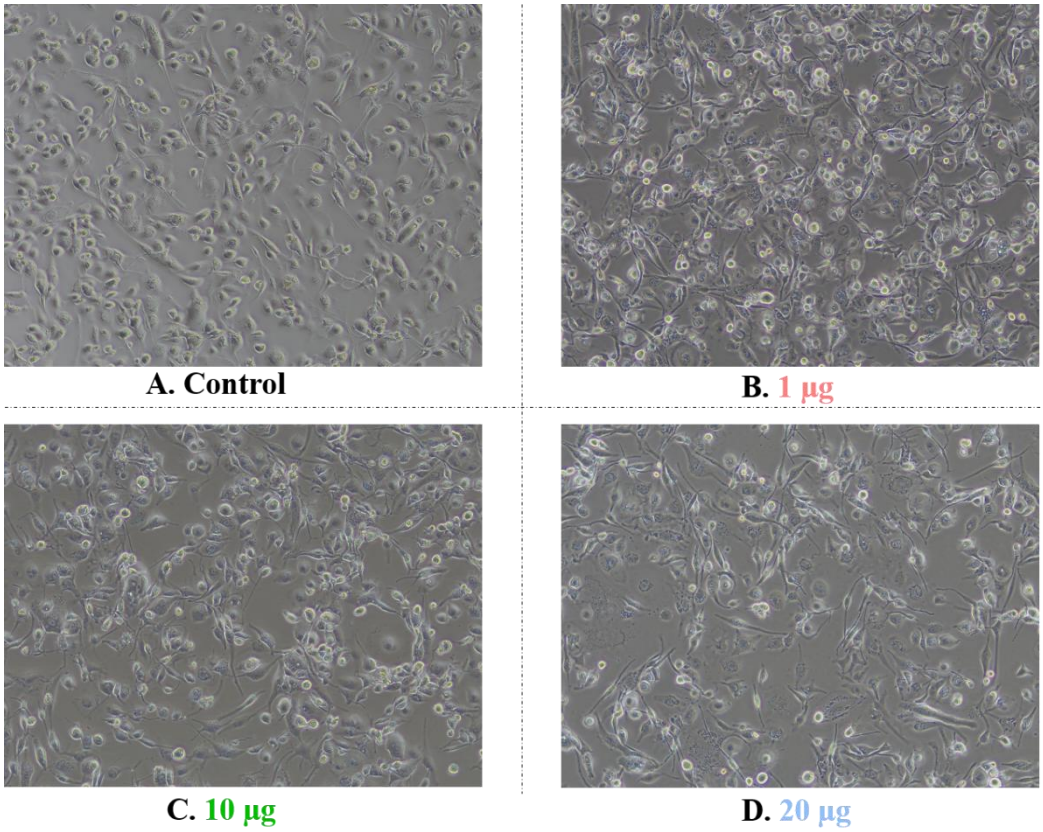


**Figure 4.42: Visualisation of THP-1-derived macrophage by plan confocal microscopy with or without treatment with *L. pneumophila* OMVs.**

Representative images of (A) untreated control, (B) 1 µg OMV, (C) 10 µg OMV, and (D) 20 µg OMV. Cell density increased after treatment with all doses of OMVs. However, 1 µg OMV displayed a higher number of cells relative to the other treatment groups. Morphological changes are also visible post-OMV treatment.

### 4.2.3.4. ROS assay

The scRNA-seq study indicated no substantial activation of ROS-associated genes after OMV treatment. Instead, a significant increase in the antioxidant gene SOD2 was observed (verified by qPCR). ROS assay were conducted to confirm the effect of OMVs on ROS generation. Treatment with 1 µg of OMVs led to a substantial decrease in ROS

levels, whereas no significant effect on ROS was observed at 10 µg and 20 µg doses (Figure 4.43A). The reduction in ROS generation at the 1 µg dosage correlates with increased expression of SOD2 (Figure 4.43B), suggesting that OMVs may have a beneficial antioxidant effect that likely contributes to both host cell survival and intracellular bacterial survival during infection.

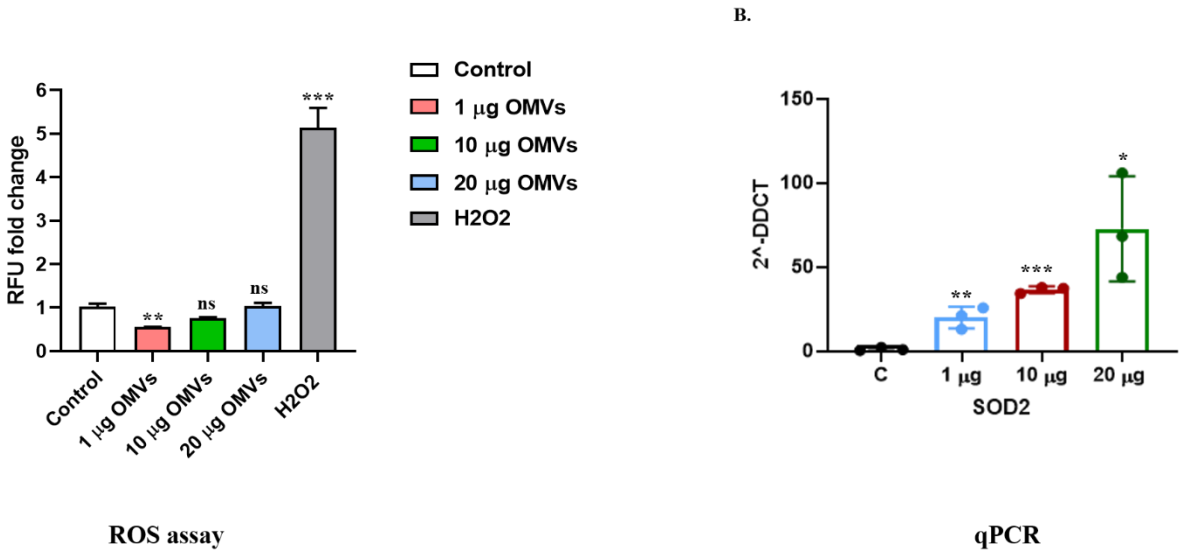


**ROS assay** **qPCR**

**Figure 4.43: *L. pneumophila* OMVs stimulate antioxidant responses and reduce ROS generation in THP-1 derived macrophages.**

(A) Reactive oxygen species (ROS) assay: THP-1-derived macrophages were exposed to increasing doses of OMVs (1, 10, and 20 µg) for 24 hours. Cellular reactive oxygen species (ROS) levels were quantified utilizing the Abcam ROS assay and shown as the fold change in relative fluorescence units (RFU) compared to untreated controls. Data are expressed as mean ± standard deviation from separate experiments. Statistical study utilized one-way ANOVA with Tukey's post hoc test with multiple comparisons. Treatment with 1 µg OMVs markedly decreased ROS generation (**$p < 0.01$), whereas higher OMV dosages had no significant impact. Hydrogen peroxide ($H_2O_2$) treatment served as a positive control for reactive oxygen species (ROS) induction (***$p < 0.001$, **$p < 0.01$). (B) Quantitative PCR analysis: The expression of the SOD2 antioxidant gene was assessed using qPCR in THP-1 macrophages after OMV treatment. SOD2 transcript levels were markedly increased at 1 µg (**$p < 0.01$), 10 µg (***$p < 0.001$), and 20 µg (*$p < 0.05$) compared to untreated controls.

#### 4.2.3.5. Active caspase-1 assay

Caspase-1 is a key mediator of the innate immune response to *L. pneumophila*. The active/cleaved form of caspase-1 induces pyroptosis, the death of infected cells. This is crucial for limiting and controlling *L. pneumophila* infection. IL-1β and IL-18 are key pro-inflammatory cytokines that activate pyroptosis. Although scRNA-seq data showed significant up-regulation of IL-1β and no up-regulation of IL-18, activation of caspase pathways was not observed. This finding was validated using an active caspase-1 staining kit. The results confirmed that OMVs, at any concentration, did not activate caspase-1 for pyroptosis, thereby favouring *L. pneumophila* survival (Figure 4.44).

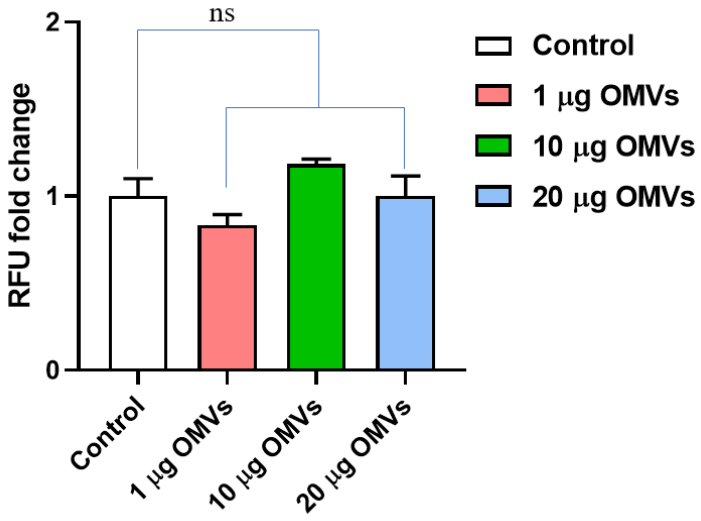


**Figure 4.44: Analysis of caspase-1 activity (Pyroptosis) in THP-1 derived macrophages following treatment with *L. pneumophila* OMV.**

The bar graph illustrates the relative activity of caspase-1 (RFU fold change) quantified with the Abcam Caspase-1 Fluorometric Assay Kit in macrophages subjected to 24-hour treatment with increasing doses of OMVs (1 μg, 10 μg, and 20 μg) in comparison to untreated controls. Data are expressed as mean ± standard deviation from separate experiments. Statistical study utilized one-way ANOVA with Tukey's post hoc test for multiple comparisons; findings indicated no significant differences (ns) in caspase-1 activity across all OMV dosages. This suggests that OMV therapy does not substantially modify caspase-1-dependent inflammasome activation under the specified experimental circumstances.

#### 4.2.3.6. Effects of OMVs on bacterial survival and replication inside host cell

Based on scRNA-seq at 12 hours and functional studies at 24 hours, it is hypothesized that *L. pneumophila* OMVs enhance bacterial survival and replication by modulating host cellular processes. To validate this, THP-1 derived macrophages were pre-treated with increasing doses of OMVs at 1 μg, 10 μg, and 20 μg, or left untreated, for 24 hours to examine the impact of OMV modulation on the macrophages' ability to facilitate bacterial survival and replication. After 24 hours, macrophages were infected with *L. pneumophila* at a MOI of 10 and incubated for 12, 24, and 48 hours. At each time interval, macrophages were lysed, and bacterial CFU were quantified. CFU counts of untreated macrophages were used to determine CFU percentages.

The bar graph below shows that OMV-pre-treated macrophages led to a considerable increase in *L. pneumophila* replication relative to untreated controls at all time points assessed. However, the highest effect was observed for 48 hours (Figure 4.45).

Bacterial replication also increased in a dose-dependent fashion with elevated OMV concentrations, suggesting that 24-hour OMV pre-treatment creates a conducive intracellular environment for *L. pneumophila* replication.

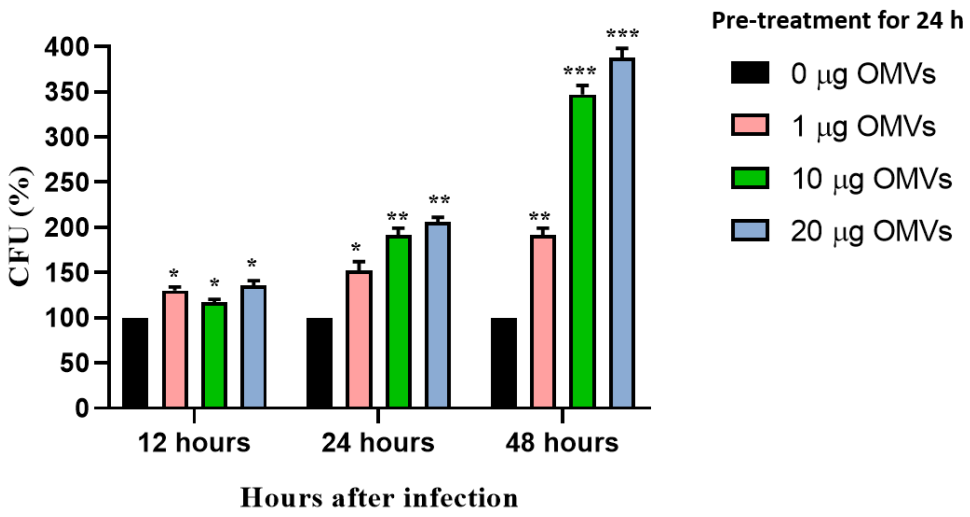


**Figure 4.45: Impact of OMV pre-treatment on the intracellular replication of *L. pneumophila* in THP-1 derived macrophages.**

THP-1 derived macrophages were subjected to a 24-hour pre-treatment with increasing doses of *L. pneumophila* OMV (1, 10, or 20 µg) or left untreated (0 µg OMV). Cells were subsequently infected with *L. pneumophila* at a multiplicity of infection (MOI) of 10. At the specified time intervals post-infection (12, 24, and 48 hours), macrophages were lysed, and viable intracellular bacteria were measured by assessing colony-forming units (CFU), normalized as a percentage of the control (0 OMV). The bar graph illustrates the mean CFU (%) ± SD for each condition over time. OMV pre-treatment resulted in substantial, dose-dependent enhancements in bacterial replication at all time intervals, particularly evident at 48 hours with elevated OMV concentrations. Statistical significance compared to untreated controls was calculated (*$p < 0.05$; **$p < 0.01$; ***$p < 0.001$). The results demonstrate that prior exposure to *L. pneumophila* OMVs promotes the intracellular proliferation of *L. pneumophila* within human macrophages.

# Chapter 5. Discussion

## 5.1. Isolation of *L. pneumophila* OMVs

The purification of outer membrane vesicles is a crucial phase in OMV research, since the selected separation method profoundly affects the subsequent analyses and functional investigations. *L. pneumophila* was grown until the log and early stationary phase for the isolation of actively releasing OMVs and to avoid OMVs originating from dead bacteria.

Both Size Exclusion Chromatography (SEC) and Density Gradient (DEG) methods are classified as intermediate in both recovery and specificity, according to the MISEV (Minimal Information for Studies of Extracellular Vesicles) guidelines (Théry et al., 2018). Our comparative examination of size-exclusion chromatography using qEV1 columns versus iodixanol density gradient centrifugation for the purification of *L. pneumophila* outer membrane vesicles revealed that, although both techniques yielded pure OMVs, as confirmed by TEM, SEC provided greater recovery efficiency. Nanoparticle tracking analysis of OMV concentration and qubit-based estimation of biomolecules revealed a higher OMV yield using the SEC method. However, the size range of OMVs from both methods was comparable, with the same range (100 to 250 nm) as determined by TEM and Nanosight, with the highest fraction containing a mean

particle size of 127 nm by Optiprep and 133 nm by qEV1.

Both DEG and SEC are established methods for recovering pure OMVs from the literature. The preservation of OMV purity observed in both methodologies in our investigation aligns with existing techniques for separating *L. pneumophila* OMVs. Jung et al. demonstrated that differential ultracentrifugation combined with density gradient purification efficiently eliminates bacterial debris and contaminating proteins, yielding pure OMV preparations suitable for subsequent applications (Jung, Hoffmann, et al., 2017). However, SEC has become a favoured alternative to conventional ultracentrifugation techniques over the last decade, as it preserves vesicle integrity and requires less time (Kaddour et al., 2021). Consistent with our findings, Monguió-Tortajada et al. (2019) reported that SEC-based purification methods can achieve yields much higher than those of density gradient techniques, with recovery rates exceeding those of traditional ultracentrifugation (Monguió-Tortajada et al., 2019).

Our findings indicate that the SEC can achieve similar purity levels while providing practical benefits in processing time and significant yield enhancement. To evaluate the purity of isolated OMVs and ensure that SEC-derived samples were free from co-eluting protein contaminants, the particle-to-protein ratio was calculated for both SEC and DEG fractions (Table 5.1). The comparable ratios obtained with the two methods demonstrate that SEC effectively removes non-vesicular proteins while maintaining

high purity. Furthermore, the structural integrity of the OMVs was validated by the detection of LPS via the LAL assay and the identification of characteristic outer membrane proteins through LC-MS, confirming the presence of functionally intact vesicles.

**Table 5.1 Comparison of particle to protein ratio of OMVs obtained by SEC and DEG**

| SEC | | | | DEG | | | |
|---|---|---|---|---|---|---|---|
| **Pure Fractions** | **Particles/ml** | **Protein µg/ml** | **Particle/ protein ratio** | **Pure Fractions** | **Particles/ml** | **Protein µg/ml** | **Particle/ protein ratio** |
| 1 | $1.70 \times 10^{12}$ | 756 | $2.25 \times 10^{9}$ | 4 | $2.06 \times 10^{12}$ | 263 | $7.84 \times 10^{9}$ |
| 2 | $3.59 \times 10^{13}$ | 861 | $4.17 \times 10^{10}$ | 5 | $6.31 \times 10^{12}$ | 405 | $1.56 \times 10^{10}$ |
| 3 | $5.20 \times 10^{12}$ | 582 | $8.93 \times 10^{9}$ | 6 | $1.94 \times 10^{12}$ | 213 | $9.11 \times 10^{9}$ |

In conclusion, the iodixanol density gradient approach, although successful for OMV purification, has intrinsic drawbacks, including extended processing times, reduced recovery rates, and the risk of vesicle aggregation during high-speed centrifugation. Improved OMV yields immediately enhance experimental repeatability and decrease the culture volumes necessary for thorough molecular characterisation and functional investigations. This benefit is especially crucial for performing thorough proteomic, genomic, and transcriptomic investigations of OMV cargo. Maintained vesicular integrity during SEC purification ensures that the functional features of OMVs are

conserved, thereby preserving their biological significance for host cell interaction research.

Although more efficient and faster methods for OMV isolation have recently emerged, this project started in 2021 and utilized DEG and SEC.

## 5.2. Molecular Characterisation of *L. pneumophila* OMVs

### 5.2.1. Significance of LPS in *L. pneumophila* OMVs

LPS functions as both a structural component and an important virulence factor for Gram-negative bacteria. The presence of LPS in isolated *L. pneumophila* OMVs supports previous studies on the composition of Gram-negative bacterial OMVs.

LPS is a crucial component of *L. pneumophila* OMVs and plays an essential role in host-pathogen interactions. Previous research has shown that *L. pneumophila* actively releases LPS-enriched OMVs during both the replicative (E-phase) and transmissive (PE-phase) stages (Fernandez-Moreira et al., 2006).

The structural arrangement of *L. pneumophila* LPS makes it distinct from the endotoxins of other Gram-negative bacteria, despite their general architectural similarities. *L. pneumophila* LPS exhibits significant hydrophobicity due to long, branched fatty acids and abundant O- and N-acetyl groups. This unique composition results in a very low endotoxic potential, with approximately 1000-fold less ability to

stimulate proinflammatory cytokines than Enterobacteriaceae LPS. This could explain why the LPS detected by the LAL test was only 1.3 endotoxin units (EU) per millilitre. Nonetheless, this reduced endotoxin property does not diminish its role in pathogenesis, as *L. pneumophila* LPS is involved in several virulence mechanisms. For example, host TLR2 recognises *L. pneumophila* LPS and induces cytokine production, and *L. pneumophila* also triggers the MyD88 signalling pathway. **(**Shevchuk et al., 2011**;** Szysz et al., 2018**)**. Additionally, Seeger et al. reported that both OMV-bound and unbound LPS from *L. pneumophila* may independently help the pathogen to evade lysosomal degradation within host phagocytes and maintain this protective effect for up to 5 hours after phagocytosis **(**Seeger et al., 2010**)**.

LAL assay confirmed the presence of LPS in *L. pneumophila* OMVs, and our scRNA-seq data supported its role in pathogenesis, showing TLR2 activation in THP-1-derived macrophages in response to OMV-associated LPS and highlighting the importance of the LPS component in bacterial OMVs.

### 5.2.2. Functional diversity in the protein composition of *L. pneumophila* OMVs

Proteomic analysis of OMVs from pathogenic bacteria provides a basis for understanding OMV architecture and the regulation of virulence mechanisms mediated by OMVs. Moreover, proteomic characterisations of OMVs can help utilise OMVs as

a vaccine candidate. For example, comprehensive proteomic investigations of *N. meningitidis* OMVs laid the foundation for the discovery of MeNZB, an OMV vaccine targeting serogroup B (Oster et al., 2005).

Proteomic analysis of *L. pneumophila* OMVs revealed that they contain a diverse set of 250 proteins, predominantly cytoplasmic (188 out of 250) and some cell envelope proteins. This is one of the most interesting puzzles regarding OMV biogenesis because the outward bulging of the outer membrane likely traps nearby proteins, such as periplasmic proteins, into the vesicle. In contrast, the movement of cytoplasmic proteins lacking signal sequences to the vesiculation site is challenging due to the rigidity of the inner membrane. Nevertheless, this observation aligns with many prior studies showing that bacterial OMVs, from various species, can encapsulate not only outer membrane and periplasmic proteins but also significant quantities of cytoplasmic proteins, highlighting the complexity of OMV biogenesis and selective cargo loading (potentially as an approach for increasing the functional repertoire of vesicles) (Altindis et al., 2014; Bai et al., 2014; Lee et al., 2007). Proteome analysis of the whole secretome of *L. pneumophila* in 2008 also revealed the distinct profile of OMV proteins compared to soluble secreted proteins, confirming the selective cargo phenomenon; however, they identified only 108 proteins in OMVs, which could be attributed to conservative, less developed approaches for protein characterization (Galka et al., 2008).

Among identified proteins, many ribosomal or translation-associated proteins (including RplE, RplS, and RpsF), and metabolism-related proteins were found. The presence of translation-associated proteins in OMVs has been reported before in other Gram-negative bacteria (Lee et al., 2007). The high number of metabolism- and translation-related proteins in the *L. pneumophila* OMVs could be due to actively replicating bacteria, as OMVs were isolated from the exponential or early stationary phase of growth. The genes encoding ribosomes and their translation are typically upregulated during mid-log phase (Rolfe et al., 2012). It has been previously reported that these genes are released into OMVs and the extracellular culture supernatant (Lee et al., 2007; Niemann et al., 2011). Or the presence of translation-associated proteins in OMVs may play a role in the host cell, such as modulating host translational processes or stress adaptation; however, this mechanism remains unexplored. Additionally, the identification of metabolic enzymes and ABC transporters (e.g., HutG, DapD, AroB, PurA, MetN, SecB) is reported in previous OMV literature, highlighting the role of OMVs in bacterial fitness and competition within microbial communities (Jan, 2017; Li et al., 2016; Zakharzhevskaya et al., 2017).

The presence of cell wall and membrane biosynthesis proteins (LpxB2, LpcD1m, PlsY, MurD) in OMVs may facilitate extracellular adaptation and biofilm matrix formation, thereby increasing their role in environmental persistence and disease pathogenesis.

(Kim et al., 2018; Rather et al., 2021). The presence of heat shock proteins and molecular chaperones is reported in literature in both prokaryotic and eukaryotic extracellular vesicles, which play an essential role in OMV stability (De Maio & Hightower, 2021; Li et al., 2023). The presence of heat shock proteins HtpX, DnaK, GroEL, and GroES in *L. pneumophila* OMVs suggests these stress response proteins may assist in protein folding, improve vesicle stability, or offer protection of OMVs against adverse conditions and within the host cell (De Jonge et al., 2021). A large number of proteins related to the outer membrane and lipoprotein groups, such as Pal, LolA, Mip, LptD, and MsbA, are structural components of OMVs and are often used as quality criteria in OMV preparations, confirming the integrity and authenticity of the isolated vesicles.

Our study identified 16 known virulence factors within the OMV proteome (e.g., HSP60, Mip, dnaJ, and numerous Dot/Icm apparatus and effector proteins), providing evidence that *L. pneumophila* OMVs may function as carriers of virulence determinants to host cells. Previous literature indicates that OMV-associated virulence proteins, including HSP60 and Mip, are not only immunogenic but also actively facilitate host cell invasion and immune evasion. The presence of the SidE virulence factor (a ubiquitinating enzyme) indicates that OMVs can manipulate host ubiquitination to remodel ER pathways and help bacteria evade the immune system (Xie et al., 2023).

Moreover, the detection of type IV Dot/Icm system-encoded proteins and Type II secretion system protein ProA in OMVs supports the hypothesis that vesicle-mediated transfer of effectors enhances pathogenesis by altering host cellular processes remotely, aligning with research that suggests OMVs serve as alternative delivery mechanisms alongside traditional secretion systems (Guerrero-Mandujano et al., 2017; Jonca et al., 2021).

While this study identified proteins within *L. pneumophila* OMVs with diverse functional potential, including the ability to alter the environment, promote bacterial survival among competing microbes, and influence host cell biology, we did not assess their transfer to host cells or their direct functional activity within those cells. Additionally, the delivery route of OMV-associated virulence factors into the host cytosol requires investigation. While *L. pneumophila* OMVs have been shown to fuse directly with eukaryotic membranes, other models suggest that vesicles are internalized via endocytic pathways followed by endosomal membrane destabilization (Bielaszewska et al., 2017; O'donoghue & Krachler, 2016). This preference may be dictated by OMV heterogeneity, for instance, smaller vesicles often favor endocytosis while larger ones undergo direct fusion (Turner et al., 2018). Ultimately, OMV-host interactions are multifaceted, with the specific delivery route being dependent on OMV size, biochemical composition, and host cell type (Cecil et al., 2019).

Furthermore, a deeper understanding of these proteins could enable their manipulation for vaccine development or other therapeutic applications.

### 5.2.3. Nucleic acids associated with *L. pneumophila* OMVs: Gaps in understanding

The protein and RNA composition of bacterial extracellular vesicles has received attention. However, the relevance, origin, and functional implications of DNA found in pathogenic bacterial OMVs, such as *L. pneumophila*, remain unexplored. Although very few studies have comprehensively characterised OMV-associated DNA in other gram-negative bacteria **(**Bitto et al., 2017**;** P rez-Cruz et al., 2013**)**.

This study comprehensively characterized the DNA associated with *L. pneumophila* OMVs for the first time. Consistent with previous reports, we found that most OMV DNA is on the OMV surface, while a small proportion remains protected within OMVs even after DNase treatment **(**Biller et al., 2014**;** Bitto et al., 2017**;** P rez-Cruz et al., 2013**;** Pérez-Cruz et al., 2015**)**. Illumina sequencing confirmed that both total and internal OMV DNA comprised the entire bacterial genome, indicating that OMVs can contain a representative snapshot of the entire bacterial chromosome. The total OMV-DNA was fully aligned to the bacterial genome, a finding also observed for the total OMV-associated DNA of *P. aeruginosa* **(**Turnbull et al., 2016**)**. While the internal OMV DNA

was enriched in a few genes. Biller et al., also observed a relatively high abundance of some regions within the internal DNA of *Prochlorococcus* OMVs (a marine cyanobacterium) **(**Biller et al., 2014**)**. Similarly, Natalie et al. reported that the internal OMV-DNA of *P. aeruginosa* was selectively enriched for certain genes related to specific biological functions **(**Bitto et al., 2017**)**.

Regarding biological implication, functions related to amino acid transport and metabolism, coenzyme transport, replication, translation, and cellular biogenesis are notably enriched in the total OMV DNA of *L. pneumophila*. The presence of these functional categories probably indicates a selective advantage involved in metabolism, transport, and adaptability **(**P rez-Cruz et al., 2013**;** Renelli et al., 2004**)**. Furthermore, genes associated with replication, translation, and biogenesis indicate the possibility of OMV-mediated gene transfer or the manipulation of critical host cellular processes. However, it remains unclear whether these genes can be expressed and translated within bacterial communities or within host cells, and whether they perform the predicted functions in a biological context. Further studies are needed to determine the functional relevance and activity of OMV-associated DNA following its delivery to host cells. Extracellular DNA (eDNA) is often found attached to the surface of OMVs. According to the literature, this eDNA likely originates from bacterial lysis and plays an important role in biofilm formation and protection **(**Campoccia et al., 2021**;** Liao et al., 2014**;**

Peterson et al., 2013).

In the host-pathogen context, OMV DNA has been reported to modulate the host cell's immune response by being recognised by host TLR9 (Dorward & Garon, 1990; Kaparakis-Liaskos & Ferrero, 2015). Notably, TLR9 activation was absent in our transcriptomic data. A plausible explanation for this observation lies in the subcellular localization of the receptor. As an endosomal pattern recognition receptor, TLR9 requires the delivery of OMV-associated DNA specifically to the endocytic compartment for activation. While OMVs can be internalized via pathways such as macropinocytosis and clathrin-mediated endocytosis, *L. pneumophila* OMVs have been shown to enter host cells through direct membrane fusion (Jäger et al., 2015). By membrane fusion, OMV-derived DNA would be released directly into the cytosol, thereby bypassing the endosomal network and precluding TLR9-mediated detection. Further research into the uptake kinetics and DNA localization of *L. pneumophila* OMVs is necessary to elucidate the precise mechanism by which these vesicles bypass endosomal TLR9 activation.

It remains uncertain whether the OMV-DNA can be integrated and expressed in recipient cells; only one report stated that *P. aeruginosa*-derived OMVs can enter non-phagocytic host cells and deliver their DNA cargo into the cytoplasm or the nuclear compartment (Bitto et al., 2017). Lateral gene transfer between bacteria and human

somatic cells has also been proposed, especially in cancer samples **(**Riley et al., 2013**)**, where *Pseudomonas* spp. This suggests that OMV-mediated DNA transfer between the host and bacteria is possible and could influence host cell biology and immune signalling. Future research should explore OMV-mediated DNA integration and expression in host cells, immunogenicity, and the potential of OMVs for vaccine development.

Recent investigations have found that various RNA species, including rRNAs, tRNAs, sRNAs, and full-length mRNAs, are associated with bacterial OMVs (Ghosal et al., 2015; Han et al., 2019; Koeppen et al., 2016; Sjöström et al., 2015). However, reports on the biological effects of OMV-associated RNAs on host cells are still few. sRNAs packaged with *P. aeruginosa* OMVs can mimic eukaryotic microRNAs, target host cell mRNAs and suppressing translation. *P. aeruginosa* OMV-associated sRNA inhibited neutrophil infiltration in mouse lung models and decreased IL-8 release in human airway epithelial cells (Koeppen et al., 2016). Similarly, in *Helicobacter pylori*, OMV-mediated small non-coding RNA reduced IL-8 responses and altered TNF-α production in cultured gastric cells (Zhang et al., 2020). In contrast to other OMV-associated RNA studies conducted with uropathogenic *E. coli*, this study suggests that the OMV RNA cargo may not elicit any transcriptional responses (Dauros-Singorenko et al., 2020).

Our study confirmed the presence of low levels of RNA in *L. pneumophila* OMVs and found that small RNAs are more prevalent in OMVs than mRNA species. The predominance of small RNA species over larger RNAs is consistent with findings from other bacterial systems. This may be due to selective packaging processes that favour functionally essential regulatory RNAs, which exhibit increased stability against external nucleases (Choi et al., 2017; Joshi et al., 2021). Characterisation of this RNA content by sequencing was one of the most challenging parts of OMV cargo analysis. In this study, the SMARTer® RNA-Seq library preparation kit was used, which was designed for low-input RNA (1 ng). However, despite substantial optimisation efforts by pooling multiple OMV samples and increasing the PCR cycle number, sequencing of the OMV-associated RNA was unsuccessful. Future work is needed to maximize RNA yields through OMV concentration and to evaluate alternative low-input library kits or pre-amplification strategies.

### 5.3. Functional implications of *L. pneumophila* OMVs on host cell physiology

The dose and time profile significantly impact experimental design and the interpretation of host-OMV interactions, so both dose and exposure duration must be evaluated when assessing cellular responses to bacterial OMVs

THP-1-derived macrophages internalized *L. pneumophila* OMVs in a dose-dependent

manner at both 24 and 48 hours. At higher OMV concentrations (10 µg and 20 µg), uptake was significantly greater compared to lower concentrations (1 µg). Previous reports on *L. pneumophila* and *Brucella* support these findings, demonstrating that OMV absorption increases with OMV concentration (Jäger et al., 2015; Pollak et al., 2012). Both 24- and 48-hour time-point data indicated that, except for the 1 µg dose at 48 hours, OMV uptake did not increase further between 24 and 48 hours. Previous kinetic studies used less than 12 hours for uptake and showed an increase in uptake over time. However, our study showed that, with prolonged exposure, OMV uptake reaches equilibrium, especially at higher doses, where the availability of receptors or endocytic machinery may become limiting (Ellis & Kuehn, 2010). Nevertheless, since there are five known mechanisms of OMV uptake (as described in thesis section 1.2.3), the observed OMV uptake limit might be linked to specific uptake pathways involved. As this project did not investigate the mechanisms of OMV uptake, further studies are necessary to clarify this OMV uptake limit.

### 5.3.1. ScRNA-seq reveals how OMVs promote *L. pneumophila* pathogenesis by reprogramming host macrophage responses

Most research on *L. pneumophila* has focused on the type IV Dot/Icm secretion system and its role in altering host cell processes; however, the influence of bacterial OMVs on host cell functions remains largely unexplored. To date, research on OMV-host interactions has primarily focused on the activation of a few pro-inflammatory cytokines in immune cells rather than evaluating the overall impact on host-pathogen dynamics. More specifically, the contribution of OMVs to the pathogenesis of *L. pneumophila* and the underlying mechanisms were not understood. To investigate this, scRNA-seq analysis was performed.

Macrophages are highly plastic cells with high cellular heterogeneity (Garrido-Trigo et al., 2023). scRNA-seq was chosen to measure the transcriptomic responses of THP-1-derived macrophages upon the internalization of *L. pneumophila* OMVs, given its ability to analyse cellular heterogeneity and dynamic gene expression changes at the individual-cell level. Furthermore, scRNA-seq can identify distinct macrophage subpopulations with varying activation stages or susceptibility to OMV-induced effects. This differs from bulk RNA-seq, which averages transcriptomic signals across a mixed cell population and may obscure the diversity of cellular responses (Woo & Eyun, 2025). This insight is crucial for understanding macrophage responses to pathogens and their

products, like OMVs.

ScRNA-seq revealed that THP-1 derived macrophages clustered differently before and after treatment with *L. pneumophila* OMVs, indicating that exposure to OMVs induces distinct changes in the macrophage population. The UMAP plots show that OMV treated macrophages exhibit substantial divergence in their transcriptomes relative to controls, leading to different clusters (Figure 4.21A and B).

A differential gene expression (DEG) study using the bulk approach further showed that genes implicated in inflammation and immunological activation (including CCL1, IL23A, CSF2, CD80, and TNFAIP2) are among the most activated genes. Research indicates that bacterial OMVs predominantly stimulate pro-inflammatory pathways in macrophages via multiple signalling pathways, thereby enhancing the production of cytokines and chemokines crucial for host defence and inflammation. Genes such as CSF2 and IL23A have been previously associated with OMV-induced modification of cytokine response in both macrophage cultures and in vivo models (Ryu et al., 2023; Soult et al., 2013). As expected, DEG profiles across single-cell clusters revealed that some subpopulations responded more strongly to OMV exposure, with the most significant transcriptional changes observed in clusters 3 and 4. These DEGs were also associated with cytokines, chemokines, and stimulatory molecules, and both clusters 3 and 4 exhibited an immune profile characteristic of the M2b macrophage state,

characterised by activation of both pro-inflammatory and anti-inflammatory molecules. The qPCR analysis of specific M2b markers also validated the M2b activation status of macrophages, as indicated by the findings from clusters 3 and 4 from scRNA-seq data. Additionally, flow cytometry confirmed the expression of cell-surface markers associated with M2b macrophage activation states.

M2b polarization is a unique finding in *L. pneumophila* OMVs literature which explains the mechanism of OMV action in the pathogenesis of *L. pneumophila*. Previous literature discussed that bacteria, viruses and parasites can polarize macrophages towards an M2b state to increase their replication and survival within macrophage as M2b monocytes/macrophages lack antibacterial properties and also enhance tolerance to opportunistic infections, including *S. aureus, methicillin-resistant S. aureus (MRSA), E. faecalis, C. albicans,* and *K. pneumoniae* (L.-x. Wang et al., 2019). Certain studies also indicate that M1 macrophages are not readily produced in immunosuppressed hosts, resulting in a predominance of M2b macrophages, and LD shows more prevalence in immunocompromised patients. The most likely reason for this phenomenon is that M2b slows macrophage transformation from the quiescent M0 to the M1 phenotype, thereby reducing anti-pathogen activity. Few other studies reported transcriptional changes in THP-1-derived macrophages for the pathogen *M. avium*, indicating changes in immune cell heterogeneity, including the metabolic and inflammatory reprogramming of

macrophages (Park et al., 2021). Bulk RNA sequencing after treatment with bacterial OMVs has been shown to induce metabolic reprogramming and promote M1 macrophage polarization in Raw264.7 macrophages (Ma et al., 2025). Interestingly, studies on probiotic-derived extracellular vesicles describe their beneficial role in regulating host immune function by M2b polarisation (Chen et al., 2024), as it reduces the damage to host cells, but opportunistic pathogens can take advantage of this state for their survival. Hence, M2b macrophage polarization represents a regulatory 'double-edged sword' whose impact is strictly context-dependent. While probiotic-derived vesicles leverage this phenotype to promote anti-inflammatory homeostasis, enhance barrier integrity, and protect the host (Kim et al., 2020; X Wang et al., 2023; Zhang et al., 2025), pathogens such as *L. pneumophila* subvert the same pathway to facilitate intracellular replication and immune evasion (Jung et al., 2016). Thus, while M2b induction is a shared immunological response, its biological significance shifts from host protection to pathogen survival depending on whether the stimulus is symbiotic or pathogenic.

Investigation of host cell surface receptors revealed that the above immune responses are possibly generated by activation of TLR2 and CLEC4E. The involvement of TLR2 and CLEC4E in *L. pneumophila* recognition is consistent with the literature, with TLR2 reportedly mediating macrophage responses to *L. pneumophila's* components that

include lipoproteins and LPS, while CLEC4E is activated by *L. pneumophila* membrane glycolipids (Shim et al., 2009; Stegmann et al., 2024). This implies the importance of LPS and glycolipids present in bacterial OMVs in activating the host immune response. The activation of the NLRP3 intracellular receptor by OMVs aligns with previous research indicating that NLRP3 is crucial to the immunological response to *L. pneumophila* infection, as shown in studies reported earlier (Zamboni et al., 2006).

Significant downregulation of the STING1 cytosolic receptor was observed, which is essential for interferon gamma production and antibacterial immunity. A previous study showed that wild-type Bone marrow-derived macrophages (BMDM) produce strong interferon-β and are anti-bacterial. In contrast, STING-deficient cells were more susceptible to *L. pneumophila* infection (Ruiz-Moreno et al., 2018). *L. pneumophila* OMVs downregulate this receptor as an escape mechanism to prevent the host cell from interferon gamma immunity. Downregulation of STING1 was observed in conjunction with the absence of interferon gamma production genes in all macrophage sub-populations. Similarly, other antibacterial responses, such as reactive oxygen species and reactive nitrogen species, were not induced. Instead, antioxidant genes were activated to prevent oxidative damage to both the host and bacteria. Results of the gene expression study were verified by ROS assay, where no production of reactive species

was observed. Collectively, OMV-induced activation of antioxidant genes, in addition to M2b polarization, creates a permissive and protective environment within the host cell that supports bacterial replication.

KEGG pathway analysis revealed strong activation of immune signalling cascades following OMV treatment, including IL-17, TNF, NF-κB, chemokine, JAK-STAT, C-type lectin receptor, NOD-like receptor, and cytokine–cytokine receptor interactions signalling pathways. Among these, NF-κB, TNF, and IL-17 signalling are well-documented as central components of the innate immune response against *L. pneumophila* (Ge et al., 2009; Guillemot et al., 2022; Kimizuka et al., 2012). Notably, changes in the JAK-STAT pathway, which controls cell growth, differentiation, and immunity, suggest that OMVs affect more than just traditional inflammatory responses and reveal novel aspects of *L. pneumophila* interaction with host cells.

Overwhelming immune activation by OMVs was also verified by a cytokine array, which showed that 46 out of 105 cytokines/chemokines/growth factors were activated. Where co-induction of pro-inflammatory and anti-inflammatory cytokines is observed, proving the M2b activation state of the macrophage. Secondly, the heterogeneity of cytokine responses to different doses of OMV was observed. Lastly, the induction of more cytokines at 24 hours was also observed, highlighting the activation of the innate

immune system, while a decrease in cytokine responses at 48 hours can be related to the host cell transition from acute infection to resolution.

### 5.3.2. *L. pneumophila* OMVs support host survival and increase bacterial replication inside the host

To determine the host cell viability, we used the MTT assay. No decrease in host cell viability was observed after 24 hours of incubation with *L. pneumophila* OMVs. Instead, a significant increase in cell viability was observed at 1 µg OMV. The maintenance and enhancement of host cell viability can be explained by the activation of the M2b macrophage state by these vesicles, which promote cell survival and immuno-regulatory activity. This finding aligned with a prior study where no cytotoxicity was observed until 96 hours of incubation of THP-1 derived macrophages with increasing concentrations of *L. pneumophila* OMVs, and they observed a significant increase in cell viability at a 1 µg OMV dose compared to a 10 µg OMV dose (Jung et al., 2016). Similarly, *L. pneumophila* OMVs did not induce cell death in alveolar epithelial cells and promoted amoeba growth in another study (Galka et al., 2008). In amoebae, OMV exposure may increase host cell growth by providing additional nutrients like peptides, as OMVs contain a significant no. of proteins.

In this study, the cytokine array showed that low OMV dose induced higher cytokine response than high OMV dose did. This suggests a threshold effect, where optimal OMV concentrations more effectively stimulate cellular pathways that support cell viability and immune activation, while higher doses may dampen these responses

While in vitro experiments consistently show increased or unchanged cell viability, analysis of human lung tissue explants after 24 hours of treatment with *L. pneumophila* OMVs showed significant damage in alveolar septa (Jäger et al., 2014), highlighting the diverse consequences of OMV interactions (Fan et al., 2023). The cytotoxicity of OMVs to host cells may depend on multiple factors, including the host type, the OMV dose, and the duration of exposure. As the current study is limited to THP-1 derived macrophages, other host types and dosages can confirm the cytotoxic potential of *L. pneumophila*.

Caspase 1 plays a crucial role in the body's innate immunity against *L. pneumophila*. Active caspase-1 measurement also confirmed that OMVs at any concentration did not activate caspase-1 for pyroptosis, thereby favouring host cell survival.

The above findings indicate that *L. pneumophila* OMVs modulate host cell functions to enhance cell viability. To determine whether this modulation also favours bacterial replication, we compared the growth and replication of *L. pneumophila* in OMV treated

and untreated macrophages. OMV pre-treatment at all studied concentrations (1, 10, and 20 μg) led to a substantial enhancement in intracellular proliferation of *L. pneumophila* at 12-, 24-, and 48-hours post-infection, compared with macrophages not exposed to OMVs.

### 5.3.3. OMVs contribute to the pathogenesis of *L. pneumophila* and present a promising therapeutic strategy

These findings provide direct evidence that OMV-mediated transformation of macrophages enhances their susceptibility to *L. pneumophila* replication. Over time, pre-exposed cells display higher CFU percentages, which shows that OMVs have a long-lasting influence on the cellular environment. The result implies that OMVs prepare macrophages for a protective state that reduces apoptosis and inflammatory responses, thereby helping intracellular bacteria survive and extend their niche.

The capacity of OMVs to boost host cell viability, combined with the apparent increase in bacterial replication, supports the concept that *L. pneumophila* OMVs are strategic virulence factors. This mechanism likely contributes to the establishment and progression of *L. pneumophila* infection in human body, highlighting OMVs as key modulators in host-pathogen interactions.

Targeting OMVs presents a promising therapeutic strategy; approaches may include inhibiting OMV biogenesis, blocking OMV-host cell interactions, or neutralizing OMV-associated virulence factors. Such interventions could disrupt the ability of *L. pneumophila* to manipulate host cells, thereby reducing bacterial survival and disease severity. Nevertheless, further research is required to introduce OMV-targeted therapies, which may pave the way for novel treatments against Legionnaires' disease and other gram-negative bacterial infections.

# Chapter 6. Conclusion and future directions

## 6.1. Conclusion

The current research presents a significant advancement in understanding *L. pneumophila* OMVs by providing a comprehensive characterization of OMV biomolecules and elucidating OMVs' contribution to LD pathogenesis.

Our explorations regarding OMV biomolecules are summarized as follows:

1. This study demonstrated that proteins constitute a large portion of *L. pneumophila* OMV biomolecules. While these proteins may play a direct role in *L. pneumophila* pathogenesis, their transfer to host cells and specific functions were not investigated in this project and require further exploration.
2. DNA was found both inside (internal DNA) and outside of OMVs. Interestingly, both OMV total and OMV internal DNA cover the whole bacterial genome. However, the DNA read density and enrichment were varied between internal and total DNA. While host TLR9 can recognize DNA associated with OMVs, it was not found to be activated in scRNA-seq data, which could be linked to the low concentration of DNA associated with *L. pneumophila* OMVs.

Therefore, the direct role of OMV-DNA in host-pathogen interactions remains uncertain.

3. RNA was found in very lower amounts than protein and DNA, making sequencing unfeasible highlighting the need to optimize RNA extraction and sequencing methods for future molecular profiling of OMVs. RNA associated with OMVs may play a role, particularly in modulating host-pathogen interactions and in activating receptors such as TLR7 and TLR8. Here, *L. pneumophila* OMV-RNA did not activate TLR7 and TLR8, probably due to very low RNA concentration as shown by ScRNA-seq data.
4. Finally, *L. pneumophila* LPS was identified as a component of the bacterium's OMVs that play a crucial role in activating host TLR2. ScRNA-seq data demonstrated the significant TLR2 activation, underscoring the importance of LPS in *L. pneumophila* OMVs.

The observations described below illustrate how *L. pneumophila* OMVs modulate host cell functions and may contribute to the pathogenesis of *L. pneumophila* and LD:

1. ScRNA-seq demonstrated the heterogeneity of the macrophage population and identified that clusters 3 and 4 respond more to *L. pneumophila* OMVs.
2. Most DEGs in clusters 3 and 4 were related to the immune response, including TNFAIP2, CCL1, CSF2, and IL6, which preferentially produced an immunoregulatory M2b phenotype. The induction of an M2b immunoregulatory phenotype in macrophages by OMVs is a critical insight, as this state supports bacterial persistence while minimizing host cell damage.
3. The absence of classical bactericidal responses including oxidative genes, interferon genes, and pyroptosis further emphasized the sophisticated the strategies employed by *L. pneumophila* OMVs to manipulate host defenses, for pathogen's advantage.
4. Using cytokine array, the upregulation of a broad spectrum of inflammatory and anti-inflammatory cytokines, and chemokines confirmed the functional impact of OMVs on host signalling networks.
5. Pathway analysis from both transcriptional (sc-RNA-seq) and proteins (cytokine array) identified the activation of chemokine signalling, IL-17

signalling and NF-κB signalling pathways. Based on KEGG analysis and supporting literature, we hypothesize that M2b polarization is predominantly mediated by activation of the NF-κB signaling pathway, which is known to induce a mixed cytokine profile essential for establishing the M2b activation state.

6. Finally, OMV-driven macrophage modulation promoted the survival of both the host cell and intracellular bacteria, as demonstrated by a significant increase in *L. pneumophila* replication in macrophages pre-exposed to OMVs. These results highlight the complex and unique function of *L. pneumophila* OMVs in facilitating pathogen persistence and replication by promoting host survival.

## 6.2. Limitations and future directions

Current research also presents certain limitations that should be addressed in future research, as outlined below:

1. While the study comprehensively characterized the protein, DNA, and RNA content of *L. pneumophila* OMVs in vitro, it did not directly assess the uptake or transfer of these OMV components into host cells, leaving the mechanisms of host cell interaction unresolved.

2. The scRNA-seq analysis was conducted at the 12-hour time point, which may not capture the earliest immune responses and PRR activation induced by OMVs. However, the transcriptional profiles observed at 12 hours were largely consistent with the functional assay results obtained at 24 hours.
3. The experiments were conducted using THP-1 derived macrophages in vitro, which may not fully recapitulate the complexity of immune responses in the human body.
4. Although we characterized the components of OMVs and identified the overall modulatory effects of OMVs on host cells, we were unable to pinpoint the specific OMV component responsible for these effects at this stage of the study. Further research is needed to identify and experimentally validate the exact OMV components driving this modulation.

**Translational Prospects:**

Our understanding of OMVs in pathogen pathogenesis remains at an early stage. The precise mechanisms of OMV uptake by host cells and their stability within the host environment are still not fully understood. However, if future studies confirm and validate the critical role of OMVs in aggravating disease pathogenesis, targeting their mechanisms of action could open new avenues for therapeutic intervention.

Furthermore, as *L. pneumophila* OMVs have been shown to be non-cytotoxic to host cells while effectively eliciting immune responses, they present a promising platform for the development of safe vaccines and drug delivery systems. Unlike some peptide-based therapeutics and vaccine approaches that can cause host cell damage or adverse reactions, OMVs offer the potential for targeted delivery and immunogenicity without compromising host cell viability.

# Appendices

## Appendix 1: *L. pneumophila* OMV proteome

| Gene name | Protein | Description | Pfams | MW [kDa] | calc. pI | ave abu% | Beta-barrel c | Adhesin | Class | Location (Vaxign) | Location (CELLO) |
|---|---|---|---|---|---|---|---|---|---|---|---|
| rplQ | Large ribosomal subunit protein bL17 | structural constituent of ribosome | PF01196 | 14.45 | 10.67 | 0.858938 | N\|0.000 | 0.037 | Cyt | Cytoplasmic | Cytoplasmic |
| infB | Translation initiation factor IF-2 | One of the essential components for the initiation of protein synthesis. Protects formylmethionyl-tRNA from spontaneous hydrolysis and promotes its binding to the 30S ribosomal subunits. Also involved in the hydrolysis of GTP during the formation of the 70S ribosomal complex | PF08364, PF03144, PF11987, PF04760, PF04760, PF00009 | 94.71 | 5.16 | 0.011102 | N\|0.000 | 0.043 | Cyt | Cytoplasmic | Cytoplasmic |
| rpsG | Small ribosomal subunit protein uS7 | One of the primary rRNA binding proteins, it binds directly to 16S rRNA where it nucleates assembly of the head domain of the 30S subunit. Is located at | PF00177 | 19.79 | 10.65 | 0.838212 | N\|0.000 | 0.046 | Cyt | Cytoplasmic | Cytoplasmic |

| | | | | | | | | | | | |
|---|---|---|---|---|---|---|---|---|---|---|---|
| | | the subunit interface close to the decoding center, probably blocks exit of the E-site tRNA | | | | | | | | | |
| frr | Ribosome-recycling factor | Responsible for the release of ribosomes from messenger RNA at the termination of protein biosynthesis. May increase the efficiency of translation by recycling ribosomes from one round of translation to another | PF01765 | 20.87 | 6.82 | 0.312217 | N\|0.000 | 0.056 | Cyt | Cytoplasmic | Cytoplasmic |
| valS | Valine--tRNA ligase | amino acids such as threonine, to avoid such errors, it has a posttransfer editing activity that hydrolyzes mischarged Thr-tRNA(Val) in a tRNA-dependent manner | PF10458, PF08264, PF00133 | 106.44 | 6.69 | 0.008713 | N\|0.000 | 0.057 | Cyt | Cytoplasmic | Cytoplasmic |
| lysS | Lysine--tRNA ligase | Belongs to the class-II aminoacyl-tRNA synthetase family | PF00152, PF01336 | 57.87 | 5.48 | 0.049605 | N\|0.000 | 0.059 | Cyt | Cytoplasmic | Cytoplasmic |
| rpsS | Small ribosomal subunit protein uS19 | Protein S19 forms a complex with S13 that binds strongly to the 16S ribosomal RNA | PF00203 | 10.32 | 11.07 | 0.03578 | N\|0.000 | 0.063 | Cyt | Cytoplasmic | Cytoplasmic |

| | | | | | | | | | | | |
|---|---|---|---|---|---|---|---|---|---|---|---|
| groES | Co-chaperonin GroES | Binds to Cpn60 in the presence of Mg-ATP and suppresses the ATPase activity of the latter | PF00166 | 10.48 | 5.93 | 3.216242 | N\|0.000 | 0.063 | Cyt | Cytoplasmic | Cytoplasmic |
| rplE | Large ribosomal subunit protein uL5 | This is 1 of the proteins that binds and probably mediates the attachment of the 5S RNA into the large ribosomal subunit, where it forms part of the central protuberance. In the 70S ribosome it contacts protein S13 of the 30S subunit (bridge B1b), connecting the 2 subunits | PF00281, PF00673 | 20.94 | 10.14 | 0.901172 | N\|0.000 | 0.065 | Cyt | Cytoplasmic | Cytoplasmic |
| rpoC | DNA-directed RNA polymerase subunit beta' | DNA-dependent RNA polymerase catalyzes the transcription of DNA into RNA using the four ribonucleoside triphosphates as substrates | PF04983, PF00623, PF04998, PF05000, PF04997 | 155.68 | 6.82 | 0.671169 | N\|0.000 | 0.065 | Cyt | Cytoplasmic | Cytoplasmic |
| lepA | Elongation factor 4 | Required for accurate and efficient protein synthesis under certain stress | PF00679, | 67.77 | 6.9 | 0.060093 | N\|0.000 | 0.066 | Cyt | Cytoplasmic | Cytoplasmic |

| | | | | | | | | | | | |
|---|---|---|---|---|---|---|---|---|---|---|---|
| | | conditions. May act as a fidelity factor of the translation reaction, by catalyzing a one-codon backward translocation of tRNAs on improperly translocated ribosomes. Back- translocation proceeds from a post-translocation (POST) complex to a pre-translocation (PRE) complex, thus giving elongation factor G a second chance to translocate the tRNAs correctly. Binds to ribosomes in a GTP-dependent manner | PF00009, PF03144, PF06421 | | | | | | | Membrane | |
| ligA | DNA ligase | DNA ligase that catalyzes the formation of phosphodiester linkages between 5'-phosphoryl and 3'-hydroxyl groups in double-stranded DNA using NAD as a coenzyme and as the energy source for the reaction. It is essential for DNA replication and repair of damaged DNA | PF03120, PF12826, PF00533, PF03119, PF01653, PF145 | 74.59 | 6.3 | 0.001747 | N\|0.000 | 0.066 | Cyt | Cytoplasmic | Cytoplasmic |

| | | | | | | | | | | | |
|---|---|---|---|---|---|---|---|---|---|---|---|
| | | | 20 | | | | | | | | |
| rpoB | DNA-directed RNA polymerase subunit beta | Together with LptE, is involved in the assembly of lipopolysaccharide (LPS) at the surface of the outer membrane | PF04561, PF04561, PF04565, PF04563, PF10385, PF00562, PF04560 | 152.74 | 5.28 | 0.244903 | N\|0.000 | 0.066 | Cyt | Cytoplasmic | Cytoplasmic |
| uvrC | UvrABC system protein C | The UvrABC repair system catalyzes the recognition and processing of DNA lesions. UvrC both incises the 5' and 3' sides of the lesion. The N-terminal half is responsible for the 3' incision and the C-terminal half is responsible for the 5' incision | PF01541, PF02151, PF14520, PF084 | 70.41 | 9.56 | 0.005446 | N\|0.000 | 0.068 | Cyt | Cytoplasmic | Cytoplasmic |

| | | | | | | | | | | | |
|---|---|---|---|---|---|---|---|---|---|---|---|
| | | | 59 | | | | | | | | |
| rplS | Large ribosomal subunit protein bL19 | This protein is located at the 30S-50S ribosomal subunit interface and may play a role in the structure and function of the aminoacyl-tRNA binding site | PF01245 | 13.67 | 10.97 | 1.901326 | N\|0.000 | 0.069 | Cyt | Cytoplasmic | Cytoplasmic |
| nuoC | NADH-quinone oxidoreductase subunit C | NDH-1 shuttles electrons from NADH, via FMN and iron- sulfur (Fe-S) centers, to quinones in the respiratory chain. The immediate electron acceptor for the enzyme in this species is believed to be ubiquinone. Couples the redox reaction to proton translocation (for every two electrons transferred, four hydrogen ions are translocated across the cytoplasmic membrane), and thus conserves the redox energy in a proton gradient | PF00329 | 26.56 | 5.57 | 0.210646 | N\|0.000 | 0.07 | Cyt | Cytoplasmic | Cytoplasmic |
| rpmB | Large ribosomal subunit protein bL28 | structural constituent of ribosome | PF00830 | 9.08 | 11.73 | 2.552614 | N\|0.000 | 0.072 | Cyt | Cytoplasmic | Cytoplasmic |
| prfC | Peptide chain release factor 3 | Increases the formation of ribosomal termination complexes and stimulates activities of RF-1 and RF-2. It binds guanine nucleotides and has strong | PF03144, PF16658, | 59.48 | 6.47 | 0.001864 | N\|0.000 | 0.072 | Cyt | Cytoplasmic | Cytoplasmic |

| | | | | | | | | | | | |
|---|---|---|---|---|---|---|---|---|---|---|---|
| | | preference for UGA stop codons. It may interact directly with the ribosome. The stimulation of RF- 1 and RF-2 is significantly reduced by GTP and GDP, but not by GMP | PF00009 | | | | | | | | |
| secA | Protein translocase subunit SecA | Catalyzes the formation of 5-methyl-uridine at position 1939 (m5U1939) in 23S rRNA | PF02810, PF21090, PF07517, PF07516, PF01043 | 102 | 5.63 | 0.159176 | N\|0.000 | 0.074 | Cyt | Cytoplasmic | Cytoplasmic |
| hutH | Histidine ammonia-lyase | Molecular chaperone. Has ATPase activity | PF00221 | 54.73 | 6.05 | 0.003535 | N\|0.000 | 0.076 | Cyt | Cytoplasmic | Cytoplasmic |
| guaA | GMP synthase [glutamine-hydrolyzing] | Catalyzes the synthesis of GMP from XMP | PF00117, PF00958, PF025 | 58.68 | 6.04 | 0.010724 | N\|0.000 | 0.079 | Cyt | Cytoplasmic | Cytoplasmic |

| | | | | | | | | | | | |
|---|---|---|---|---|---|---|---|---|---|---|---|
| | | | 40 | | | | | | | | |
| ankX | Phosphocholine transferase AnkX | - | PF12796, PF12796, PF12796 | 107.16 | 8.19 | 0.009062 | N\|0.000 | 0.081 | Cyt | Cytoplasmic | Cytoplasmic |
| infA | Translation initiation factor IF-1 | One of the essential components for the initiation of protein synthesis. Stabilizes the binding of IF-2 and IF-3 on the 30S subunit to which N-formylmethionyl-tRNA(fMet) subsequently binds. Helps modulate mRNA selection, yielding the 30S pre- initiation complex (PIC). Upon addition of the 50S ribosomal subunit IF-1, IF-2 and IF-3 are released leaving the mature 70S translation initation complex | PF01176 | 8.34 | 9.73 | 0.185133 | N\|0.000 | 0.082 | Cyt | Cytoplasmic | Cytoplasmic |
| hslU | ATP-dependent protease ATPase subunit HslU | this subunit has chaperone activity. The binding of ATP and its subsequent hydrolysis by HslU are essential for unfolding of protein substrates subsequently hydrolyzed by HslV. HslU | PF07724, PF00004 | 49.43 | 5.15 | 0.116103 | N\|0.000 | 0.082 | Cyt | Cytoplasmic | Cytoplasmic |

| | | | | | | | | | | | |
|---|---|---|---|---|---|---|---|---|---|---|---|
| | | recognizes the N-terminal part of its protein substrates and unfolds these before they are guided to HslV for hydrolysis | | | | | | | | | |
| tsf | Elongation factor Ts | Associates with the EF-Tu.GDP complex and induces the exchange of GDP to GTP. It remains bound to the aminoacyl-tRNA.EF- Tu.GTP complex up to the GTP hydrolysis stage on the ribosome | PF00889 | 32.12 | 5.05 | 0.313646 | N\|0.000 | 0.083 | Cyt | Cytoplasmic | Cytoplasmic |
| accA | Acetyl-coenzyme A carboxylase carboxyl transferase subunit alpha | Component of the acetyl coenzyme A carboxylase (ACC) complex. First, biotin carboxylase catalyzes the carboxylation of biotin on its carrier protein (BCCP) and then the CO(2) group is transferred by the carboxyltransferase to acetyl-CoA to form malonyl-CoA | PF03255 | 35.51 | 6.18 | 0.492254 | N\|0.000 | 0.085 | Cyt | Cytoplasmic | Cytoplasmic |
| prfA | Peptide chain release factor 1 | Peptide chain release factor 1 directs the termination of translation in response to the peptide chain termination codons UAG and UAA | PF03462, PF00472 | 41.11 | 4.85 | 0.014914 | N\|0.000 | 0.087 | Cyt | Cytoplasmic | Cytoplasmic |
| thrS | Threonine--tRNA ligase | Catalyzes the attachment of threonine to tRNA(Thr) in a two-step reaction L- | PF02824, | 72.86 | 6.51 | 0.011378 | N\|0.000 | 0.089 | Cyt | Cytoplasmic | Cytoplasmic |

| | | | | | | | | | | | |
|---|---|---|---|---|---|---|---|---|---|---|---|
| | | threonine is first activated by ATP to form Thr-AMP and then transferred to the acceptor end of tRNA(Thr) | PF03129, PF07973, PF00587 | | | | | | | | |
| pnp | Polyribonucleotide nucleotidyltransferase | Involved in mRNA degradation. Catalyzes the phosphorolysis of single-stranded polyribonucleotides processively in the 3'- to 5'-direction | PF03726, PF03725, PF03725, PF00013, PF00575, PF01138, PF01138 | 80.13 | 4.71 | 0.008286 | N\|0.000 | 0.09 | Cyt | Cytoplasmic | Cytoplasmic |
| gcvH | Glycine cleavage system H protein | The glycine cleavage system catalyzes the degradation of glycine. The H protein | PF01597 | 13.85 | 3.95 | 0.032595 | N\|0.000 | 0.091 | Cyt | Unknown | Cytoplasmic |

| | | | | | | | | | | | |
|---|---|---|---|---|---|---|---|---|---|---|---|
| | | shuttles the methylamine group of glycine from the P protein to the T protein | | | | | | | | | |
| glyA | Serine hydroxymethyltransferase | Catalyzes the reversible interconversion of serine and glycine with tetrahydrofolate (THF) serving as the one-carbon carrier. This reaction serves as the major source of one-carbon groups required for the biosynthesis of purines, thymidylate, methionine, and other important biomolecules. Also exhibits THF- independent aldolase activity toward beta-hydroxyamino acids, producing glycine and aldehydes, via a retro-aldol mechanism | PF00464 | 45.58 | 6.84 | 0.063193 | N\|0.000 | 0.092 | Cyt | Cytoplasmic | Cytoplasmic |
| proS | Proline--tRNA ligase | Catalyzes the attachment of proline to tRNA(Pro) in a two-step reaction proline is first activated by ATP to form Pro- AMP and then transferred to the acceptor end of tRNA(Pro). As ProRS can inadvertently accommodate and process non-cognate amino acids such as alanine and cysteine, to avoid such errors it has two additional | PF00587, PF04073, PF03129 | 64.2 | 5.83 | 0.001615 | N\|0.000 | 0.092 | Cyt | Cytoplasmic | Cytoplasmic |

| | | | | | | | | | | | |
|---|---|---|---|---|---|---|---|---|---|---|---|
| | | distinct editing activities against alanine. One activity is designated as 'pretransfer' editing and involves the tRNA(Pro)-independent hydrolysis of activated Ala-AMP. The other activity is designated 'posttransfer' editing and involves deacylation of mischarged Ala-tRNA(Pro). The misacylated Cys-tRNA(Pro) is not edited by ProRS | | | | | | | | | |
| pnp | Polyribonucleotide nucleotidyltransferase | Involved in mRNA degradation. Catalyzes the phosphorolysis of single-stranded polyribonucleotides processively in the 3'- to 5'-direction | PF00575, PF03725, PF03725, PF00013, PF01138, PF01138, PF037 | 80.03 | 4.81 | 0.087459 | N\|0.000 | 0.092 | Cyt | Cytoplasmic | Cytoplasmic |

| | | | | | | | | | | | |
|---|---|---|---|---|---|---|---|---|---|---|---|
| | | | 26 | | | | | | | | |
| icmW | Type 4 adapter protein IcmW | - | | 17.33 | 4.66 | 0.069223 | N\|0.000 | 0.093 | Cyt | Cytoplasmic | Cytoplasmic |
| aroB | 3-dehydroquinate synthase | Catalyzes the conversion of 3-deoxy-D-arabino- heptulosonate 7-phosphate (DAHP) to dehydroquinate (DHQ) | PF01761 | 40.91 | 6.98 | 0.003016 | N\|0.000 | 0.093 | Cyt | Cytoplasmic | Cytoplasmic |
| pyrF | Orotidine 5'-phosphate decarboxylase | Catalyzes the decarboxylation of orotidine 5'- monophosphate (OMP) to uridine 5'-monophosphate (UMP) | PF00215 | 25.23 | 6.68 | 0.013404 | N\|0.000 | 0.094 | Cyt | Cytoplasmic | Cytoplasmic |
| gltX | Glutamate--tRNA ligase | Catalyzes the attachment of glutamate to tRNA(Glu) in a two-step reaction glutamate is first activated by ATP to form Glu-AMP and then transferred to the acceptor end of tRNA(Glu) | PF00749, PF19269 | 53.56 | 6.37 | 0.030226 | N\|0.000 | 0.095 | Cyt | Cytoplasmic | Cytoplasmic |
| fabZ | 3-hydroxyacyl-[acyl-carrier-protein] dehydratase FabZ | HNH nucleases | PF07977 | 17.05 | 7.62 | 0.088397 | N\|0.000 | 0.096 | Cyt | Cytoplasmic | Cytoplasmic |
| hemC | Porphobilinogen deaminase | Tetrapolymerization of the monopyrrole PBG into the hydroxymethylbilane pre-uroporphyrinogen in several discrete steps | PF01379, PF03900 | 33.99 | 7.18 | 0.017795 | N\|0.000 | 0.096 | Cyt | Cytoplasmic | Cytoplasmic |
| pheT | Phenylalanine--tRNA | Belongs to the phenylalanyl-tRNA | PF034 | 88.2 | 4.94 | 0.0051 | N\|0.0 | 0.097 | Cyt | Cytoplas | Cytoplasmic |

| | | | | | | | | | | | |
|---|---|---|---|---|---|---|---|---|---|---|---|
| | ligase beta subunit | synthetase beta subunit family. Type 1 subfamily | 83, PF17759, PF01588, PF03147, PF03484 | 2 | | 11 | 00 | | | mic | |
| minE | Cell division topological specificity factor | Prevents the cell division inhibition by proteins MinC and MinD at internal division sites while permitting inhibition at polar sites. This ensures cell division at the proper site by restricting the formation of a division septum at the midpoint of the long axis of the cell | PF03776 | 10.24 | 5.87 | 0.202847 | N\|0.000 | 0.098 | Cyt | Cytoplasmic | Cytoplasmic |
| atpA2 | ATP synthase subunit alpha 2 | Produces ATP from ADP in the presence of a proton gradient across the membrane. The alpha chain is a regulatory subunit | PF00006, PF00306, PF02874 | 55.54 | 5.42 | 0.681782 | N\|0.000 | 0.099 | Cyt | Cytoplasmic | Cytoplasmic |

| | | | | | | | | | | | |
|---|---|---|---|---|---|---|---|---|---|---|---|
| purA | Adenylosuccinate synthetase | Plays an important role in the de novo pathway of purine nucleotide biosynthesis. Catalyzes the first committed step in the biosynthesis of AMP from IMP | PF00709 | 47.49 | 6.07 | 0.040956 | N\|0.000 | 0.1 | Cyt | Cytoplasmic | Cytoplasmic |
| proA | Gamma-glutamyl phosphate reductase | Thiamine biosynthesis protein | | 46.18 | 7.93 | 0.012694 | N\|0.000 | 0.101 | Cyt | Cytoplasmic | Cytoplasmic |
| tig | Trigger factor | Involved in protein export. Acts as a chaperone by maintaining the newly synthesized protein in an open conformation. Functions as a peptidyl-prolyl cis-trans isomerase | PF05698, PF05697, PF00254 | 50.8 | 5.02 | 0.192188 | N\|0.000 | 0.102 | Cyt | Cytoplasmic | Cytoplasmic |
| pepA | Probable cytosol aminopeptidase | Presumably involved in the processing and regular turnover of intracellular proteins. Catalyzes the removal of unsubstituted N-terminal amino acids from various peptides | PF00883, PF02789 | 52.62 | 5.68 | 0.06208 | N\|0.000 | 0.102 | Cyt | Cytoplasmic | Cytoplasmic |
| alaS | Alanine--tRNA ligase | Catalyzes the attachment of alanine to tRNA(Ala) in a two-step reaction alanine is first activated by ATP to form Ala-AMP and then transferred to the acceptor | PF02272, PF01411, | 96.28 | 6.26 | 0.019408 | N\|0.000 | 0.102 | Cyt | Cytoplasmic | Cytoplasmic |

| | | | | | | | | | | | |
|---|---|---|---|---|---|---|---|---|---|---|---|
| | | end of tRNA(Ala). Also edits incorrectly charged Ser-tRNA(Ala) and Gly-tRNA(Ala) via its editing domain | PF07973 | | | | | | | | |
| ileS | Isoleucine--tRNA ligase | Adenylosuccinate lyase C-terminal | PF08264, PF00133, PF06827 | 105.65 | 6.44 | 0.015553 | N\|0.000 | 0.102 | Cyt | Cytoplasmic | Cytoplasmic |
| serS | Serine--tRNA ligase | Catalyzes the attachment of serine to tRNA(Ser). Is also able to aminoacylate tRNA(Sec) with serine, to form the misacylated tRNA L-seryl-tRNA(Sec), which will be further converted into selenocysteinyl-tRNA(Sec) | PF00587, PF02403 | 48.16 | 6.25 | 0.0367 | N\|0.000 | 0.104 | Cyt | Cytoplasmic | Cytoplasmic |
| asnS | Asparagine--tRNA ligase | tRNA synthetases class II (D, K and N) | PF01336, PF00152 | 53.22 | 5.36 | 0.020523 | N\|0.000 | 0.104 | Cyt | Cytoplasmic | Cytoplasmic |
| lolD | Lipoprotein-releasing system ATP-binding protein LolD | sphinganine-1-phosphate aldolase activity | PF00005 | 25.13 | 8.27 | 0.039015 | N\|0.000 | 0.106 | Cyt | Cytoplasmic Membran | Cytoplasmic |

| | | | | | | | | | | | |
|---|---|---|---|---|---|---|---|---|---|---|---|
| | | | | | | | | | | e | |
| rplN | Large ribosomal subunit protein uL14 | Binds to 23S rRNA. Forms part of two intersubunit bridges in the 70S ribosome | PF00238 | 13.36 | 11.33 | 0.271016 | N\|0.000 | 0.107 | Cyt | Cytoplasmic | Cytoplasmic |
| rplO | Large ribosomal subunit protein uL15 | Binds to the 23S rRNA | PF00828 | 15.38 | 11.13 | 0.589344 | N\|0.000 | 0.107 | Cyt | Cytoplasmic | Cytoplasmic |
| kmo | Kynurenine 3-monooxygenase | Catalyzes the hydroxylation of L-kynurenine (L-Kyn) to form 3-hydroxy-L-kynurenine (L-3OHKyn). Required for synthesis of quinolinic acid | PF01494 | 51.32 | 6.68 | 0.00527 | N\|0.000 | 0.108 | Cyt | Cytoplasmic | Cytoplasmic |
| nuoB | NADH-quinone oxidoreductase subunit B | NDH-1 shuttles electrons from NADH, via FMN and iron- sulfur (Fe-S) centers, to quinones in the respiratory chain. The immediate electron acceptor for the enzyme in this species is believed to be ubiquinone. Couples the redox reaction to proton translocation (for every two electrons transferred, four hydrogen ions are translocated across the cytoplasmic membrane), and thus conserves the redox energy in a proton gradient | PF01058 | 17.54 | 8.57 | 0.865183 | N\|0.000 | 0.11 | Cyt | Cytoplasmic Membrane | Unknow |
| dotL | Type 4 coupling protein DotL | - | PF12696 | 87.52 | 5.05 | 0.092445 | Y\|0.327 | 0.11 | Cyt | Cytoplasmic | Unknow |

| | | | | | | | | | | | |
|---|---|---|---|---|---|---|---|---|---|---|---|
| | | | | | | | | | | Membrane | |
| ccmA | Cytochrome c biogenesis ATP-binding export protein CcmA | once thought to export heme, this seems not to be the case, but its exact role is uncertain. Responsible for energy coupling to the transport system | PF00005 | 22.56 | 6.78 | 0.02007 | N\|0.000 | 0.111 | Cyt | Cytoplasmic Membrane | Cytoplasmic |
| hisS | Histidine--tRNA ligase | Part of the Sec protein translocase complex. Interacts with the SecYEG preprotein conducting channel. Has a central role in coupling the hydrolysis of ATP to the transfer of proteins into and across the cell membrane, serving both as a receptor for the preprotein-SecB complex and as an ATP-driven molecular motor driving the stepwise translocation of polypeptide chains across the membrane | PF03129, PF13393 | 48.42 | 5.11 | 0.023018 | N\|0.000 | 0.113 | Cyt | Cytoplasmic | Cytoplasmic |
| coaD | Phosphopantetheine adenylyltransferase | Reversibly transfers an adenylyl group from ATP to 4'- phosphopantetheine, yielding dephospho-CoA (dPCoA) and pyrophosphate | PF01467 | 19.23 | 8.9 | 0.015048 | N\|0.000 | 0.115 | Cyt | Cytoplasmic | Cytoplasmic |
| rplB | Large ribosomal subunit | One of the primary rRNA binding | PF039 | 30.0 | 11.3 | 0.1748 | N\|0.0 | 0.116 | Cyt | Cytoplas | Unknow |

| | | | | | | | | | | | |
|---|---|---|---|---|---|---|---|---|---|---|---|
| | protein uL2 | proteins. Required for association of the 30S and 50S subunits to form the 70S ribosome, for tRNA binding and peptide bond formation. It has been suggested to have peptidyltransferase activity | 47, PF00181 | 9 | 7 | 98 | 00 | | | mic | |
| lpxB2 | Lipid-A-disaccharide synthase 2 | Condensation of UDP-2,3-diacylglucosamine and 2,3-diacylglucosamine-1-phosphate to form lipid A disaccharide, a precursor of lipid A, a phosphorylated glycolipid that anchors the lipopolysaccharide to the outer membrane of the cell | PF02684 | 43.72 | 9.98 | 0.0049 | N\|0.000 | 0.116 | Cyt | Cytoplasmic | Unknow |
| clpX | ATP-dependent Clp protease ATP-binding subunit ClpX | ATP-dependent specificity component of the Clp protease. It directs the protease to specific substrates. Can perform chaperone functions in the absence of ClpP | PF10431, PF07724, PF06689 | 46.65 | 5.07 | 0.020679 | N\|0.000 | 0.116 | Cyt | Cytoplasmic | Cytoplasmic |
| | Putative phosphoenolpyruvate synthase regulatory protein | Bifunctional serine threonine kinase and phosphorylase involved in the regulation of the phosphoenolpyruvate synthase (PEPS) by catalyzing its phosphorylation | PF03618 | 30.78 | 7.45 | 0.019781 | N\|0.000 | 0.119 | Cyt | Cytoplasmic | Cytoplasmic |

| | | | | | | | | | | | |
|---|---|---|---|---|---|---|---|---|---|---|---|
| | | dephosphorylation | | | | | | | | | |
| rpsB | Small ribosomal subunit protein uS2 | Belongs to the universal ribosomal protein uS2 family | PF00318 | 28.75 | 7.15 | 0.309856 | N\|0.000 | 0.12 | Cyt | Cytoplasmic | Cytoplasmic |
| sidJ | Calmodulin-dependent glutamylase SidJ | Catalyzes the reversible conversion of 2-phosphoglycerate into phosphoenolpyruvate. It is essential for the degradation of carbohydrates via glycolysis | | 100.22 | 7.09 | 0.041296 | Y\|1.000 | 0.121 | Cyt | Unknown | OuterMembrane |
| helA | Protein HelA | Belongs to the resistance-nodulation-cell division (RND) (TC 2.A.6) family | PF00873 | 115.84 | 9.6 | 0.004807 | N\|0.000 | 0.124 | Cyt | Cytoplasmic Membrane | InnerMembrane |
| upp | Uracil phosphoribosyltransferase | Catalyzes the conversion of uracil and 5-phospho-alpha- D-ribose 1-diphosphate (PRPP) to UMP and diphosphate | PF14681 | 23.9 | 6.68 | 0.001658 | N\|0.000 | 0.127 | Cyt | Cytoplasmic | Cytoplasmic |
| drrA | Multifunctional virulence effector protein DrrA | DrrA phosphatidylinositol 4-phosphate binding domain | PF20879, PF20851, PF14860 | 73.43 | 5.95 | 0.277487 | N\|0.000 | 0.129 | Cyt | Cytoplasmic | Cytoplasmic |
| rppH | RNA pyrophosphohydrolase | Accelerates the degradation of transcripts by removing pyrophosphate from the 5'- | PF00293 | 20.71 | 10.25 | 0.036655 | N\|0.000 | 0.13 | Cyt | Cytoplasmic | Cytoplasmic |

| | | | | | | | | | | | |
|---|---|---|---|---|---|---|---|---|---|---|---|
| | | end of triphosphorylated RNA, leading to a more labile monophosphorylated state that can stimulate subsequent ribonuclease cleavage | | | | | | | | | |
| orn | Oligoribonuclease | 3'-to-5' exoribonuclease specific for small oligoribonucleotides | PF00929 | 21.74 | 5.34 | 0.044835 | N\|000 | 0.13 | Cyt | Cytoplasmic | Cytoplasmic |
| fusA | Elongation factor G | DNA-dependent RNA polymerase catalyzes the transcription of DNA into RNA using the four ribonucleoside triphosphates as substrates | PF00009, PF03144, PF03764, PF14492, PF00679 | 77.04 | 5.19 | 0.104639 | N\|000 | 0.131 | Cyt | Cytoplasmic | Cytoplasmic |
| atpD | ATP synthase subunit beta | Produces ATP from ADP in the presence of a proton gradient across the membrane. The catalytic sites are hosted primarily by the beta subunits | PF00006, PF02874 | 50.03 | 4.75 | 0.395866 | N\|000 | 0.132 | Cyt | Cytoplasmic | Cytoplasmic |
| cysS | Cysteine--tRNA ligase | cysteine-tRNA ligase activity | PF01406, | 51.65 | 5.9 | 0.038753 | N\|000 | 0.132 | Cyt | Cytoplasmic | Cytoplasmic |

| | | | | | | | | | | | |
|---|---|---|---|---|---|---|---|---|---|---|---|
| | | | PF09190 | | | | | | | | |
| | Probable sphingosine-1-phosphate lyase | nuclear chromosome segregation | PF00282 | 66.56 | 7.04 | 0.011695 | N\|0.000 | 0.132 | Cyt | Cytoplasmic | Unknow |
| dapD | 2,3,4,5-tetrahydropyridine-2,6-dicarboxylate N-succinyltransferase | N-succinyltransferase activity | PF14805, PF14602 | 30.08 | 5.66 | 0.029771 | N\|0.000 | 0.133 | Cyt | Cytoplasmic | Cytoplasmic |
| lem3 | Phosphocholine hydrolase Lem3 | Ankyrin repeat | | 64.75 | 6.3 | 0.015747 | N\|0.000 | 0.133 | Cyt | Cytoplasmic | Cytoplasmic |
| copA | Copper-exporting P-type ATPase | amino acids such as valine, to avoid such errors it has two additional distinct tRNA(Ile)-dependent editing activities. One activity is designated as 'pretransfer' editing and involves the hydrolysis of activated Val-AMP. The other activity is designated 'posttransfer' editing and involves deacylation of mischarged Val-tRNA(Ile) | PF19335, PF00702, PF00122 | 78.26 | 6.65 | 0.006963 | N\|0.000 | 0.133 | Cyt | Cytoplasmic Membrane | InnerMembrane |
| fur | Ferric uptake regulation protein | Ferric uptake regulator family | PF01475 | 15.37 | 6.22 | 0.025402 | N\|0.000 | 0.134 | Cyt | Cytoplasmic | Cytoplasmic |
| rpmC | Large ribosomal subunit | structural constituent of ribosome | PF008 | 7.37 | 10.8 | 9.8482 | N\|0.0 | 0.135 | Cyt | Cytoplas | Cytoplasmic |

| | | | | | | | | | | | |
|---|---|---|---|---|---|---|---|---|---|---|---|
| | protein uL29 | | 31 | | 7 | 15 | 00 | | | mic | |
| pdxJ | Pyridoxine 5'-phosphate synthase | Catalyzes the complicated ring closure reaction between the two acyclic compounds 1-deoxy-D-xylulose-5-phosphate (DXP) and 3-amino-2-oxopropyl phosphate (1-amino-acetone-3-phosphate or AAP) to form pyridoxine 5'-phosphate (PNP) and inorganic phosphate | PF03740 | 27.83 | 5.74 | 0.04857 | N\|0.000 | 0.135 | Cyt | Cytoplasmic | Cytoplasmic |
| pgk | Phosphoglycerate kinase | phosphotransferase activity, carboxyl group as acceptor | PF00162 | 42.56 | 4.79 | 0.018156 | N\|0.000 | 0.138 | Cyt | Cytoplasmic | Cytoplasmic |
| ddl | D-alanine--D-alanine ligase | Belongs to the D-alanine--D-alanine ligase family | PF01820, PF07478 | 40.41 | 5.39 | 0.004826 | N\|0.000 | 0.14 | Cyt | Cytoplasmic | Cytoplasmic |
| nuoD | NADH-quinone oxidoreductase subunit D | NDH-1 shuttles electrons from NADH, via FMN and iron- sulfur (Fe-S) centers, to quinones in the respiratory chain. The immediate electron acceptor for the enzyme in this species is believed to be ubiquinone. Couples the redox reaction to proton translocation (for every two | PF00346 | 48.18 | 6.95 | 0.325854 | N\|0.000 | 0.14 | Cyt | Cytoplasmic | Cytoplasmic |

| | | | | | | | | | | | |
|---|---|---|---|---|---|---|---|---|---|---|---|
| | | electrons transferred, four hydrogen ions are translocated across the cytoplasmic membrane), and thus conserves the redox energy in a proton gradient | | | | | | | | | |
| htpG | Chaperone protein HtpG | The beta subunit is responsible for the synthesis of L- tryptophan from indole and L-serine | PF13589, PF00183 | 71.06 | 5.38 | 0.305615 | N\|0.000 | 0.14 | Cyt | Cytoplasmic | Cytoplasmic |
| murG | UDP-N-acetylglucosamine--N-acetylmuramyl-(pentapeptide) pyrophosphoryl-undecaprenol N-acetylglucosamine transferase | Cell wall formation. Catalyzes the transfer of a GlcNAc subunit on undecaprenyl-pyrophosphoryl-MurNAc-pentapeptide (lipid intermediate I) to form undecaprenyl-pyrophosphoryl-MurNAc-(pentapeptide)GlcNAc (lipid intermediate II) | PF04101, PF03033 | 39.66 | 9.13 | 0.025057 | N\|0.000 | 0.142 | Cyt | Cytoplasmic Membrane | Unknow |
| potA | Spermidine/putrescine import ATP-binding protein PotA | E1-E2 ATPase | PF00005, PF08402 | 41.39 | 6.01 | 0.021184 | N\|0.000 | 0.145 | Cyt | Cytoplasmic Membrane | Cytoplasmic |
| nusB | Transcription antitermination protein | Involved in transcription antitermination. Required for transcription of ribosomal | PF01029 | 16.97 | 5.29 | 0.062545 | N\|0.000 | 0.149 | Cyt | Cytoplasmic | Cytoplasmic |

| | | | | | | | | | | | |
|---|---|---|---|---|---|---|---|---|---|---|---|
| | NusB | RNA (rRNA) genes. Binds specifically to the boxA antiterminator sequence of the ribosomal RNA (rrn) operons | | | | | | | | | |
| tuf1; tuf2 | Elongation factor Tu | This protein promotes the GTP-dependent binding of aminoacyl-tRNA to the A-site of ribosomes during protein biosynthesis | PF00009, PF03143, PF03144 | 43.18 | 5.04 | 1.242886 | N\|0.000 | 0.149 | Cyt | Cytoplasmic | Cytoplasmic |
| rpsC | Small ribosomal subunit protein uS3 | Binds the lower part of the 30S subunit head. Binds mRNA in the 70S ribosome, positioning it for translation | PF07650, PF00189 | 24.12 | 10.79 | 0.415313 | N\|0.000 | 0.15 | Cyt | Cytoplasmic | Cytoplasmic |
| dapA | 4-hydroxy-tetrahydrodipicolinate synthase | Catalyzes the condensation of (S)-aspartate-beta- semialdehyde (S)-ASA and pyruvate to 4-hydroxy-tetrahydrodipicolinate (HTPA) | PF00701 | 31.56 | 6.43 | 0.098478 | N\|0.000 | 0.151 | Cyt | Cytoplasmic | Cytoplasmic |
| surA | Chaperone SurA | Chaperone involved in the correct folding and assembly of outer membrane proteins. Recognizes specific patterns of aromatic residues and the orientation of their side chains, which are found more | PF13616, PF09312, PF006 | 48.52 | 8.24 | 0.179772 | N\|0.000 | 0.151 | Spl | Periplasmic | Cytoplasmic |

| | | | | | | | | | | | |
|---|---|---|---|---|---|---|---|---|---|---|---|
| | | frequently in integral outer membrane proteins. May act in both early periplasmic and late outer membrane-associated steps of protein maturation | 39 | | | | | | | | |
| rplR | Large ribosomal subunit protein uL18 | This is one of the proteins that binds and probably mediates the attachment of the 5S RNA into the large ribosomal subunit, where it forms part of the central protuberance | PF00861 | 13.01 | 11.39 | 1.655471 | N\|0.000 | 0.153 | Cyt | Cytoplasmic | Cytoplasmic |
| folD | Bifunctional protein FolD | Catalyzes the oxidation of 5,10-methylenetetrahydrofolate to 5,10-methenyltetrahydrofolate and then the hydrolysis of 5,10-methenyltetrahydrofolate to 10-formyltetrahydrofolate | PF02882, PF00763 | 31.7 | 7.74 | 0.026733 | N\|0.000 | 0.154 | Cyt | Cytoplasmic | Cytoplasmic |
| rplY | Large ribosomal subunit protein bL25 | This is one of the proteins that binds to the 5S RNA in the ribosome where it forms part of the central protuberance | PF01386, PF14693 | 23.99 | 6.51 | 0.05049 | N\|0.000 | 0.155 | Cyt | Cytoplasmic | Cytoplasmic |
| pyrG | CTP synthase | Catalyzes the ATP-dependent amination of UTP to CTP with either L-glutamine or ammonia as the source of nitrogen. | PF06418, PF0011 | 60.73 | 6.77 | 0.015156 | N\|0.000 | 0.156 | Cyt | Cytoplasmic | Cytoplasmic |

| | | | | | | | | | | | |
|---|---|---|---|---|---|---|---|---|---|---|---|
| | | Regulates intracellular CTP levels through interactions with the four ribonucleotide triphosphates | 7 | | | | | | | | |
| sidE | Ubiquitinating enzyme SidE | Bifunctional enzyme with both catalase and broad- spectrum peroxidase activity | PF12252, PF19048, PF19049 | 169.45 | 6.14 | 0.006557 | N\|0.000 | 0.157 | Cyt | Cytoplasmic | Cytoplasmic |
| rpsF | Small ribosomal subunit protein bS6 | Binds together with S18 to 16S ribosomal RNA | PF01250 | 13.13 | 9.73 | 0.087385 | N\|0.000 | 0.158 | Cyt | Cytoplasmic | Cytoplasmic |
| clpP | ATP-dependent Clp protease proteolytic subunit | Cleaves peptides in various proteins in a process that requires ATP hydrolysis. Has a chymotrypsin-like activity. Plays a major role in the degradation of misfolded proteins | PF00574 | 23.83 | 5.65 | 0.003376 | N\|0.000 | 0.158 | Cyt | Cytoplasmic | Cytoplasmic |
| pheS | Phenylalanine--tRNA ligase alpha subunit | Belongs to the class-II aminoacyl-tRNA synthetase family. Phe-tRNA synthetase alpha subunit type 1 subfamily | PF02912, PF01409 | 38.27 | 6.74 | 0.019498 | N\|0.000 | 0.158 | Cyt | Cytoplasmic | Cytoplasmic |
| lipA | Lipoyl synthase | Catalyzes the radical-mediated insertion of two sulfur atoms into the C-6 and C-8 | PF04055 | 36.78 | 7.88 | 0.018526 | N\|0.000 | 0.16 | Cyt | Cytoplasmic | Cytoplasmic |

| | | | | | | | | | | | |
|---|---|---|---|---|---|---|---|---|---|---|---|
| | | positions of the octanoyl moiety bound to the lipoyl domains of lipoate-dependent enzymes, thereby converting the octanoylated domains into lipoylated derivatives | | | | | | | | | |
| der | GTPase Der | GTPase that plays an essential role in the late steps of ribosome biogenesis | PF01926, PF01926, PF14714 | 51.32 | 9.97 | 0.020305 | N\|0.000 | 0.16 | Cyt | Cytoplasmic | Cytoplasmic |
| glmM | Phosphoglucosamine mutase | Catalyzes the conversion of glucosamine-6-phosphate to glucosamine-1-phosphate | PF00408, PF02879, PF02880, PF02878 | 48.36 | 6.72 | 0.003085 | N\|0.000 | 0.163 | Cyt | Cytoplasmic | Cytoplasmic |
| plsX | Phosphate acyltransferase | Catalyzes the reversible formation of acyl-phosphate (acyl-PO(4)) from acyl-acyl-carrier-protein (acyl-ACP). This | PF02504 | 36.75 | 8.15 | 0.334337 | N\|0.000 | 0.164 | Cyt | Cytoplasmic | Cytoplasmic |

| | | | | | | | | | | | |
|---|---|---|---|---|---|---|---|---|---|---|---|
| | | enzyme utilizes acyl-ACP as fatty acyl donor, but not acyl-CoA | | | | | | | | | |
| psd | Phosphatidylserine decarboxylase proenzyme | Catalyzes the formation of phosphatidylethanolamine (PtdEtn) from phosphatidylserine (PtdSer) | PF02666 | 31.97 | 8.44 | 0.085085 | N\|0.000 | 0.165 | Cyt | Cytoplasmic Membrane | Unknow |
| aroQ | 3-dehydroquinate dehydratase | Catalyzes a trans-dehydration via an enolate intermediate | PF01220 | 15.78 | 6.89 | 0.002542 | N\|0.000 | 0.169 | Cyt | Cytoplasmic | Cytoplasmic |
| hemH | Ferrochelatase | Catalyzes the GTP-dependent ribosomal translocation step during translation elongation. During this step, the ribosome changes from the pre-translocational (PRE) to the post- translocational (POST) state as the newly formed A-site-bound peptidyl-tRNA and P-site-bound deacylated tRNA move to the P and E sites, respectively. Catalyzes the coordinated movement of the two tRNA molecules, the mRNA and conformational changes in the ribosome | PF00762 | 37.81 | 8.51 | 0.044331 | N\|0.000 | 0.169 | Cyt | Cytoplasmic | Cytoplasmic |
| rplM | Large ribosomal subunit protein uL13 | This protein is one of the early assembly proteins of the 50S ribosomal subunit, | PF00572 | 16.4 | 10.42 | 0.504644 | N\|0.000 | 0.171 | Cyt | Cytoplasmic | Unknow |

| | | | | | | | | | | | |
|---|---|---|---|---|---|---|---|---|---|---|---|
| | | although it is not seen to bind rRNA by itself. It is important during the early stages of 50S assembly | | | | | | | | | |
| hslV | ATP-dependent protease subunit HslV | Protease subunit of a proteasome-like degradation complex believed to be a general protein degrading machinery | PF00227 | 19.71 | 6.8 | 0.10511 | N\|0.000 | 0.173 | Cyt | Cytoplasmic | Cytoplasmic |
| rplX | Large ribosomal subunit protein uL24 | One of the proteins that surrounds the polypeptide exit tunnel on the outside of the subunit | PF17136, PF00467 | 12.09 | 10.63 | 0.122289 | N\|0.000 | 0.174 | Cyt | Cytoplasmic | Cytoplasmic |
| sucC | Succinate--CoA ligase [ADP-forming] subunit beta | Succinyl-CoA synthetase functions in the citric acid cycle (TCA), coupling the hydrolysis of succinyl-CoA to the synthesis of either ATP or GTP and thus represents the only step of substrate-level phosphorylation in the TCA. The beta subunit provides nucleotide specificity of the enzyme and binds the substrate succinate, while the binding sites for coenzyme A and phosphate are found in the alpha subunit | PF08442, PF00549 | 41.73 | 5.53 | 0.133195 | N\|0.000 | 0.176 | Cyt | Cytoplasmic | Cytoplasmic |
| tyrS | Tyrosine--tRNA ligase | Catalyzes the attachment of tyrosine to | PF005 | 45.3 | 7.08 | 0.0174 | N\|0.0 | 0.179 | Cyt | Cytoplas | Cytoplasmic |

| | | | | | | | | | | | |
|---|---|---|---|---|---|---|---|---|---|---|---|
| | | tRNA(Tyr) in a two-step reaction tyrosine is first activated by ATP to form Tyr- AMP and then transferred to the acceptor end of tRNA(Tyr) | 79 | 6 | | 53 | 00 | | | mic | |
| gcvT | Aminomethyltransferase | Transfers a palmitate residue from the sn-1 position of a phospholipid to the N-linked hydroxymyristate on the proximal unit of lipid A or its precursors | PF01571, PF08669 | 39.52 | 6.7 | 0.019616 | N\|0.000 | 0.18 | Cyt | Cytoplasmic | Cytoplasmic |
| rpmA | Large ribosomal subunit protein bL27 | Belongs to the bacterial ribosomal protein bL27 family | PF01016 | 10.1 | 10.77 | 0.057375 | N\|0.000 | 0.181 | Cyt | Cytoplasmic | Cytoplasmic |
| rpsD | Small ribosomal subunit protein uS4 | One of the primary rRNA binding proteins, it binds directly to 16S rRNA where it nucleates assembly of the body of the 30S subunit | PF00163, PF01479 | 23.26 | 10.64 | 0.569818 | N\|0.000 | 0.181 | Cyt | Cytoplasmic | Unknow |
| metK | S-adenosylmethionine synthase | Catalyzes the formation of S-adenosylmethionine (AdoMet) from methionine and ATP. The overall synthetic reaction is composed of two sequential steps, AdoMet formation and the subsequent tripolyphosphate hydrolysis which occurs prior to release of AdoMet from the enzyme | PF00438, PF02772, PF02773 | 42.01 | 5.79 | 0.08117 | N\|0.000 | 0.181 | Cyt | Cytoplasmic | Cytoplasmic |

| | | | | | | | | | | | |
|---|---|---|---|---|---|---|---|---|---|---|---|
| gcvPB | Probable glycine dehydrogenase (decarboxylating) subunit 2 | The glycine cleavage system catalyzes the degradation of glycine. The P protein binds the alpha-amino group of glycine through its pyridoxal phosphate cofactor | PF21478, PF00266 | 53.37 | 8.51 | 0.017038 | N\|0.000 | 0.181 | Cyt | Cytoplasmic | Unknow |
| kup1 | Probable potassium transport system protein Kup 1 | Transport of potassium into the cell | PF02705 | 70.79 | 8.9 | 0.010232 | Y\|0.803 | 0.183 | Cyt | Cytoplasmic Membrane | InnerMembrane |
| leuS | Leucine--tRNA ligase | leucyl-tRNA aminoacylation | PF13603, PF09334, PF08264, PF00133 | 94.09 | 6.33 | 0.025454 | N\|0.000 | 0.183 | Cyt | Cytoplasmic | Cytoplasmic |
| ftsW | Probable peptidoglycan glycosyltransferase FtsW | Peptidoglycan polymerase that is essential for cell division | PF01098 | 43.44 | 9.67 | 0.042435 | N\|0.000 | 0.184 | Cyt | Cytoplasmic Membrane | InnerMembrane |
| rbfA | Ribosome-binding factor A | One of several proteins that assist in the late maturation steps of the functional | PF02033 | 13.83 | 8.91 | 1.2558 | N\|0.000 | 0.185 | Cyt | Cytoplasmic | Cytoplasmic |

| | | | | | | | | | | | |
|---|---|---|---|---|---|---|---|---|---|---|---|
| | | core of the 30S ribosomal subunit. Associates with free 30S ribosomal subunits (but not with 30S subunits that are part of 70S ribosomes or polysomes). Required for efficient processing of 16S rRNA. May interact with the 5'-terminal helix region of 16S rRNA | | | | | | | | | |
| ravZ | Cysteine protease RavZ | Catalyzes the NADPH-dependent reduction of L-glutamate 5-phosphate into L-glutamate 5-semialdehyde and phosphate. The product spontaneously undergoes cyclization to form 1-pyrroline-5- carboxylate | | 56.25 | 4.73 | 0.04429 | N\|0.000 | 0.186 | Cyt | Cytoplasmic | Unknow |
| metG | Methionine--tRNA ligase | Is required not only for elongation of protein synthesis but also for the initiation of all mRNA translation through initiator tRNA(fMet) aminoacylation | PF19303, PF09334, PF01588 | 75.9 | 6.22 | 0.034297 | N\|0.000 | 0.186 | Cyt | Cytoplasmic | Cytoplasmic |
| glmS | Glutamine--fructose-6-phosphate aminotransferase [isomerizing] | Catalyzes the first step in hexosamine metabolism, converting fructose-6P into glucosamine-6P using glutamine as a nitrogen source | PF01380, PF01380, | 66.4 | 6.62 | 0.051707 | N\|0.000 | 0.187 | Cyt | Cytoplasmic | Cytoplasmic |

| | | | | | | | | | | | |
|---|---|---|---|---|---|---|---|---|---|---|---|
| | | | PF13522 | | | | | | | | |
| aspS | Aspartate--tRNA(Asp/Asn) ligase | Aspartyl-tRNA synthetase with relaxed tRNA specificity since it is able to aspartylate not only its cognate tRNA(Asp) but also tRNA(Asn). Reaction proceeds in two steps L-aspartate is first activated by ATP to form Asp-AMP and then transferred to the acceptor end of tRNA(Asp Asn) | PF02938, PF00152, PF01336 | 66.93 | 6.21 | 0.009911 | N\|0.000 | 0.189 | Cyt | Cytoplasmic | Cytoplasmic |
| kup2 | Probable potassium transport system protein Kup 2 | Transport of potassium into the cell | PF02705 | 70.81 | 7.66 | 0.008203 | N\|0.000 | 0.189 | Cyt | Cytoplasmic Membrane | InnerMembrane |
| rpsM | Small ribosomal subunit protein uS13 | Located at the top of the head of the 30S subunit, it contacts several helices of the 16S rRNA. In the 70S ribosome it contacts the 23S rRNA (bridge B1a) and protein L5 of the 50S subunit (bridge B1b), connecting the 2 subunits | PF00416 | 13.14 | 11.72 | 1.041585 | N\|0.000 | 0.191 | Cyt | Cytoplasmic | Cytoplasmic |
| atpG | ATP synthase gamma chain | Produces ATP from ADP in the presence of a proton gradient across the membrane. | PF00231 | 32.59 | 9.5 | 0.326609 | N\|0.000 | 0.191 | Cyt | Cytoplasmic | Cytoplasmic |

| | | | | | | | | | | | |
|---|---|---|---|---|---|---|---|---|---|---|---|
| | | The gamma chain is believed to be important in regulating ATPase activity and the flow of protons through the CF(0) complex | | | | | | | | | |
| ndk | Nucleoside diphosphate kinase | histidyl-tRNA aminoacylation | PF00334 | 15.59 | 5.26 | 0.236317 | N\|0.000 | 0.193 | Cyt | Extracellular | Cytoplasmic |
| | UPF0434 protein LPC_1374 | Belongs to the UPF0434 family | PF03966 | 6.96 | 8.04 | 0.346153 | -- | 0.195 | Cyt | Unknown | Cytoplasmic |
| msbA | ATP-dependent lipid A-core flippase | - | PF00005, PF00664 | 65.43 | 9.47 | 0.016378 | N\|0.000 | 0.195 | Cyt | Cytoplasmic Membrane | InnerMembrane |
| rplU | Large ribosomal subunit protein bL21 | This protein binds to 23S rRNA in the presence of protein L20 | PF00829 | 11.76 | 10.57 | 1.314958 | N\|0.000 | 0.196 | Cyt | Cytoplasmic | Cytoplasmic |
| | UPF0761 membrane protein LPC_2650 | Virulence factor BrkB | PF03631 | 47.19 | 9.05 | 0.037303 | Y\|0.988 | 0.197 | Cyt | Cytoplasmic Membrane | InnerMembrane |
| asd | Aspartate-semialdehyde dehydrogenase | Catalyzes the NADPH-dependent formation of L-aspartate- semialdehyde (L-ASA) by the reductive dephosphorylation of L- aspartyl-4- | PF02774, PF01118 | 37.72 | 5.98 | 0.024082 | N\|0.000 | 0.199 | Cyt | Cytoplasmic | Cytoplasmic |

| | | | | | | | | | | | |
|---|---|---|---|---|---|---|---|---|---|---|---|
| | | phosphate | | | | | | | | | |
| dnaK | Chaperone protein DnaK | Heat shock 70 kDa protein | PF00012 | 70.07 | 4.68 | 0.266322 | N\|0.000 | 0.199 | Cyt | Cytoplasmic | Cytoplasmic |
| infC | Translation initiation factor IF-3 | IF-3 binds to the 30S ribosomal subunit and shifts the equilibrum between 70S ribosomes and their 50S and 30S subunits in favor of the free subunits, thus enhancing the availability of 30S subunits on which protein synthesis initiation begins | PF05198, PF00707 | 20.39 | 10.44 | 0.612632 | N\|0.000 | 0.202 | Cyt | Cytoplasmic | Cytoplasmic |
| rplV | Large ribosomal subunit protein uL22 | The globular domain of the protein is located near the polypeptide exit tunnel on the outside of the subunit, while an extended beta-hairpin is found that lines the wall of the exit tunnel in the center of the 70S ribosome | PF00237 | 12.02 | 10.28 | 0.822998 | N\|0.000 | 0.205 | Cyt | Cytoplasmic | Unknow |
| adk | Adenylate kinase | Catalyzes the reversible transfer of the terminal phosphate group between ATP and AMP. Plays an important role in cellular energy homeostasis and in adenine nucleotide metabolism | PF00406, PF05191 | 24.12 | 5.64 | 0.052093 | N\|0.000 | 0.205 | Cyt | Cytoplasmic | Cytoplasmic |
| sidD | Adenosine | Transport of potassium into the cell | PF215 | 57.1 | 5.24 | 0.2029 | N\|0.0 | 0.205 | Cyt | Cytoplas | Cytoplasmic |

| | | | | | | | | | | | |
|---|---|---|---|---|---|---|---|---|---|---|---|
| | monophosphate-protein hydrolase SidD | | 11, PF21513 | 6 | | 41 | 00 | | | mic | |
| aroK | Shikimate kinase | Catalyzes the specific phosphorylation of the 3-hydroxyl group of shikimic acid using ATP as a cosubstrate | PF01202 | 19.83 | 4.76 | 0.120625 | N\|0.000 | 0.206 | Cyt | Cytoplasmic | Cytoplasmic |
| groEL | Chaperonin GroEL | Prevents misfolding and promotes the refolding and proper assembly of unfolded polypeptides generated under stress conditions | PF00118 | 58.17 | 5.02 | 0.317455 | N\|0.000 | 0.207 | Cyt | Cytoplasmic | Cytoplasmic |
| murD | UDP-N-acetylmuramoylalanine--D-glutamate ligase | Cell wall formation. Catalyzes the addition of glutamate to the nucleotide precursor UDP-N-acetylmuramoyl-L-alanine (UMA) | PF21799, PF08245, PF02875 | 48.13 | 5.79 | 0.006168 | N\|0.000 | 0.209 | Cyt | Cytoplasmic | Cytoplasmic |
| rpsN | Small ribosomal subunit protein uS14 | Binds 16S rRNA, required for the assembly of 30S particles and may also be responsible for determining the conformation of the 16S rRNA at the A site | PF00253 | 11.76 | 11.35 | 1.022785 | N\|0.000 | 0.21 | Cyt | Cytoplasmic | Unknow |
| rplJ | Large ribosomal subunit | Forms part of the ribosomal stalk, playing | PF004 | 19.2 | 10.4 | 0.6918 | N\|0.0 | 0.21 | Cyt | Cytoplas | Unknow |

| | | | | | | | | | | | |
|---|---|---|---|---|---|---|---|---|---|---|---|
| | protein uL10 | a central role in the interaction of the ribosome with GTP-bound translation factors | 66 | 9 | | 66 | 00 | | | mic | |
| nuoI | NADH-quinone oxidoreductase subunit I | NDH-1 shuttles electrons from NADH, via FMN and iron- sulfur (Fe-S) centers, to quinones in the respiratory chain. The immediate electron acceptor for the enzyme in this species is believed to be ubiquinone. Couples the redox reaction to proton translocation (for every two electrons transferred, four hydrogen ions are translocated across the cytoplasmic membrane), and thus conserves the redox energy in a proton gradient | PF12838 | 19.29 | 7.99 | 1.002597 | N\|0.000 | 0.214 | Cyt | Cytoplasmic | Cytoplasmic |
| dlpA | Protein DlpA | Isocitrate/isopropylmalate dehydrogenase | PF03737, PF00180 | 67.71 | 6.72 | 0.01013 | N\|0.000 | 0.215 | Cyt | Cytoplasmic | Cytoplasmic |
| trpA | Tryptophan synthase alpha chain | The alpha subunit is responsible for the aldol cleavage of indoleglycerol phosphate to indole and glyceraldehyde 3- phosphate | PF00290 | 29.97 | 5.38 | 0.019306 | N\|0.000 | 0.216 | Cyt | Cytoplasmic | Cytoplasmic |

| | | | | | | | | | | | |
|---|---|---|---|---|---|---|---|---|---|---|---|
| metN | Methionine import ATP-binding protein MetN | Part of the ABC transporter complex MetNIQ involved in methionine import. Responsible for energy coupling to the transport system | PF00005, PF09383 | 37.59 | 5.14 | 0.155767 | N\|0.000 | 0.217 | Cyt | Cytoplasmic Membrane | Cytoplasmic |
| grpE | Protein GrpE | Participates actively in the response to hyperosmotic and heat shock by preventing the aggregation of stress-denatured proteins, in association with DnaK and GrpE. It is the nucleotide exchange factor for DnaK and may function as a thermosensor. Unfolded proteins bind initially to DnaJ | PF01025 | 22.83 | 4.95 | 0.200353 | N\|0.000 | 0.219 | Cyt | Cytoplasmic | Cytoplasmic |
| rpsO | Small ribosomal subunit protein uS15 | Forms an intersubunit bridge (bridge B4) with the 23S rRNA of the 50S subunit in the ribosome | PF00312 | 10.85 | 10.33 | 4.288138 | N\|0.000 | 0.22 | Cyt | Cytoplasmic | Cytoplasmic |
| recA | Protein RecA | Can catalyze the hydrolysis of ATP in the presence of single-stranded DNA, the ATP-dependent uptake of single-stranded DNA by duplex DNA, and the ATP-dependent hybridization of homologous single-stranded DNAs. It interacts with LexA causing its activation and leading to | PF00154, PF21096 | 37.96 | 5.08 | 0.045075 | N\|0.000 | 0.22 | Cyt | Cytoplasmic | Cytoplasmic |

| | | | | | | | | | | | |
|---|---|---|---|---|---|---|---|---|---|---|---|
| | | its autocatalytic cleavage | | | | | | | | | |
| xseA | Exodeoxyribonuclease 7 large subunit | Bidirectionally degrades single-stranded DNA into large acid-insoluble oligonucleotides, which are then degraded further into small acid-soluble oligonucleotides | PF02601, PF13742 | 49.46 | 9.2 | 0.003857 | N\|0.000 | 0.222 | Cyt | Cytoplasmic | Unknow |
| dotN | Type 4 apparatus protein DotN | TraM recognition site of TraD and TraG | | 24.43 | 7.58 | 0.051453 | N\|0.000 | 0.223 | Cyt | Unknown | Unknow |
| | Putative glutamate--cysteine ligase 2-1 | ATP-dependent carboxylate-amine ligase which exhibits weak glutamate--cysteine ligase activity | PF04107 | 44.74 | 9.17 | 0.040083 | N\|0.000 | 0.224 | Cyt | Cytoplasmic | Cytoplasmic |
| rplP | Large ribosomal subunit protein uL16 | Binds 23S rRNA and is also seen to make contacts with the A and possibly P site tRNAs | PF00252 | 15.76 | 11.56 | 0.804858 | N\|0.000 | 0.228 | Cyt | Cytoplasmic | Cytoplasmic |
| ihfA | Integration host factor subunit alpha | This protein is one of the two subunits of integration host factor, a specific DNA-binding protein that functions in genetic recombination as well as in transcriptional and translational control | PF00216 | 10.99 | 10.44 | 1.810265 | N\|0.000 | 0.234 | Cyt | Cytoplasmic | Cytoplasmic |
| hfq | RNA-binding protein Hfq | RNA chaperone that binds small regulatory RNA (sRNAs) and mRNAs to facilitate mRNA translational regulation | PF17209 | 9.53 | 6.24 | 0.053338 | N\|0.000 | 0.237 | Cyt | Cytoplasmic | Cytoplasmic |

| | | | | | | | | | | | |
|---|---|---|---|---|---|---|---|---|---|---|---|
| | | in response to envelope stress, environmental stress and changes in metabolite concentrations. Also binds with high specificity to tRNAs | | | | | | | | | |
| rlmL | Ribosomal RNA large subunit methyltransferase K/L | Specifically methylates the guanine in position 2445 (m2G2445) and the guanine in position 2069 (m7G2069) of 23S rRNA | PF01170, PF10672, PF02926 | 80.18 | 9.34 | 0.007695 | N\|0.000 | 0.239 | Cyt | Cytoplasmic | Cytoplasmic |
| rpoA | DNA-directed RNA polymerase subunit alpha | DNA-dependent RNA polymerase catalyzes the transcription of DNA into RNA using the four ribonucleoside triphosphates as substrates | PF01000, PF03118, PF01193 | 36.77 | 4.99 | 1.296842 | N\|0.000 | 0.24 | Cyt | Cytoplasmic | Cytoplasmic |
| rph | Ribonuclease PH | Phosphorolytic exoribonuclease that removes nucleotide residues following the -CCA terminus of tRNA and adds nucleotides to the ends of RNA molecules by using nucleoside diphosphates as substrates | PF03725, PF01138 | 26.14 | 6.52 | 0.22533 | N\|0.000 | 0.243 | Cyt | Cytoplasmic | Cytoplasmic |

| | | | | | | | | | | | |
|---|---|---|---|---|---|---|---|---|---|---|---|
| tdh | L-threonine 3-dehydrogenase | Catalyzes the NAD( )-dependent oxidation of L-threonine to 2-amino-3-ketobutyrate | PF08240, PF00107 | 37.22 | 6.64 | 0.003519 | N\|0.000 | 0.246 | Cyt | Cytoplasmic | Cytoplasmic |
| rlmD | 23S rRNA (uracil(1939)-C(5))-methyltransferase RlmD | ammonia-lyase activity | PF05958, PF01938 | 50.58 | 7.58 | 0.483554 | N\|0.000 | 0.247 | Cyt | Cytoplasmic | Cytoplasmic |
| murB | UDP-N-acetylenolpyruvoylglucosamine reductase | Cell wall formation | PF01565, PF02873 | 33.42 | 6.71 | 0.009381 | N\|0.000 | 0.248 | Cyt | Unknown | Cytoplasmic |
| rplI | Large ribosomal subunit protein bL9 | Binds to the 23S rRNA | PF03948, PF01281 | 16.53 | 6.53 | 0.066204 | N\|0.000 | 0.25 | Cyt | Cytoplasmic | Cytoplasmic |
| pyrH | Uridylate kinase | Catalyzes the reversible phosphorylation of UMP to UDP | PF00696 | 26.53 | 8.79 | 0.024405 | N\|0.000 | 0.252 | Cyt | Cytoplasmic | Cytoplasmic |
| atpF | ATP synthase subunit b | Component of the F(0) channel, it forms part of the peripheral stalk, linking F(1) to F(0) | PF00430 | 17.46 | 6.82 | 0.171531 | N\|0.000 | 0.254 | Cyt | Cytoplasmic Membrane | Unknow |

| | | | | | | | | | | | |
|---|---|---|---|---|---|---|---|---|---|---|---|
| dotZ | Type 4 apparatus protein DotZ | Major role in the synthesis of nucleoside triphosphates other than ATP. The ATP gamma phosphate is transferred to the NDP beta phosphate via a ping-pong mechanism, using a phosphorylated active-site intermediate | | 33.85 | 5.49 | 0.140345 | N\|0.000 | 0.255 | Cyt | Cytoplasmic | Unknow |
| trpB | Tryptophan synthase beta chain | Protein of unknown function (DUF520) | PF00291 | 43.31 | 6.97 | 0.031697 | N\|0.000 | 0.256 | Cyt | Cytoplasmic | Cytoplasmic |
| greA | Transcription elongation factor GreA | Necessary for efficient RNA polymerase transcription elongation past template-encoded arresting sites. The arresting sites in DNA have the property of trapping a certain fraction of elongating RNA polymerases that pass through, resulting in locked ternary complexes. Cleavage of the nascent transcript by cleavage factors such as GreA or GreB allows the resumption of elongation from the new 3'terminus. GreA releases sequences of 2 to 3 nucleotides | PF03449, PF01272 | 17.73 | 5.09 | 0.018252 | N\|0.000 | 0.262 | Cyt | Cytoplasmic | Cytoplasmic |
| lvgA | Type 4 adapter protein LvgA | Involved in unsaturated fatty acids biosynthesis. Catalyzes the dehydration of short chain beta-hydroxyacyl-ACPs and long chain saturated and | | 23.51 | 5.54 | 0.078667 | Y\|0.306 | 0.264 | Cyt | Cytoplasmic | Cytoplasmic |

| | | | | | | | | | | | |
|---|---|---|---|---|---|---|---|---|---|---|---|
| | | unsaturated beta-hydroxyacyl-ACPs | | | | | | | | | |
| rsmH | Ribosomal RNA small subunit methyltransferase H | Specifically methylates the N4 position of cytidine in position 1402 (C1402) of 16S rRNA | PF01795 | 34.59 | 9.31 | 0.027077 | N\|0.000 | 0.264 | Cyt | Cytoplasmic | Cytoplasmic |
| mdh | Malate dehydrogenase | Catalyzes the reversible oxidation of malate to oxaloacetate | PF00056, PF02866 | 36.02 | 5.24 | 0.445882 | N\|0.000 | 0.268 | Cyt | Unknown | Unknow |
| ppa | Inorganic pyrophosphatase | Catalyzes the hydrolysis of inorganic pyrophosphate (PPi) forming two phosphate ions | PF00719 | 20.05 | 5.27 | 0.011794 | N\|0.000 | 0.271 | Cyt | Cytoplasmic | Cytoplasmic |
| rpsH | Small ribosomal subunit protein uS8 | One of the primary rRNA binding proteins, it binds directly to 16S rRNA central domain where it helps coordinate assembly of the platform of the 30S subunit | PF00410 | 14.68 | 10.28 | 0.294666 | N\|0.000 | 0.273 | Cyt | Cytoplasmic | Cytoplasmic |
| obg | GTPase Obg | An essential GTPase which binds GTP, GDP and possibly (p)ppGpp with moderate affinity, with high nucleotide exchange rates and a fairly low GTP hydrolysis rate. Plays a role in control of the cell cycle, stress response, ribosome | PF01018, PF01926 | 36.78 | 6.68 | 0.005113 | N\|0.000 | 0.275 | Cyt | Cytoplasmic | Cytoplasmic |

| | | | | | | | | | | | |
|---|---|---|---|---|---|---|---|---|---|---|---|
| | | biogenesis and in those bacteria that undergo differentiation, in morphogenesis control | | | | | | | | | |
| dotM | Type 4 apparatus protein DotM | Catalyzes the ferrous insertion into protoporphyrin IX | | 43.82 | 8.01 | 0.06148 | N\|0.000 | 0.275 | Cyt | Cytoplasmic Membrane | InnerMembrane |
| thi5 | 4-amino-5-hydroxymethyl-2-methylpyrimidine phosphate synthase | - | PF09084 | 35.28 | 5.71 | 0.013252 | N\|0.000 | 0.277 | Cyt | Cytoplasmic | Cytoplasmic |
| lpxD1 | UDP-3-O-acylglucosamine N-acyltransferase 1 | Catalyzes the N-acylation of UDP-3-O-acylglucosamine using 3-hydroxyacyl-ACP as the acyl donor. Is involved in the biosynthesis of lipid A, a phosphorylated glycolipid that anchors the lipopolysaccharide to the outer membrane of the cell | PF04613, PF00132, PF00132, PF00132 | 37.3 | 7.18 | 0.024278 | N\|0.000 | 0.281 | Cyt | Cytoplasmic | Cytoplasmic |
| sdeA | Ubiquitinating/deubiquitinating enzyme SdeA | lyase activity | PF19048, PF122 | 169.08 | 6.22 | 0.098296 | N\|0.000 | 0.282 | Cyt | Cytoplasmic | Cytoplasmic |

| | | | | | | | | | | | |
|---|---|---|---|---|---|---|---|---|---|---|---|
| | | | 52, PF19049 | | | | | | | | |
| lgt | Phosphatidylglycerol--prolipoprotein diacylglyceryl transferase | Transfers the N-acyl diglyceride group on what will become the N-terminal cysteine of membrane lipoproteins | PF01790 | 29.35 | 8.81 | 0.110738 | N\|0.000 | 0.284 | Cyt | Cytoplasmic Membrane | InnerMembrane |
| argS | Arginine--tRNA ligase | arginyl-tRNA aminoacylation | PF03485, PF00750, PF00750, PF05746 | 65.73 | 5.4 | 0.024877 | N\|0.000 | 0.29 | Cyt | Cytoplasmic | Cytoplasmic |
| | Nucleoid-associated protein lpg2755 | Binds to DNA and alters its conformation. May be involved in regulation of gene expression, nucleoid organization and DNA protection | PF02575 | 12.34 | 4.48 | 0.381137 | N\|0.000 | 0.293 | Cyt | Unknown | Cytoplasmic |
| dapB | 4-hydroxy-tetrahydrodipicolinate reductase | Catalyzes the conversion of 4-hydroxy-tetrahydrodipicolinate (HTPA) to tetrahydrodipicolinate | PF05173, PF0111 | 26.51 | 7.31 | 0.090847 | N\|0.000 | 0.3 | Cyt | Cytoplasmic | Cytoplasmic |

| | | | | | | | | | | | |
|---|---|---|---|---|---|---|---|---|---|---|---|
| | | | 3 | | | | | | | | |
| hisF | Imidazole glycerol phosphate synthase subunit HisF | Regulatory DnaK co-chaperone. Direct interaction between DnaK and DjlA is needed for the induction of the wcaABCDE operon, involved in the synthesis of a colanic acid polysaccharide capsule, possibly through activation of the RcsB RcsC phosphotransfer signaling pathway. The colanic acid capsule may help the bacterium survive conditions outside the host | PF00977 | 23.02 | 5.11 | 0.045623 | N\|0.000 | 0.312 | Cyt | Cytoplasmic | Cytoplasmic |
| atpH | ATP synthase subunit delta | F(1)F(0) ATP synthase produces ATP from ADP in the presence of a proton or sodium gradient. F-type ATPases consist of two structural domains, F(1) containing the extramembraneous catalytic core and F(0) containing the membrane proton channel, linked together by a central stalk and a peripheral stalk. During catalysis, ATP synthesis in the catalytic domain of F(1) is coupled via a rotary mechanism of the central stalk | PF00213 | 19.91 | 5.35 | 0.301377 | N\|0.000 | 0.315 | Cyt | Cytoplasmic | Cytoplasmic |

| | | | | | | | | | | | |
|---|---|---|---|---|---|---|---|---|---|---|---|
| | | subunits to proton translocation | | | | | | | | | |
| | Nucleotide-binding protein lpg1167 | Part of the ABC transporter complex PotABCD involved in spermidine putrescine import. Responsible for energy coupling to the transport system | PF04461 | 18.52 | 6.55 | 0.05663 | N\|0.000 | 0.317 | Cyt | Cytoplasmic | Cytoplasmic |
| rimK | Probable alpha-L-glutamate ligase | cellular protein modification process | PF08443, PF18030 | 32.89 | 10.05 | 0.042601 | N\|0.000 | 0.317 | Cyt | Cytoplasmic | Cytoplasmic |
| rplL | Large ribosomal subunit protein bL12 | Forms part of the ribosomal stalk which helps the ribosome interact with GTP-bound translation factors. Is thus essential for accurate translation | PF16320, PF00542 | 12.91 | 4.27 | 0.720581 | N\|0.000 | 0.322 | Cyt | Unknown | Cytoplasmic |
| murA2 | UDP-N-acetylglucosamine 1-carboxyvinyltransferase 2 | Cell wall formation. Adds enolpyruvyl to UDP-N- acetylglucosamine | PF00275 | 45.23 | 6.61 | 0.00401 | N\|0.000 | 0.326 | Cyt | Cytoplasmic | Cytoplasmic |
| eno | Enolase | Involved in lipid A export and possibly also in glycerophospholipid export and for biogenesis of the outer membrane. Transmembrane domains (TMD) form a pore in the inner membrane and the ATP-binding domain (NBD) is responsible for | PF03952, PF00113 | 46.23 | 5.63 | 0.016976 | N\|0.000 | 0.327 | Cyt | Cytoplasmic | Cytoplasmic |

| | | | | | | | | | | | |
|---|---|---|---|---|---|---|---|---|---|---|---|
| | | energy generation | | | | | | | | | |
| glmU | Bifunctional protein GlmU | Catalyzes the last two sequential reactions in the de novo biosynthetic pathway for UDP-N-acetylglucosamine (UDP-GlcNAc). The C-terminal domain catalyzes the transfer of acetyl group from acetyl coenzyme A to glucosamine-1-phosphate (GlcN-1-P) to produce N-acetylglucosamine-1-phosphate (GlcNAc-1-P), which is converted into UDP-GlcNAc by the transfer of uridine 5-monophosphate (from uridine 5-triphosphate), a reaction catalyzed by the N-terminal domain | PF00132, PF00132, PF12804 | 50.51 | 6.9 | 0.003123 | N\|0.000 | 0.328 | Cyt | Cytoplasmic | Cytoplasmic |
| astD | N-succinylglutamate 5-semialdehyde dehydrogenase | Catalyzes the NAD-dependent reduction of succinylglutamate semialdehyde into succinylglutamate | PF00171 | 54.58 | 6.62 | 0.013657 | N\|0.000 | 0.328 | Cyt | Cytoplasmic | Cytoplasmic |
| | UPF0145 protein LPC_0273 | Putative heavy-metal-binding | PF01906 | 11.21 | 7.41 | 0.040837 | N\|0.000 | 0.329 | Cyt | Unknown | Cytoplasmic |
| tpiA | Triosephosphate isomerase | Involved in the gluconeogenesis. Catalyzes stereospecifically the conversion of dihydroxyacetone | PF00121 | 27.52 | 6.86 | 0.01677 | N\|0.000 | 0.329 | Cyt | Cytoplasmic | Unknow |

| | | | | | | | | | | | |
|---|---|---|---|---|---|---|---|---|---|---|---|
| | | phosphate (DHAP) to D-glyceraldehyde-3-phosphate (G3P) | | | | | | | | | |
| ruvA | Holliday junction branch migration complex subunit RuvA | The RuvA-RuvB complex in the presence of ATP renatures cruciform structure in supercoiled DNA with palindromic sequence, indicating that it may promote strand exchange reactions in homologous recombination. RuvAB is a helicase that mediates the Holliday junction migration by localized denaturation and reannealing. RuvA stimulates, in the presence of DNA, the weak ATPase activity of RuvB | PF14520, PF07499, PF01330 | 22.11 | 7.15 | 0.026771 | N\|0.000 | 0.33 | Cyt | Cytoplasmic | Cytoplasmic |
| hemE | Uroporphyrinogen decarboxylase | Catalyzes the decarboxylation of four acetate groups of uroporphyrinogen-III to yield coproporphyrinogen-III | PF01208 | 39.4 | 6.71 | 0.009276 | N\|0.000 | 0.333 | Cyt | Cytoplasmic | Cytoplasmic |
| acn | Aconitate hydratase A | Catalyzes the isomerization of citrate to isocitrate via cis-aconitate | PF00330, PF00694 | 98.22 | 6.48 | 0.081833 | N\|0.000 | 0.333 | Cyt | Cytoplasmic | Unknow |
| dcd | dCTP deaminase | dCTP deaminase activity | PF00692 | 21.14 | 5.8 | 0.042377 | N\|0.000 | 0.339 | Cyt | Cytoplasmic | Cytoplasmic |

| | | | | | | | | | | | |
|---|---|---|---|---|---|---|---|---|---|---|---|
| dnaJ | Chaperone protein DnaJ | ATP binding to DnaK triggers the release of the substrate protein, thus completing the reaction cycle. Several rounds of ATP-dependent interactions between DnaJ, DnaK and GrpE are required for fully efficient folding. Also involved, together with DnaK and GrpE, in the DNA replication of plasmids through activation of initiation proteins | PF01556, PF00684, PF00226 | 41.29 | 8.26 | 0.02158 | Y\|0.296 | 0.339 | Cyt | Unknown | Cytoplasmic |
| htpX | Protease HtpX | The glycine cleavage system catalyzes the degradation of glycine | PF01435 | 30.26 | 6.43 | 0.057933 | N\|0.000 | 0.343 | Cyt | Cytoplasmic Membrane | InnerMembrane |
| pyrD | Dihydroorotate dehydrogenase (quinone) | Catalyzes the conversion of dihydroorotate to orotate with quinone as electron acceptor | PF01180 | 36.66 | 7.6 | 0.170063 | N\|0.000 | 0.346 | Cyt | Cytoplasmic Membrane | Cytoplasmic |
| kup3 | Probable potassium transport system protein Kup 3 | Catalyzes the transfer of an acyl group from acyl- phosphate (acyl-PO(4)) to glycerol-3-phosphate (G3P) to form lysophosphatidic acid (LPA). This enzyme utilizes acyl-phosphate as fatty | PF02705 | 68.88 | 9.47 | 0.012195 | N\|0.000 | 0.347 | Cyt | Cytoplasmic Membrane | InnerMembrane |

| | | | | | | | | | | | |
|---|---|---|---|---|---|---|---|---|---|---|---|
| | | acyl donor, but not acyl-CoA or acyl-ACP | | | | | | | | | |
| lly | 4-hydroxyphenylpyruvate dioxygenase | Hydroxyphenylpyruvate dioxygenase, HPPD, N-terminal | PF00903, PF14696 | 38.93 | 6.29 | 0.1564 | N\|0.000 | 0.349 | Cyt | Cytoplasmic | Cytoplasmic |
| ubiE | Ubiquinone/menaquinone biosynthesis C-methyltransferase UbiE | Methyltransferase required for the conversion of demethylmenaquinol (DMKH2) to menaquinol (MKH2) and the conversion of 2-polyprenyl-6-methoxy-1,4-benzoquinol (DDMQH2) to 2- polyprenyl-3-methyl-6-methoxy-1,4-benzoquinol (DMQH2) | PF01209 | 28.32 | 8.02 | 0.026139 | N\|0.000 | 0.351 | Cyt | Cytoplasmic | Cytoplasmic |
| pyrE | Orotate phosphoribosyltransferase | Catalyzes the transfer of a ribosyl phosphate group from 5-phosphoribose 1-diphosphate to orotate, leading to the formation of orotidine monophosphate (OMP) | | 23.5 | 6.52 | 0.017845 | N\|0.000 | 0.355 | Cyt | Cytoplasmic | Cytoplasmic |
| | Uncharacterized protein in pal 5'region | ABC-type transport auxiliary lipoprotein component | | 11.47 | 6.51 | 0.119568 | N\|0.000 | 0.361 | Cyt | Unknown | Unknow |
| plsY | Glycerol-3-phosphate acyltransferase | - | PF02660 | 30.47 | 10.26 | 0.398683 | N\|0.000 | 0.363 | Cyt | Cytoplasmic Membrane | InnerMembrane |

| | | | | | | | | | | | |
|---|---|---|---|---|---|---|---|---|---|---|---|
| rpsE | Small ribosomal subunit protein uS5 | Located at the back of the 30S subunit body where it stabilizes the conformation of the head with respect to the body | PF00333, PF03719 | 17.7 | 10.51 | 0.488436 | N\|0.000 | 0.366 | Cyt | Cytoplasmic | Cytoplasmic |
| coaX | Type III pantothenate kinase | Catalyzes the phosphorylation of pantothenate (Pan), the first step in CoA biosynthesis | PF03309 | 27.75 | 8.36 | 0.003064 | N\|0.000 | 0.366 | Cyt | Cytoplasmic | Cytoplasmic |
| hisH1 | Imidazole glycerol phosphate synthase subunit HisH 1 | IGPS catalyzes the conversion of PRFAR and glutamine to IGP, AICAR and glutamate. The HisH subunit provides the glutamine amidotransferase activity that produces the ammonia necessary to HisF for the synthesis of IGP and AICAR | PF00117 | 23.31 | 5 | 0.045911 | N\|0.000 | 0.379 | Cyt | Cytoplasmic | Cytoplasmic |
| rpsK | Small ribosomal subunit protein uS11 | Located on the platform of the 30S subunit, it bridges several disparate RNA helices of the 16S rRNA. Forms part of the Shine-Dalgarno cleft in the 70S ribosome | PF00411 | 14.35 | 11.07 | 0.823646 | N\|0.000 | 0.391 | Cyt | Cytoplasmic | Cytoplasmic |
| purC | Phosphoribosylaminoimidazole-succinocarboxamide synthase | phosphoribosylaminoimidazolesuccinocarboxamide synthase activity | PF01259 | 35.92 | 5.4 | 0.006923 | N\|0.000 | 0.397 | Cyt | Cytoplasmic | Cytoplasmic |

| | | | | | | | | | | | |
|---|---|---|---|---|---|---|---|---|---|---|---|
| tolB | Tol-Pal system protein TolB | involved in the tonB-independent uptake of proteins | PF04052, PF07676, PF07676, PF07676 | 45.4 | 9.08 | 1.496746 | N\|0.000 | 0.4 | Spl | Periplasmic | OuterMembrane |
| aroC | Chorismate synthase | Catalyzes the anti-1,4-elimination of the C-3 phosphate and the C-6 proR hydrogen from 5-enolpyruvylshikimate-3-phosphate (EPSP) to yield chorismate, which is the branch point compound that serves as the starting substrate for the three terminal pathways of aromatic amino acid biosynthesis. This reaction introduces a second double bond into the aromatic ring system | PF01264 | 38.41 | 8.45 | 0.022685 | N\|0.000 | 0.406 | Cyt | Cytoplasmic | Unknow |
| gatB | Aspartyl/glutamyl-tRNA(Asn/Gln) amidotransferase subunit B | Allows the formation of correctly charged Asn-tRNA(Asn) or Gln-tRNA(Gln) through the transamidation of misacylated Asp- tRNA(Asn) or Glu- | PF02934, PF02637 | 53.55 | 6.07 | 0.003737 | N\|0.000 | 0.411 | Cyt | Cytoplasmic | Cytoplasmic |

| | | | | | | | | | | | |
|---|---|---|---|---|---|---|---|---|---|---|---|
| | | tRNA(Gln) in organisms which lack either or both of asparaginyl-tRNA or glutaminyl-tRNA synthetases. The reaction takes place in the presence of glutamine and ATP through an activated phospho-Asp-tRNA(Asn) or phospho-Glu-tRNA(Gln) | | | | | | | | | |
| grlA | Probable monothiol glutaredoxin GrlA | Glutaredoxin | PF00462 | 9.85 | 4.11 | 0.064549 | N\|0.000 | 0.418 | Cyt | Unknown | Cytoplasmic |
| rplF | Large ribosomal subunit protein uL6 | This protein binds to the 23S rRNA, and is important in its secondary structure. It is located near the subunit interface in the base of the L7 L12 stalk, and near the tRNA binding site of the peptidyltransferase center | PF00347, PF00347 | 19.44 | 10.36 | 0.026302 | N\|0.000 | 0.426 | Cyt | Cytoplasmic | Periplasmic |
| lpxD2 | UDP-3-O-acylglucosamine N-acyltransferase 2 | Catalyzes the N-acylation of UDP-3-O-acylglucosamine using 3-hydroxyacyl-ACP as the acyl donor. Is involved in the biosynthesis of lipid A, a phosphorylated glycolipid that anchors the lipopolysaccharide to the outer membrane of the cell | PF00132, PF04613 | 36.57 | 9.06 | 0.007213 | N\|0.000 | 0.428 | Cyt | Unknown | Cytoplasmic |

| | | | | | | | | | | | |
|---|---|---|---|---|---|---|---|---|---|---|---|
| | Putative pterin-4-alpha-carbinolamine dehydratase | 4-alpha-hydroxytetrahydrobiopterin dehydratase activity | PF01329 | 12.9 | 6.22 | 0.379562 | N\|0.000 | 0.43 | Cyt | Cytoplasmic | Cytoplasmic |
| mavE | Effector protein MavE | One of the proteins required for the normal export of preproteins out of the cell cytoplasm. It is a molecular chaperone that binds to a subset of precursor proteins, maintaining them in a translocation-competent state. It also specifically binds to its receptor SecA | | 23.93 | 9.25 | 0.046672 | N\|0.000 | 0.43 | Cyt | Unknown | Unknow |
| yidC | Membrane protein insertase YidC | Required for the insertion and or proper folding and or complex formation of integral membrane proteins into the membrane. Involved in integration of membrane proteins that insert both dependently and independently of the Sec translocase complex, as well as at least some lipoproteins. Aids folding of multispanning membrane proteins | PF14849, PF02096 | 62.52 | 8.99 | 0.484573 | N\|0.000 | 0.435 | Cyt | Cytoplasmic Membrane | Unknow |
| djlA | Co-chaperone protein DjlA | Outer membrane protein assembly factor BamB | PF00226, PF05099 | 34.14 | 9.77 | 0.022069 | N\|0.000 | 0.449 | Cyt | Cytoplasmic Membrane | Periplasmic |

| | | | | | | | | | | | |
|---|---|---|---|---|---|---|---|---|---|---|---|
| aguA | Putative agmatine deiminase | polyamine metabolic process | PF04371 | 39.4 | 5.2 | 0.007981 | N\|0.000 | 0.453 | Cyt | Cytoplasmic | Cytoplasmic |
| rplW | Large ribosomal subunit protein uL23 | One of the early assembly proteins it binds 23S rRNA. One of the proteins that surrounds the polypeptide exit tunnel on the outside of the ribosome. Forms the main docking site for trigger factor binding to the ribosome | PF00276 | 11.26 | 10.79 | 0.057629 | N\|0.000 | 0.46 | Cyt | Cytoplasmic | Unknow |
| purB | Adenylosuccinate lyase | Catalyzes the conversion of N-formimidoyl-L-glutamate to L-glutamate and formamide | PF08328, PF00206 | 51.41 | 6.36 | 0.012005 | N\|0.000 | 0.461 | Cyt | Cytoplasmic | Unknow |
| pal | Peptidoglycan-associated lipoprotein | OmpA family | PF00691 | 18.91 | 7.16 | 19.31846 | N\|0.000 | 0.464 | Lp | Outer Membrane | Unknow |
| efp | Elongation factor P | Involved in peptide bond synthesis. Alleviates ribosome stalling that occurs when 3 or more consecutive Pro residues or the sequence PPG is present in a protein, possibly by augmenting the peptidyl transferase activity of the ribosome. Modification of Lys-34 is | PF09285, PF01132, PF08207 | 20.93 | 4.56 | 0.139952 | N\|0.000 | 0.469 | Cyt | Cytoplasmic | Cytoplasmic |

| | | | | | | | | | | | |
|---|---|---|---|---|---|---|---|---|---|---|---|
| | | required for alleviation | | | | | | | | | |
| katG2 | Catalase-peroxidase 2 | Belongs to the peptidase M48B family | PF00141, PF00141 | 82.93 | 8.43 | 0.446752 | N\|0.000 | 0.478 | Spl | Unknown | Periplasmic |
| hemL | Glutamate-1-semialdehyde 2,1-aminomutase | intramolecular transferase activity, transferring amino groups | PF00202 | 46.17 | 5.42 | 0.031974 | N\|0.000 | 0.481 | Cyt | Cytoplasmic | Cytoplasmic |
| rplD | Large ribosomal subunit protein uL4 | Forms part of the polypeptide exit tunnel | PF00573 | 22.71 | 10.15 | 0.213868 | N\|0.000 | 0.485 | Cyt | Cytoplasmic | Unknow |
| lptD | LPS-assembly protein LptD | - | PF04453, PF03968 | 95.98 | 7.03 | 0.073194 | Y\|1 | 0.485 | Spl | Outer Membrane | OuterMembrane |
| lolA | Outer-membrane lipoprotein carrier protein | Participates in the translocation of lipoproteins from the inner membrane to the outer membrane. Only forms a complex with a lipoprotein if the residue after the N-terminal Cys is not an aspartate (The Asp acts as a targeting signal to indicate that the lipoprotein should stay in the inner membrane) | PF03548 | 22.86 | 10.19 | 0.031336 | N\|0.000 | 0.493 | Spl | Periplasmic | Periplasmic |

| | | | | | | | | | | | |
|---|---|---|---|---|---|---|---|---|---|---|---|
| rplC | Large ribosomal subunit protein uL3 | One of the primary rRNA binding proteins, it binds directly near the 3'-end of the 23S rRNA, where it nucleates assembly of the 50S subunit | PF00297 | 22.99 | 10.89 | 0.148913 | N\|0.000 | 0.498 | Cyt | Cytoplasmic | Periplasmic |
| dotY | Type 4 apparatus protein DotY | Dot/Icm substrate protein | | 25.53 | 4.94 | 0.056743 | N\|0.000 | 0.5 | Cyt | Cytoplasmic | Cytoplasmic |
| | UPF0422 protein lpl2888 | Forms passive diffusion pores that allow small molecular weight hydrophilic materials across the outer membrane | | 57.5 | 8.64 | 0.917717 | Y\|0.963 | 0.508 | Spl | Outer Membrane | OuterMembrane |
| secB | Protein-export protein SecB | Part of the ABC transporter complex LolCDE involved in the translocation of lipoproteins, in an ATP-dependent manner | PF02556 | 18.33 | 4.58 | 0.394636 | N\|0.000 | 0.516 | Cyt | Cytoplasmic | Cytoplasmic |
| hutG | Formimidoylglutamase | [glutamine synthetase]-adenylyl-L-tyrosine phosphorylase | PF00491 | 35.84 | 6.17 | 0.011716 | N\|0.000 | 0.539 | Cyt | Cytoplasmic | Cytoplasmic |
| dsbA | Thiol:disulfide interchange protein DsbA | Thiol disulfide interchange protein | PF01323 | 23.15 | 9.22 | 0.152766 | N\|0.000 | 0.544 | Spl | Periplasmic | Periplasmic |
| panB | 3-methyl-2-oxobutanoate hydroxymethyltransferase | Catalyzes the reversible reaction in which hydroxymethyl group from 5,10-methylenetetrahydrofolate is transferred onto alpha-ketoisovalerate to form ketopantoate | PF02548 | 28.58 | 7.41 | 0.006833 | N\|0.000 | 0.548 | Cyt | Unknown | Periplasmic |

| | | | | | | | | | | | |
|---|---|---|---|---|---|---|---|---|---|---|---|
| hmgA | Homogentisate 1,2-dioxygenase | Involved in the catabolism of homogentisate (2,5-dihydroxyphenylacetate or 2,5-OH-PhAc), a central intermediate in the degradation of phenylalanine and tyrosine. Catalyzes the oxidative ring cleavage of the aromatic ring of homogentisate to yield maleylacetoacetate | PF04209, PF20510 | 47.49 | 6.41 | 0.004971 | N\|0.000 | 0.548 | Cyt | Unknown | Extracellular |
| thyA | Thymidylate synthase | Catalyzes the reductive methylation of 2'-deoxyuridine- 5'-monophosphate (dUMP) to 2'-deoxythymidine-5'-monophosphate (dTMP) while utilizing 5,10-methylenetetrahydrofolate (mTHF) as the methyl donor and reductant in the reaction, yielding dihydrofolate (DHF) as a by-product. This enzymatic reaction provides an intracellular de novo source of dTMP, an essential precursor for DNA biosynthesis | PF00303 | 30.17 | 6.6 | 0.048571 | N\|0.000 | 0.573 | Cyt | Cytoplasmic | Cytoplasmic |
| | Zinc metalloproteinase | Fungalysin/Thermolysin Propeptide Motif | PF02868, | 60.72 | 5.2 | 0.051565 | N\|0.000 | 0.578 | Spl | Extracellular | Periplasmic |

| | | | | | | | | | | | |
|---|---|---|---|---|---|---|---|---|---|---|---|
| | | | PF07504, PF01447 | | | | | | | | |
| mnmA | tRNA-specific 2-thiouridylase MnmA | Catalyzes the 2-thiolation of uridine at the wobble position (U34) of tRNA, leading to the formation of s(2)U34 | PF20258, PF20259, PF03054 | 40.66 | 7.08 | 0.019706 | N\|0.000 | 0.58 | Cyt | Cytoplasmic | Periplasmic |
| pagP | Lipid A acyltransferase PagP | IGPS catalyzes the conversion of PRFAR and glutamine to IGP, AICAR and glutamate. The HisF subunit catalyzes the cyclization activity that produces IGP and AICAR from PRFAR using the ammonia provided by the HisH subunit | PF07017 | 21.22 | 8.81 | 0.452227 | Y\|1 | 0.583 | Spl | Outer Membrane | Extracellular |
| rplA | Large ribosomal subunit protein uL1 | Binds directly to 23S rRNA. The L1 stalk is quite mobile in the ribosome, and is involved in E site tRNA release | PF00687 | 24.52 | 10.31 | 1.714945 | N\|0.000 | 0.586 | Cyt | Cytoplasmic | Periplasmic |
| rplK | Large ribosomal subunit protein uL11 | Forms part of the ribosomal stalk which helps the ribosome interact with GTP-bound translation factors | PF03946, PF002 | 15.09 | 10.36 | 0.04235 | N\|0.000 | 0.619 | Cyt | Cytoplasmic | Periplasmic |

| | | | | | | | | | | | |
|---|---|---|---|---|---|---|---|---|---|---|---|
| | | | 98 | | | | | | | | |
| sodB | Superoxide dismutase [Fe] | radicals which are normally produced within the cells and which are toxic to biological systems | PF02777, PF00081 | 21.64 | 6.39 | 0.066639 | N\|0.000 | 0.725 | Cyt | Periplasmic | Extracellular |
| dapF | Diaminopimelate epimerase | Catalyzes the stereoinversion of LL-2,6-diaminoheptanedioate (L,L-DAP) to meso-diaminoheptanedioate (meso-DAP), a precursor of L-lysine and an essential component of the bacterial peptidoglycan | PF01678, PF01678 | 29.95 | 5.26 | 0.018156 | N\|0.000 | 0.792 | Cyt | Cytoplasmic | Cytoplasmic |
| | Outer membrane protein MIP | peptidyl-prolyl cis-trans isomerase | PF00254, PF01346 | 24.87 | 9.81 | 12.2831 | N\|0.000 | 0.809 | Spl | Outer Membrane | OuterMembrane |
| bamB | Outer membrane protein assembly factor BamB | Part of the outer membrane protein assembly complex, which is involved in assembly and insertion of beta-barrel proteins into the outer membrane | PF13360, PF13360 | 41.22 | 9.4 | 0.390834 | N\|0.000 | 0.83 | Lp | Outer Membrane | Unknow |

## Appendix 2: GO terms and KEGG pathways in Clusters 0, 1, 2, 5, 6, 7

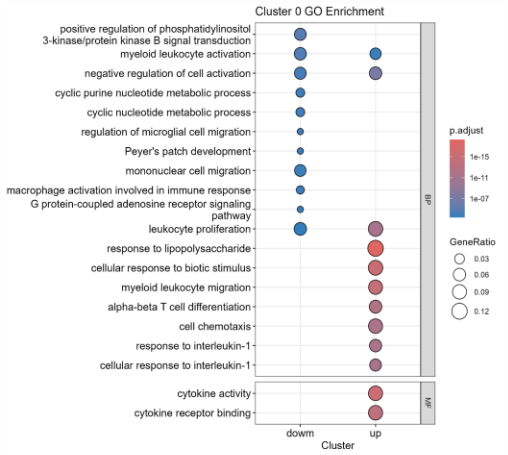


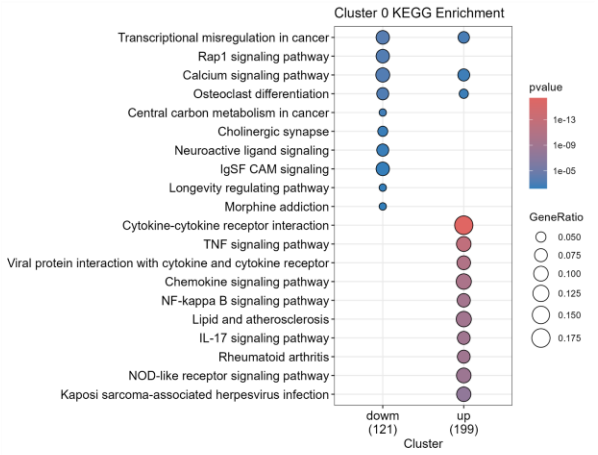


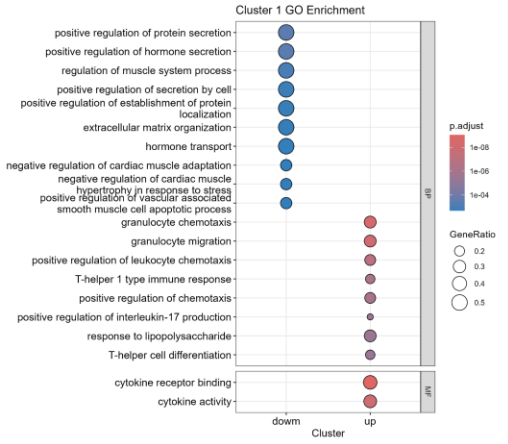


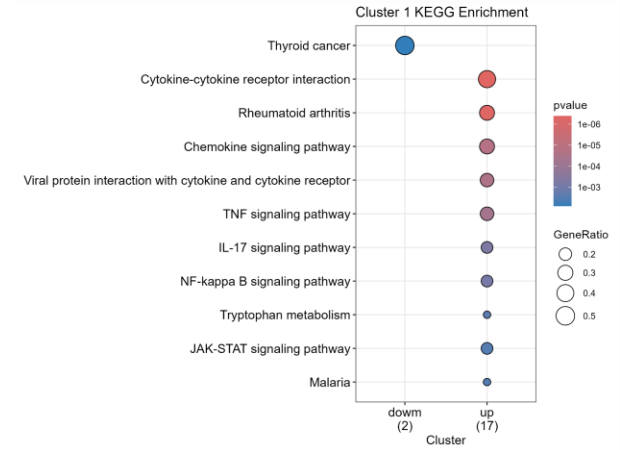

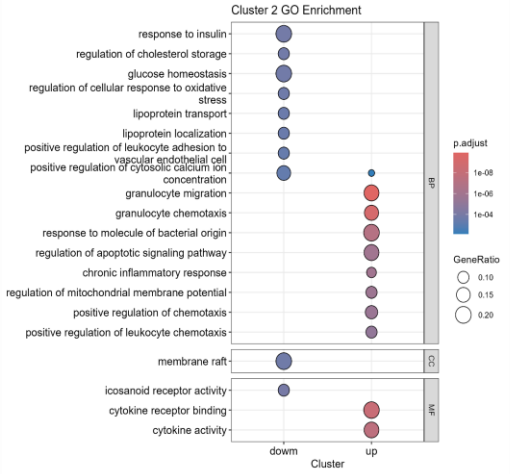
Cluster 2 GO Enrichment
response to insulin
regulation of cholesterol storage
glucose homeostasis
regulation of cellular response to oxidative stress
lipoprotein transport
lipoprotein localization
positive regulation of leukocyte adhesion to vascular endothelial cell
positive regulation of cytosolic calcium ion concentration
granulocyte migration
granulocyte chemotaxis
response to molecule of bacterial origin
regulation of apoptotic signaling pathway
chronic inflammatory response
regulation of mitochondrial membrane potential
positive regulation of chemotaxis
positive regulation of leukocyte chemotaxis
membrane raft
icosanoid receptor activity
cytokine receptor binding
cytokine activity
BP
CC
MF
p.adjust
1e-08
1e-06
1e-04
GeneRatio
0.10
0.15
0.20
dowm
up
Cluster

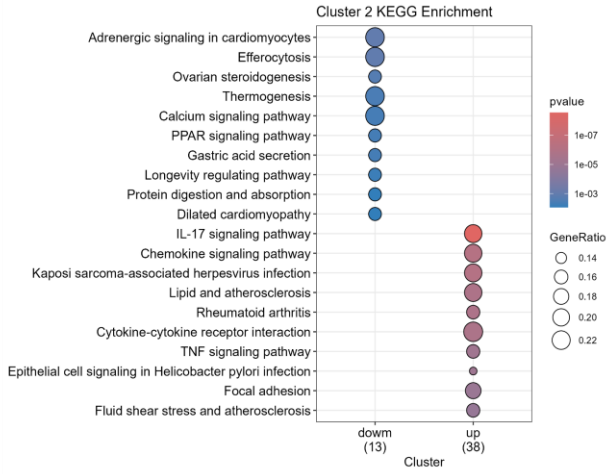
Cluster 2 KEGG Enrichment
Adrenergic signaling in cardiomyocytes
Efferocytosis
Ovarian steroidogenesis
Thermogenesis
Calcium signaling pathway
PPAR signaling pathway
Gastric acid secretion
Longevity regulating pathway
Protein digestion and absorption
Dilated cardiomyopathy
IL-17 signaling pathway
Chemokine signaling pathway
Kaposi sarcoma-associated herpesvirus infection
Lipid and atherosclerosis
Rheumatoid arthritis
Cytokine-cytokine receptor interaction
TNF signaling pathway
Epithelial cell signaling in Helicobacter pylori infection
Focal adhesion
Fluid shear stress and atherosclerosis
pvalue
1e-07
1e-05
1e-03
GeneRatio
0.14
0.16
0.18
0.20
0.22
dowm
(13)
up
(38)
Cluster

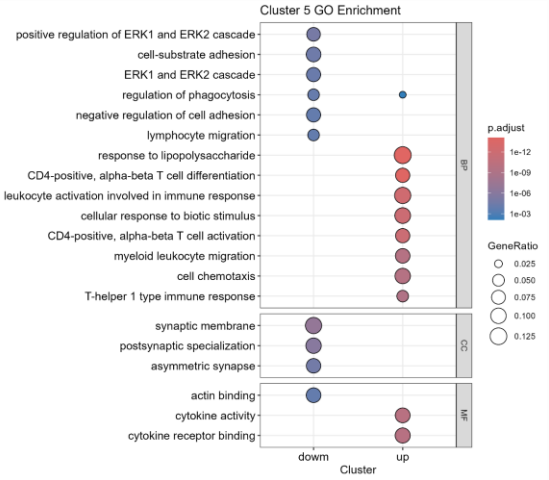
Cluster 5 GO Enrichment
positive regulation of ERK1 and ERK2 cascade
cell-substrate adhesion
ERK1 and ERK2 cascade
regulation of phagocytosis
negative regulation of cell adhesion
lymphocyte migration
response to lipopolysaccharide
CD4-positive, alpha-beta T cell differentiation
leukocyte activation involved in immune response
cellular response to biotic stimulus
CD4-positive, alpha-beta T cell activation
myeloid leukocyte migration
cell chemotaxis
T-helper 1 type immune response
synaptic membrane
postsynaptic specialization
asymmetric synapse
actin binding
cytokine activity
cytokine receptor binding
BP
CC
MF
p.adjust
1e-12
1e-09
1e-06
1e-03
GeneRatio
0.025
0.050
0.075
0.100
0.125
dowm
up
Cluster

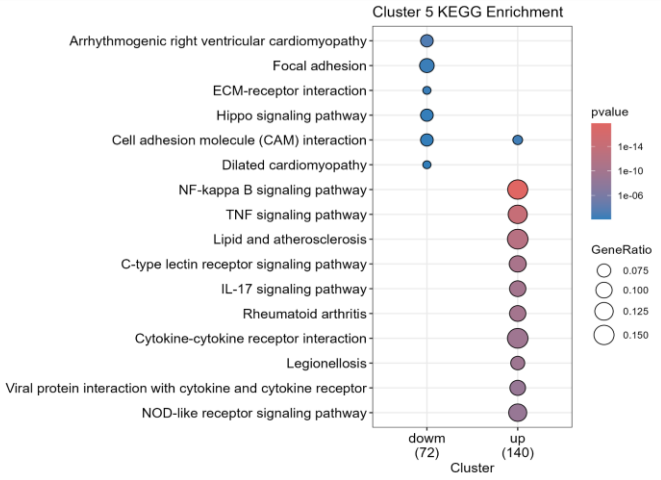
Cluster 5 KEGG Enrichment
Arrhythmogenic right ventricular cardiomyopathy
Focal adhesion
ECM-receptor interaction
Hippo signaling pathway
Cell adhesion molecule (CAM) interaction
Dilated cardiomyopathy
NF-kappa B signaling pathway
TNF signaling pathway
Lipid and atherosclerosis
C-type lectin receptor signaling pathway
IL-17 signaling pathway
Rheumatoid arthritis
Cytokine-cytokine receptor interaction
Legionellosis
Viral protein interaction with cytokine and cytokine receptor
NOD-like receptor signaling pathway
pvalue
1e-14
1e-10
1e-06
GeneRatio
0.075
0.100
0.125
0.150
dowm
(72)
up
(140)
Cluster

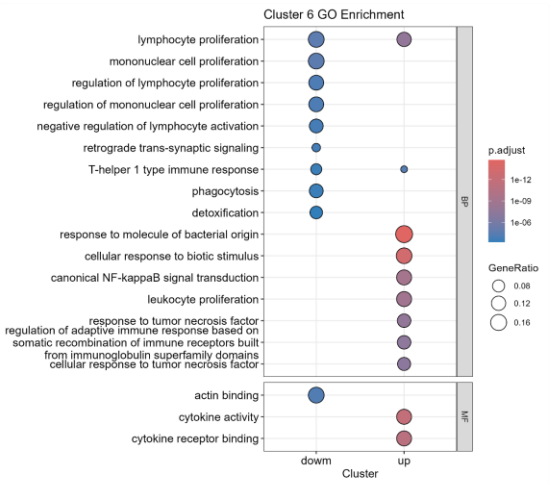
Cluster 6 GO Enrichment
lymphocyte proliferation
mononuclear cell proliferation
regulation of lymphocyte proliferation
regulation of mononuclear cell proliferation
negative regulation of lymphocyte activation
retrograde trans-synaptic signaling
T-helper 1 type immune response
phagocytosis
detoxification
response to molecule of bacterial origin
cellular response to biotic stimulus
canonical NF-kappaB signal transduction
leukocyte proliferation
response to tumor necrosis factor
regulation of adaptive immune response based on somatic recombination of immune receptors built from immunoglobulin superfamily domains
cellular response to tumor necrosis factor
actin binding
cytokine activity
cytokine receptor binding
BP
MF
p.adjust
1e-12
1e-09
1e-06
GeneRatio
0.08
0.12
0.16
dowm
up
Cluster

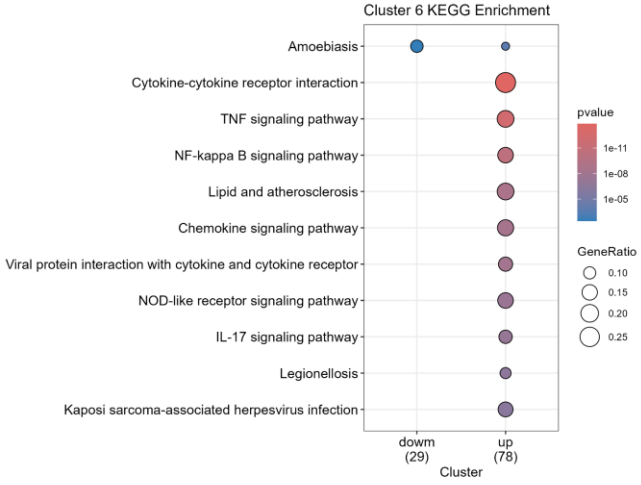
Cluster 6 KEGG Enrichment
Amoebiasis
Cytokine-cytokine receptor interaction
TNF signaling pathway
NF-kappa B signaling pathway
Lipid and atherosclerosis
Chemokine signaling pathway
Viral protein interaction with cytokine and cytokine receptor
NOD-like receptor signaling pathway
IL-17 signaling pathway
Legionellosis
Kaposi sarcoma-associated herpesvirus infection
pvalue
1e-11
1e-08
1e-05
GeneRatio
0.10
0.15
0.20
0.25
dowm
(29)
up
(78)
Cluster

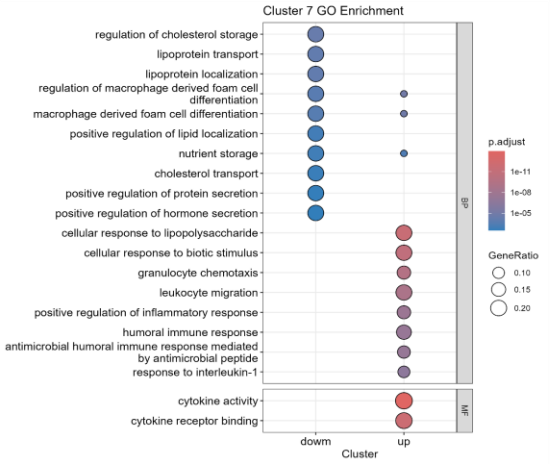
Cluster 7 GO Enrichment
regulation of cholesterol storage
lipoprotein transport
lipoprotein localization
regulation of macrophage derived foam cell differentiation
macrophage derived foam cell differentiation
positive regulation of lipid localization
nutrient storage
cholesterol transport
positive regulation of protein secretion
positive regulation of hormone secretion
cellular response to lipopolysaccharide
cellular response to biotic stimulus
granulocyte chemotaxis
leukocyte migration
positive regulation of inflammatory response
humoral immune response
antimicrobial humoral immune response mediated by antimicrobial peptide
response to interleukin-1
cytokine activity
cytokine receptor binding
BP
MF
p.adjust
1e-11
1e-08
1e-05
GeneRatio
0.10
0.15
0.20
dowm
up
Cluster

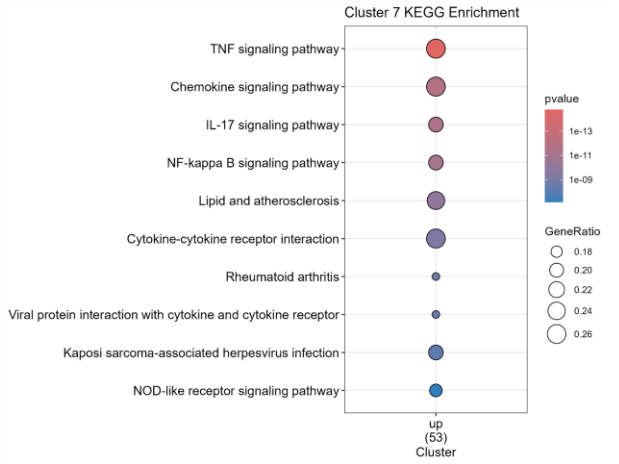
Cluster 7 KEGG Enrichment
TNF signaling pathway
Chemokine signaling pathway
IL-17 signaling pathway
NF-kappa B signaling pathway
Lipid and atherosclerosis
Cytokine-cytokine receptor interaction
Rheumatoid arthritis
Viral protein interaction with cytokine and cytokine receptor
Kaposi sarcoma-associated herpesvirus infection
NOD-like receptor signaling pathway
pvalue
1e-13
1e-11
1e-09
GeneRatio
0.18
0.20
0.22
0.24
0.26
up
(53)
Cluster

**Appendix 3: qPCR fold changes of cytokines in THP-1 derived macrophages after treatment with *L. pneumophila* OMVs**

| Markers | 24 h | | | | 48 h | | | |
|---|---|---|---|---|---|---|---|---|
| | 1 µg Fold change | 10 µg Fold change | 20 µg Fold change | Significance | 1 µg Fold change | 10 µg Fold change | 20 µg Fold change | Significance |
| **CCL4** | 1 ± 0.265 | 1.6 ± 0.358 | 1.2 ± 0.183 | ns | 1.07 ± 0.054 | 1.48 ± 0.124 | 1.55 ± 0.253 | ns |
| **VEGF** | 1.1 ± 0.101 | 1.3 ± 0.283 | 0.9 ± 0.236 | ns | 0.7 ± 0.143 | 0.81 ± 0.527 | 0.61 ± 0.048 | ns |
| **IL6** | 1 ± 0.172 | 2.1 ± 0.458 | 1.8 ± 0.316 | ns | 0.88 ± 0.187 | 1.64 ± 0.199 | 4.18 ± 0.390 | * at 20 µg |
| **IL1β** | 0.95 ± 0.164 | 1.16 ± 0.361 | 1.52 ± 0.254 | ns | 0.82 ± 0.085 | 1.03 ± 0.048 | 1.18 ± 0.159 | ns |
| **IL4** | 2.1 ± 0.209 | 1.4 ± 0.212 | 0.7 ± 0.169 | ns | 1.21 ± 0.215 | 0.65 ± 0.093 | 1.3 ± 0.182 | ns |
| **IL10** | 1 ± 0.340 | 1.59 ± 0.434 | 1.52 ± 0.265 | ns | 0.88 ± 0.227 | 1.61 ± 0.218 | 3.61 ± 0.290 | * at 20 µg |
| **TGFβ** | 0.78 ± 0.154 | 2.55 ± 0.226 | 1.51 ± 0.206 | * at 10 µg | 0.91± 0.217 | 1.05 ± 0.094 | 1.21 ± 0.151 | ns |
| **iNOS** | 0.64 ± 0.142 | 1.16 ± 0.053 | 0.92 ± 0.127 | ns | 0.82 ± 0.128 | 1.1 ± 0.054 | 1.06 ± 0.043 | ns |
| **ARG1** | 0.82 ± 0.286 | 1.52 ± 0.03 | 1.2 ± 0.06 | ns | 1.06 ± 0.087 | 0.78 ± 0.079 | 0.55 ± 0.110 | ns |
| **SOD2** | 0.8 ± 0.244 | 1.53 ± 0.237 | 1.56 ± 0.075 | ns | 0.87 ± 0.076 | 1.11 ± 0.108 | 1.48 ± 0.099 | ns |

| | | | | | | | | |
|---|---|---|---|---|---|---|---|---|
| **IL-12** | 1.2 ± 0.054 | 1.4 ± 0.042 | 1 ± 0.254 | ns | 1.12 ± 0.054 | 1.45 ± 0.124 | 1.38 ± 0.122 | ns |
| **TNF alpha** | 1 ± 0.150 | 0.95 ± 0.125 | 1.2 ± 0.162 | ns | 1.24 ± 0.058 | 3.5 ± 0.125 | 4.95 ± 0.256 | * at 20 µg |

**Appendix 4: Blot images of Cytokine array data from triplicates at 24 and 48 hours**

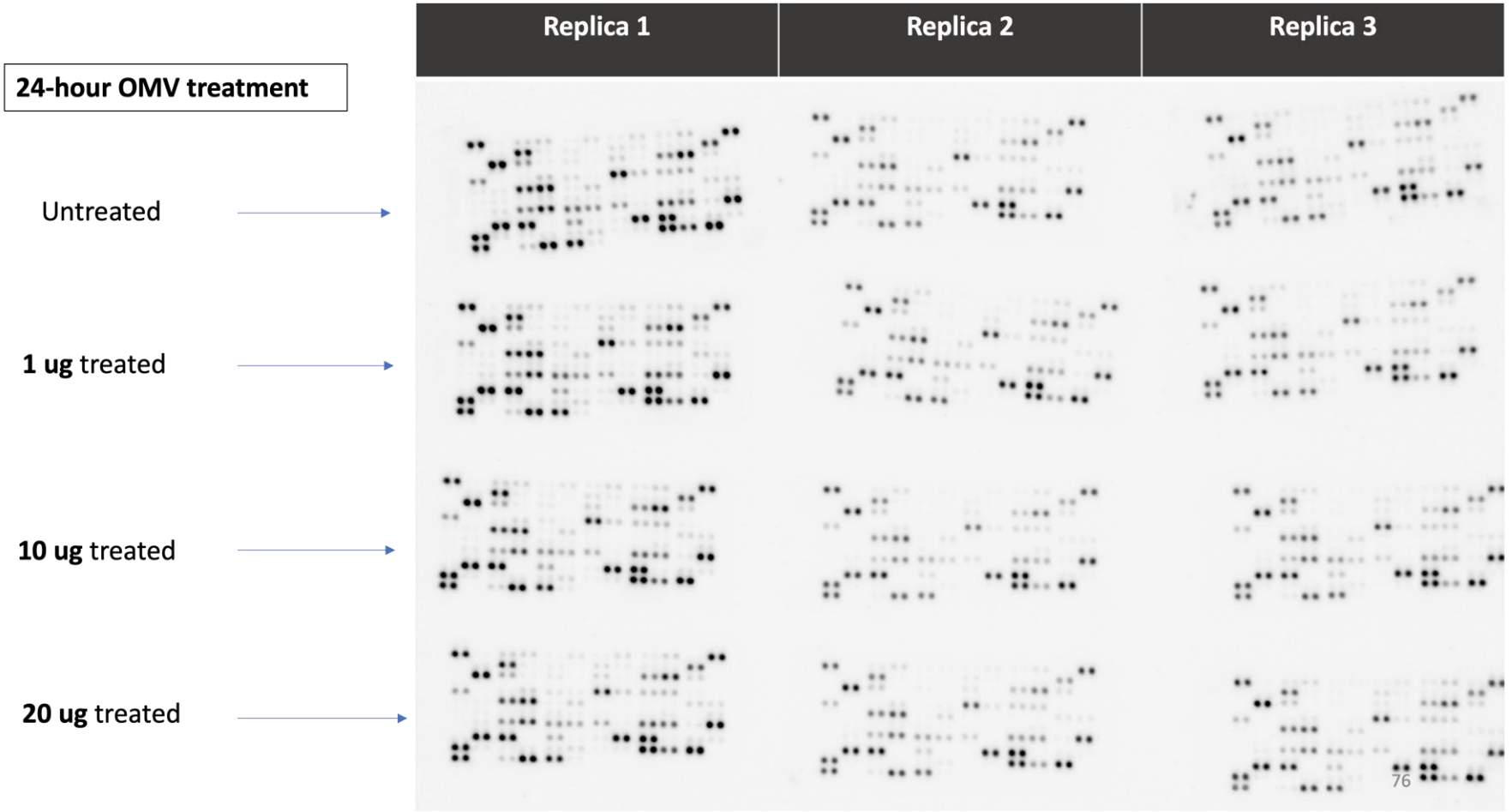

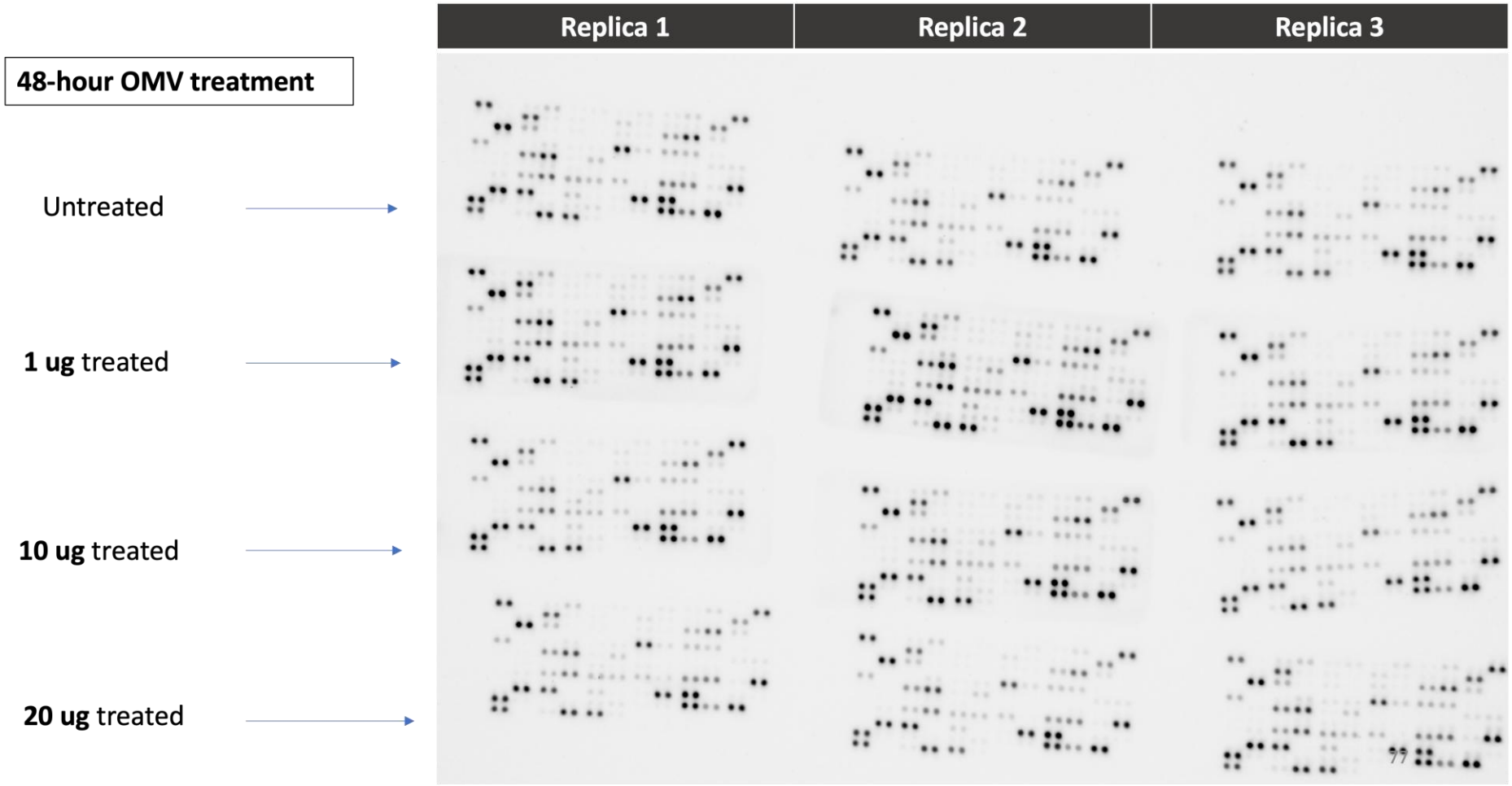
Replica 1
Replica 2
Replica 3
48-hour OMV treatment
Untreated
1 ug treated
10 ug treated
20 ug treated

**Appendix 5: Dot plot of 46 cytokines list (significant in cytokine array data) also found differentially expressed in scRNA-seq data**

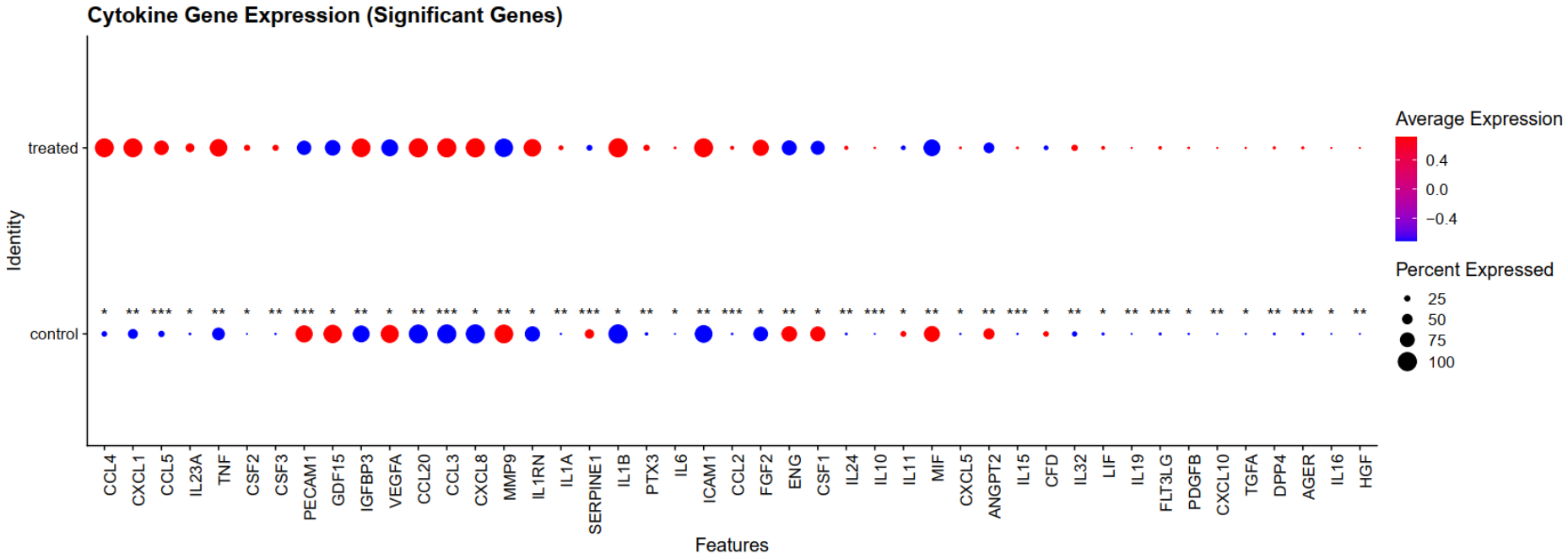

# References


Aachoui, Y., Leaf, I. A., Hagar, J. A., Fontana, M. F., Campos, C. G., Zak, D. E., Tan, M. H., Cotter, P. A., Vance, R. E., & Aderem, A. (2013). Caspase-11 protects against bacteria that escape the vacuole. *science*, *339*(6122), 975-978.

Abu Khweek, A., & Amer, A. O. (2018). Factors mediating environmental biofilm formation by Legionella pneumophila. *Frontiers in cellular and infection microbiology*, *8*, 38.

Akhter, A., Caution, K., Khweek, A. A., Tazi, M., Abdulrahman, B. A., Abdelaziz, D. H., Voss, O. H., Doseff, A. I., Hassan, H., & Azad, A. K. (2012). Caspase-11 promotes the fusion of phagosomes harboring pathogenic bacteria with lysosomes by modulating actin polymerization. *Immunity*, *37*(1), 35-47.

Alan, R., Ezekowitz, B., & Gordon, S. (1984). Alterations of surface properties by macrophage activation: expression of receptors for Fc and mannose-terminal glycoproteins and differentiation antigens. *Macrophage Activation*, 33-56.

Allam, C., Mouton, W., Testaert, H., Ginevra, C., Fessy, N., Ibranosyan, M., Descours, G., Beraud, L., Guillemot, J., & Chapalain, A. (2023). Hyper-inflammatory profile and immunoparalysis in patients with severe Legionnaires' disease. *Frontiers in Cellular and Infection Microbiology*, *13*, 1252515.

Allgaier, J., Lagu, T., Haessler, S., Imrey, P. B., Deshpande, A., Guo, N., & Rothberg, M. B. (2021). Risk factors, management, and outcomes of Legionella pneumonia in a large, nationally representative sample. *Chest*, *159*(5), 1782-1792.

Altindis, E., Fu, Y., & Mekalanos, J. J. (2014). Proteomic analysis of Vibrio cholerae outer membrane vesicles. *Proceedings of the National Academy of Sciences*, *111*(15), E1548-E1556.

Anderson, C. F., & Mosser, D. M. (2002). A novel phenotype for an activated macrophage: the type 2 activated macrophage. *Journal of leukocyte biology*, *72*(1), 101-106.

Arango Duque, G., & Descoteaux, A. (2014). Macrophage cytokines: involvement in immunity and infectious diseases. *Frontiers in immunology*, *5*, 491.

Archer, K. A., Alexopoulou, L., Flavell, R. A., & Roy, C. R. (2009). Multiple MyD88-dependent responses contribute to pulmonary clearance of Legionella pneumophila. *Cellular microbiology*, *11*(1), 21-36.

Archer, K. A., & Roy, C. R. (2006). MyD88-dependent responses involving toll-like receptor 2 are important for protection and clearance of Legionella pneumophila in a mouse model of Legionnaires' disease. *Infection and immunity*, *74*(6), 3325-3333.

Arnett, E., Lehrer, R. I., Pratikhya, P., Lu, W., & Seveau, S. (2011). Defensins enable macrophages to inhibit the intracellular proliferation of Listeria monocytogenes. *Cellular microbiology*, *13*(4), 635-651.

Asrat, S., Dugan, A. S., & Isberg, R. R. (2014). The frustrated host response to Legionella pneumophila is bypassed by MyD88-dependent translation of pro-inflammatory cytokines. *PLoS pathogens*, *10*(7), e1004229.

Auwerx, J. (1991). The human leukemia cell line, THP-1: a multifacetted model for the study of monocyte-macrophage differentiation. *Experientia*, *47*(1), 22-31.

Avila-Calderón, E. D., Ruiz-Palma, M. D. S., Aguilera-Arreola, M. G., Velázquez-Guadarrama, N., Ruiz, E. A., Gomez-Lunar, Z., Witonsky, S., & Contreras-Rodríguez, A. (2021). Outer membrane vesicles of gram-negative bacteria: an outlook on biogenesis. *Frontiers in Microbiology*, *12*, 557902.

Awad, F., Assrawi, E., Jumeau, C., Georgin-Lavialle, S., Cobret, L., Duquesnoy, P., Piterboth, W., Thomas, L., Stankovic-Stojanovic, K., & Louvrier, C. (2017). Impact of human monocyte and macrophage polarization on NLR expression and NLRP3 inflammasome activation. *PloS one*, *12*(4), e0175336.

Ayesha, A., Chow, F. W.-N., & Leung, P. H.-M. (2023). Role of Legionella pneumophila outer membrane vesicles in host-pathogen interaction. *Frontiers in Microbiology*, *14*, 1270123.

Bach, F. H., Ferran, C., Hechenleitner, P., Mark, W., Koyamada, N., Miyatake, T., Winkler, H., Badrichant, A., Candinas, D., & Hancock, W. W. (1997). Accommodation of vascularized xenografts: expression of "protective genes" by donor endothelial cells in a host Th2 cytokine environment. *Nature medicine*, *3*(2), 196-204.

Bai, J., Kim, S. I., Ryu, S., & Yoon, H. (2014). Identification and characterization of outer membrane vesicle-associated proteins in Salmonella enterica serovar Typhimurium. *Infection and immunity*, *82*(10), 4001-4010.

Baskic, D., Vukovic, V. R., Popovic, S., Djurdjevic, P., Zaric, M., Nikolic, I., Zelen, I., Mitrovic, M., Avramovic, D., & Mijailovic, Z. (2017). Cytokine profile in chronic hepatitis C: An observation. *Cytokine*, *96*, 185-188.

Bastiaan-Net, S., Chanput, W., Hertz, A., Zwittink, R. D., Mes, J. J., & Wichers, H. J. (2013). Biochemical and functional characterization of recombinant fungal immunomodulatory proteins (rFIPs). *International immunopharmacology*, *15*(1), 167-175.

Battesti, A., Majdalani, N., & Gottesman, S. (2011). The RpoS-mediated general stress response in Escherichia coli. *Annual review of microbiology*, *65*, 189-213.

Bauman, S. J., & Kuehn, M. J. (2009). Pseudomonas aeruginosa vesicles associate with and are internalized by human lung epithelial cells. *BMC microbiology*, *9*(1), 1-12.

Beauté, J. (2017). Legionnaires' disease in Europe, 2011 to 2015. *Eurosurveillance*, *22*(27), 30566.

Bedard, K., & Krause, K.-H. (2007). The NOX family of ROS-generating NADPH oxidases: physiology and pathophysiology. *Physiological reviews*, *87*(1), 245-313.

Belyi, Y. (2020). Targeting eukaryotic mRNA translation by Legionella pneumophila. *Frontiers in molecular biosciences*, *7*, 80.

Belyi, Y., Levanova, N., & Schroeder, G. N. (2022). Glycosylating effectors of Legionella pneumophila:

Finding the sweet spots for host cell subversion. *Biomolecules*, *12*(2), 255.

Benoit, M., Desnues, B., & Mege, J.-L. (2008). Macrophage polarization in bacterial infections. *The Journal of immunology*, *181*(6), 3733-3739.

Bernadac, A., Gavioli, M., Lazzaroni, J.-C., Raina, S., & Lloubès, R. (1998). Escherichia coli tol-pal mutants form outer membrane vesicles. *Journal of bacteriology*, *180*(18), 4872-4878.

Bewley, M. A., Marriott, H. M., Tulone, C., Francis, S. E., Mitchell, T. J., Read, R. C., Chain, B., Kroemer, G., Whyte, M. K., & Dockrell, D. H. (2011). A cardinal role for cathepsin d in co-ordinating the host-mediated apoptosis of macrophages and killing of pneumococci. *PLoS pathogens*, *7*(1), e1001262.

Bhat, N., & Fitzgerald, K. A. (2014). Recognition of cytosolic DNA by c GAS and other STING-dependent sensors. *European journal of immunology*, *44*(3), 634-640.

Bielaszewska, M., Rüter, C., Bauwens, A., Greune, L., Jarosch, K.-A., Steil, D., Zhang, W., He, X., Lloubes, R., & Fruth, A. (2017). Host cell interactions of outer membrane vesicle-associated virulence factors of enterohemorrhagic Escherichia coli O157: Intracellular delivery, trafficking and mechanisms of cell injury. *PLoS pathogens*, *13*(2), e1006159.

Bielaszewska, M., Rüter, C., Kunsmann, L., Greune, L., Bauwens, A., Zhang, W., Kuczius, T., Kim, K. S., Mellmann, A., & Schmidt, M. A. (2013). Enterohemorrhagic Escherichia coli hemolysin employs outer membrane vesicles to target mitochondria and cause endothelial and epithelial apoptosis. *PLoS pathogens*, *9*(12), e1003797.

Biller, S. J., Schubotz, F., Roggensack, S. E., Thompson, A. W., Summons, R. E., & Chisholm, S. W. (2014). Bacterial vesicles in marine ecosystems. *science*, *343*(6167), 183-186.

Biondo, C., Mancuso, G., Midiri, A., Signorino, G., Domina, M., Lanza Cariccio, V., Venza, M., Venza, I., Teti, G., & Beninati, C. (2014). Essential role of interleukin-1 signaling in host defenses against group B streptococcus. *MBio*, *5*(5), 10.1128/mbio. 01428-01414.

Biswas, S. K., & Mantovani, A. (2010). Macrophage plasticity and interaction with lymphocyte subsets: cancer as a paradigm. *Nature immunology*, *11*(10), 889-896.

Bitto, N. J., Chapman, R., Pidot, S., Costin, A., Lo, C., Choi, J., D'Cruze, T., Reynolds, E. C., Dashper, S. G., & Turnbull, L. (2017). Bacterial membrane vesicles transport their DNA cargo into host cells. *Scientific Reports*, *7*(1), 7072.

Bomberger, J. M., MacEachran, D. P., Coutermarsh, B. A., Ye, S., O'Toole, G. A., & Stanton, B. A. (2009). Long-distance delivery of bacterial virulence factors by Pseudomonas aeruginosa outer membrane vesicles. *PLoS pathogens*, *5*(4), e1000382.

Borthwick, L. (2016). The IL-1 cytokine family and its role in inflammation and fibrosis in the lung. Seminars in immunopathology,

Brieland, J. K., Jackson, C., Hurst, S., Loebenberg, D., Muchamuel, T., Debets, R., Kastelein, R., Churakova, T., Abrams, J., & Hare, R. (2000). Immunomodulatory role of endogenous interleukin-18 in gamma interferon-mediated resolution of replicative Legionella pneumophila lung infection. *Infection and immunity*, *68*(12), 6567-6573.

Broggi, A., & Granucci, F. (2015). Microbe-and danger-induced inflammation. *Molecular immunology*, *63*(2), 127-133.

Brown, G. D., Willment, J. A., & Whitehead, L. (2018). C-type lectins in immunity and homeostasis. *Nature Reviews Immunology*, *18*(6), 374-389.

Brown, L., Wolf, J. M., Prados-Rosales, R., & Casadevall, A. (2015). Through the wall: extracellular vesicles in Gram-positive bacteria, mycobacteria and fungi. *Nature Reviews Microbiology*, *13*(10), 620-630.

Brüggemann, H., Hagman, A., Jules, M., Sismeiro, O., Dillies, M. A., Gouyette, C., Kunst, F., Steinert, M., Heuner, K., & Coppée, J. Y. (2006). Virulence strategies for infecting phagocytes deduced from the in vivo transcriptional program of Legionella pneumophila. *Cellular microbiology*, *8*(8), 1228-1240.

Buse, H. Y., Brehm, A., Santo Domingo, J. W., & Ashbolt, N. J. (2011). Screening-level assays for potentially human-infectious environmental Legionella spp. *The Journal of Microbiology*, *49*(2), 200-207.

Byrne, B., & Swanson, M. S. (1998). Expression of Legionella pneumophila virulence traits in response to growth conditions. *Infection and immunity*, *66*(7), 3029-3034.

Cairo, G., Recalcati, S., Mantovani, A., & Locati, M. (2011). Iron trafficking and metabolism in macrophages: contribution to the polarized phenotype. *Trends in immunology*, *32*(6), 241-247.

Calvano, S. E., Xiao, W., Richards, D. R., Felciano, R. M., Baker, H. V., Cho, R. J., Chen, R. O., Brownstein, B. H., Cobb, J. P., & Tschoeke, S. K. (2005). A network-based analysis of systemic inflammation in humans. *Nature*, *437*(7061), 1032-1037.

Campoccia, D., Montanaro, L., & Arciola, C. R. (2021). Extracellular DNA (eDNA). A major ubiquitous element of the bacterial biofilm architecture. *International journal of molecular sciences*, *22*(16), 9100.

Cañas, M.-A., Fábrega, M.-J., Giménez, R., Badia, J., & Baldomà, L. (2018). Outer membrane vesicles from probiotic and commensal Escherichia coli activate NOD1-mediated immune responses in intestinal epithelial cells. *Frontiers in Microbiology*, *9*, 498.

Canton, J. (2014). Phagosome maturation in polarized macrophages. *Journal of leukocyte biology*, *96*(5), 729-738.

Case, C. L., Shin, S., & Roy, C. R. (2009). Asc and Ipaf Inflammasomes direct distinct pathways for caspase-1 activation in response to Legionella pneumophila. *Infection and immunity*, *77*(5), 1981-1991.

Casson, C. N., Copenhaver, A. M., Zwack, E. E., Nguyen, H. T., Strowig, T., Javdan, B., Bradley, W. P., Fung, T. C., Flavell, R. A., & Brodsky, I. E. (2013). Caspase-11 activation in response to bacterial secretion systems that access the host cytosol. *PLoS pathogens*, *9*(6), e1003400.

Cazalet, C., Gomez-Valero, L., Rusniok, C., Lomma, M., Dervins-Ravault, D., Newton, H. J., Sansom, F. M., Jarraud, S., Zidane, N., & Ma, L. (2010). Analysis of the Legionella longbeachae genome and transcriptome uncovers unique strategies to cause Legionnaires' disease. *PLoS genetics*,

*6*(2), e1000851.

Cecil, J. D., O'Brien-Simpson, N. M., Lenzo, J. C., Holden, J. A., Singleton, W., Perez-Gonzalez, A., Mansell, A., & Reynolds, E. C. (2017). Outer membrane vesicles prime and activate macrophage inflammasomes and cytokine secretion in vitro and in vivo. *Frontiers in immunology*, *8*, 1017.

Cecil, J. D., Sirisaengtaksin, N., O'Brien-Simpson, N. M., & Krachler, A. M. (2019). Outer membrane vesicle-host cell interactions. *Microbiology spectrum*, *7*(1), 10.1128/microbiolspec. psib-0001-2018.

Cellier, M. F. (2017). Developmental control of NRAMP1 (SLC11A1) expression in professional phagocytes. *Biology*, *6*(2), 28.

Chacon-Salinas, R., Serafin-Lopez, J., Ramos-Payan, R., Méndez-Aragón, P., Hernandez-Pando, R., Van Soolingen, D., Flores-Romo, L., Estrada-Parra, S., & Estrada-García, I. (2005). Differential pattern of cytokine expression by macrophages infected in vitro with different Mycobacterium tuberculosis genotypes. *Clinical & Experimental Immunology*, *140*(3), 443-449.

Chanput, W., Mes, J. J., Savelkoul, H. F., & Wichers, H. J. (2013). Characterization of polarized THP-1 macrophages and polarizing ability of LPS and food compounds. *Food & function*, *4*(2), 266-276.

Chanput, W., Mes, J. J., & Wichers, H. J. (2014). THP-1 cell line: an in vitro cell model for immune modulation approach. *International immunopharmacology*, *23*(1), 37-45.

Chanput, W., Reitsma, M., Kleinjans, L., Mes, J. J., Savelkoul, H. F., & Wichers, H. J. (2012). β-Glucans are involved in immune-modulation of THP-1 macrophages. *Molecular nutrition & food research*, *56*(5), 822-833.

Chatterjee, S., & Das, J. (1967). Electron microscopic observations on the excretion of cell-wall material by Vibrio cholerae. *Microbiology*, *49*(1), 1-11.

Chauhan, D., & Shames, S. R. (2021). Pathogenicity and Virulence of Legionella: Intracellular replication and host response. *Virulence*, *12*(1), 1122-1144.

Chen, X., Li, Q., Xie, J., & Nie, S. (2024). Immunomodulatory effects of Probiotic-Derived extracellular vesicles: opportunities and challenges. *Journal of Agricultural and Food Chemistry*, *72*(35), 19259-19273.

Chiu, Y.-H., MacMillan, J. B., & Chen, Z. J. (2009). RNA polymerase III detects cytosolic DNA and induces type I interferons through the RIG-I pathway. *Cell*, *138*(3), 576-591.

Chizzolini, C., Chicheportiche, R., Alvarez, M., de Rham, C., Roux-Lombard, P., Ferrari-Lacraz, S., & Dayer, J.-M. (2008). Prostaglandin E2 synergistically with interleukin-23 favors human Th17 expansion. *Blood, The Journal of the American Society of Hematology*, *112*(9), 3696-3703.

Chizzolini, C., Dufour, A. M., & Brembilla, N. C. (2018). Is there a role for IL-17 in the pathogenesis of systemic sclerosis? *Immunology Letters*, *195*, 61-67.

Chmiela, M., Walczak, N., & Rudnicka, K. (2018). Helicobacter pylori outer membrane vesicles involvement in the infection development and Helicobacter pylori-related diseases. *Journal of*

*biomedical science*, *25*, 1-11.

Choi, J.-W., Um, J.-H., Cho, J.-H., & Lee, H.-J. (2017). Tiny RNAs and their voyage via extracellular vesicles: Secretion of bacterial small RNA and eukaryotic microRNA. *Experimental biology and medicine*, *242*(15), 1475-1481.

Christoforidis, S., Miaczynska, M., Ashman, K., Wilm, M., Zhao, L., Yip, S.-C., Waterfield, M. D., Backer, J. M., & Zerial, M. (1999). Phosphatidylinositol-3-OH kinases are Rab5 effectors. *Nature cell biology*, *1*(4), 249-252.

Cianciotto, N. P. (2005). Type II secretion: a protein secretion system for all seasons. *Trends in microbiology*, *13*(12), 581-588.

Coers, J., Vance, R. E., Fontana, M. F., & Dietrich, W. F. (2007). Restriction of Legionella pneumophila growth in macrophages requires the concerted action of cytokine and Naip5/Ipaf signalling pathways. *Cellular microbiology*, *9*(10), 2344-2357.

Conza, L., Casati, S., Limoni, C., & Gaia, V. (2013). Meteorological factors and risk of community-acquired Legionnaires' disease in Switzerland: an epidemiological study. *BMJ open*, *3*(3), e002428.

Copenhaver, A. M., Casson, C. N., Nguyen, H. T., Fung, T. C., Duda, M. M., Roy, C. R., & Shin, S. (2014). Alveolar macrophages and neutrophils are the primary reservoirs for Legionella pneumophila and mediate cytosolic surveillance of type IV secretion. *Infection and immunity*, *82*(10), 4325-4336.

Corraliza, I., Campo, M., Soler, G., & Modolell, M. (1994). Determination of arginase activity in macrophages: a micromethod. *Journal of immunological methods*, *174*(1-2), 231-235.

Cullom, A. C., Martin, R. L., Song, Y., Williams, K., Williams, A., Pruden, A., & Edwards, M. A. (2020). Critical review: propensity of premise plumbing pipe materials to enhance or diminish growth of Legionella and other opportunistic pathogens. *Pathogens*, *9*(11), 957.

Cunha, B. (2006). The atypical pneumonias: clinical diagnosis and importance. *Clinical Microbiology and Infection*, *12*, 12-24.

Cunha, C. B., & Cunha, B. A. (2017). Legionnaire's disease since Philadelphia: lessons learned and continued progress. *Infectious Disease Clinics*, *31*(1), 1-5.

Currie, S. L., & Beattie, T. K. (2015). Compost and Legionella longbeachae: an emerging infection? *Perspectives in public health*, *135*(6), 309-315.

Daëron, M. (1997). Fc receptor biology. *Annual review of immunology*, *15*(1), 203-234.

Daigneault, M., Preston, J. A., Marriott, H. M., Whyte, M. K., & Dockrell, D. H. (2010). The identification of markers of macrophage differentiation in PMA-stimulated THP-1 cells and monocyte-derived macrophages. *PloS one*, *5*(1), e8668.

Darrah, P. A., Hondalus, M. K., Chen, Q., Ischiropoulos, H., & Mosser, D. M. (2000). Cooperation between reactive oxygen and nitrogen intermediates in killing of Rhodococcus equi by activated macrophages. *Infection and immunity*, *68*(6), 3587-3593.

Dauros-Singorenko, P., Hong, J., Swift, S., Phillips, A., & Blenkiron, C. (2020). Effect of the extracellular

vesicle RNA cargo from uropathogenic Escherichia coli on bladder cells. *Frontiers in molecular biosciences*, *7*, 580913.

Davis, M. J., Tsang, T. M., Qiu, Y., Dayrit, J. K., Freij, J. B., Huffnagle, G. B., & Olszewski, M. A. (2013). Macrophage M1/M2 polarization dynamically adapts to changes in cytokine microenvironments in Cryptococcus neoformans infection. *MBio*, *4*(3), 10.1128/mbio. 00264-00213.

de Freitas, M. C. R., de Almeida, P. E., Vieira, W. V., Ferreira-Machado, A. B., Resende, J. A., da Silva, V. L., & Diniz, C. G. (2022). Inflammatory modulation and outer membrane vesicles (OMV) production associated to Bacteroides fragilis response to subinhibitory concentrations of metronidazole during experimental infection. *Anaerobe*, *73*, 102504.

De Jonge, E. F., Balhuizen, M. D., Van Boxtel, R., Wu, J., Haagsman, H. P., & Tommassen, J. (2021). Heat shock enhances outer-membrane vesicle release in Bordetella spp. *Current research in microbial sciences*, *2*, 100009.

De Leon, J. A., Qiu, J., Nicolai, C. J., Counihan, J. L., Barry, K. C., Xu, L., Lawrence, R. E., Castellano, B. M., Zoncu, R., & Nomura, D. K. (2017). Positive and negative regulation of the master metabolic regulator mTORC1 by two families of Legionella pneumophila effectors. *Cell reports*, *21*(8), 2031-2038.

De Maio, A., & Hightower, L. E. (2021). Heat shock proteins and the biogenesis of cellular membranes. *Cell Stress and Chaperones*, *26*(1), 15-18.

Deatherage, B. L., & Cookson, B. T. (2012). Membrane vesicle release in bacteria, eukaryotes, and archaea: a conserved yet underappreciated aspect of microbial life. *Infection and immunity*, *80*(6), 1948-1957.

Descamps, D., Le Gars, M., Balloy, V., Barbier, D., Maschalidi, S., Tohme, M., Chignard, M., Ramphal, R., Manoury, B., & Sallenave, J.-M. (2012). Toll-like receptor 5 (TLR5), IL-1β secretion, and asparagine endopeptidase are critical factors for alveolar macrophage phagocytosis and bacterial killing. *Proceedings of the National Academy of Sciences*, *109*(5), 1619-1624.

Desjardins, M., Celis, J. E., Van Meer, G., Dieplinger, H., Jahraus, A., Griffiths, G., & Huber, L. A. (1994). Molecular characterization of phagosomes. *Journal of biological chemistry*, *269*(51), 32194-32200.

Desjardins, M., Huber, L. A., Parton, R. G., & Griffiths, G. (1994). Biogenesis of phagolysosomes proceeds through a sequential series of interactions with the endocytic apparatus. *The Journal of cell biology*, *124*(5), 677-688.

Devoe, I., & Gilchrist, J. (1973). Release of endotoxin in the form of cell wall blebs during in vitro growth of Neisseria meningitidis. *The Journal of experimental medicine*, *138*(5), 1156-1167.

Dinarello, C. A. (2000). Proinflammatory cytokines. *Chest*, *118*(2), 503-508.

Dinarello, C. A. (2007). Historical insights into cytokines. *European journal of immunology*, *37*(S1), S34-S45.

Dorward, D. W., & Garon, C. F. (1990). DNA is packaged within membrane-derived vesicles of Gram-

negative but not Gram-positive bacteria. *Applied and environmental microbiology*, *56*(6), 1960-1962.

Dubern, J.-F., & Diggle, S. P. (2008). Quorum sensing by 2-alkyl-4-quinolones in Pseudomonas aeruginosa and other bacterial species. *Molecular Biosystems*, *4*(9), 882-888.

Dupke, S., Buchholz, U., Fastner, J., Förster, C., Frank, C., Lewin, A., Rickerts, V., & Selinka, H.-C. (2023). Impact of climate change on waterborne infections and intoxications. *Journal of health monitoring*, *8*(Suppl 3), 62.

Efeyan, A., Zoncu, R., & Sabatini, D. M. (2012). Amino acids and mTORC1: from lysosomes to disease. *Trends in molecular medicine*, *18*(9), 524-533.

Eisele, N. A., Ruby, T., Jacobson, A., Manzanillo, P. S., Cox, J. S., Lam, L., Mukundan, L., Chawla, A., & Monack, D. M. (2013). Salmonella require the fatty acid regulator PPARδ for the establishment of a metabolic environment essential for long-term persistence. *Cell host & microbe*, *14*(2), 171-182.

El Kasmi, K. C., Qualls, J. E., Pesce, J. T., Smith, A. M., Thompson, R. W., Henao-Tamayo, M., Basaraba, R. J., König, T., Schleicher, U., & Koo, M.-S. (2008). Toll-like receptor–induced arginase 1 in macrophages thwarts effective immunity against intracellular pathogens. *Nature immunology*, *9*(12), 1399-1406.

Ellis, T. N., & Kuehn, M. J. (2010). Virulence and immunomodulatory roles of bacterial outer membrane vesicles. *Microbiology and molecular biology reviews*, *74*(1), 81-94.

Escoll, P., Rolando, M., & Buchrieser, C. (2016). Modulation of host autophagy during bacterial infection: sabotaging host munitions for pathogen nutrition. *Frontiers in immunology*, *7*, 81.

Escoll, P., Rolando, M., Gomez-Valero, L., & Buchrieser, C. (2014). From amoeba to macrophages: exploring the molecular mechanisms of Legionella pneumophila infection in both hosts. *Molecular mechanisms in Legionella pathogenesis*, 1-34.

Escoll, P., Song, O.-R., Viana, F., Steiner, B., Lagache, T., Olivo-Marin, J.-C., Impens, F., Brodin, P., Hilbi, H., & Buchrieser, C. (2017). Legionella pneumophila modulates mitochondrial dynamics to trigger metabolic repurposing of infected macrophages. *Cell host & microbe*, *22*(3), 302-316. e307.

Eshwara, V. K., Mukhopadhyay, C., & Rello, J. (2020). Community-acquired bacterial pneumonia in adults: An update. *Indian Journal of Medical Research*, *151*(4), 287-302.

Fabroni, C., Gori, A., Prignano, F., & Lotti, T. (2010). A severe complication of anti-TNF alfa treatment. *Giornale Italiano di Dermatologia e Venereologia: Organo Ufficiale, Societa Italiana di Dermatologia e Sifilografia*, *145*(6), 775-777.

Fan, M., Kiefer, P., Charki, P., Hedberg, C., Seibel, J., Vorholt, J. A., & Hilbi, H. (2023). The Legionella autoinducer LAI-1 is delivered by outer membrane vesicles to promote interbacterial and interkingdom signaling. *Journal of biological chemistry*, *299*(12).

Fernandez-Moreira, E., Helbig, J. H., & Swanson, M. S. (2006). Membrane vesicles shed by Legionella pneumophila inhibit fusion of phagosomes with lysosomes. *Infection and immunity*, *74*(6),

3285-3295.

Fernández-Serrano, S., Dorca, J., Coromines, M., Carratalà, J., Gudiol, F., & Manresa, F. (2003). Molecular inflammatory responses measured in blood of patients with severe community-acquired pneumonia. *Clinical and Vaccine Immunology*, *10*(5), 813-820.

Ferreira-Coimbra, J., Sarda, C., & Rello, J. (2020). Burden of community-acquired pneumonia and unmet clinical needs. *Advances in therapy*, *37*(4), 1302-1318.

Finsel, I., & Hilbi, H. (2015). Formation of a pathogen vacuole according to L egionella pneumophila: how to kill one bird with many stones. *Cellular microbiology*, *17*(7), 935-950.

Fischer, S., Stegmann, F., Gnanapragassam, V. S., & Lepenies, B. (2022). From structure to function–Ligand recognition by myeloid C-type lectin receptors. *Computational and structural biotechnology journal*, *20*, 5790-5812.

Flannagan, R. S., Cosío, G., & Grinstein, S. (2009). Antimicrobial mechanisms of phagocytes and bacterial evasion strategies. *Nature Reviews Microbiology*, *7*(5), 355-366.

FLESHER, A. R., ITO, S., MANSHEIM, B. J., & KASPER, D. L. (1979). The Cell Envelope of the Legionnaires' Disease Bacterium: Morphologic and Biochemical Characteristics. *Annals of Internal Medicine*, *90*(4), 628-630.

Fliermans, C. (1996). Ecology of Legionella: from data to knowledge with a little wisdom. *Microbial Ecology*, *32*, 203-228.

Franchi, L., Warner, N., Viani, K., & Nuñez, G. (2009). Function of Nod-like receptors in microbial recognition and host defense. *Immunological reviews*, *227*(1), 106-128.

Fraser, D. W., Tsai, T. R., Orenstein, W., Parkin, W. E., Beecham, H. J., Sharrar, R. G., Harris, J., Mallison, G. F., Martin, S. M., & McDade, J. E. (1977). Legionnaires' disease: description of an epidemic of pneumonia. *New England Journal of Medicine*, *297*(22), 1189-1197.

Frutuoso, M. S., Hori, J. I., Pereira, M. S., Junior, D. S., Sônego, F., Kobayashi, K. S., Flavell, R. A., Cunha, F. Q., & Zamboni, D. S. (2010). The pattern recognition receptors Nod1 and Nod2 account for neutrophil recruitment to the lungs of mice infected with Legionella pneumophila. *Microbes and infection*, *12*(11), 819-827.

Fujita, M., Ikegame, S., Harada, E., Ouchi, H., Inoshima, I., Watanabe, K., Yoshida, S.-i., & Nakanishi, Y. (2008). TNF receptor 1 and 2 contribute in different ways to resistance to Legionella pneumophila-induced mortality in mice. *Cytokine*, *44*(2), 298-303.

Futai, M., Oka, T., Sun-Wada, G.-h., Moriyama, Y., Kanazawa, H., & Wada, Y. (2000). Luminal acidification of diverse organelles by V-ATPase in animal cells. *Journal of Experimental Biology*, *203*(1), 107-116.

Galán, J. E. (2009). Common themes in the design and function of bacterial effectors. *Cell host & microbe*, *5*(6), 571-579.

Galka, F., Wai, S. N., Kusch, H., Engelmann, S., Hecker, M., Schmeck, B., Hippenstiel, S., Uhlin, B. E., & Steinert, M. (2008). Proteomic characterization of the whole secretome of Legionella pneumophila and functional analysis of outer membrane vesicles. *Infection and immunity*, *76*(5),

1825-1836.

Gan, N., Guan, H., Huang, Y., Yu, T., Fu, J., Nakayasu, E. S., Puvar, K., Das, C., Wang, D., & Ouyang, S. (2020). Legionella pneumophila regulates the activity of UBE 2N by deamidase-mediated deubiquitination. *The EMBO Journal*, *39*(4), e102806.

Gan, N., Nakayasu, E. S., Hollenbeck, P. J., & Luo, Z.-Q. (2019). Legionella pneumophila inhibits immune signalling via MavC-mediated transglutaminase-induced ubiquitination of UBE2N. *Nature microbiology*, *4*(1), 134-143.

Gankema, H., Wensink, J., Guinée, P. A., Jansen, W. H., & Witholt, B. (1980). Some characteristics of the outer membrane material released by growing enterotoxigenic Escherichia coli. *Infection and immunity*, *29*(2), 704-713.

Garau, J., & Calbo, E. (2008). Community-acquired pneumonia. *The Lancet*, *371*(9611), 455-458.

Garrido-Trigo, A., Corraliza, A. M., Veny, M., Dotti, I., Melón-Ardanaz, E., Rill, A., Crowell, H. L., Corbí, Á., Gudiño, V., & Esteller, M. (2023). Macrophage and neutrophil heterogeneity at single-cell spatial resolution in human inflammatory bowel disease. *Nature communications*, *14*(1), 4506.

Gattarello, S., Lagunes, L., Vidaur, L., Solé-Violán, J., Zaragoza, R., Vallés, J., Torres, A., Sierra, R., Sebastian, R., & Rello, J. (2015). Improvement of antibiotic therapy and ICU survival in severe non-pneumococcal community-acquired pneumonia: a matched case–control study. *Critical care*, *19*, 1-12.

Ge, J., & Shao, F. (2011). Manipulation of host vesicular trafficking and innate immune defence by Legionella Dot/Icm effectors. *Cellular microbiology*, *13*(12), 1870-1880.

Ge, J., Xu, H., Li, T., Zhou, Y., Zhang, Z., Li, S., Liu, L., & Shao, F. (2009). A Legionella type IV effector activates the NF-κB pathway by phosphorylating the IκB family of inhibitors. *Proceedings of the National Academy of Sciences*, *106*(33), 13725-13730.

Geissmann, F., Jung, S., & Littman, D. R. (2003). Blood monocytes consist of two principal subsets with distinct migratory properties. *Immunity*, *19*(1), 71-82.

Gerber, J. S., & Mosser, D. M. (2001). Reversing lipopolysaccharide toxicity by ligating the macrophage Fcγ receptors. *The Journal of immunology*, *166*(11), 6861-6868.

Ghosal, A., Upadhyaya, B. B., Fritz, J. V., Heintz-Buschart, A., Desai, M. S., Yusuf, D., Huang, D., Baumuratov, A., Wang, K., & Galas, D. (2015). The extracellular RNA complement of Escherichia coli. *Microbiologyopen*, *4*(2), 252-266.

Glick, T. H., Gregg, M. B., Berman, B., Mallison, G., RHODES JR, W. W., & Kassanoff, I. (1978). Pontiac fever: an epidemic of unknown etiology in a health department: I. Clinical and epidemiologic aspects. *American journal of epidemiology*, *107*(2), 149-160.

Gold, E. S., Underhill, D. M., Morrissette, N. S., Guo, J., McNiven, M. A., & Aderem, A. (1999). Dynamin 2 is required for phagocytosis in macrophages. *Journal of Experimental Medicine*, *190*(12), 1849-1856.

Gomez-Valero, L., Rusniok, C., Carson, D., Mondino, S., Pérez-Cobas, A. E., Rolando, M., Pasricha, S.,

Reuter, S., Demirtas, J., & Crumbach, J. (2019). More than 18,000 effectors in the Legionella genus genome provide multiple, independent combinations for replication in human cells. *Proceedings of the National Academy of Sciences*, *116*(6), 2265-2273.

Gonçalves, I. G., Simões, L. C., & Simões, M. L. (2021). Legionella pneumophila.

Gordon, S. (2016). Phagocytosis: an immunobiologic process. *Immunity*, *44*(3), 463-475.

Graham, F. F., Finn, N., White, P., Hales, S., & Baker, M. G. (2022). Global perspective of Legionella infection in community-acquired pneumonia: a systematic review and meta-analysis of observational studies. *International journal of Environmental research and public health*, *19*(3), 1907.

Green, E. R., & Mecsas, J. (2016). Bacterial secretion systems: an overview. *Virulence mechanisms of bacterial pathogens*, 213-239.

Grenier, D., & Mayrand, D. (1987). Functional characterization of extracellular vesicles produced by Bacteroides gingivalis. *Infection and immunity*, *55*(1), 111-117.

Griffin Jr, F. M., Bianco, C., & Silverstein, S. (1975). Characterization of the macrophage receptro for complement and demonstration of its functional independence from the receptor for the Fc portion of immunoglobulin G. *The Journal of experimental medicine*, *141*(6), 1269-1277.

Gruenberg, J. (2001). The endocytic pathway: a mosaic of domains. *Nature reviews Molecular cell biology*, *2*(10), 721-730.

Guerrero-Mandujano, A., Hernández-Cortez, C., Ibarra, J. A., & Castro-Escarpulli, G. (2017). The outer membrane vesicles: secretion system type zero. *Traffic*, *18*(7), 425-432.

Guillemot, J., Ginevra, C., Allam, C., Kay, E., Gilbert, C., Doublet, P., Jarraud, S., & Chapalain, A. (2022). TNF-α response in macrophages depends on clinical Legionella pneumophila isolates genotypes. *Virulence*, *13*(1), 160-173.

Han, E.-C., Choi, S.-Y., Lee, Y., Park, J.-W., Hong, S.-H., & Lee, H.-J. (2019). Extracellular RNAs in periodontopathogenic outer membrane vesicles promote TNF-α production in human macrophages and cross the blood–brain barrier in mice. *The FASEB Journal*, *33*(12), 13412.

Happel, K. I., Zheng, M., Young, E., Quinton, L. J., Lockhart, E., Ramsay, A. J., Shellito, J. E., Schurr, J. R., Bagby, G. J., & Nelson, S. (2003). Cutting edge: roles of Toll-like receptor 4 and IL-23 in IL-17 expression in response to Klebsiella pneumoniae infection. *The Journal of immunology*, *170*(9), 4432-4436.

Harrington, L. E., Hatton, R. D., Mangan, P. R., Turner, H., Murphy, T. L., Murphy, K. M., & Weaver, C. T. (2005). Interleukin 17–producing CD4+ effector T cells develop via a lineage distinct from the T helper type 1 and 2 lineages. *Nature immunology*, *6*(11), 1123-1132.

Hawn, T. R., Berrington, W. R., Smith, I. A., Uematsu, S., Akira, S., Aderem, A., Smith, K. D., & Skerrett, S. J. (2007). Altered inflammatory responses in TLR5-deficient mice infected with Legionella pneumophila. *The Journal of immunology*, *179*(10), 6981-6987.

Hawn, T. R., Smith, K. D., Aderem, A., & Skerrett, S. J. (2006). Myeloid differentiation primary response gene (88)—and toll-like receptor 2—deficient mice are susceptible to infection with aerosolized

Legionella pneumophila. *Journal of Infectious Diseases*, *193*(12), 1693-1702.

Hempstead, A. D., & Isberg, R. R. (2015). Inhibition of host cell translation elongation by Legionella pneumophila blocks the host cell unfolded protein response. *Proceedings of the National Academy of Sciences*, *112*(49), E6790-E6797.

Hibbs, M. L., Bonadonna, L., Scott, B. M., McKenzie, I., & Hogarth, P. M. (1988). Molecular cloning of a human immunoglobulin G Fc receptor. *Proceedings of the National Academy of Sciences*, *85*(7), 2240-2244.

Hoekstra, D., van der Laan, J. W., de Leij, L., & Witholt, B. (1976). Release of outer membrane fragments from normally growing Escherichia coli. *Biochimica et Biophysica Acta (BBA)-Biomembranes*, *455*(3), 889-899.

Holm, C. K., Paludan, S. R., & Fitzgerald, K. A. (2013). DNA recognition in immunity and disease. *Current opinion in immunology*, *25*(1), 13-18.

Hoppe, J., Ünal, C. M., Thiem, S., Grimpe, L., Goldmann, T., Gaßler, N., Richter, M., Shevchuk, O., & Steinert, M. (2017). PilY1 promotes Legionella pneumophila infection of human lung tissue explants and contributes to bacterial adhesion, host cell invasion, and twitching motility. *Frontiers in cellular and infection microbiology*, *7*, 63.

Hornung, V., & Latz, E. (2010). Intracellular DNA recognition. *Nature Reviews Immunology*, *10*(2), 123-130.

Horstman, A. L., & Kuehn, M. J. (2000). Enterotoxigenic Escherichia coli secretes active heat-labile enterotoxin via outer membrane vesicles. *Journal of biological chemistry*, *275*(17), 12489-12496.

Horwitz, M. A. (1983a). Formation of a novel phagosome by the Legionnaires' disease bacterium (Legionella pneumophila) in human monocytes. *The Journal of experimental medicine*, *158*(4), 1319-1331.

Horwitz, M. A. (1983b). The Legionnaires' disease bacterium (Legionella pneumophila) inhibits phagosome-lysosome fusion in human monocytes. *The Journal of experimental medicine*, *158*(6), 2108-2126.

Horwitz, M. A., & Maxfield, F. R. (1984). Legionella pneumophila inhibits acidification of its phagosome in human monocytes. *The Journal of cell biology*, *99*(6), 1936-1943.

Hoshino, K., Takeuchi, O., Kawai, T., Sanjo, H., Ogawa, T., Takeda, Y., Takeda, K., & Akira, S. (1999). Cutting edge: Toll-like receptor 4 (TLR4)-deficient mice are hyporesponsive to lipopolysaccharide: evidence for TLR4 as the Lps gene product. *The Journal of immunology*, *162*(7), 3749-3752.

Imlay, J. A., & Linn, S. (1988). DNA damage and oxygen radical toxicity. *science*, *240*(4857), 1302-1309.

Irizarry, R. A., Bolstad, B. M., Collin, F., Cope, L. M., Hobbs, B., & Speed, T. P. (2003). Summaries of Affymetrix GeneChip probe level data. *Nucleic acids research*, *31*(4), e15-e15.

Ivanov, S. S., & Roy, C. R. (2013). Pathogen signatures activate a ubiquitination pathway that modulates

the function of the metabolic checkpoint kinase mTOR. *Nature immunology*, *14*(12), 1219-1228.

Jäger, J., Keese, S., Roessle, M., Steinert, M., & Schromm, A. B. (2015). Fusion of L egionella pneumophila outer membrane vesicles with eukaryotic membrane systems is a mechanism to deliver pathogen factors to host cell membranes. *Cellular microbiology*, *17*(5), 607-620.

Jäger, J., Marwitz, S., Tiefenau, J., Rasch, J., Shevchuk, O., Kugler, C., Goldmann, T., & Steinert, M. (2014). Human lung tissue explants reveal novel interactions during Legionella pneumophila infections. *Infection and immunity*, *82*(1), 275-285.

Jan, A. T. (2017). Outer membrane vesicles (OMVs) of gram-negative bacteria: a perspective update. *Frontiers in Microbiology*, *8*, 1053.

Jenkins, S. J., Ruckerl, D., Thomas, G. D., Hewitson, J. P., Duncan, S., Brombacher, F., Maizels, R. M., Hume, D. A., & Allen, J. E. (2013). IL-4 directly signals tissue-resident macrophages to proliferate beyond homeostatic levels controlled by CSF-1. *Journal of Experimental Medicine*, *210*(11), 2477-2491.

Jenner, R. G., & Young, R. A. (2005). Insights into host responses against pathogens from transcriptional profiling. *Nature Reviews Microbiology*, *3*(4), 281-294.

Jonca, J., Waleron, M., Czaplewska, P., Bogucka, A., Steć, A., Dziomba, S., Jasiecki, J., Rychłowski, M., & Waleron, K. (2021). Membrane vesicles of Pectobacterium as an effective protein secretion system. *International journal of molecular sciences*, *22*(22), 12574.

Joshi, B., Singh, B., Nadeem, A., Askarian, F., Wai, S. N., Johannessen, M., & Hegstad, K. (2021). Transcriptome profiling of Staphylococcus aureus associated extracellular vesicles reveals presence of small RNA-cargo. *Frontiers in molecular biosciences*, *7*, 566207.

Jouanguy, E., Döffinger, R., Dupuis, S., Pallier, A., Altare, F., & Casanova, J.-L. (1999). IL-12 and IFN-γ in host defense against mycobacteria and salmonella in mice and men. *Current opinion in immunology*, *11*(3), 346-351.

Jung, A. L., Herkt, C. E., Schulz, C., Bolte, K., Seidel, K., Scheller, N., Sittka-Stark, A., Bertrams, W., & Schmeck, B. (2017). Legionella pneumophila infection activates bystander cells differentially by bacterial and host cell vesicles. *Scientific Reports*, *7*(1), 6301.

Jung, A. L., Hoffmann, K., Herkt, C. E., Schulz, C., Bertrams, W., & Schmeck, B. (2017). Legionella pneumophila outer membrane vesicles: isolation and analysis of their pro-inflammatory potential on macrophages. *Journal of Visualized Experiments: JoVE*(120), 55146.

Jung, A. L., Stoiber, C., Herkt, C. E., Schulz, C., Bertrams, W., & Schmeck, B. (2016). Legionella pneumophila-derived outer membrane vesicles promote bacterial replication in macrophages. *PLoS pathogens*, *12*(4), e1005592.

Kaddour, H., Tranquille, M., & Okeoma, C. M. (2021). The past, the present, and the future of the size exclusion chromatography in extracellular vesicles separation. *Viruses*, *13*(11), 2272.

Kadurugamuwa, J. L., & Beveridge, T. J. (1995). Virulence factors are released from Pseudomonas aeruginosa in association with membrane vesicles during normal growth and exposure to gentamicin: a novel mechanism of enzyme secretion. *Journal of bacteriology*, *177*(14), 3998-

4008.

Kakihana, Y., Ito, T., Nakahara, M., Yamaguchi, K., & Yasuda, T. (2016). Sepsis-induced myocardial dysfunction: pathophysiology and management. *Journal of intensive care*, *4*, 1-10.

Kaparakis-Liaskos, M., & Ferrero, R. L. (2015). Immune modulation by bacterial outer membrane vesicles. *Nature Reviews Immunology*, *15*(6), 375-387.

Kaparakis, M., Turnbull, L., Carneiro, L., Firth, S., Coleman, H. A., Parkington, H. C., Le Bourhis, L., Karrar, A., Viala, J., & Mak, J. (2010). Bacterial membrane vesicles deliver peptidoglycan to NOD1 in epithelial cells. *Cellular microbiology*, *12*(3), 372-385.

Kaplan, G. (1977). Differences in the mode of phagocytosis with Fc and C3 receptors in macrophages. *Scandinavian journal of immunology*, *6*(8), 797-807.

Karthikeyan, R., Gayathri, P., Gunasekaran, P., Jagannadham, M. V., & Rajendhran, J. (2019). Comprehensive proteomic analysis and pathogenic role of membrane vesicles of Listeria monocytogenes serotype 4b reveals proteins associated with virulence and their possible interaction with host. *International Journal of Medical Microbiology*, *309*(3-4), 199-212.

Kawai, T., & Akira, S. (2009). The roles of TLRs, RLRs and NLRs in pathogen recognition. *International immunology*, *21*(4), 317-337.

Kawai, T., & Akira, S. (2010). The role of pattern-recognition receptors in innate immunity: update on Toll-like receptors. *Nature immunology*, *11*(5), 373-384.

Kawamoto, Y., Morinaga, Y., Kimura, Y., Kaku, N., Kosai, K., Uno, N., Hasegawa, H., & Yanagihara, K. (2017). TNF-α inhibits the growth of Legionella pneumophila in airway epithelial cells by inducing apoptosis. *Journal of Infection and Chemotherapy*, *23*(1), 51-55.

Kawasaki, T., & Kawai, T. (2014). Toll-like receptor signaling pathways. *Frontiers in immunology*, *5*, 461.

Keestra-Gounder, A. M., & Tsolis, R. M. (2017). NOD1 and NOD2: beyond peptidoglycan sensing. *Trends in immunology*, *38*(10), 758-767.

Kellermann, M., Scharte, F., & Hensel, M. (2021). Manipulation of host cell organelles by intracellular pathogens. *International journal of molecular sciences*, *22*(12), 6484.

Kessler, D. S., Levy, D. E., & Darnell Jr, J. E. (1988). Two interferon-induced nuclear factors bind a single promoter element in interferon-stimulated genes. *Proceedings of the National Academy of Sciences*, *85*(22), 8521-8525.

Khweek, A. A., & Amer, A. (2010). Replication of Legionella pneumophila in human cells: why are we susceptible? *Frontiers in Microbiology*, *1*, 133.

Kim, J. H., Yoon, Y. J., Lee, J., Choi, E.-J., Yi, N., Park, K.-S., Park, J., Lötvall, J., Kim, Y.-K., & Gho, Y. S. (2013). Outer membrane vesicles derived from Escherichia coli up-regulate expression of endothelial cell adhesion molecules in vitro and in vivo. *PloS one*, *8*(3), e59276.

Kim, S. J., Chang, J., Rimal, B., Yang, H., & Schaefer, J. (2018). Surface proteins and the formation of biofilms by Staphylococcus aureus. *Biochimica et Biophysica Acta (BBA)-Biomembranes*, *1860*(3), 749-756.

Kim, W., Lee, E. J., Bae, I.-H., Myoung, K., Kim, S. T., Park, P. J., Lee, K.-H., Pham, A. V. Q., Ko, J., & Oh, S. H. (2020). Lactobacillus plantarum-derived extracellular vesicles induce anti-inflammatory M2 macrophage polarization in vitro. *Journal of extracellular vesicles*, *9*(1), 1793514.

Kimizuka, Y., Kimura, S., Saga, T., Ishii, M., Hasegawa, N., Betsuyaku, T., Iwakura, Y., Tateda, K., & Yamaguchi, K. (2012). Roles of interleukin-17 in an experimental Legionella pneumophila pneumonia model. *Infection and immunity*, *80*(3), 1121-1127.

Kiszewski, A., Becerril, E., Aguilar, L., Kader, I., Myers, W., Portaels, F., & Hernandez Pando, R. (2006). The local immune response in ulcerative lesions of Buruli disease. *Clinical & Experimental Immunology*, *143*(3), 445-451.

Kitao, T., Nagai, H., & Kubori, T. (2020). Divergence of Legionella effectors reversing conventional and unconventional ubiquitination. *Frontiers in cellular and infection microbiology*, *10*, 448.

Knoke, L. R., Abad Herrera, S., Götz, K., Justesen, B. H., Günther Pomorski, T., Fritz, C., Schäkermann, S., Bandow, J. E., & Aktas, M. J. F. i. m. (2020). Agrobacterium tumefaciens small lipoprotein atu8019 is involved in selective outer membrane vesicle (OMV) docking to bacterial cells. *11*, 1228.

Koeppen, K., Hampton, T. H., Jarek, M., Scharfe, M., Gerber, S. A., Mielcarz, D. W., Demers, E. G., Dolben, E. L., Hammond, J. H., & Hogan, D. A. (2016). A novel mechanism of host-pathogen interaction through sRNA in bacterial outer membrane vesicles. *PLoS pathogens*, *12*(6), e1005672.

Kohanski, M. A., Dwyer, D. J., Hayete, B., Lawrence, C. A., & Collins, J. J. (2007). A common mechanism of cellular death induced by bactericidal antibiotics. *Cell*, *130*(5), 797-810.

Kolls, J. K., McCray Jr, P. B., & Chan, Y. R. (2008). Cytokine-mediated regulation of antimicrobial proteins. *Nature Reviews Immunology*, *8*(11), 829-835.

Koriyama, T., Yamakuchi, M., Takenouchi, K., Oyama, Y., Takenaka, H., Nagakura, T., Masamoto, I., & Hashiguchi, T. (2019). Legionella pneumophila infection-mediated regulation of RICTOR via miR-218 in U937 macrophage cells. *Biochemical and Biophysical Research Communications*, *508*(2), 608-613.

Kotewicz, K. M., Ramabhadran, V., Sjoblom, N., Vogel, J. P., Haenssler, E., Zhang, M., Behringer, J., Scheck, R. A., & Isberg, R. R. (2017). A single Legionella effector catalyzes a multistep ubiquitination pathway to rearrange tubular endoplasmic reticulum for replication. *Cell host & microbe*, *21*(2), 169-181.

Kulp, A., & Kuehn, M. J. (2010). Biological functions and biogenesis of secreted bacterial outer membrane vesicles. *Annual review of microbiology*, *64*, 163-184.

Kumar, H., Kawai, T., & Akira, S. (2009). Pathogen recognition in the innate immune response. *Biochemical Journal*, *420*(1), 1-16.

Kunishima, H., Takemura, H., Yamamoto, H., Kanemitsu, K., & Shimada, J. (2000). Evaluation of the activity of antimicrobial agents against Legionella pneumophila multiplying in a human

monocytic cell line, THP-1, and an alveolar epithelial cell line, A549. *Journal of Infection and Chemotherapy*, *6*, 206-210.

Lanternier, F., Tubach, F., Ravaud, P., Salmon, D., Dellamonica, P., Bretagne, S., Couret, M., Bouvard, B., Debandt, M., & Gueit, I. (2013). Incidence and risk factors of Legionella pneumophila pneumonia during anti-tumor necrosis factor therapy: a prospective French study. *Chest*, *144*(3), 990-998.

Lappann, M., Danhof, S., Guenther, F., Olivares-Florez, S., Mordhorst, I. L., & Vogel, U. (2013). In vitro resistance mechanisms of N eisseria meningitidis against neutrophil extracellular traps. *Molecular microbiology*, *89*(3), 433-449.

Lee, E. Y., Bang, J. Y., Park, G. W., Choi, D. S., Kang, J. S., Kim, H. J., Park, K. S., Lee, J. O., Kim, Y. K., & Kwon, K. H. (2007). Global proteomic profiling of native outer membrane vesicles derived from Escherichia coli. *Proteomics*, *7*(17), 3143-3153.

LeibundGut-Landmann, S., Weidner, K., Hilbi, H., & Oxenius, A. (2011). Nonhematopoietic cells are key players in innate control of bacterial airway infection. *The Journal of immunology*, *186*(5), 3130-3137.

Li, J., Azam, F., & Zhang, S. (2016). Outer membrane vesicles containing signalling molecules and active hydrolytic enzymes released by a coral pathogen Vibrio shilonii AK1. *Environmental microbiology*, *18*(11), 3850-3866.

Li, Y., Cao, H., Qiu, D., Wang, N., Wang, Y., Wen, T., Wang, J., & Zhu, H. (2023). The proteomics analysis of extracellular vesicles revealed the possible function of heat shock protein 60 in Helicobacter pylori infection. *Cancer Cell International*, *23*(1), 272.

Liao, S., Klein, M. I., Heim, K. P., Fan, Y., Bitoun, J. P., Ahn, S.-J., Burne, R. A., Koo, H., Brady, L. J., & Wen, Z. T. (2014). Streptococcus mutans extracellular DNA is upregulated during growth in biofilms, actively released via membrane vesicles, and influenced by components of the protein secretion machinery. *Journal of bacteriology*, *196*(13), 2355-2366.

Lippmann, J., Müller, H. C., Naujoks, J., Tabeling, C., Shin, S., Witzenrath, M., Hellwig, K., Kirschning, C. J., Taylor, G. A., & Barchet, W. (2011). Dissection of a type I interferon pathway in controlling bacterial intracellular infection in mice. *Cellular microbiology*, *13*(11), 1668-1682.

Lippmann, J., Rothenburg, S., Deigendesch, N., Eitel, J., Meixenberger, K., Van Laak, V., Slevogt, H., N'guessan, P. D., Hippenstiel, S., & Chakraborty, T. (2008). IFNβ responses induced by intracellular bacteria or cytosolic DNA in different human cells do not require ZBP1 (DLM-1/DAI). *Cellular microbiology*, *10*(12), 2579-2588.

Liu, H., Geng, Z., & Su, J. (2022). Engineered mammalian and bacterial extracellular vesicles as promising nanocarriers for targeted therapy. *Extracell Vesicles Circ Nucleic Acids*, *3*(2), 63-86.

Liu, X., & Shin, S. (2019). Viewing Legionella pneumophila pathogenesis through an immunological lens. *Journal of molecular biology*, *431*(21), 4321-4344.

Logan, S. M., & Trust, T. (1982). Outer membrane characteristics of Campylobacter jejuni. *Infection and immunity*, *38*(3), 898-906.

Loo, Y.-M., & Gale, M. (2011). Immune signaling by RIG-I-like receptors. *Immunity*, *34*(5), 680-692.

Lugo-Villarino, G., Vérollet, C., Maridonneau-Parini, I., & Neyrolles, O. (2011). Macrophage polarization: convergence point targeted by mycobacterium tuberculosis and HIV. *Frontiers in immunology*, *2*, 43.

Ma, D., Zhang, Y., Zhang, J., Shi, J., Gao, S., Long, F., Wang, X., Pu, X., Sun, J., & Liang, S. (2025). Outer membrane vesicles derived from probiotic Escherichia coli Nissle 1917 promote metabolic remodeling and M1 polarization of RAW264. 7 macrophages. *Frontiers in immunology*, *16*, 1501174.

Maas, S. L., Breakefield, X. O., & Weaver, A. M. (2017). Extracellular vesicles: unique intercellular delivery vehicles. *Trends in cell biology*, *27*(3), 172-188.

Mackaness, G. (1962). Cellular resistance to infection. *Journal of Experimental Medicine*, *116*(3), 381-406.

Malaviya, R., & Abraham, S. N. (2000). Role of mast cell leukotrienes in neutrophil recruitment and bacterial clearance in infectious peritonitis. *Journal of leukocyte biology*, *67*(6), 841-846.

Maldonado, R., Wei, R., Kachlany, S., Kazi, M., & Balashova, N. (2011). Cytotoxic effects of Kingella kingae outer membrane vesicles on human cells. *Microbial pathogenesis*, *51*(1-2), 22-30.

Manning, A. J., & Kuehn, M. J. (2011). Contribution of bacterial outer membrane vesicles to innate bacterial defense. *BMC microbiology*, *11*(1), 1-15.

Månsson, A., Mörgelin, M., Jendholm, J., & Vidakovics, M. L. A. P. (2010). B cell activation by outer membrane vesicles--a novel virulence mechanism. *PLoS pathogens*, *6*(1).

Marie-Anaïs, F., Mazzolini, J., Herit, F., & Niedergang, F. (2016). Dynamin-actin cross talk contributes to phagosome formation and closure. *Traffic*, *17*(5), 487-499.

Martinez, F. O., & Gordon, S. (2014). The M1 and M2 paradigm of macrophage activation: time for reassessment. *F1000prime reports*, *6*, 13.

Martinez, F. O., Sica, A., Mantovani, A., & Locati, M. (2008). Macrophage activation and polarization. *Front biosci*, *13*(13), 453-461.

Martinez, J. L., Sánchez, M. B., Martínez-Solano, L., Hernandez, A., Garmendia, L., Fajardo, A., & Alvarez-Ortega, C. (2009). Functional role of bacterial multidrug efflux pumps in microbial natural ecosystems. *FEMS microbiology reviews*, *33*(2), 430-449.

Mascarenhas, D. P., Pereira, M. S., Manin, G. Z., Hori, J. I., & Zamboni, D. S. (2015). Interleukin 1 receptor–driven neutrophil recruitment accounts to MyD88–dependent pulmonary clearance of Legionella pneumophila infection in vivo. *The Journal of infectious diseases*, *211*(2), 322-330.

Maurin, M., Hammer, L., Gestin, B., Timsit, J.-F., Rogeaux, O., Delavena, F., Tous, J., Epaulard, O., Brion, J.-P., & Croizé, J. (2010). Quantitative real-time PCR tests for diagnostic and prognostic purposes in cases of legionellosis. *Clinical Microbiology and Infection*, *16*(4), 379-384.

McBroom, A. J., Johnson, A. P., Vemulapalli, S., & Kuehn, M. J. (2006). Outer membrane vesicle production by Escherichia coli is independent of membrane instability. *Journal of bacteriology*, *188*(15), 5385-5392.

McBroom, A. J., & Kuehn, M. J. (2007). Release of outer membrane vesicles by Gram-negative bacteria is a novel envelope stress response. *Molecular microbiology*, *63*(2), 545-558.

Mechnikov, I. i. I. i. (1988). Immunity in infective diseases. *Reviews of infectious diseases*, *10*(1), 223-227.

Mentasti, M., Fry, N., Afshar, B., Palepou-Foxley, C., Naik, F., & Harrison, T. (2012). Application of Legionella pneumophila-specific quantitative real-time PCR combined with direct amplification and sequence-based typing in the diagnosis and epidemiological investigation of Legionnaires' disease. *European Journal of Clinical Microbiology & Infectious Diseases*, *31*, 2017-2028.

Miettinen, M., Matikainen, S., Vuopio-Varkila, J., Pirhonen, J., Varkila, K., Kurimoto, M., & Julkunen, I. (1998). Lactobacilli and streptococci induce interleukin-12 (IL-12), IL-18, and gamma interferon production in human peripheral blood mononuclear cells. *Infection and immunity*, *66*(12), 6058-6062.

Miller, L. S., Pietras, E. M., Uricchio, L. H., Hirano, K., Rao, S., Lin, H., O'Connell, R. M., Iwakura, Y., Cheung, A. L., & Cheng, G. (2007). Inflammasome-mediated production of IL-1β is required for neutrophil recruitment against Staphylococcus aureus in vivo. *The Journal of immunology*, *179*(10), 6933-6942.

Mills, C. D., Kincaid, K., Alt, J. M., Heilman, M. J., & Hill, A. M. (2000). M-1/M-2 macrophages and the Th1/Th2 paradigm. *The Journal of immunology*, *164*(12), 6166-6173.

Molofsky, A. B., Byrne, B. G., Whitfield, N. N., Madigan, C. A., Fuse, E. T., Tateda, K., & Swanson, M. S. (2006). Cytosolic recognition of flagellin by mouse macrophages restricts Legionella pneumophila infection. *The Journal of experimental medicine*, *203*(4), 1093-1104.

Molofsky, A. B., & Swanson, M. S. (2003). Legionella pneumophila CsrA is a pivotal repressor of transmission traits and activator of replication. *Molecular microbiology*, *50*(2), 445-461.

Molofsky, A. B., & Swanson, M. S. (2004). Differentiate to thrive: lessons from the Legionella pneumophila life cycle. *Molecular microbiology*, *53*(1), 29-40.

Mondino, S., Schmidt, S., Rolando, M., Escoll, P., Gomez-Valero, L., & Buchrieser, C. (2020). Legionnaires' disease: state of the art knowledge of pathogenesis mechanisms of Legionella. *Annual Review of Pathology: Mechanisms of Disease*, *15*(1), 439-466.

Monguió-Tortajada, M., Gálvez-Montón, C., Bayes-Genis, A., Roura, S., & Borràs, F. E. (2019). Extracellular vesicle isolation methods: rising impact of size-exclusion chromatography. *Cellular and Molecular Life Sciences*, *76*(12), 2369-2382.

Monroe, K. M., McWhirter, S. M., & Vance, R. E. (2009). Identification of host cytosolic sensors and bacterial factors regulating the type I interferon response to Legionella pneumophila. *PLoS pathogens*, *5*(11), e1000665.

Moscardini, A., Di Pietro, S., Signore, G., Parlanti, P., Santi, M., Gemmi, M., & Cappello, V. (2020). Uranium-free X solution: a new generation contrast agent for biological samples ultrastructure. *Scientific Reports*, *10*(1), 11540.

Mosser, D. (1994). Receptors on phagocytic cells involved in microbial recognition. *Immunology series*, *60*, 99-114.

Mosser, D. M. (2003). The many faces of macrophage activation. *Journal of Leucocyte Biology*, *73*(2), 209-212.

Muñoz Carrillo, J. L., Castro García, F. P., Gutiérrez Coronado, O., Moreno García, M. A., & Contreras Cordero, J. F. (2017). Physiology and pathology of innate immune response against pathogens.

Murphy, T. F. (2006). The role of bacteria in airway inflammation in exacerbations of chronic obstructive pulmonary disease. *Current opinion in infectious diseases*, *19*(3), 225-230.

Murray, H., Juangbhanich, C., Nathan, C., & Cohn, Z. (1979). Macrophage oxygen-dependent antimicrobial activity. II. The role of oxygen intermediates. *Journal of Experimental Medicine*, *150*(4), 950-964.

Murray, H. W. (1994). Interferon-gamma and host antimicrobial defense: current and future clinical applications. *The American journal of medicine*, *97*(5), 459-467.

Nathan, C. F., Murray, H. W., Wiebe, M. E., & Rubin, B. Y. (1983). Identification of interferon-gamma as the lymphokine that activates human macrophage oxidative metabolism and antimicrobial activity. *The Journal of experimental medicine*, *158*(3), 670-689.

Nau, G. J., Richmond, J. F., Schlesinger, A., Jennings, E. G., Lander, E. S., & Young, R. A. (2002). Human macrophage activation programs induced by bacterial pathogens. *Proceedings of the National Academy of Sciences*, *99*(3), 1503-1508.

Naujoks, J., Lippmann, J., Suttorp, N., & Opitz, B. (2018). Innate sensing and cell-autonomous resistance pathways in Legionella pneumophila infection. *International Journal of Medical Microbiology*, *308*(1), 161-167.

Naujoks, J., Tabeling, C., Dill, B. D., Hoffmann, C., Brown, A. S., Kunze, M., Kempa, S., Peter, A., Mollenkopf, H.-J., & Dorhoi, A. (2016). IFNs modify the proteome of Legionella-containing vacuoles and restrict infection via IRG1-derived itaconic acid. *PLoS pathogens*, *12*(2), e1005408.

Newton, C. A., Perkins, I., Widen, R. H., Friedman, H., & Klein, T. W. (2007). Role of Toll-like receptor 9 in Legionella pneumophila-induced interleukin-12 p40 production in bone marrow-derived dendritic cells and macrophages from permissive and nonpermissive mice. *Infection and immunity*, *75*(1), 146-151.

Newton, H. J., Ang, D. K., Van Driel, I. R., & Hartland, E. L. (2010). Molecular pathogenesis of infections caused by Legionella pneumophila. *Clinical microbiology reviews*, *23*(2), 274-298.

Newton, K., & Dixit, V. M. (2012). Signaling in innate immunity and inflammation. *Cold Spring Harbor perspectives in biology*, *4*(3), a006049.

Niemann, G. S., Brown, R. N., Gustin, J. K., Stufkens, A., Shaikh-Kidwai, A. S., Li, J., McDermott, J. E., Brewer, H. M., Schepmoes, A., & Smith, R. D. (2011). Discovery of novel secreted virulence factors from Salmonella enterica serovar Typhimurium by proteomic analysis of culture supernatants. *Infection and immunity*, *79*(1), 33-43.

Ninio, S., & Roy, C. R. (2007). Effector proteins translocated by Legionella pneumophila: strength in numbers. *Trends in microbiology*, *15*(8), 372-380.

Novick, D. (2013). Interleukin-18 and IL-18 binding protein. *Frontiers in immunology*, *4*(289).

Nowotny, A., Behling, U., Hammond, B., Lai, C., Listgarten, M., Pham, P., & Sanavi, F. (1982). Release of toxic microvesicles by Actinobacillus actinomycetemcomitans. *Infection and immunity*, *37*(1), 151-154.

O'donoghue, E. J., & Krachler, A. M. (2016). Mechanisms of outer membrane vesicle entry into host cells. *Cellular microbiology*, *18*(11), 1508-1517.

Odegaard, J. I., & Chawla, A. (2011). Alternative macrophage activation and metabolism. *Annual Review of Pathology: Mechanisms of Disease*, *6*(1), 275-297.

Oliva, G., Sahr, T., & Buchrieser, C. (2018). The life cycle of L. pneumophila: cellular differentiation is linked to virulence and metabolism. *Frontiers in Cellular and Infection Microbiology*, *8*, 3.

Optenhövel, M., Mellmann, A., & Kuczius, T. (2023). Occurrence and prevalence of Legionella species in dental chair units in Germany with a focus on risk factors. *European Journal of Clinical Microbiology & Infectious Diseases*, *42*(10), 1235-1244.

Orench-Rivera, N., & Kuehn, M. J. (2016). Environmentally controlled bacterial vesicle-mediated export. *Cellular microbiology*, *18*(11), 1525-1536.

Oster, P., Lennon, D., O'Hallahan, J., Mulholland, K., Reid, S., & Martin, D. (2005). MeNZB™: a safe and highly immunogenic tailor-made vaccine against the New Zealand Neisseria meningitidis serogroup B disease epidemic strain. *Vaccine*, *23*(17-18), 2191-2196.

P rez-Cruz, C., Carri n, O., Delgado, L., Martinez, G., L pez-Iglesias, C., & Mercade, E. (2013). New type of outer membrane vesicle produced by the Gram-negative bacterium Shewanella vesiculosa M7T: implications for DNA content. *Applied and environmental microbiology*, *79*(6), 1874-1881.

Pacelli, R., Wink, D. A., Cook, J. A., Krishna, M. C., DeGraff, W., Friedman, N., Tsokos, M., Samuni, A., & Mitchell, J. B. (1995). Nitric oxide potentiates hydrogen peroxide-induced killing of Escherichia coli. *Journal of Experimental Medicine*, *182*(5), 1469-1479.

Paciello, I., Silipo, A., Lembo-Fazio, L., Curcurù, L., Zumsteg, A., Noël, G., Ciancarella, V., Sturiale, L., Molinaro, A., & Bernardini, M. L. (2013). Intracellular Shigella remodels its LPS to dampen the innate immune recognition and evade inflammasome activation. *Proceedings of the National Academy of Sciences*, *110*(46), E4345-E4354.

Pampaka, D., Gómez-Barroso, D., López-Perea, N., Carmona, R., & Portero, R. C. (2022). Meteorological conditions and Legionnaires' disease sporadic cases-a systematic review. *Environmental Research*, *214*, 114080.

Park, B., Park, G., Kim, J., Lim, S. A., & Lee, K.-M. (2017). Innate immunity against Legionella pneumophila during pulmonary infections in mice. *Archives of pharmacal research*, *40*, 131-145.

Park, H.-T., Park, W. B., Kim, S., Lim, J.-S., Nah, G., & Yoo, H. S. (2021). Revealing immune responses

in the Mycobacterium avium subsp. paratuberculosis-infected THP-1 cells using single cell RNA-sequencing. *PloS one*, *16*(7), e0254194.

Pérez-Cruz, C., Delgado, L., López-Iglesias, C., & Mercade, E. (2015). Outer-inner membrane vesicles naturally secreted by gram-negative pathogenic bacteria. *PloS one*, *10*(1), e0116896.

Perez-Riverol, Y., Bai, J., Bandla, C., García-Seisdedos, D., Hewapathirana, S., Kamatchinathan, S., Kundu, D. J., Prakash, A., Frericks-Zipper, A., & Eisenacher, M. (2022). The PRIDE database resources in 2022: a hub for mass spectrometry-based proteomics evidences. *Nucleic acids research*, *50*(D1), D543-D552.

Personnic, N., Striednig, B., & Hilbi, H. (2018). Legionella quorum sensing and its role in pathogen–host interactions. *Current opinion in microbiology*, *41*, 29-35.

Peterson, B. W., van der Mei, H. C., Sjollema, J., Busscher, H. J., & Sharma, P. K. (2013). A distinguishable role of eDNA in the viscoelastic relaxation of biofilms. *MBio*, *4*(5), 10.1128/mbio. 00497-00413.

Phillips, R. J., Lutz, M., & Premack, B. (2005). Differential signaling mechanisms regulate expression of CC chemokine receptor-2 during monocyte maturation. *Journal of inflammation*, *2*, 1-14.

Podinovskaia, M., VanderVen, B. C., Yates, R. M., Glennie, S., Fullerton, D., Mwandumba, H. C., & Russell, D. G. (2013). Dynamic quantitative assays of phagosomal function. *Current Protocols in Immunology*, *102*(1), 14.34. 11-14.34. 14.

Pollak, C. N., Delpino, M. V., Fossati, C. A., & Baldi, P. C. (2012). Outer membrane vesicles from Brucella abortus promote bacterial internalization by human monocytes and modulate their innate immune response. *PloS one*, *7*(11), e50214.

Polverino, E., Torres, A., Menendez, R., Cillóniz, C., Valles, J. M., Capelastegui, A., Marcos, M. A., Alfageme, I., Zalacain, R., & Almirall, J. (2013). Microbial aetiology of healthcare associated pneumonia in Spain: a prospective, multicentre, case–control study. *Thorax*, *68*(11), 1007-1014.

Protection, C. f. H. (2024). *Communicable Diseases*.

Qin, T., Zhou, H., Ren, H., & Liu, W. (2017). Distribution of secretion systems in the genus Legionella and its correlation with pathogenicity. *Frontiers in Microbiology*, *8*, 388.

Qiu, J., & Luo, Z.-Q. (2017). Hijacking of the host ubiquitin network by Legionella pneumophila. *Frontiers in cellular and infection microbiology*, *7*, 487.

Qiu, J., Sheedlo, M. J., Yu, K., Tan, Y., Nakayasu, E. S., Das, C., Liu, X., & Luo, Z.-Q. (2016). Ubiquitination independent of E1 and E2 enzymes by bacterial effectors. *Nature*, *533*(7601), 120-124.

Qualls, J. E., Neale, G., Smith, A. M., Koo, M.-S., DeFreitas, A. A., Zhang, H., Kaplan, G., Watowich, S. S., & Murray, P. J. (2010). Arginine usage in mycobacteria-infected macrophages depends on autocrine-paracrine cytokine signaling. *Science signaling*, *3*(135), ra62-ra62.

Rabinovitch, M. (1995). Professional and non-professional phagocytes: an introduction. *Trends in cell biology*, *5*(3), 85-87.

Rather, M. A., Gupta, K., & Mandal, M. (2021). Microbial biofilm: formation, architecture, antibiotic

resistance, and control strategies. *Brazilian Journal of Microbiology*, *52*(4), 1701-1718.

Reimer, S. L., Beniac, D. R., Hiebert, S. L., Booth, T. F., Chong, P. M., Westmacott, G. R., Zhanel, G. G., & Bay, D. C. (2021). Comparative analysis of outer membrane vesicle isolation methods with an Escherichia coli tolA mutant reveals a hypervesiculating phenotype with outer-inner membrane vesicle content. *Frontiers in Microbiology*, *12*, 628801.

Reis, F. C., Borges, B. S., Jozefowicz, L. J., Sena, B. A., Garcia, A. W., Medeiros, L. C., Martins, S. T., Honorato, L., Schrank, A., & Vainstein, M. H. (2019). A novel protocol for the isolation of fungal extracellular vesicles reveals the participation of a putative scramblase in polysaccharide export and capsule construction in Cryptococcus gattii. *MSphere*, *4*(2), 10.1128/msphere. 00080-00019.

Renelli, M., Matias, V., Lo, R. Y., & Beveridge, T. J. (2004). DNA-containing membrane vesicles of Pseudomonas aeruginosa PAO1 and their genetic transformation potential. *Microbiology*, *150*(7), 2161-2169.

Riley, D. R., Sieber, K. B., Robinson, K. M., White, J. R., Ganesan, A., Nourbakhsh, S., & Dunning Hotopp, J. C. (2013). Bacteria-human somatic cell lateral gene transfer is enriched in cancer samples. *PLoS computational biology*, *9*(6), e1003107.

Rivas-Santiago, B., Hernandez-Pando, R., Carranza, C., Juarez, E., Contreras, J. L., Aguilar-Leon, D., Torres, M., & Sada, E. (2008). Expression of cathelicidin LL-37 during Mycobacterium tuberculosis infection in human alveolar macrophages, monocytes, neutrophils, and epithelial cells. *Infection and immunity*, *76*(3), 935-941.

Roach, D. R., Bean, A. G., Demangel, C., France, M. P., Briscoe, H., & Britton, W. J. (2002). TNF regulates chemokine induction essential for cell recruitment, granuloma formation, and clearance of mycobacterial infection. *The Journal of immunology*, *168*(9), 4620-4627.

Rodríguez-Prados, J.-C., Través, P. G., Cuenca, J., Rico, D., Aragonés, J., Martin-Sanz, P., Cascante, M., & Boscá, L. (2010). Substrate fate in activated macrophages: a comparison between innate, classic, and alternative activation. *The Journal of immunology*, *185*(1), 605-614.

Rodriguez, K. R., Bruns, A. M., & Horvath, C. M. (2014). MDA5 and LGP2: accomplices and antagonists of antiviral signal transduction. *Journal of virology*, *88*(15), 8194-8200.

Roier, S., Zingl, F. G., Cakar, F., Durakovic, S., Kohl, P., Eichmann, T. O., Klug, L., Gadermaier, B., Weinzerl, K., & Prassl, R. J. N. c. (2016). A novel mechanism for the biogenesis of outer membrane vesicles in Gram-negative bacteria. *7*(1), 1-13.

Rolfe, M. D., Rice, C. J., Lucchini, S., Pin, C., Thompson, A., Cameron, A. D., Alston, M., Stringer, M. F., Betts, R. P., & Baranyi, J. (2012). Lag phase is a distinct growth phase that prepares bacteria for exponential growth and involves transient metal accumulation. *Journal of bacteriology*, *194*(3), 686-701.

Rompikuntal, P. K., Thay, B., Khan, M. K., Alanko, J., Penttinen, A.-M., Asikainen, S., Wai, S. N., & Oscarsson, J. (2012). Perinuclear localization of internalized outer membrane vesicles carrying active cytolethal distending toxin from Aggregatibacter actinomycetemcomitans. *Infection and*

*immunity*, *80*(1), 31-42.

Rottenberg, M. n. E., Gigliotti-Rothfuchs, A., & Wigzell, H. (2002). The role of IFN-γ in the outcome of chlamydial infection. *Current opinion in immunology*, *14*(4), 444-451.

Rowbotham, T. J. (1980). Preliminary report on the pathogenicity of Legionella pneumophila for freshwater and soil amoebae. *Journal of clinical pathology*, *33*(12), 1179-1183.

Roy, C. R., Berger, K. H., & Isberg, R. R. (1998). Legionella pneumophila DotA protein is required for early phagosome trafficking decisions that occur within minutes of bacterial uptake. *Molecular microbiology*, *28*(3), 663-674.

Roy, C. R., & Isberg, R. R. (1997). Topology of Legionella pneumophila DotA: an inner membrane protein required for replication in macrophages. *Infection and immunity*, *65*(2), 571-578.

Ruiz-Moreno, J. S., Hamann, L., Shah, J. A., Verbon, A., Mockenhaupt, F. P., Puzianowska-Kuznicka, M., Naujoks, J., Sander, L. E., Witzenrath, M., & Cambier, J. C. (2018). The common HAQ STING variant impairs cGAS-dependent antibacterial responses and is associated with susceptibility to Legionnaires' disease in humans. *PLoS pathogens*, *14*(1), e1006829.

Ruiz-Spinelli, A., Waterer, G., & Rello, J. (2023). Severe community-acquired pneumonia in the post COVID-19 era. *Current Opinion in Critical Care*, *29*(5), 400-406.

Rutherford, S. T., & Bassler, B. L. (2012). Bacterial quorum sensing: its role in virulence and possibilities for its control. *Cold Spring Harbor perspectives in medicine*, *2*(11), a012427.

Ryu, S., Ni, K., Wang, C., Sivanantham, A., Carnino, J. M., Ji, H.-L., & Jin, Y. (2023). Bacterial outer membrane vesicles promote lung inflammatory responses and macrophage activation via multi-signaling pathways. *Biomedicines*, *11*(2), 568.

Sahoo, M., Ceballos-Olvera, I., del Barrio, L., & Re, F. (2011). Role of the inflammasome, IL-1β, and IL-18 in bacterial infections. *The Scientific World Journal*, *11*(1), 2037-2050.

Samuelsson, J., Hallström, L. P., Marrone, G., & Dias, J. G. (2023). Legionnaires' disease in the EU/EEA*: increasing trend from 2017 to 2019. *Eurosurveillance*, *28*(11), 2200114.

Sartorio, M. G., Pardue, E. J., Feldman, M. F., & Haurat, M. F. (2021). Bacterial outer membrane vesicles: from discovery to applications. *Annual review of microbiology*, *75*(1), 609-630.

Schaale, K., Brandenburg, J., Kispert, A., Leitges, M., Ehlers, S., & Reiling, N. (2013). Wnt6 is expressed in granulomatous lesions of Mycobacterium tuberculosis–infected mice and is involved in macrophage differentiation and proliferation. *The Journal of immunology*, *191*(10), 5182-5195.

Scheithauer, L., Karagöz, M. S., Mayer, B. E., & Steinert, M. (2023). Protein sociology of ProA, Mip and other secreted virulence factors at the Legionella pneumophila surface. *Frontiers in Cellular and Infection Microbiology*, *13*, 1140688.

Schell, U., Simon, S., & Hilbi, H. (2016). Inflammasome recognition and regulation of the Legionella flagellum. *Inflammasome Signaling and Bacterial Infections*, 161-181.

Schooling, S. R., & Beveridge, T. J. (2006). Membrane vesicles: an overlooked component of the matrices of biofilms. *Journal of bacteriology*, *188*(16), 5945-5957.

Schultz, H., Hume, J., Zhang, D. S., Gioannini, T. L., & Weiss, J. P. (2007). A novel role for the

bactericidal/permeability increasing protein in interactions of gram-negative bacterial outer membrane blebs with dendritic cells. *The Journal of Immunology*, *179*(4), 2477-2484.

Seeger, E. M., Thuma, M., Fernandez-Moreira, E., Jacobs, E., Schmitz, M., & Helbig, J. H. (2010). Lipopolysaccharide of Legionella pneumophila shed in a liquid culture as a nonvesicular fraction arrests phagosome maturation in amoeba and monocytic host cells. *FEMS microbiology letters*, *307*(2), 113-119.

Shames, S. R., Liu, L., Havey, J. C., Schofield, W. B., Goodman, A. L., & Roy, C. R. (2017). Multiple Legionella pneumophila effector virulence phenotypes revealed through high-throughput analysis of targeted mutant libraries. *Proceedings of the National Academy of Sciences*, *114*(48), E10446-E10454.

Sharma, S., & Fitzgerald, K. A. (2011). Innate immune sensing of DNA. *PLoS pathogens*, *7*(4), e1001310.

Shevchuk, O., Jäger, J., & Steinert, M. (2011). Virulence properties of the Legionella pneumophila cell envelope. *Frontiers in Microbiology*, *2*, 74.

Shim, H. K., Kim, J. Y., Kim, M. J., Sim, H. S., Park, D. W., Sohn, J. W., & Kim, M. J. (2009). Legionella lipoprotein activates toll-like receptor 2 and induces cytokine production and expression of costimulatory molecules in peritoneal macrophages. *Experimental & molecular medicine*, *41*(10), 687-694.

Shin, D. M., Yuk, J. M., Lee, H. M., Lee, S. H., Son, J. W., Harding, C. V., Kim, J. M., Modlin, R. L., & Jo, E. K. (2010). Mycobacterial lipoprotein activates autophagy via TLR2/1/CD14 and a functional vitamin D receptor signalling. *Cellular microbiology*, *12*(11), 1648-1665.

Shin, S., Case, C. L., Archer, K. A., Nogueira, C. V., Kobayashi, K. S., Flavell, R. A., Roy, C. R., & Zamboni, D. S. (2008). Type IV secretion-dependent activation of host MAP kinases induces an increased proinflammatory cytokine response to Legionella pneumophila. *PLoS pathogens*, *4*(11), e1000220.

Shinozawa, Y., Matsumoto, T., Uchida, K., Tsujimoto, S., Iwakura, Y., & Yamaguchi, K. (2002). Role of interferon-gamma in inflammatory responses in murine respiratory infection with Legionella pneumophila. *Journal of medical microbiology*, *51*(3), 225-230.

Si-Tahar, M., Touqui, L., & Chignard, M. (2009). Innate immunity and inflammation–two facets of the same anti-infectious reaction. *Clinical & Experimental Immunology*, *156*(2), 194-198.

Sica, A., & Mantovani, A. (2012). Macrophage plasticity and polarization: in vivo veritas. *The Journal of clinical investigation*, *122*(3), 787-795.

Sjöström, A. E., Sandblad, L., Uhlin, B. E., & Wai, S. N. (2015). Membrane vesicle-mediated release of bacterial RNA. *Scientific Reports*, *5*(1), 15329.

Sobota, A., Strzelecka-Kiliszek, A., Gładkowska, E., Yoshida, K., Mrozinska, K., & Kwiatkowska, K. (2005). Binding of IgG-opsonized particles to FcγR is an active stage of phagocytosis that involves receptor clustering and phosphorylation. *The Journal of immunology*, *175*(7), 4450-4457.

Söderberg, M. A., Dao, J., Starkenburg, S. R., & Cianciotto, N. P. (2008). Importance of type II secretion

for survival of Legionella pneumophila in tap water and in amoebae at low temperatures. *Applied and environmental microbiology*, *74*(17), 5583-5588.

Soult, M. C., Lonergan, N. E., Shah, B., Kim, W.-K., Britt, L., & Sullivan, C. J. (2013). Outer membrane vesicles from pathogenic bacteria initiate an inflammatory response in human endothelial cells. *journal of surgical research*, *184*(1), 458-466.

Stegmann, F., Diersing, C., & Lepenies, B. (2024). Legionella pneumophila modulates macrophage functions through epigenetic reprogramming via the C-type lectin receptor Mincle. *Iscience*, *27*(9).

Stein, M., Keshav, S., Harris, N., & Gordon, S. (1992). Interleukin 4 potently enhances murine macrophage mannose receptor activity: a marker of alternative immunologic macrophage activation. *The Journal of experimental medicine*, *176*(1), 287-292.

Stetson, D. B., & Medzhitov, R. (2006). Type I interferons in host defense. *Immunity*, *25*(3), 373-381.

Stout, J. E., & Yu, V. L. (1997). Legionellosis. *New England Journal of Medicine*, *337*(10), 682-687.

Stow, J. L., & Murray, R. Z. (2013). Intracellular trafficking and secretion of inflammatory cytokines. *Cytokine & growth factor reviews*, *24*(3), 227-239.

Sturgill-Koszycki, S., Schlesinger, P. H., Chakraborty, P., Haddix, P. L., Collins, H. L., Fok, A. K., Allen, R. D., Gluck, S. L., Heuser, J., & Russell, D. G. (1994). Lack of acidification in Mycobacterium phagosomes produced by exclusion of the vesicular proton-ATPase. *science*, *263*(5147), 678-681.

Susa, M., Ticac, B., Rukavina, T., Doric, M., & Marre, R. (1998). Legionella pneumophila infection in intratracheally inoculated T cell-depleted or-nondepleted A/J mice. *The Journal of immunology*, *160*(1), 316-321.

Swanson, J. A. (2008). Shaping cups into phagosomes and macropinosomes. *Nature reviews Molecular cell biology*, *9*(8), 639-649.

Szysz, M. P., Wołczańska, A., & Chmiel, E. (2018). Biological role of Legionella pneumophila lipopolysaccharide. *Biomed. J. Sci. Tech. Res*, *4*, 3739-3741.

Takahashi, K. (2001). Development and differentiation of macrophages and related cells historical review and current concepts. *Journal of clinical and experimental hematopathology*, *41*(1), 1-31.

Takeuchi, O., & Akira, S. (2010). Pattern recognition receptors and inflammation. *Cell*, *140*(6), 805-820.

Teruya, H., Higa, F., Akamine, M., Ishikawa, C., Okudaira, T., Tomimori, K., Mukaida, N., Tateyama, M., Heuner, K., & Fujita, J. (2007). Mechanisms of Legionella pneumophila-induced interleukin-8 expression in human lung epithelial cells. *BMC microbiology*, *7*, 1-16.

Tesh, M. J., & Miller, R. D. (1981). Amino acid requirements for Legionella pneumophila growth. *Journal of Clinical Microbiology*, *13*(5), 865-869.

Thay, B., Damm, A., Kufer, T. A., Wai, S. N., & Oscarsson, J. (2014). Aggregatibacter actinomycetemcomitans outer membrane vesicles are internalized in human host cells and trigger NOD1-and NOD2-dependent NF-κB activation. *Infection and immunity*, *82*(10), 4034-4046.

Théry, C., Witwer, K. W., Aikawa, E., Alcaraz, M. J., Anderson, J. D., Andriantsitohaina, R., Antoniou, A., Arab, T., Archer, F., & Atkin-Smith, G. K. (2018). Minimal information for studies of extracellular vesicles 2018 (MISEV2018): a position statement of the International Society for Extracellular Vesicles and update of the MISEV2014 guidelines. *Journal of extracellular vesicles*, *7*(1), 1535750.

Thurlow, L. R., Hanke, M. L., Fritz, T., Angle, A., Aldrich, A., Williams, S. H., Engebretsen, I. L., Bayles, K. W., Horswill, A. R., & Kielian, T. (2011). Staphylococcus aureus biofilms prevent macrophage phagocytosis and attenuate inflammation in vivo. *The Journal of immunology*, *186*(11), 6585-6596.

Tilney, L. G., Harb, O. S., Connelly, P. S., Robinson, C. G., & Roy, C. R. (2001). How the parasitic bacterium Legionella pneumophila modifies its phagosome and transforms it into rough ER: implications for conversion of plasma membrane to the ER membrane. *Journal of cell science*, *114*(24), 4637-4650.

Tosi, M. F. (2005). Innate immune responses to infection. *Journal of Allergy and Clinical Immunology*, *116*(2), 241-249.

Toyofuku, M. (2019). Bacterial communication through membrane vesicles. *Bioscience, Biotechnology, and Biochemistry*, *83*(9), 1599-1605.

Toyofuku, M., Nomura, N., & Eberl, L. (2019). Types and origins of bacterial membrane vesicles. *Nature Reviews Microbiology*, *17*(1), 13-24.

TR, H. (2003). A common dominant TLR5 stop codon polymorphism abolishes flagellin signaling and is associated with susceptibility to legionnaires' disease. *Journal of Experimental Medicine*, *198*, 1563-1572.

Treacy-Abarca, S., & Mukherjee, S. (2015). Legionella suppresses the host unfolded protein response via multiple mechanisms. *Nature communications*, *6*(1), 7887.

Tsuchiya, S., Kobayashi, Y., Goto, Y., Okumura, H., Nakae, S., Konno, T., & Tada, K. (1982). Induction of maturation in cultured human monocytic leukemia cells by a phorbol diester. *Cancer research*, *42*(4), 1530-1536.

Tsuchiya, S., Yamabe, M., Yamaguchi, Y., Kobayashi, Y., Konno, T., & Tada, K. (1980). Establishment and characterization of a human acute monocytic leukemia cell line (THP-1). *International journal of cancer*, *26*(2), 171-176.

Turnbull, L., Toyofuku, M., Hynen, A. L., Kurosawa, M., Pessi, G., Petty, N. K., Osvath, S. R., Cárcamo-Oyarce, G., Gloag, E. S., & Shimoni, R. (2016). Explosive cell lysis as a mechanism for the biogenesis of bacterial membrane vesicles and biofilms. *Nature communications*, *7*(1), 11220.

Turner, L., Bitto, N. J., Steer, D. L., Lo, C., D'Costa, K., Ramm, G., Shambrook, M., Hill, A. F., Ferrero, R. L., & Kaparakis-Liaskos, M. (2018). Helicobacter pylori outer membrane vesicle size determines their mechanisms of host cell entry and protein content. *Frontiers in immunology*, *9*, 1466.

Underhill, D. M., & Goodridge, H. S. (2012). Information processing during phagocytosis. *Nature*

*Reviews Immunology*, *12*(7), 492-502.

van Lookeren Campagne, M., Wiesmann, C., & Brown, E. J. (2007). Macrophage complement receptors and pathogen clearance. *Cellular microbiology*, *9*(9), 2095-2102.

Vanaja, S. K., Russo, A. J., Behl, B., Banerjee, I., Yankova, M., Deshmukh, S. D., & Rathinam, V. A. (2016). Bacterial outer membrane vesicles mediate cytosolic localization of LPS and caspase-11 activation. *Cell*, *165*(5), 1106-1119.

Varghese, P. M., Murugaiah, V., Beirag, N., Temperton, N., Khan, H. A., Alrokayan, S. H., Al-Ahdal, M. N., Nal, B., Al-Mohanna, F. A., & Sim, R. B. (2021). C4b binding protein acts as an innate immune effector against influenza A virus. *Frontiers in immunology*, *11*, 585361.

Vatansever, F., de Melo, W. C., Avci, P., Vecchio, D., Sadasivam, M., Gupta, A., Chandran, R., Karimi, M., Parizotto, N. A., & Yin, R. (2013). Antimicrobial strategies centered around reactive oxygen species–bactericidal antibiotics, photodynamic therapy, and beyond. *FEMS microbiology reviews*, *37*(6), 955-989.

Vats, D., Mukundan, L., Odegaard, J. I., Zhang, L., Smith, K. L., Morel, C. R., Greaves, D. R., Murray, P. J., & Chawla, A. (2006). Oxidative metabolism and PGC-1β attenuate macrophage-mediated inflammation. *Cell metabolism*, *4*(1), 13-24.

Verma, V., Kumar, P., Gupta, S., Yadav, S., Dhanda, R. S., Thorlacius, H., & Yadav, M. (2020). α-Hemolysin of uropathogenic E. coli regulates NLRP3 inflammasome activation and mitochondrial dysfunction in THP-1 macrophages. *Scientific Reports*, *10*(1), 12653.

Vinzing, M., Eitel, J., Lippmann, J., Hocke, A. C., Zahlten, J., Slevogt, H., Günther, S., Schmeck, B., Hippenstiel, S., & Flieger, A. (2008). NAIP and Ipaf control Legionella pneumophila replication in human cells. *The Journal of immunology*, *180*(10), 6808-6815.

Wagner, C., Khan, A. S., Kamphausen, T., Schmausser, B., Ünal, C., Lorenz, U., Fischer, G., Hacker, J., & Steinert, M. (2007). Collagen binding protein Mip enables Legionella pneumophila to transmigrate through a barrier of NCI-H292 lung epithelial cells and extracellular matrix. *Cellular microbiology*, *9*(2), 450-462.

Walter, P., & Ron, D. (2011). The unfolded protein response: from stress pathway to homeostatic regulation. *science*, *334*(6059), 1081-1086.

Wang, B., Tian, Y., & Yin, Q. (2019). AIM2 inflammasome assembly and signaling. *Structural immunology*, 143-155.

Wang, H., Lu, J., Li, K., Ren, H., Shi, Y., Qin, T., Duan, X., & Fang, M. (2018). The virulence of Legionella pneumophila is positively correlated with its ability to stimulate NF-κB activation. *Future Microbiology*, *13*(11), 1247-1259.

Wang, L.-x., Zhang, S.-x., Wu, H.-j., Rong, X.-l., & Guo, J. (2019). M2b macrophage polarization and its roles in diseases. *Journal of leukocyte biology*, *106*(2), 345-358.

Wang, X., Lin, S., Wang, L., Cao, Z., Zhang, M., Zhang, Y., Liu, R., & Liu, J. (2023). Versatility of bacterial outer membrane vesicles in regulating intestinal homeostasis. *Science Advances*, *9*(11), eade5079.

Wang, X., Lin, S., Wang, L., Cao, Z., Zhang, M., Zhang, Y., Liu, R., & Liu, J. (2023). Versatility of bacterial outer membrane vesicles in regulating intestinal homeostasis. Sci. Adv. 9, eade5079. In.

Wensink, J., & Witholt, B. (1981). Outer-membrane vesicles released by normally growing Escherichia coli contain very little lipoprotein. *European journal of biochemistry*, *116*(2), 331-335.

Woo, H., & Eyun, S.-i. (2025). Applications and techniques of single-cell RNA sequencing across diverse species. *Briefings in bioinformatics*, *26*(4), bbaf354.

Woodhead, M. (2002). Community-acquired pneumonia in Europe: causative pathogens and resistance patterns. *European Respiratory Journal*, *20*(36 suppl), 20s-27s.

Wright, E. K., Goodart, S. A., Growney, J. D., Hadinoto, V., Endrizzi, M. G., Long, E. M., Sadigh, K., Abney, A. L., Bernstein-Hanley, I., & Dietrich, W. F. (2003). Naip5 affects host susceptibility to the intracellular pathogen Legionella pneumophila. *Current Biology*, *13*(1), 27-36.

Wynn, T. A., Chawla, A., & Pollard, J. W. (2013). Macrophage biology in development, homeostasis and disease. *Nature*, *496*(7446), 445-455.

Xie, Y., Zhang, Y., Wang, Y., & Feng, Y. (2023). Mechanism and modulation of SidE family proteins in the pathogenesis of Legionella pneumophila. *Pathogens*, *12*(4), 629.

Xiong, L., Yamasaki, S., Chen, H., Shi, L., & Mo, Z. (2017). Intracellular growth and morphological characteristics of Legionella pneumophila during invasion and proliferation in different cells. *Biological and Pharmaceutical Bulletin*, *40*(7), 1035-1042.

Xu, F., Kang, Y., Zhang, H., Piao, Z., Yin, H., Diao, R., Xia, J., & Shi, L. (2013). Akt1-mediated regulation of macrophage polarization in a murine model of Staphylococcus aureus pulmonary infection. *The Journal of infectious diseases*, *208*(3), 528-538.

Yaron, S., Kolling, G. L., Simon, L., & Matthews, K. R. (2000). Vesicle-mediated transfer of virulence genes from Escherichia coli O157: H7 to other enteric bacteria. *Applied and environmental microbiology*, *66*(10), 4414-4420.

Ye, P., Garvey, P. B., Zhang, P., Nelson, S., Bagby, G., Summer, W. R., Schwarzenberger, P., Shellito, J. E., & Kolls, J. K. (2001). Interleukin-17 and lung host defense against Klebsiella pneumoniae infection. *American journal of respiratory cell and molecular biology*, *25*(3), 335-340.

Yu, V. L., Plouffe, J. F., Pastoris, M. C., Stout, J. E., Schousboe, M., Widmer, A., Summersgill, J., File, T., Heath, C. M., & Paterson, D. L. (2002). Distribution of Legionella species and serogroups isolated by culture in patients with sporadic community-acquired legionellosis: an international collaborative survey. *The Journal of infectious diseases*, *186*(1), 127-128.

Zakharzhevskaya, N. B., Vanyushkina, A. A., Altukhov, I. A., Shavarda, A. L., Butenko, I. O., Rakitina, D. V., Nikitina, A. S., Manolov, A. I., Egorova, A. N., & Kulikov, E. E. (2017). Outer membrane vesicles secreted by pathogenic and nonpathogenic Bacteroides fragilis represent different metabolic activities. *Scientific Reports*, *7*(1), 5008.

Zamboni, D. S., Kobayashi, K. S., Kohlsdorf, T., Ogura, Y., Long, E. M., Vance, R. E., Kuida, K., Mariathasan, S., Dixit, V. M., & Flavell, R. A. (2006). The Birc1e cytosolic pattern-recognition

receptor contributes to the detection and control of Legionella pneumophila infection. *Nature immunology*, *7*(3), 318-325.

Zhang, B., Wang, N., He, G., Chen, T., Zong, J., Shen, C., Wang, Y., Li, C., Yin, X., & Meng, Y. (2025). Akkermansia muciniphila-Derived Outer Membrane Vesicles as a Novel Therapeutic Approach for Mastitis: Insights From In Vitro and Vivo Studies. *The FASEB Journal*, *39*(13), e70770.

Zhang, H., Zhang, Y., Song, Z., Li, R., Ruan, H., Liu, Q., & Huang, X. (2020). sncRNAs packaged by Helicobacter pylori outer membrane vesicles attenuate IL-8 secretion in human cells. *International Journal of Medical Microbiology*, *310*(1), 151356.

Zhang, Y., Liang, S., Deng, Z., Zhao, Z., & Han, X. (2024). High-glucose conditions attenuate the response of macrophages to Legionella pneumophila infection by inhibiting NOD1 and MAPK signaling. *International immunopharmacology*, *134*, 112254.